Printing Cells and Co-cultures for Osteoarthritis Models

A thesis submitted to the Faculty of Science, Agriculture and Engineering for the Degree of Doctor of Philosophy (Integrated)

By

Joseph Dudman

School of Engineering

Newcastle University

February 2020

Abstract

Osteoarthritis is a multifactorial disease characterised by the degradation of cartilage and bone tissue within the joint. Research into novel therapies is currently limited by the throughput and replicative accuracy of early-stage *in vitro* disease models.

Biofabrication represents an emerging technology which allows for the selective deposition of cells and material in order to create complex cell-laden structures. The aim of this research was to characterise a combination of inkjet and valve-based drop-on-demand printing processes for the construction of osteoarthritis tissue models.

An inkjet printing platform was characterised to deposit material at the picolitre-scale. Single cell printing was achieved, with biological analysis confirming that the printing process does not significantly affect cellular viability or function.

A valve printing process was applied for the production of cellular aggregates that could be used for both *in vitro* osteoarthritis research and *in vivo* therapeutic applications. Reliable jetting performance was demonstrated, enabling material deposition at the nanolitre-scale. Cell printing was achieved across a concentration range of 1-20 million cells per mL, with biological analysis of printed cells revealing no significant effects on viability or function. No discernible impact on aggregate tissue structure was observed as a result of the printing process, confirming its suitability for the manufacture of tissue aggregates.

A bioprinted co-culture tissue model comprised of mesenchymal stromal cell and chondrocyte cell types was successfully generated using a 3D insert culture format. Cell proliferation was maintained over a 14 day period, alongside an increase in tissue density and cellular organisation.

In combination, this research has demonstrated the suitability of inkjet and valve printing processes to selectively deposit cells. Bioprinted aggregate and insert-based 3D tissue models were validated using the valve printing technique, providing an effective method to scale up the manufacture of *in vitro* platforms for osteoarthritis research applications.

Acknowledgements

Firstly, I would like to acknowledge the support of Versus Arthritis, the Engineering and Physical Sciences Research Council and the Centre for Doctoral Training in Additive Manufacturing and 3D Printing for providing the funding and support that made this project possible.

I would like to thank my supervisory team, Dr. Ana Ferreira-Duarte, Dr. Piergiorgio Gentile, Dr. Xiao Wang and Professor Kenny Dalgarno for providing me with essential support and guidance over the past four years that has enabled me to undertake this PhD and develop as an independent scientist.

I would like to acknowledge the support of the Newcastle University Bio-imaging facility staff for providing the equipment training and facilities that were used throughout this work.

I would also like to acknowledge the support of Xin Xu of the Newcastle University Biobank facility for performing all of the sample sectioning that was required for this project.

I would like to thank the members of the Versus Arthritis Tissue Engineering Centre at the Universities of York and Keele for providing me with technical resources and support surrounding the biological analysis techniques used within this research.

I would like to thank my friends and colleagues in both Newcastle and on the CDT programme for making the experience so enjoyable and conference attendances so memorable.

I would also like to acknowledge the support of Dr. Mhairi Morris, my undergraduate degree project supervisor, who provided me with the inspiration to pursue a PhD.

I would like to thank my friends and family for supporting and encouraging me throughout the project.

Finally, I would like to thank Melissa Jackson for providing an indispensable sounding board and voice of reason throughout the last four years.

Table of Contents

Table of Figures

Table of Tables

Table of Equations

Table of Abbreviations

2D	-	2-Dimensional
3D	-	3-Dimensional
ACI	-	Autologous Chondrocyte Implantation
ADAMTS	-	A Disintegrin and Metalloproteinase with Thrombospondin Motifs
CJ	-	Continuous Jetting
COX-2	-	Cyclooxygenase-2
CV	-	Coefficient of Variation
DAPI	-	4',6-Diamidino-2-phenylindole
DMEM	-	Dulbecco's Modified Eagle's Medium
DoD	-	Drop-on-Demand
ECM	-	Extracellular Matrix
EdU	-	5-Ethynyl-2'-deoxyuridine
FITC	-	Fluorescein Isothiocyanate
F-actin	-	Filamentous Actin
HTS	-	High-Throughput Screening
IL-1β	-	Interleukin-1 beta
MMP	-	Matrix Metalloproteinase
MSC	-	Mesenchymal Stromal Cell
NF-κβ	-	Nuclear Factor kappa beta
OA	-	Osteoarthritis
PBS	-	Phosphate Buffered Saline
PDMS	-	Polydimethylsiloxane
PLL	-	Poly-L-Lysine
TIMP	-	Tissue Inhibitor of Metalloproteinase
TNF-α	-	Tumour Necrosis Factor alpha
VEGF	-	Vascular Endothelial Growth Factor

Chapter 1. Introduction

Osteoarthritis (OA) is a chronic disease that involves the breakdown of cartilage and bone tissue within the joint. Current treatment strategies range from holistic approaches to strengthen the underlying joint and manage pain to full joint replacement surgery (National Institute for Health and Care Excellence, 2014). Although the development of novel pharmaceuticals and cellular therapies provide promising alternatives to traditional treatment methods, further research is required to fully ascertain the causes and mechanisms of the disease, as well as to explore the efficacy of therapies currently under development (Loeser, Collins and Diekman, 2016; Mobasheri and Batt, 2016; Armoiry *et al.*, 2019).

In order to perform such research, developments within the field of *in vitro* tissue modelling are essential, as novel OA models may provide a mechanism by which it would be possible to facilitate the high-throughput screening of drug candidates or therapies in a short time span, and at a low cost to the end user. However, a current challenge in *in vitro* modelling is the ability to generate models which are user-friendly, scalable, and wholly replicative of the OA joint *in vivo* (DiMasi, Grabowski and Hansen, 2016).

A key feature of 3D *in vitro* models is the ability to recapitulate the spatial organisation and cell-cell contact that exists within *in vivo* living tissue, a feature that is lost with traditional 2D monolayer culture approaches. Techniques which support this approach include aggregate culture, and those that utilise supportive inserts as exogenous extracellular matrix to improve cellular support (McMurtrey, 2016; Nath and Devi, 2016; Melissaridou *et al.*, 2019). However, in spite of these developments, such 3D formats are currently limited to low-throughput applications due to the labour-intensive requirements during setup, and increased cost and complexity when compared to traditional 2D culture techniques (Joshi and Lee, 2015).

Biofabrication is an emerging field in which liquid handling and additive manufacturing processes are applied for the deposition of cells and materials to generate cell-laden structures. A range of different techniques have been developed to enable the selective deposition of cellular material, including inkjet, valve, laser-assisted and extrusion based processes. These techniques have been successfully utilised to generate cell, tissue and biomaterial structures for tissue engineering and regenerative medicine applications.

Of these techniques, droplet-based processes such as inkjet and valve printing show the most potential for cell printing applications due to the inherent scalability of each process, comparatively low cost of operation and demonstrated biocompatibility with a range of cell types (Xu *et al.*, 2005; Gudapati, Dey and Ozbolat, 2016; Tse *et al.*, 2016).

Early research by Wilson and Boland first investigated the potential of using inkjet printing technology to deposit a combination of cell types in 2003 (Wilson and Boland, 2003). More recent projects, such as the work by Park *et al.* in 2017, have demonstrated that the inkjet printing process can be used to deposit a range cell types with a sufficient accuracy and precision to enable the production of complex cellular patterns without affecting cellular viability (J. A. Park *et al.*, 2017).

Valve printing processes have also been explored for the deposition of cellular material. Indeed, work by Faulkner-Jones *et al.* in 2013 successfully demonstrated the application of valve printing processes to generate cellular aggregates. This is further supported by work from Lee *et al.* in 2014, which used these techniques to generate human skin equivalents, and Horvath *et al.* in 2015 to construct an *in vitro* human alveolar tissue model (Faulkner-Jones *et al.*, 2013; Lee *et al.*, 2014; Horvath *et al.*, 2015).

Despite such research however, droplet-based techniques are currently limited by the lack of process validation for cell printing applications, as well as the associated nozzle clogging and performance issues that have been reported when dispensing cell-containing ink solutions (Parsa *et al.*, 2010; Chahal, Ahmadi and Cheung, 2012). In addition, little is known about the impact of mechanical forces induced by each printing process on cell types, and moreover how these factors might influence the mechano-responsive cell types involved in *in vitro* OA models.

Nevertheless, droplet-based bioprinting techniques present a range of opportunities to automate and scale up the manufacture of *in vitro* tissue models for osteoarthritis research, as well as providing a potential mechanism to generate 3-dimensional tissues for *in vivo* therapeutic applications.

1.1 Aims and Objectives

The overall aim of this thesis is to evaluate the potential of using bioprinting techniques for the construction of *in vitro* osteoarthritis tissue models.

To achieve this aim a number of specific objectives are defined:

1. To evaluate the performance of an inkjet printing process for the selective deposition of cellular material
2. To characterise the cell printing performance of a valve printing technique
3. To assess the effects of each printing process on cellular viability and function
4. To apply droplet-based bioprinting processes to manufacture tissue aggregates
5. To print and characterise a novel cartilage tissue model for osteoarthritis research

1.2 Thesis Structure

This thesis is organised into 7 chapters with chapter 1 providing an introduction to the research area alongside the aims and objectives defined for this project.

Chapter 2 provides a literature review of the underlying concepts of the thesis. This includes a review of osteoarthritis pathophysiology, treatment and available disease models, alongside considerations surrounding high-throughput screening. Information is provided on the field of biofabrication, with a focus on drop-on-demand bioprinting processes and bioink design, in order to explore its suitability for high-throughput model generation.

Chapter 3 contains the methodologies for work performed in this thesis, including the biological culture and analysis techniques used across the individual chapters. In addition, this chapter provides an overview of the bioprinting setup used for inkjet and valve printing applications.

Chapter 4 presents novel research into the application of a piezoelectric inkjet printing technique for the selective deposition of single cells. Material and cell printing performance characterisation is presented in response to changes in printer parameters. Evaluation of the biocompatibility of the inkjet printing process is also reported, alongside a combination of novel methods to reduce cellular agglomeration during printing.

Chapter 5 reports an investigation into the application of a drop-on-demand valve printing process for the production of 3D cell aggregates. Material and cell printing performance

characterisation is presented alongside biological analysis of printed cells and tissue aggregates.

Chapter 6 presents a bioprinted osteoarthritis tissue model generated using the valve printing process upon well-based inserts, alongside biological characterisation of the culture format.

Chapter 7 provides an overall discussion on the results displayed within this thesis and their impact on the fields of biofabrication and osteoarthritis research. It also provides recommendations for future work.

Chapter 2. Literature Review

2.1 Osteoarthritis

2.1.1 Significance

Osteoarthritis is a chronic joint disease characterised by the degradation of cartilage and underlying bone that leads to disability and pain as the disease progresses. It is most common amongst load-bearing joints within the knee, hip, hands and spine, with age-related articular tissue changes having been shown to contribute to disease pathophysiology (Loeser, Collins and Diekman, 2016). Globally, OA was responsible for approximately 17.1 million years lived with disability in 2010, representing an increase of 64 % since 1990 (Vos *et al.*, 2012).

The most common joint affected by the disease is the knee, with a global prevalence of radiographically confirmed symptomatic OA within this joint estimated to be 3.8 % (Cross *et al.*, 2014). Peak incidence occurs at 50 years of age, with hip OA prevalence most strongly correlating with increasing age. Risk factors include obesity, age, ethnicity, female gender, joint injury, joint laxity, muscle weakness and reduced bone density (Chaganti and Lane, 2011).

2.1.2 Pathophysiology

Osteoarthritis is a multifactorial disease whereby biochemical changes within the cartilage and underlying bone combine with morphological damage, resulting in gross cartilage tissue loss through degradative processes. Although not a causative agent, inflammation is considered critical in the pathogenesis of the disease. Inflammatory mediators such as cytokines and prostaglandins released by cartilage, bone and synovium result in local tissue changes and synovitis, a characteristic symptom in OA patients (Berenbaum, 2013). The bone tissue response is also thought to play a considerable role in the development of OA, characterised radiographically within this tissue by osteophyte formation, joint space narrowing, subchondral sclerosis and cyst formation (Kellgren and Lawrence, 1957). Examples of the changes leading to the development of osteoarthritis is shown in Figure 2.1.

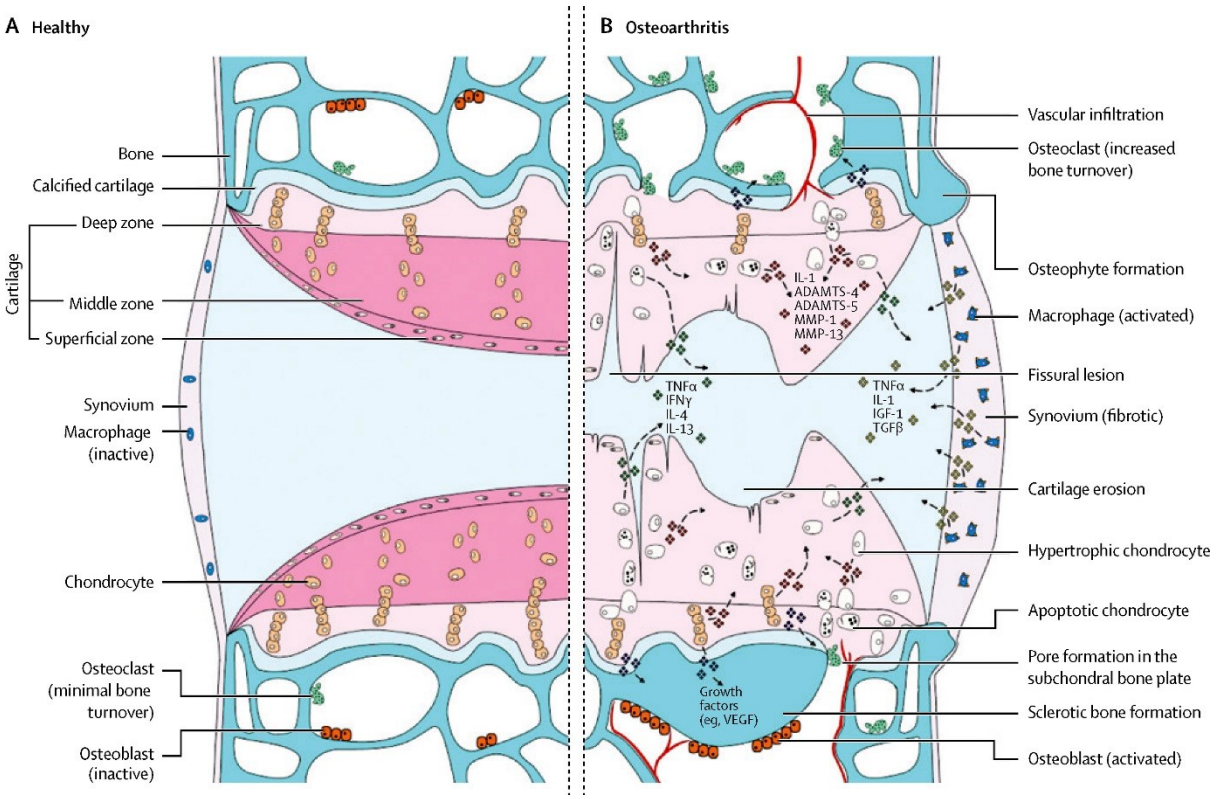

Figure 2.1 – Osteoarthritis development within an articular joint. Reproduced from (Glyn-Jones et al., 2015).

Osteoarthritis is thought to be initiated by non-physiological joint loading disrupting the homeostatic mechanisms that maintain a healthy joint. Risk factors presented in Figure 2.2 such as ligament damage and joint laxity or weakness contribute towards this by causing abnormal alignment of the joint, increasing load on specific regions of cartilage. In addition, under-loading and over-loading are also known to induce degradative processes within healthy joint tissue through reduced limb use or the absorption of excessive and prolonged impact forces.

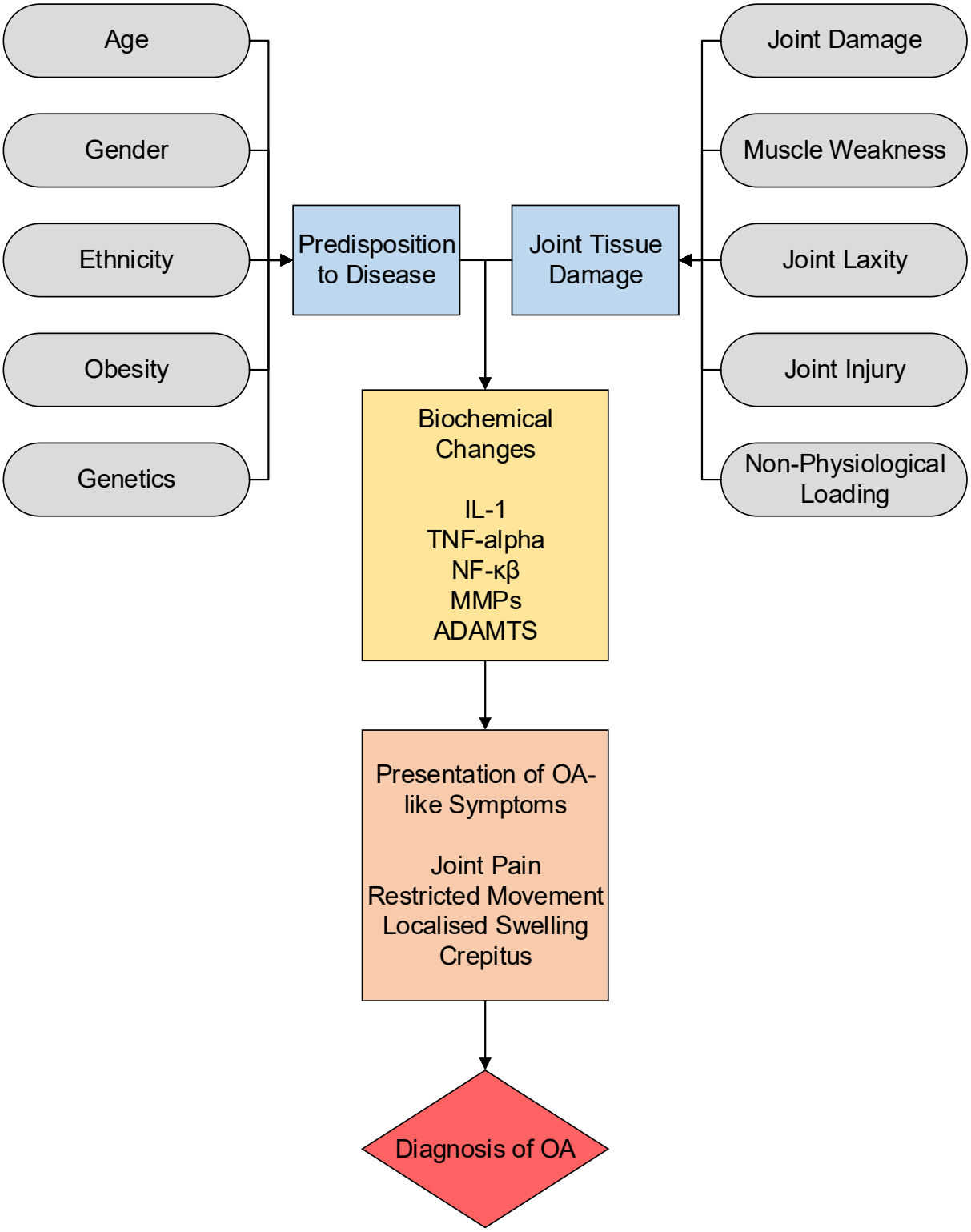

Figure 2.2 – A flow diagram depicting the pathogenesis of osteoarthritis. IL-1 – Interleukin-1, TNF-alpha – Tumour necrosis factor alpha, NF-κβ – Nuclear factor kappa beta, MMP – Matrix metalloproteinase, ADAMTS - A disintegrin and metalloproteinase with thrombospondin motifs. Adapted from (Dieppe and Lohmander, 2005).

Healthy cartilage is comprised of chondrocytes and extracellular matrix (ECM), which represent approximately 1-5 % and 95-99 % of the total tissue volume respectively (Bhosale

and Richardson, 2008). Type II collagen is the most abundant ECM component within articular cartilage tissue and accounts for approximately 50 % of the total protein content. The fibril network of collagen provides tensile strength to the tissue during loading. Aggrecan is also an integral ECM component, conferring resistance to compressive forces during joint loading. Variations in chondrocyte cell density, size, shape, maturation status and orientation are present across different regions within cartilage tissue, alongside differences in ECM fibre composition, orientation and density. This is highlighted in the diagram in Figure 2.3 below.

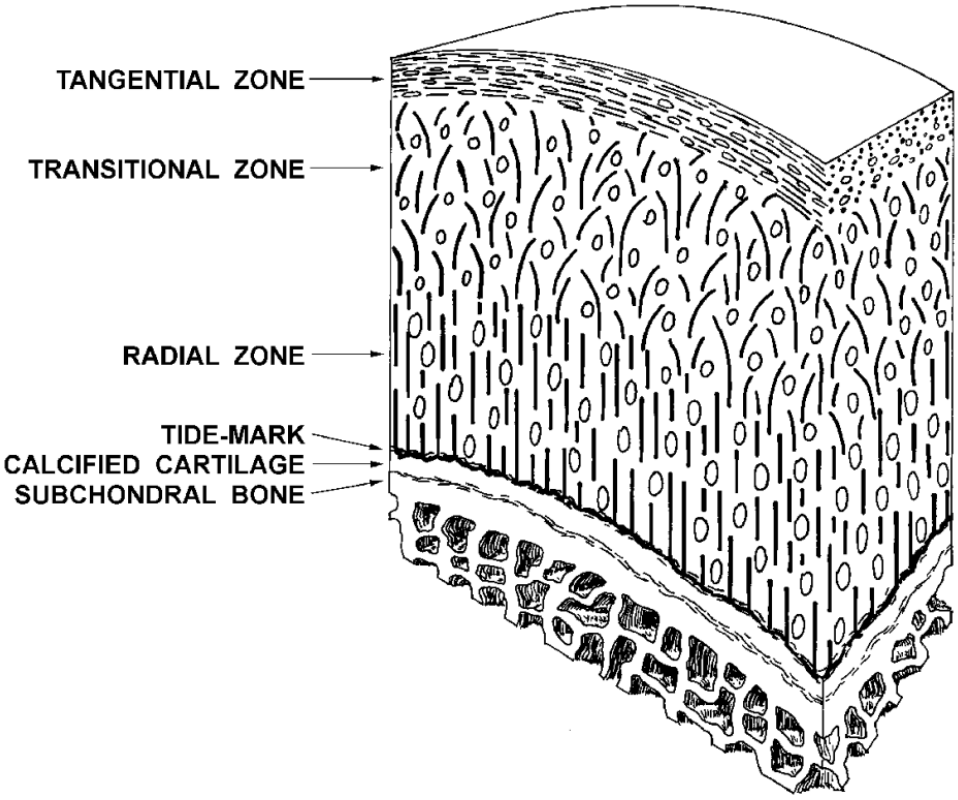

Figure 2.3 – Diagram displaying the stratification of hyaline cartilage tissue into different regions. Variations in ECM composition and fibre orientation, alongside chondrocyte cell density, maturation status, shape, size and orientation are present between each region. Reproduced from (Cova and Toffanin, 2002).

Biochemical processes within the joint can damage cartilage ECM and increase catabolic activity in response to initiating factors such as those highlighted in Figure 2.4, leading to development of OA. Enzymes responsible for the breakdown of ECM collagen fibrils and proteoglycans include matrix metalloproteinases (MMPs) and a disintegrin and metalloproteinase with thrombospondin motifs (ADAMTS) (Cawston and Wilson, 2006; Rengel, Ospelt and Gay, 2007). Specific isoforms of the enzymes implicated in osteoarthritis include ADAMTS 4 and 5, which are secreted from chondrocyte cells into the extracellular

space, and collagenases MMP-1 and 13, which are secreted by macrophage, fibroblast and chondrocyte cells (Cawston and Wilson, 2006; Gendron *et al.*, 2007).

However, it's important to appreciate that whilst MMP activity may be significant pathologically, MMP activity is also crucial within a healthy joint, whereby they initiate osteoclastic resorption by removing surface collagen from bone tissue prior to demineralisation (Rengel, Ospelt and Gay, 2007). This process is balanced against the functionality of osteoblasts which synthesise crosslinked collagen, osteocalcin, osteopontin and hydroxyapatite to generate mineralised bone tissue. As such, MMP inhibition therapies can only be used for the treatment of OA if drug action can be selectively targeted towards degradative processes.

Aggrecan degradation occurs via the activity of differentially regulated ADAMTS-4 and ADAMTS-5 aggrecanases. Conflicting research exists in determining the enzyme primarily responsible for the development of osteoarthritis, with the results of animal models contrasting with those of human studies (Glasson *et al.*, 2005; Gendron *et al.*, 2007). ADAMTS-5 has been demonstrated to have a greater role in proteolysis of ECM and is constitutively expressed. However, ADAMTS-4 has been shown to respond to interleukin-1 beta (IL-1β) and tumour necrosis factor-alpha (TNF-α), with its upregulation transcriptionally dependant on nuclear factor-kappa beta (NF-κβ), a key signalling molecule elevated during the development of OA (Glasson *et al.*, 2005; Bondeson *et al.*, 2008; Verma and Dalal, 2011).

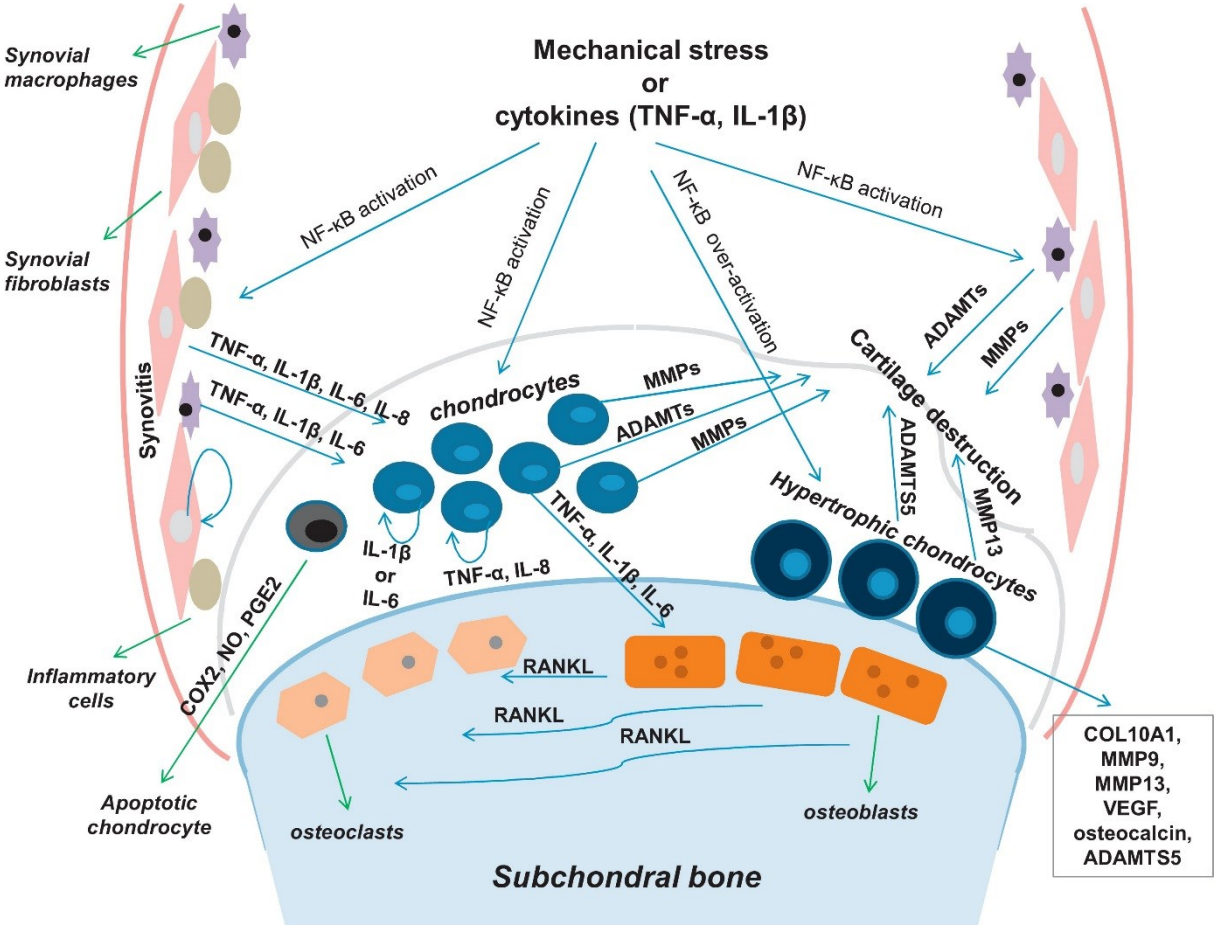

Figure 2.4 – The nuclear factor-kappa beta (NF-κβ) signalling network in osteoarthritis. Reproduced from (Rigoglou and Papavassiliou, 2013). MMPs – Matrix metalloproteinases. ADAMTS – A disintegrin and metalloproteinase with thrombospondin motifs. COX-2 – Cyclooxygenase-2. NO – Nitric oxide. TNF-α – Tumour necrosis factor-alpha. IL-1β – Interleukin-1 beta. PGE2 – Prostaglandin E2. RANKL – Receptor activator of nuclear factor kappa-B ligand. VEGF – Vascular endothelial growth factor. COL – Collagen.

MMP activity also plays a role in chemokine processing, protease activity status modulation and cell membrane shedding (Löffek, Schilling and Franzke, 2011). Research has suggested that each MMP subtype is responsible for a specific role in the degradation process through location specific functions across cartilage tissue. This includes MMP 1, 8 and 13, each belonging to the collagenase group, MMP 2 and 9, belonging to the gelatinase group, and MMP 3, 7, 10 and 11, belonging to the stromelysin group, as well as other membrane-specific and non-specific MMPs. MMP mRNA is upregulated in response to IL-1β signalling as well as MMP-specific responses to tissue inhibitors of metalloproteinases (TIMPs) (Brew, Dinakarpandian and Nagase, 2000; Mountain *et al.*, 2007; Lin *et al.*, 2009; Brew and Nagase, 2010).

MMPs have also been shown to be co-expressed in OA patient tissue samples indicating a potential co-regulation mechanism (Martel-Pelletier, Welsch and Pelletier, 2001; Kevorkian

et al., 2004). Cartilage breakdown products such as fibronectin components then enter the synovial fluid as a result and irritate the synovial membrane lining, causing the release of inflammatory mediators. Such breakdown products have been shown to have a significant role in disease progression through indirectly mediating cartilage destruction (Yasuda, 2006; Pérez-García *et al.*, 2016). Mononuclear inflammatory cells are also recruited which in turn secrete IL-1β and TNF-α, further upregulating protease production via local chondrocytes and fibroblasts within the synovium.

As a further consequence of non-physiological mechanical stimulation, pro-inflammatory signalling cascades are activated which induce synovitis. Secreted IL-1β and TNF-α further activate mitogen-activated protein kinases as a result of chondrocyte loading, a critical pathway for transducing the mechanical forces of cartilage shear and compression into biological responses (Fitzgerald *et al.*, 2008).

NF-κβ is also activated in OA, initiating a wide range of chondrocyte signalling pathways. Vascular endothelial growth factor (VEGF) expression is then stimulated, leading to the upregulation of ADAMTS-5 and MMPs 1, 2, 3, 9 and 13, further contributing to enzymatic tissue degradation.

Cyclooxygenase-2 (COX-2) expression is considered an important mediator in osteoarthritis inflammation. An increase in COX-2 expression has been linked to prostaglandin-E2 synthesis local to disease sites. In addition, prostaglandin synthesis has been shown to upregulate COX-2 and interleukin-6 at inflammatory sites (Anderson *et al.*, 1996). Prostaglandin-E2 has also been shown to be a significant catabolic mediator within cartilage tissue. Both prostaglandin-E2 and nitric oxide release by IL-1β have been shown to be upregulated by mitogen-activated protein kinase, activator protein-1 and NF-κβ within chondrocytes (Chowdhury *et al.*, 2008).

In contrast to overloading-induced OA, much less is known about the specific signalling pathways that lead to cartilage degradation within under loaded tissue such as that of an immobilised joint. Nitric oxide synthase, VEGF, prothrombin and hypoxia inducible factor 1-alpha (HIF-1α) expression have been shown to increase following immobilisation, however the upstream or downstream effects in relation to osteoarthritis are not fully understood (Trudel, Uhthoff and Laneuville, 2005; Basso and Heersche, 2006; Sakamoto *et al.*, 2009).

Although cartilage degradation remains a hallmark of OA, a number of other changes relating to other joint tissues such as bone also occur and contribute to its development. Moreover, there is clear dynamic between cartilage and underlying bone within OA pathophysiology, with osteoblast and osteoclast dysfunction resulting in net bone resorption, and the development of osteophytes; a key radiological feature associated with OA development (Junker *et al.*, 2016). This feature is induced by the cytokines IL-1β and TNF-α, which promotes the differentiation of osteoclasts within bone tissue, disrupting the homeostatic balance of bone modelling and bone resorption (Rengel, Ospelt and Gay, 2007).

Changes to the subchondral bone have been previously associated with disease pathogenesis, with subchondral bone-modifying drugs considered as potential treatment options for OA (Bellido *et al.*, 2011; Castañeda *et al.*, 2012). In addition, pro-inflammatory signalling pathways elevated during OA development have been associated with subchondral bone sclerosis and hypo-mineralisation as a result of abnormal bone remodelling and tissue damage (Li *et al.*, 2013).

2.1.3 Current Treatment Strategies

Treatment for OA are stratified according to disease progression and are outlined in Figure 2.5. Initial treatment includes the use of exercise regimens to strengthen the muscles surrounding the joint and improve posture. Changes to a patient's diet are often advised where obesity is present, due to it being a recognised risk factor in the pathogenesis of the disease wherein it promotes overloading of the afflicted joint.

Painkillers such as paracetamol or non-steroidal anti-inflammatory drugs (NSAIDs) may be prescribed in order to manage symptoms in early stages of the disease. As the disease progresses, opioids and local corticosteroid injections are also used to manage pain where paracetamol or NSAIDs have proved to be ineffective. COX-2 inhibitors may also be incorporated into the treatment regime to reduce localised inflammation. If symptoms cannot be effectively managed through lifestyle modifications, pain management and anti-inflammatories alone, additional options may be explored including the use of assistive devices or surgical procedures to improve symptoms.

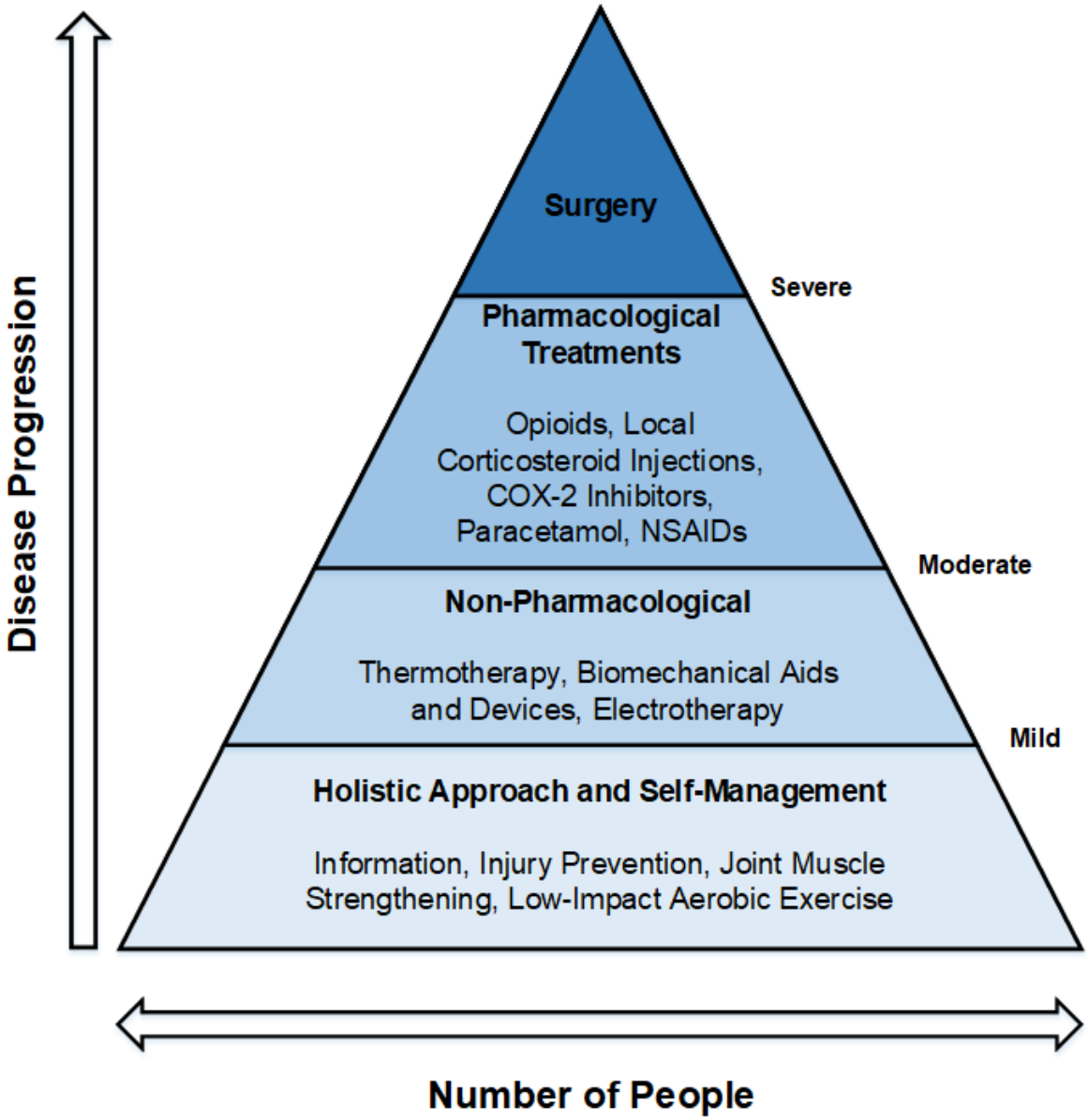

Figure 2.5 – Diagram representing the treatment pathway for OA at various stages of disease progression in accordance with current National Institute for Health and Care Excellence clinical guidelines for OA management. NSAIDs – Non-steroidal anti-inflammatory drugs, COX-2 – Cyclooxygenase-2. Adapted from (Dieppe and Lohmander, 2005).

Traditional surgical options for knee OA include arthrodesis, osteotomy and arthroplasty whereby the joint is fused, realigned or replaced respectively. More recent surgical methods include microfracture surgery, whereby small fractures are created in the underlying bone. This results in an influx of cells and signalling factors that generate a clot to stimulate cartilage repair (Erggelet and Vavken, 2016).

Mosaicplasty, also known as osteochondral transplantation, can also be used to repair cartilage tissue. This is performed by harvesting and transplanting a number of small

cylindrical osteochondral plugs taken from the less weight-bearing regions of the patellofemoral area and inserting them into defect regions following the drilling of cylindrical holes within affected tissue.

Tissue engineering approaches have also been utilised as a treatment methodology. Autologous matrix-induced chondrogenesis is a technique whereby microfracture surgery is combined with the implantation of a bi-layer collagen membrane in order to restore large defect areas that would be difficult to repair using microfracture surgery alone. This improves the defect fill and clot stability at the defect site.

Finally, the most recently adopted surgery for OA is autologous chondrocyte implantation (ACI). This is a cellular therapy performed to repair chondral defect sites, whereby a 2-300 milligram sample of cartilage tissue is obtained via arthroscopic surgery from a healthy, reduced weight-bearing area of the patellofemoral region such as the superior ridge of the medial or lateral femoral condyle. The cell matrix is then enzymatically removed from this sample in order to isolate a population of healthy chondrocytes. These cells are grown *ex vivo* for 4-6 weeks in order to generate a cell number sufficient to repair the damaged area. A second surgical procedure is then performed to apply the expanded chondrocytes to the defect area. This surgery may be expanded further by utilising an implantable scaffold to provide support to the surgical site, however previous versions have relied upon a collagen membrane or periosteal flap. A clear limitation to the ACI procedure is that it requires multiple surgical procedures in order to repair the damaged area unlike other techniques. In addition, comprehensive laboratory practices are required to screen and select cells during the *ex vivo* growth period that will be most likely to form healthy hyaline cartilage following implantation, in order to minimise fibrocartilage formation.

A review article published by Niemeyer *et al.* of the German Society of Orthopaedics and Trauma highlights the importance of considering the range of techniques available for the treatment of cartilage defects as a spectrum of cartilage-related treatments, with indication-dependent advantages as opposed to competing treatment options. This is significant given the authors observations of current research suggesting that autologous chondrocyte implantation provides superior performance over alternative therapies at a defect size of >3-4 cm^2, with >2.5 cm^2 considered for active sports patients. Defects of <2-3 cm^2 are considered to be suitable candidates for mosaicplasty. Autologous chondrocyte implantation is reported to be superior in comparison to microfracture surgery in terms of the quality of

subsequent repair tissue however the author indicates a lack of studies outlining the functional superiority of this technique in comparison to mosaicplasty for periosteum repair (Niemeyer *et al.*, 2016).

Previous work by Elvidge *et al.* has evaluated the efficacy of ACI in comparison to traditional microfracture surgery within the UK. This work assessed the clinical outcomes of each type of surgery in relation to cost and quality-adjusted life years gained. ACI was estimated to reduce the lifetime probability of knee replacement by 50 % in comparison to microfracture surgery. Quality-adjusted life years were increased from 15.85 to 16.57 when using ACI, with an associated cost of £8,008 and £23,307 respectively. The cost per quality adjusted life year was calculated to be £21,245, representing cost-effectiveness in line with UK clinical thresholds whilst providing substantial patient benefits. This outcome, alongside the high incidence and associated morbidity of the disease, provides a clear objective for the generation of cost-effective clinical solutions to reduce the burden of osteoarthritis amongst the UK population. Current state-of-the-art treatments such as ACI therefore provide a temporary benchmark for new treatments to surpass in order to demonstrate clinical viability and may offer further opportunity to develop research into this new therapeutic area (Elvidge, Bullement and Hatswell, 2016).

However, despite these recommendations, the efficacy of ACI surgery in comparison to more conventional procedures is not unanimously recognised. A randomised controlled trial funded by the French Ministry for Social Affairs and Health analysed the functional outcomes of third generation ACI in comparison to single-stage mosaicplasty over a period of 24 months using the international knee documentation committee scoring system for patients with isolated symptomatic femoral chondral defects. The Cartipatch® solid agarose-alginate scaffold was selected for this study. Functional outcomes were found to be significantly worse in the Cartipatch® group when compared to those treated via mosaicplasty after 24 months, with patients also exhibiting a greater number of recorded adverse events. This included the development of an infection within the Cartipatch® group. A two-fold increase in morbidity was observed when comparing the Cartipatch® and mosaicplasty treatment groups, which the authors attributed to the multi-stage surgical procedure required for ACI therapy. This research did not include data on the cost effectiveness of each treatment, however the cost of Cartipatch® would have likely been significantly larger than

mosaicplasty due to the increased number of procedures required and associated costs with scaffold production (Clav *et al.*, 2016).

In 2017, the National Institute for Health and Care Excellence published an updated technical appraisal report recommending the use of ACI as an option for the treatment of articular cartilage defects of the knee under specific conditions, based upon cost-effectiveness calculations incorporating a maximum cell cost of £16,000 per patient. These conditions include the requirements for patients to have not had previous articular cartilage defect surgery, have minimal osteoarthritic knee joint damage, and possess a cartilage defect of greater than 2 cm^2 in size (National Institute for Health and Care Excellence, 2005; Mistry *et al.*, 2015; National Institute for Health and Care Excellence, 2017).

2.1.4 Novel Therapies

Future treatment methods may include the use of gene therapy or targeted pharmacotherapy in order to treat OA. Such treatments have the potential to significantly improve the quality of life for patients diagnosed with OA by reducing associated symptoms, slowing progression or completely eliminating the disease. Therapies such as these would also provide new treatment options between the early and later stages of progression, reducing the need for high-risk surgical intervention. However, a lack of understanding of the pathophysiology of OA as well as concerns over the safety and cost effectiveness of such treatments currently limit development (Evans, Ghivizzani and Robbins, 2013; Thysen, Luyten and Lories, 2015; Madry and Cucchiarini, 2016).

One potential method for treating osteoarthritis involves the use of drugs that affect subchondral bone metabolism. Strontium ranelate is an example of a drug that induces reduced bone-resorption and increased bone formation, having been previously licensed for the treatment of osteoporosis. This particular drug could therefore be used as an anabolic stimulant to encourage bone generation, treating the bone related symptoms of OA (Tat *et al.*, 2011).

Inhibition of the IL-1β pathway is also considered to be a potential therapeutic target for future treatment due its critical role in OA disease pathophysiology. This includes developing methodologies to block the function of IL-1β converting enzyme, pathway receptors or receptor antagonist. So far such methods have failed to provide clinically relevant effects on OA when tested in human studies (Jotanovic *et al.*, 2012; Shin *et al.*, 2013).

A similar methodology has been trailed on the TNF-α pathway through the generation of TNF-α antagonists such as Adalimumab, a drug currently prescribed in the UK for the treatment of rheumatoid arthritis. Adalimumab has been shown to have considerable therapeutic benefits in patients suffering from knee OA (Maksymowych *et al.*, 2012). In contrast, the drug Anakinra failed to demonstrate similar disease-modifying effects when compared with a placebo for the treatment of OA. This was despite having a similar mode of action, being well tolerated, and having been extensively prescribed for the treatment of rheumatoid arthritis (Chevalier *et al.*, 2009). Such results emphasise the need for an improved understanding of OA pathophysiology in order to more reliably identify treatment targets and predict patient outcomes.

Inhibition of the OA-implicated ADAMTS isoforms is also an attractive therapeutic target. Inhibition of ADAMTS-4 and 5 would work to reduce cartilage degradation, limiting the development of more serious disease manifestations. However, non-specific inhibition of both enzymes is likely to have negative implications where such enzymes are required for normal physiological functions across different tissues within the body (Verma and Dalal, 2011). Alternatively, pharmacotherapy may target the endogenous inhibitor of ADAMTS-4 and 5, tissue inhibitor of metalloproteinases (TIMP)-3, in order to arrest enzymatic degradation of tissue within the joint and subsequent inflammatory signalling (Verma and Dalal, 2011).

A range of cell-based therapies are also being researched as potential OA treatments. This includes the use of mesenchymal stromal cell (MSC) based therapies whereby cells are injected directly within the OA joint. Cells are commonly sourced from adipose tissue or bone marrow concentrate and are applied to the defect area. A wide range of cell sources, screening and culture conditions, and implantation parameters have been assessed across a number of studies. Conflicting research outcomes and insufficient clinical trials data have failed to provide sufficient evidence to justify therapeutic use (Pas *et al.*, 2017; Hurley *et al.*, 2018; Xing *et al.*, 2018). As a result, there are no MSC injection therapies currently recommended for use within the UK.

Chondrosphere® is an aggregate based therapy representing a fourth-generation derivative of the ACI surgical procedure. During this surgery, a cartilage sample is collected from the patient for cell isolation and cultured *ex vivo* for 8-10 weeks. The cells are then seeded into hydrogel-coated 96-well plates to induce cell aggregation. The aggregates generated are

then coalesced into larger tissues prior to implantation at the defect site at a density of 10-70 aggregates per cm^2 (Foldager *et al.*, 2012). The National Institute for Health and Care Excellence currently recommend Chondrosphere® therapy as an option for the treatment of OA under same conditions as ACI surgical procedures, at an estimated cost effectiveness of £18,000 per quality-adjusted life year (National Institute for Health and Care Excellence, 2018; Armoiry *et al.*, 2019).

However, despite the recent advances in OA therapies, it is crucial to emphasise that next-generation treatments are currently hindered by our relatively limited understanding of the complex disease pathophysiology and multifactorial nature of OA (Berenbaum, 2013; Glyn-Jones *et al.*, 2015; Mobasheri and Batt, 2016). Therefore, further research is required to better understand the key signalling pathways involved in disease progression.

There also remains a significant gap between the range of early-stage and late-stage treatments currently available, as previously illustrated. This results in a significant proportion of patients falling short of thresholds justifying surgical intervention whilst being burdened with poorly managed symptoms from limited early-stage treatment options. Future treatments must be able to target the disease at an earlier stage to delay the onset of symptoms and reduce the proportion of patients requiring invasive surgical procedures. This requires the detection and validation of potential therapeutic compounds or cellular therapies at an earlier stage within the pharmaceutical research and development process.

2.1.5 Pharmaceutical Research and Development Process

The development of novel pharmacotherapies requires extensive screening, optimisation and validation in order to determine potential lead compounds for further study. Once selected, lead compounds or cell therapies are then tested extensively *in vitro* to determine their biological compatibility and effectiveness at reducing OA-like pathophysiology. Following preliminary testing, the pharmacotherapy then undergoes a series of pre-clinical testing steps, followed by clinical trials, before being approved for clinical use. A breakdown of this process is presented in Figure 2.6.

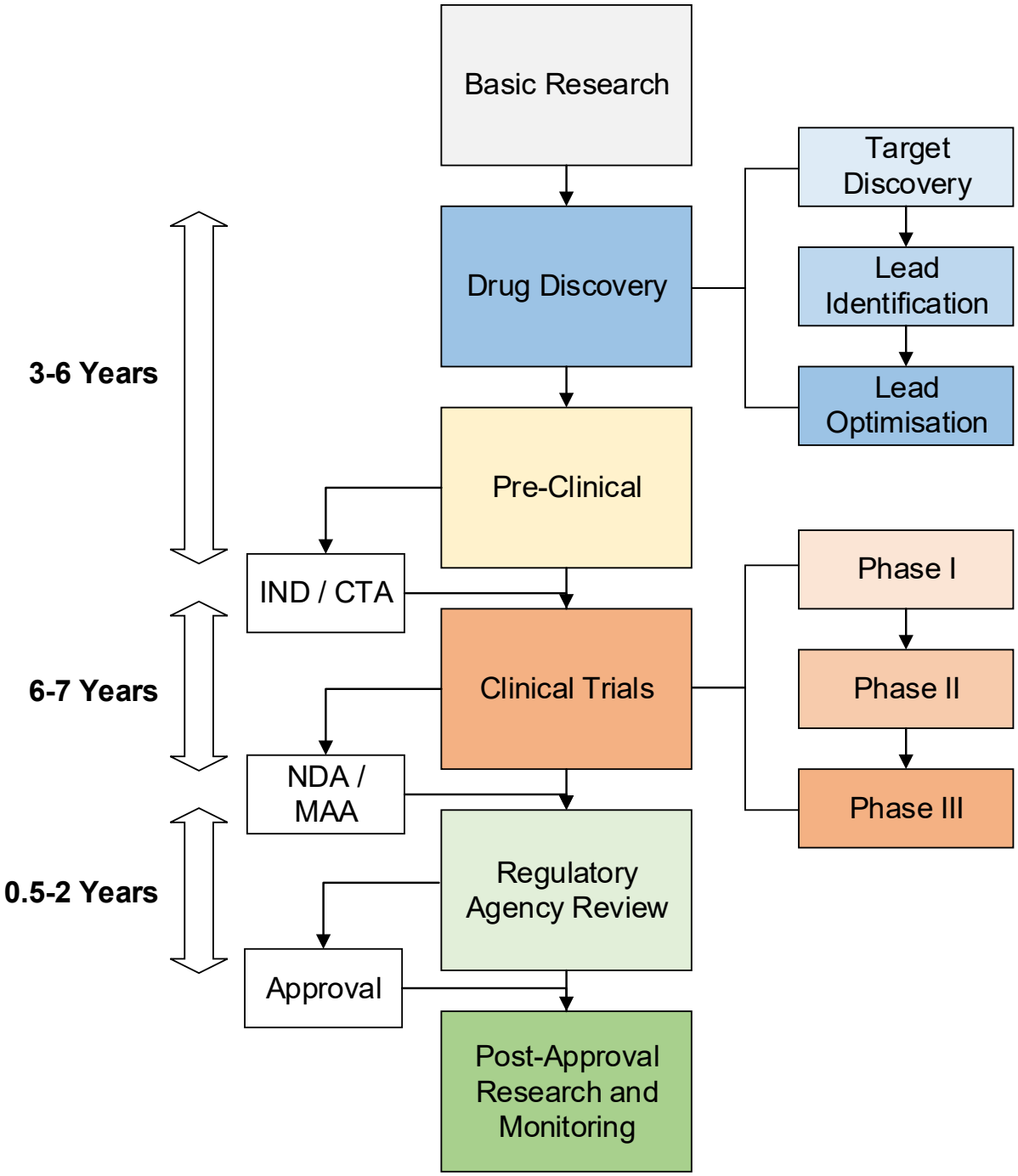

Figure 2.6 – Flow diagram depicting the pharmaceutical research and development process of bringing a drug to market. IND – Investigational new drug. CTA – Clinical trials authorisation. NDA – New drug application. MAA – Marketing authorisation application. Adapted from (Paul et al., 2010).

The cost of drug discovery has been previously estimated to have reached in excess of $2.8 billion dollars (DiMasi, Grabowski and Hansen, 2016). Increases in the cost of the development process, alongside a reduction in the number of lead compounds progressing to clinical trials, has led to a reduction in research and development productivity and

increased total costs (Paul *et al.*, 2010). Previous analysis of productivity across the sector has revealed the need to increase the productivity of early phase testing of potential lead compounds (Dimitri, 2011).

Increased productivity within this area requires further developments within the fields of automation and high-throughput screening to increase the speed of candidate screening and reduce the associated cost, alongside improvements to the quality of testing methodologies to decrease the probability of detecting and developing false positives (Shun *et al.*, 2011; Zhang *et al.*, 2012; Imaduwage *et al.*, 2017).

As a result, there is growing interest in the development of disease models to better recapitulate OA *in vitro* and provide a more comprehensive screening platform to bridge the gap between lead discovery and preclinical trials.

2.2 Models of Osteoarthritis

A variety of different types of model are currently employed to study the pathophysiology of osteoarthritis, as well as to assess the efficacy of potential new treatments. This includes both *in vitro* and *in vivo* systems, with each approach possessing specific advantages and disadvantages in comparison to the gold standard of human clinical trials. These are outlined in Figure 2.7.

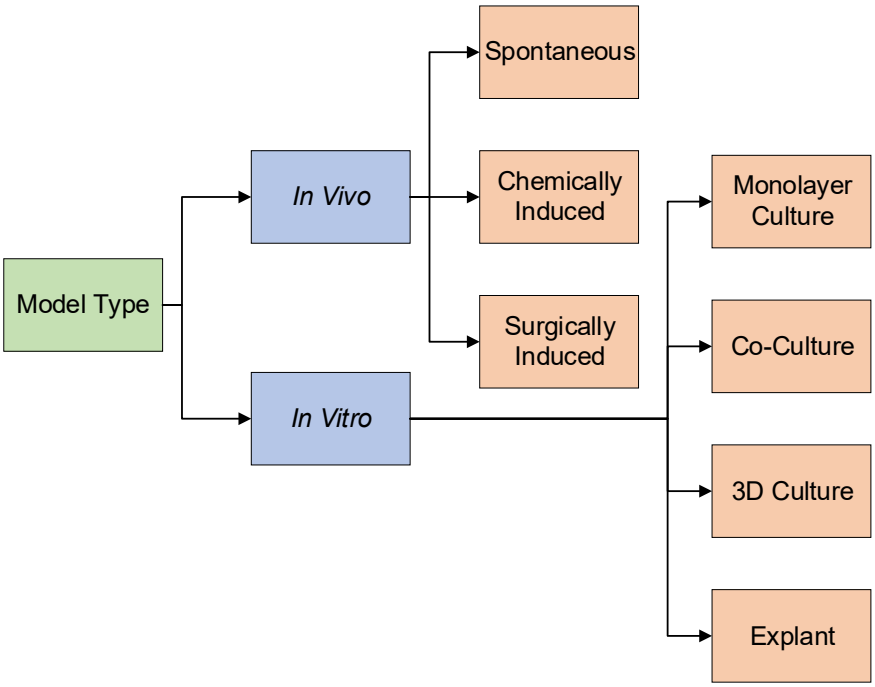

Figure 2.7 – Classification of in vivo and in vitro tissue models that have been used to study osteoarthritis.

In vivo mammalian models are typically used in the later stages of drug development or for larger research studies where the presence of full body physiological functions is required. Such models are able to more accurately replicate the pathophysiological changes caused by osteoarthritis within humans when compared to *in vitro* platforms. As a result, *in vivo* models generally provide a more replicative environment for research and pharmacological-screening applications, at the expense of the cost, throughput and the welfare implications of animal use within scientific research (Thysen, Luyten and Lories, 2015).

There are a number of different types of *in vivo* mammalian models. These can be defined by the mechanism through which osteoarthritis is induced. Spontaneous models rely on the development of osteoarthritis pathophysiology within the animal over a period of time (Kyostio-Moore *et al.*, 2011). This includes the use of genetic modifications to induce structural changes within cartilage collagen fibres that promote tissue dysfunction. Such modifications can increase cartilage catabolic activity or reduce functionality, thus prematurely inducing tissue degradation and OA like symptoms (Hu *et al.*, 2006; Kim and Cheon, 2012; McCoy, 2015). With chemical models, a local injection is given to induce joint degradation, resulting in the development of subsequent pathological processes that are characteristic of OA (Thakur *et al.*, 2012; Van Lent *et al.*, 2012; Kuyinu *et al.*, 2016). Surgical models rely on physical modifications to the joint anatomy to impair function and induce degradative changes (Moskowitz *et al.*, 1973; Pond and Nuki, 1973; Armstrong *et al.*, 1993).

Skeletally mature animals generally provide a more replicative model of OA to that of the human condition, with spontaneous models providing a better method for drugs testing applications (McCoy, 2015). In addition, the anatomy of the joint and body mass of larger species is also more similar to that of humans making histological, surgical, gait and wear analysis data more comparable to human studies. Pain-based research represents one of the areas of OA research that is most reliant on animal model use for early-stage research and therapy development. This is due to the difficulties in replicating pain signalling *in vitro* as a result of our poor understanding of pain mechanics and the associated markers of pain. Mammalian models remain critical for understanding and developing therapies for pain management, a key treatment target (Malfait, Little and McDougall, 2013; Teeple *et al.*, 2013).

Despite these features, there remains a number of significant factors that limit the use of *in vivo* animal models for OA research. This includes challenges surrounding inter-laboratory

variability, animal welfare concerns, high setup and running costs, and extensive assessment periods required for treatment screening (Vincent *et al.*, 2012).

As a consequence, there is an increasing demand within the field to minimise animal model use where possible, in accordance with the principles of the 3R's (Replacement, Reduction and Refinement) in research (Russell and Burch, 1959). This framework has pushed for the development of improved experimental design when utilising animal models for OA research to reduce the number of animals used and nociception experienced where possible (Madden *et al.*, 2012). In addition, increasing pressure is now placed on research where animal models are used to ensure that the experiment contributes significantly to the sector's body of knowledge.

A key outcome of such initiatives is the increased development and adoption of *in vitro* models for early-stage OA research applications. Such models provide an alternative mechanism to reduce animal model use and associated welfare concerns, whilst simultaneously reducing the costs and lead times associated with drug discovery (Astashkina, Mann and Grainger, 2012; Johnson, Argyle and Clements, 2016). Critical features of such models include the need to accurately replicate the pathophysiological nature of the disease, high-throughput and low cost of operation, as well as the ability to monitor biological response using real-time or near real-time cellular markers (Szymański, Markowicz and Mikiciuk-Olasik, 2012). Explant-based *in vitro* models have also been researched as a potential method to recapitulate conditions within the joint, but they are limited to low-throughput applications due to the limited supply of new tissue sources (Song *et al.*, 2007; Amin *et al.*, 2009; Geurts *et al.*, 2018).

A range of factors must be considered when developing an effective *in vitro* model of OA. This includes the cell types used, culture format, analysis techniques employed and the method of inducing an OA-like pathophysiology within the tissue.

2.2.1 Cell Types

Selection of appropriate cell types for use within disease models requires consideration of the availability of each cell type, growth rate in culture, degree of characterisation data available within the literature and phenotype stability over extended culture periods.

There are two different classifications of cultured cell types, including both primary and immortalised cells. Primary cells are cells that have been isolated from human or animal

tissue. This can be performed through enzymatic or mechanical methods in order to enable culture *in vitro*. Primary cell types have a limited life span and are heterogeneous in nature, reflecting conditions within the body. As a result, primary cell culture requires bespoke protocols and the total cell yield is finite. It is also important to consider the significant intra-donor variability between each source of primary cells, as well as potential availability issues when sourcing donated material for long term culture (Ketterl *et al.*, 2015; Trivedi *et al.*, 2019).

Immortalised cell lines are a homogenous population of cells that can be continually cultured over an extensive period of time. This cell type is generated through the immortalisation of a primary cell type via genetic or biochemical mechanisms. These cells are often commercially available and are usually associated with a range of established protocols and culture conditions. Due to the continuous rate of growth, such cell lines provide a limitless source of cells, making them highly suitable for high-throughput applications. Despite this, it is important to consider the potential for genetic drift that can occur through repeated cell divisions, as well as the limited replicability of a homogenous population of cells to the heterogeneous environment found within living tissue (Torsvik *et al.*, 2014; Gutbier *et al.*, 2018). Previous research has explored the use of both primary and immortalised cell types for the construction of *in vitro* osteochondral disease models, with cell type selection based upon the intended function of the model (Solorio *et al.*, 2010; Mohanraj *et al.*, 2014; Murphy *et al.*, 2016; Yeung *et al.*, 2018).

The pathogenesis of osteoarthritis involves a range of different cell types, including cells that would normally reside in the cartilage, bone and synovium of an articular joint. MSCs represent a multipotent heterogeneous population of cells that possess mesodermal differentiation capabilities into osteogenic, chondrogenic and adipogenic cell types, as indicated in Figure 2.8, and also have the ability to produce local immunomodulatory effects. Additional research has also explored the potential for MSCs to commit to ectodermal and endodermal lineages (Hermann *et al.*, 2006; Jeon *et al.*, 2007; Karnieli *et al.*, 2007; Mahay, Terenghi and Shawcross, 2008). Because of these properties, MSCs are considered to have a range of potential applications across the fields of tissue engineering, osteoarthritis treatment and *in vitro* disease model construction (Frith and Genever, 2008; Caplan, 2009; van Griensven *et al.*, 2019).

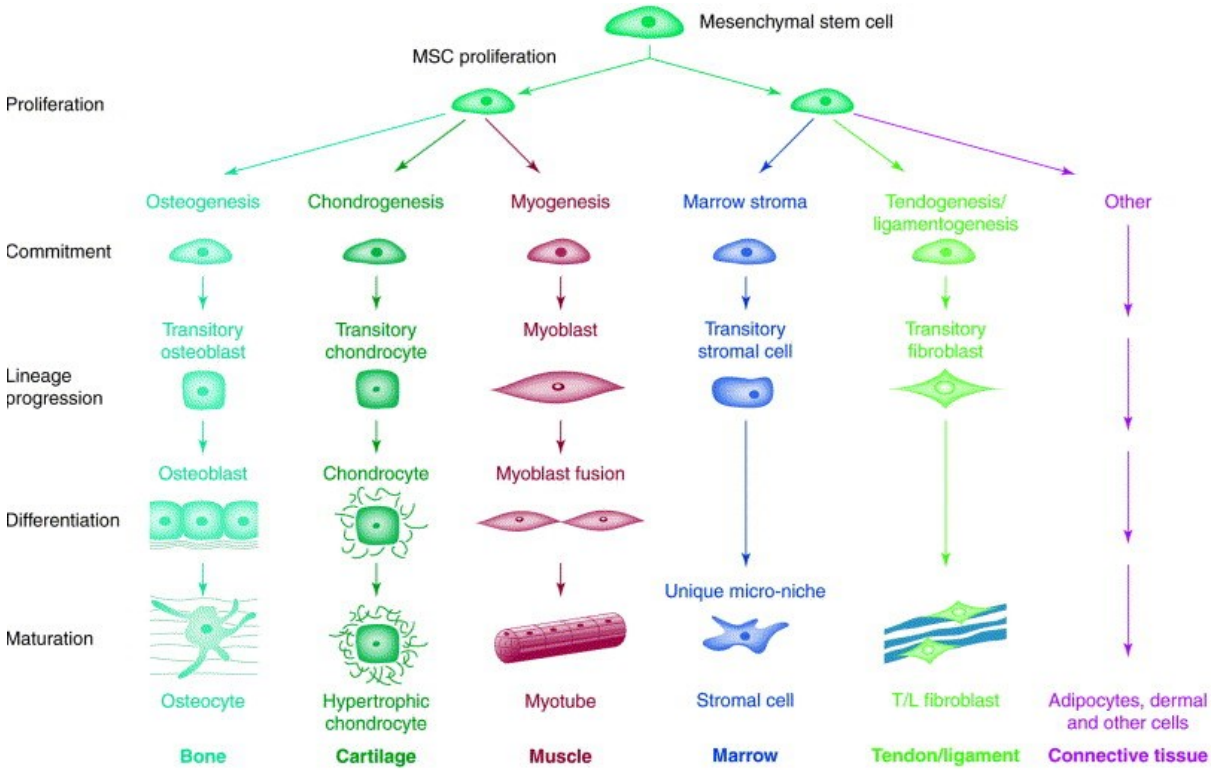

Figure 2.8 – Diagram depicting the mesenchymal stromal cell differentiation pathways that lead to the formation of articular joint tissue. Reproduced from (Caplan and Bruder, 2001).

MSCs were first isolated from the bone marrow by Friedenstein *et al.* in the 1970s and are defined as being colony-forming and fibroblastic in morphology, with plastic adherence and tri-lineage differentiation potential (Friedenstein, Chailakhjan and Lalykin, 1970; Friedenstein, Gorskaja and Kulagina, 1976). Other common sources of MSCs include adipose tissue, umbilical cord tissue and peripheral blood, with the source of MSCs having been shown to affect cellular functionality and surface marker expression (Hass *et al.*, 2011; C. Li *et al.*, 2015; Secunda *et al.*, 2015; Elahi *et al.*, 2016; Heo *et al.*, 2016).

Cell surface antigens commonly used to define MSC populations include expression of CD105, CD73 and CD90, and negative expression of CD45, CD34, CD14 or CD11b, CD79a or CD19 and HLA-DR (Dominici *et al.*, 2006). MSCs are typically sourced from the bone marrow and are grown in primary culture, however more recent research has explored the potential of developing immortalised MSC lines due to the challenges associated with large-scale primary cell culture (James *et al.*, 2015; Sawada *et al.*, 2016).

One example of such a cell line is the human bone marrow derived MSC generated and characterised by James et al. in 2015. This heterogeneous population of cells was isolated for a single donor and immortalised through the use of a lentiviral expression system to

overexpress telomerase reverse transcriptase, enabling continual culture *in vitro*. Four distinct single-cell-derived colonies were isolated and characterised from this subpopulation, with each colony displaying varying degrees of tri-lineage differentiation capacity. The resulting colonies were named Y101, Y102, Y201 and Y202. A high degree of cell characterisation has been performed on each line, including characterisation of the bone marrow derived MSC cell surface marker profiles, gene expression profiling, differentiation assays, lineage tracing and growth kinetics (James *et al.*, 2015). Previous research has demonstrated that the Y201 cell line responds similarly to changes in the mechanical properties of its microenvironment as primary MSCs, with a virally delivered fluorescent reporter construct successfully delivered to detect and report substrate stiffness (Dobre *et al.*, 2018). The Y201 cell line has also been shown to be capable of tri-lineage differentiation into osteoblasts, adipocytes and chondrocytes, representing key cell types involved in the pathogenesis of OA. These factors make Y201 cells highly suited for applications within osteochondral tissue models.

One of the challenges when developing an *in vitro* model of OA is that cell types such as chondrocytes are particularly prone to dedifferentiation into fibroblasts after short periods in culture and require a specific cellular environment (Caron *et al.*, 2012; Ma *et al.*, 2013; Minegishi, Hosokawa and Tsumaki, 2013). In normal joint tissue, chondrocytes are suspended within an extensive ECM. This matrix has an important effect on cellular behaviour and tissue function that is challenging to replicate accurately *in vitro* (Bhosale and Richardson, 2008; Atala *et al.*, 2012). Novel 3-dimensional (3D) culture formats provide a potential methodology to overcome such challenges through simulating the spatial organisation, ECM production and cell-cell contact that is present within living tissue.

A number of immortalised cell types are available that were originally sourced from differentiated tissue within the articular joint. This includes the human chondrocyte cell lines SW-1353 and TC28a2 that have been previously used for osteoarthritis research. The SW-1353 cell line was derived from the primary chondrosarcoma of a 72 year-old female. Previous research comparing the SW-1353 cell line to primary chondrocyte culture has demonstrated significant differences in gene expression in response to the IL-1β cell mediator, resulting in only a limited ability to replicate primary cells (Gebauer *et al.*, 2005).

The TC28a2 cell line was derived from costal cartilage of a 15 year-old female. Previous research has demonstrated that the TC28a2 cells display a similar response to IL-1β as

primary human chondrocyte cultures (Goldring *et al.*, 1994). Additional research into the molecular phenotype of the TC28a2 cell line observed that the cells display reduced expression of genes involved in matrix synthesis and turnover when compared with primary chondrocyte cells, as well as a more rapid rate of proliferation (Finger *et al.*, 2003). More recent research has demonstrated the potential for using the TC28a2 cell line to study sex hormone and insulin receptor interactions within the context of OA research (Claassen *et al.*, 2011).

Primary chondrocytes have also been used across a range of research applications, however are prone to the limitations of primary culture as previously discussed. This includes reported changes to chondrocyte gene expression in response to extended periods of culture, resulting in a loss of chondrogenic phenotype and subsequent ability to generate cartilage tissue (Schnabel *et al.*, 2002; Dehne *et al.*, 2010; Ma *et al.*, 2013). As a result, the selection of an optimal cell line to study osteoarthritis *in vitro* remains highly dependent upon the model culture format.

2.2.2 Culture Format

A range of different culture formats have been previously employed to recapitulate conditions within the joint. This includes primitive methods such as 2-dimensional (2D) monolayer culture of a single cell type to insert-based 3D culture systems incorporating a range of different cell types as depicted in Figure 2.9.

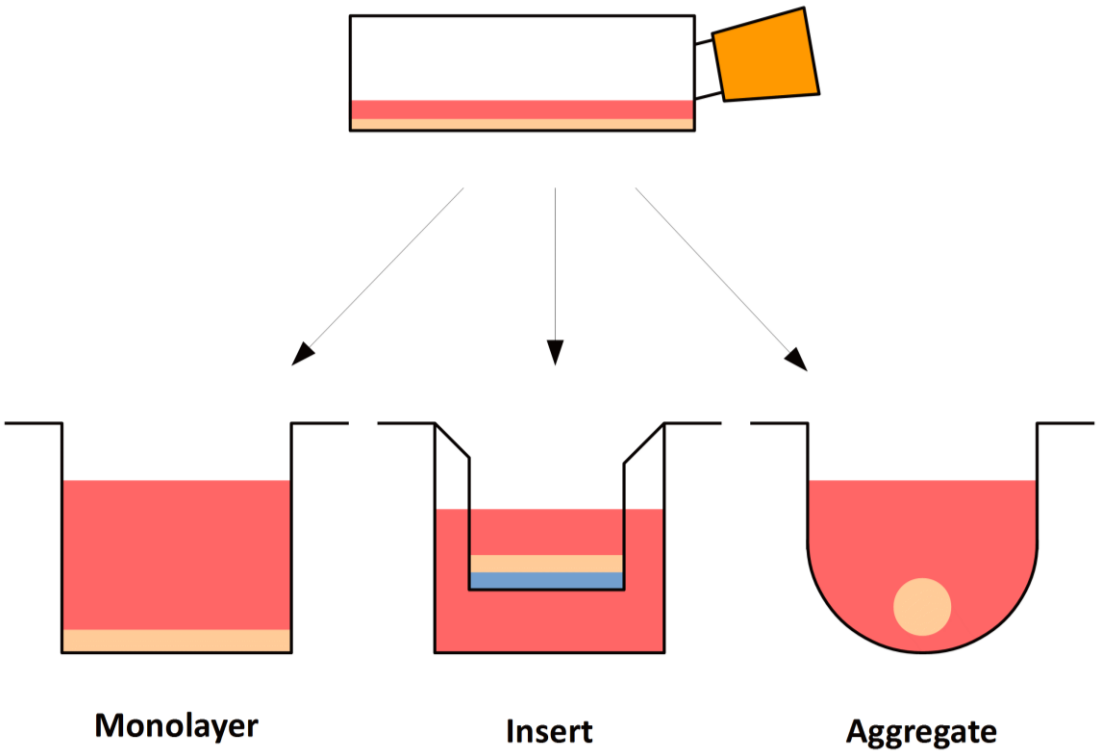

Figure 2.9 – Well-based cell culture techniques commonly used to generate in vitro disease models.

Monolayer culture is a 2D cell culture technique widely employed within OA research due to its low cost and complexity as well as high scalability for larger experiments. With this technique, a single cell type is cultured in a simple monolayer and responses to the application of various chemical factors or environmental modifications are studied. The major downside to this method is that without a 3D architecture, these cultures show a lack of complex cellular organisation and a corresponding lack of ECM. As previously described, ECM components form a crucial element of OA pathophysiology, and so its presence is of vital importance. Due to these factors, monolayer culture techniques are considered to provide a gross oversimplification of the complex and multicellular nature of the joint, whereby a variety of different cell types interact continuously through various mechanisms in order to maintain normal tissue functions (Birgersdotter, Sandberg and Ernberg, 2005; Miki *et al.*, 2012). This can lead to misleading research outcomes that provide a poor prediction of the *in vivo* response (Edmondson *et al.*, 2014). Replication of these factors *in vitro* is therefore critical in order to fully understand the dysfunction of specific pathways or factors that lead to the onset and progression of disease. Through the use of 3D culture techniques it is possible to recapitulate a level of spatial organisation that would normally be

found within OA *in vivo* in order to better replicate disease pathology (Bhadriraju and Chen, 2002).

Co-culture techniques, including those incorporating technologies such as multi-well inserts, allow for the culture of multiple different cell types within a single spatially arranged environment. This enables further recapitulation of the *in vivo* cellular environment to decrease the discrepancies between research and clinical outcomes (Hendriks, Riesle and van Blitterswijk, 2007). Co-culture models also enable the study of interactions between multiple cell types in response to different stimuli or environmental conditions (Meretoja *et al.*, 2012; Zhang *et al.*, 2017).

Aggregate culture techniques represent one of a number of 3D cell culture methods that enable the production of a large number of micro-tissues. Such culture techniques generally allow for an increase in cell-cell contact, a reduced dependence on adherence to plastic substrates, and more replicative nutrient and waste diffusion gradients within the aggregate (Malda *et al.*, 2004; McMurtrey, 2016; Nath and Devi, 2016; Melissaridou *et al.*, 2019). In addition, aggregate culture enables a greater level of cellular spatial organisation and ECM functionality than conventional monolayer culture methods (Fennema *et al.*, 2013). Aggregate culture methods are therefore being explored for both *in vitro* research applications and *in vivo* disease treatments (National Institute for Health and Care Excellence, 2017; Ong *et al.*, 2018; Yeung *et al.*, 2018).

A number of different methods exist for the production of aggregates. These most commonly include in-well, spinner flask and hanging droplet culture. However, alternative methods such as matrix, microencapsulation and microfluidic methods have also been reported (Tung *et al.*, 2011; Kojima, Takeuchi and Sakai, 2012; Aijian and Garrell, 2015; Leung *et al.*, 2015; Lee *et al.*, 2018). Gravimetric methods, such as hanging droplet, rely upon gravitational force to move dispersed cells in suspension into a dense aggregate. Cell to cell contacts induce cell signalling responses which then encourages the growth of spherical tissue. In addition to hanging droplet, examples of this culture format include hanging well and in-well culture, as depicted in Figure 2.10.

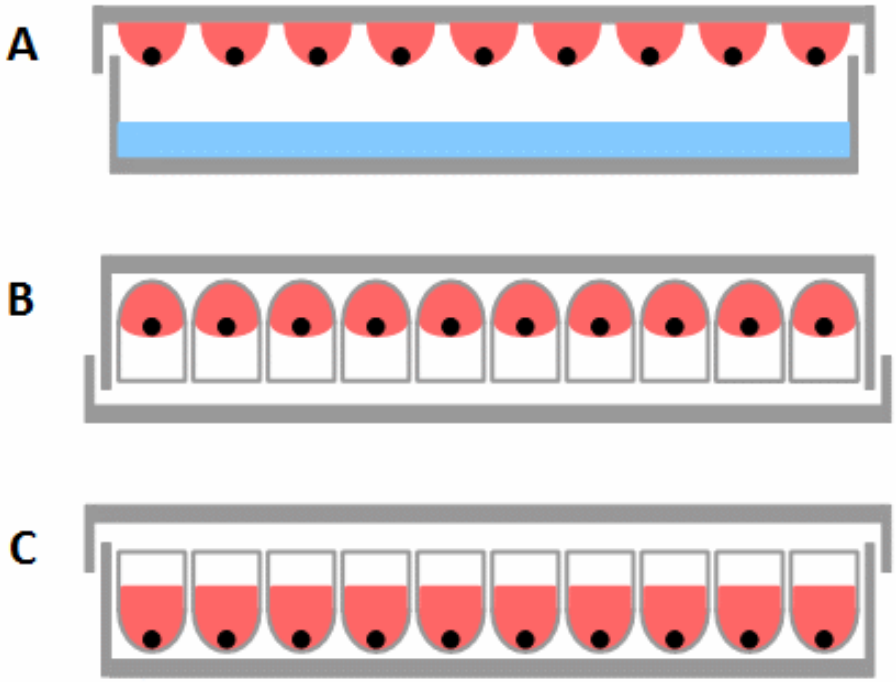

Figure 2.10 – Common cell culture techniques used for aggregate production. (A) Hanging droplet. (B) Hanging well. (C) In-well.

A number of studies have explored the application of different aggregate production techniques for the construction of micro-tissue models. In 2015, Pennock *et al*. researched the use of a well-based 3D aggregate culture technique to dedifferentiate aged human mesenchymal stromal cells into an early mesoderm-like state. The authors show that such methodologies are capable of reversing age-associated cell hypertrophy in order to restore the regeneration capacity of tissues (Pennock *et al.*, 2015).

Previous research by Marshall *et al.* has developed a 3D aggregate model that combines MSCs in undifferentiated, osteogenic and chondrogenic states with endothelial cell populations. Within these studies, cellular signalling was shown to induce tissue self-organisation within the aggregate culture format. This research demonstrates the versatility of the aggregate culture format when studying the interactions between multiple cell types (Marshall, Barnes and Genever, 2018).

Tung *et al.* demonstrates the potential use of liquid handling equipment for the production of 3D cellular aggregates, overcoming one of the more labour-intensive stages of aggregate production. Here, a liquid handling robot was used to deposit a cell-containing solution onto a custom 384-well plate insert designed to promote the formation of hanging droplets. Standard biological tests were then performed on each aggregate to demonstrate the

feasibility of using this platform for research applications. This paper provides a potential modification to existing plasticware designs in order to facilitate the use hanging droplet aggregate culture techniques within a high-throughput screening environment (Tung *et al.*, 2011).

Previous work by Choi *et al.* investigated the use of the in-well aggregate culture technique for the production of embryoid bodies from embryonic stem cells. Within this research a polymethylsiloxane (PDMS) microwell array was fabricated and cells seeded on top of the wells to promote aggregate formation. Following sedimentation, endothelial cell culture media containing neuronal differentiation additives was flowed over the cells to promote differentiation. This procedure was shown to generate homogenous sized cell aggregates for research into embryoid body differentiation. Modifying the width of the microwell inserts was found to impact aggregate size and the subsequent differentiation status of the embryoid bodies generated. This research highlights the potential of in-well aggregate culture to perform research into cellular differentiation that would not be possible using conventional monolayer culture methods (Choi *et al.*, 2010).

Research by Futrega *et al.* assessed the use of a custom nylon microwell-mesh for the high-throughput production of cartilage micro-tissues. Here, the authors develop a 6-well plate insert by casting PDMS sheets onto a polystyrene mould to generate square 2 x 2 mm, 0.8 mm deep 'V' well disks. A nylon mesh was bonded onto the surface of the disk and bone marrow derived MSCs seeded onto the mesh at a concentration of 10^6 cells per mL of cell culture media. The plate containing the insert was then centrifuged briefly in order to pass individual cells through the nylon mesh pores and into the wells to form individual pellets. Pellets formed were unable to pass back through the mesh due to the pore size, allowing for media exchange without the risk of cell loss. Cells were then harvested by removing the mesh inserts leaving individual cartilage micro-tissues loosely attached and evenly spaced across the mesh. Each micro-tissue removed yielded approximately 5 x 10^3 cells with 240 microwells per well of a 6-well plate. The chondrogenic differentiation of pellets generated via the microwell mesh culture technique was assessed and compared with pellets generated through a standardised pellet culture method. Cartilage-like micro-tissues were generated more rapidly in samples harvested from the microwell mesh when compared with control samples. This simple and scalable modification to standard cartilage pellet culture procedures was shown to increase the rate of chondrogenic differentiation whilst reducing

the challenges associated with cell handling and media exchanges due to the mechanism through which cells were entrapped within the mesh. These results provide a possible solution to some of the challenges associated with the use of liquid handling systems to automate the production and culture of 3D aggregate culture techniques (Futrega *et al.*, 2015).

An alternative method for aggregate construction was presented by Park *et al.* from research evaluating the potential of using centrifugal forces within a microfluidic chip to generate cell aggregates. A PDMS-based aggregate culture microwell disk was developed and mounted onto a rotating platform to facilitate aggregate formation. Within this work a combination of multiple different cell types were applied to the microwells sequentially in order to generate a layered effect within the resulting aggregate. Preliminary assessment of aggregate formation was assessed microscopically. This work provides a novel adaptation of conventional centrifuge-based aggregate formation protocols through the use of a potentially scalable centrifugal microfluidic system. Further research is required to assess the scalability of the microfluidic system as well as its compatibility with extended aggregate culture periods and more complex cellular analysis techniques (J. Park *et al.*, 2017).

Lee *et al.* investigated the use of in-well aggregate culture techniques to generate *in vitro* hepatic disease models. Here, a custom PDMS microwell plate was developed and assessed with interlinking concave wells to promote aggregate formation and enable inter-well diffusion. This modification allowed the flow of nutrients, waste, cytokines and cell-cell interactions alongside the diffusion of oxygen across the entire plate. Hepatic cell aggregates were found to display increased albumin secretion when compared to identical aggregates generated within standard well plates and the diffusion of material between wells was demonstrated via both a labelled albumin assay and computer simulation. This work outlines a potential method to significantly enhance conventional aggregate culture techniques through further emulating elements of the *in vivo* environment, whilst retaining a standardised culture format compatible with traditional analysis techniques and high-throughput processing systems (Lee *et al.*, 2018).

A number of limitations exist for different aggregate culture techniques. Preparation and seeding of cells for aggregate culture techniques requires both a significant amount of time and cells depending upon the particular technique employed. In addition, certain techniques such as hanging droplet culture are particularly sensitive to vibrations or surface tension

effects, limiting aggregate formation. There are also practical considerations such as the time period required for cell aggregation prior to performing experiments (Bartosh *et al.*, 2010). Aggregates also demonstrate poor compatibility with a variety of non-destructive assays that are commonly used to characterise 2D culture platforms due to the reduced rate of diffusion through the tissue (McKee and Chaudhry, 2017). Finally, media exchange and aggregate imaging during culture are often more complex to perform when compared to samples generated using monolayer culture techniques (Joshi and Lee, 2015).

Insert-based culture techniques have been developed as an alternative method to provide a 3D culture environment, whilst circumventing some of the limitations associated with aggregate culture. Such systems generally employ a standard well-plate design coupled with an intermediary porous membrane suspended within each well. Polycarbonate and polyethylene terephthalate materials are commonly used to generate the membrane, with a range of pore sizes available to selectively allow for molecular transport studies, or cell growth, migration and interactions across the substrate.

More recent designs have incorporated mechanisms to alter the membrane position within each well. This enables the gradual transfer of cells seeded onto the membrane towards the air liquid interface, a common procedure required for the production of *in vitro* skin models (Marx *et al.*, 2018; Roger *et al.*, 2019). Modifications have also been made to incorporate optional interlinked well designs to allow for media perfusion between multiple wells, as well as increase the compatibility of the insert culture format with current liquid handling systems and analysis equipment. As a result, insert-based culture techniques have been successfully incorporated in the construction of unique experimental models to assess cell migration and drug absorption (Restouin *et al.*, 2009; Larson *et al.*, 2012). These modifications also enable the use of insert-based culture systems within current high-throughput screening (HTS) workflows.

Due to the nature of the insert design it is possible to grow multiple cell types in a single well to assess cell interactions either with or without direct cell contact. Previous studies examining a combination of different cell types have demonstrated the versatility of such techniques for the construction of a wide range of different tissue models, as indicated in Table 2.1.

Tissue Model	Plate Scale (cm^2)	Insert Technology	Reference
Cartilage	1.9	Corning Transwell®	(Kubosch *et al.*, 2016)
Articular Joint	3.8	Reprocell Alvetex®	(S. Li *et al.*, 2015)
Nasal Epithelium	1.9	Corning Transwell®	(Luukkainen *et al.*, 2018)
Airway Mucosa	1.9	Corning Transwell®	(Yonker *et al.*, 2017)
Respiratory Tract	3.8	Grenier ThinCert®	(Cozens *et al.*, 2018)
Trachea	3.8	Corning Transwell®	(Kaartinen *et al.*, 1993)
Lung Cancer	1.9	Corning Transwell®	(Hassell *et al.*, 2017)
Prostate Cancer	1.9	Corning Transwell®	(Mosaad *et al.*, 2018)
Intestine	3.8	Corning Transwell®	(Kämpfer *et al.*, 2017)
Cornea	1.9	Merck Millicell®	(Mikhailova *et al.*, 2014)
Liver	9.5	Corning Transwell®	(Kang *et al.*, 2013)
Kidney	3.8	Corning Transwell®	(Vinaiphat, Charngkaew and Thongboonkerd, 2018)
Kidney	1.9	Corning Transwell®	(King *et al.*, 2017)
Skin	3.8	Reprocell Alvetex®	(Roger *et al.*, 2019)
Hippocampus	1.9	Merck Millicell®	(Ehret, Vogler and Kempermann, 2015)
Blood Brain Barrier	3.8	Corning Transwell®	(Stone, England and O'Sullivan, 2019)

Table 2.1 – Range of co-culture tissue models generated using insert-based culture techniques.

Limitations of well-insert culture formats include the higher costs of insert-based plasticware products, limited compatibility with certain cell assays and increased complexity when sectioning or imaging models (Knight, 2013; Marx *et al.*, 2018). However, despite these drawbacks, a range of previous research have demonstrated the potential for using insert-based culture models to study osteoarthritis. This includes work by Greenberg *et al.* to generate a co-culture model within a 24-well plate insert system, where within each well base a canine synovium explant was suspended within media, alongside a cartilage explant mounted onto the insert surface. The explants were cultured in medium with and without

interleukin-1β, and also contained different concentrations of hyaluronic acid. The concentrations of various biomarkers were then assessed within the culture media over time, alongside histological sectioning and analysis of the explant pairs. Two potential mechanisms of action for viscosupplementation were hypothesised as a result of the experimental outcomes. This work provides an early example of the use of a 'well-in-well' co-culture system for the evaluation of the effect of specific additives on the biochemical and histological markers of cultured tissue (Greenberg *et al.*, 2006).

A similar insert-based co-culture system was used by Osterman *et al.* to observe the effects of platelet rich plasma concentration on inflammation-related cartilage gene expression. The addition of platelet rich fibrin to the osteoarthritic cartilage and synovium co-culture was found to produce a range of anti-inflammatory effects on gene expression, however this was not found to be affected by platelet or leukocyte concentration. This paper provides further evidence of the potential of low-cost, scalable, well-based co-culture systems that utilise tissue explants and media additives to provide an early insight into the functionality of novel treatments for OA (Osterman *et al.*, 2015).

2.2.3 Analysis Techniques

The experimental value of a disease model is critically influenced by the analysis techniques employed within experimental designs. A range of possible biomarkers have been previously reported within the literature for the evaluation of OA progression *in vivo*. Research by Bay-Jensen *et al.* provides a comprehensive review of current biomarker research, as well as classifying each biomarker in accordance with the BIPED classification scheme, which incorporates the burden of disease, investigative, prognostic, efficacy of intervention and diagnostic classification elements. This research highlights a number of key biomarkers that have previously been identified within the literature as potential future targets for disease monitoring applications. In addition, it outlines the need for significant further work within the field of biomarker research to further classify and validate independent biomarker targets (Bay-Jensen *et al.*, 2016). These challenges have important ramifications when designing *in vitro* OA disease models due to the limited predictive value of current biomarkers for tracking disease progression.

Typical biomarkers used in the evaluation of OA tissue models include collagen I, II and X, aggrecan and SOX9. Expression is usually assessed by indirect immunofluorescence, enzyme-linked immunosorbent assays or mRNA expression (Wu *et al.*, 2011; Yang, Lee and Barabino,

2012; Mohanraj *et al.*, 2014; Kubosch *et al.*, 2016). This is due to changes in expression of these markers that occur during chondrogenesis (Diaz-Romero *et al.*, 2005; Graceffa *et al.*, 2019). Additional characterisation using histological staining techniques to qualitatively assess sulphated glycosaminoglycan content and tissue architecture are also commonly performed. Finally, the use of non-destructive techniques such as proteomics to analyse the secretome of disease models has also been explored to increase analysis throughput (Clutterbuck *et al.*, 2011). Careful consideration must be made to the sensitivity and specificity of each marker, as well as the compatibility of selected analysis techniques with HTS methodologies.

2.2.4 Disease Modelling

The functionality and replicative accuracy of *in vitro* models is also heavily influenced by the mechanism through which osteoarthritic processes are artificially induced. This is normally performed by either biochemical or mechanical methods.

Cytokines are commonly used within biochemical models due to the key role that they play in the degradation of joint tissue and subsequent onset of osteoarthritis. These models are relatively well understood, are lower cost and can be readily configured to suit specific research requirements. However, it is also important to understand the tissue-wide effects of such factors across each of the cell types contained within the model, as well as any effects that the spatial arrangement of cells or culture conditions will have on signalling pathway activation (Johnson, Argyle and Clements, 2016).

A wide range of different cytokines have trialled for use with OA models, yet only a small number of these have gained popularity. This is due to the fact that many cytokines are chondrocyte-derived. Successful candidates include pro-inflammatory cytokines IL-1β and TNF-α, as they are commonly used to induce further cytokine release due to their well-recognise role in OA pathogenesis (Lin *et al.*, 2009; Rahmati, Mobasheri and Mozafari, 2016). However, it is important to note that the cytokines are supplemented at a considerably higher concentration to what would normally be observed *in vivo* (Macrory *et al.*, 2009; Gabriel *et al.*, 2010; Murab *et al.*, 2013). They also require significant incubation periods under controlled conditions in order to have their target effect. Yet despite these limitations, studies have indeed been performed in order to assess the effect of cytokine concentration and exposure period on cellular responses *in vitro*.

An example of such work is by Murab *et al.*, wherein the authors use a matrix composed of silk protein with sulfonated moieties, combined with non-covalently immobilised IL-1β and TNF-α cytokines to induce an OA-like cartilage microenvironment. MMP, TIMP and ADAMTS activity were shown to be upregulated 35-fold when compared with untreated controls, with gene expression profiles of treated cells displaying similarities to profiles observed *in vivo* from patients undergoing surgical intervention. This research therefore illustrates the potent effects of exogenous cytokine supplementation in order to deliver a local and continuous OA-like microenvironment on cultured tissue (Murab *et al.*, 2013).

An alternative method of biochemically replicating OA pathophysiological processes *in vitro* is through the incubation of the model with synovial fluid taken from a human donor in substitution for specific cytokine stimulation. Research by Hoff *et al.* evaluates the influence of OA-donor synovial fluid on the cytokine stimulation of primary human chondrocytes *in vitro.* In response to synovial fluid incubation, chondrocytes actively secrete cytokines such as VEGF. The conclusions of this work, which demonstrates the activation of pro-inflammatory cytokines as a result of OA synovial fluid incubation, further complements wider research which hypothesises the presence and effects of a pro-inflammatory microenvironment on OA disease pathogenesis (Gaber *et al.*, 2012).

As an alternative to biochemically induced models, mechanically induced models utilise the application of a defined loading mechanism to directly induce cellular damage and activate signalling cascades that lead to the onset of degradative OA-like pathological processes. Such models are able to recapitulate the *in vivo* loading patterns that occur within a healthy joint, as well as the damage caused by non-physiological loading.

Mechanically induced OA model examples include work by Ikenoue *et al.* whereby an *in vitro* human articular chondrocyte monolayer was subjected to intermittent hydrostatic load bearing forces. This work demonstrated that through intermittent hydrostatic loading of 1, 5 and 10 MPa for 4 hours 4 times a day, aggrecan mRNA signal levels increased 1.4, 1.8 and 1.9-fold respectively. In addition, at 5 and 10 MPa using the same loading regime, type II collagen expression was reported to increase. This experiment highlighted the significant effects of hydrostatic loading pressure and duration of application on cellular matrix protein expression, and by implication, cartilage matrix anabolism. It also further highlighted the need to develop more advanced disease models that incorporate intermittent hydrostatic

pressure components to more accurately replicate the biological processes of OA (Ikenoue *et al.*, 2003).

The effect of mechanical stimulation on chondrocytes seeded within an agarose structure was researched by Pingguan-Murphy *et al.* Glycosaminoglycan synthesis in bi-axial-loaded chondrocytes was shown to increase when compared with unloaded and uni-axial loaded samples over the same period. The introduction of a free swelling recovery period between loading patterns further increased glycosaminoglycan production and total DNA content retrieved from samples, demonstrating an increase in cell proliferation. This paper therefore serves to further demonstrate the capabilities of a simple 3D cell seeded agarose system to determine the most fundamental effects of mechanical loading patterns on cell viability and ECM production (Pingguan-Murphy and Nawi, 2012).

Load-based models require a higher cell count than their biochemically induced counterparts and are less flexible to changes in experimental methods. Generally, such models are also more complex to set up and maintain during experimentation than biochemically induced alternatives. Research has shown that both biochemical and mechanical induction methods initiate cytokine effects, leading to similar pathophysiological changes in the treated tissue (Johnson, Argyle and Clements, 2016). It is also important to consider the impact of the mechanism for inducing OA on the reproducibility and throughput requirements of the model, with biochemically induced methods considered to be more scalable to high-throughput culture formats.

2.2.5 High-Throughput Screening

Current model platforms are labour intensive to setup, limiting the total screening throughput and experimental replication that be performed. The value of *in vitro* disease models for commercial research applications is therefore heavily influenced by their compatibility with HTS platforms. High-throughput screening represents a core technique for the analysis of potential therapeutics within the pharmaceutical sector, allowing for the analysis of more than 100,000 compounds per day (Michael *et al.*, 2008). Such systems rely upon high levels of automation and miniaturisation to rapidly screen large libraries of new chemical and biological entities, and systems are commonly standardised to allow for comparisons to be made between experiments from extensive datasets. This methodology is currently used across a range of applications including drug discovery, pharmacological profiling, drug-drug interaction studies and toxicology testing (Szymański, Markowicz and

Mikiciuk-Olasik, 2012). The widespread adoption of HTS for a range of different research applications has resulted in new challenges such as the need to develop imaging systems, automated data analysis workflows, and liquid handling systems that can be operated at a continually increasing throughput (Taylor *et al.*, 2002; Starkuviene and Pepperkok, 2007; Boutros, Heigwer and Laufer, 2015).

Research by Astashkina *et al.* highlights the growing need for HTS devices in order to accommodate the increased number of potential drug candidates in development. Primary enablers of this technology include advances in protein characterisation and combinatorial small molecule chemical synthesis capabilities within the pharmaceutical sector. High-throughput systems are able to challenge the increased economical and ethical constraints that are associated with the drug development process.

The themes highlighted in this research provide key requisites for the design and development of a truly impactful OA model for drug screening and research applications. It also highlights the need for identifying accessible biomarkers that are compatible with high-throughput system designs for the analysis of *in vitro* model functions *in situ*. Such markers must also perform predictably *in vivo* in order to evaluate the replicative accuracy of the model to that of the human disease, whilst also allowing for cross-model comparisons (Astashkina, Mann and Grainger, 2012).

In order to generate HTS-compatible models, it is necessary to scale up manufacture through automating routine laboratory tasks. Commercially available liquid handling systems provide a method to automate dispensing functions within conventional HTS well-plate formats. A variety of actuation methods are employed within such systems and can be categorised into contact and non-contact dispensing.

Contact dispensing, a dispensing system most commonly consisting of a series of solid pins or pipette tips, functions by submersing the dispensing system within a liquid. The dispensing system is then removed from the liquid and transferred to the substrate where direct contact is made, transferring retained liquid onto the substrate through surface tension or pneumatic effects.

Non-contact dispensing avoids physical contact with the substrate by directly ejecting dispensed material from an orifice placed above the substrate. Through this method the

practical limitations of surface tension on minimum droplet volume can be overcome, enabling the deposition of material down to the picolitre-scale.

Recent developments within the field of bioprinting have exploited a combination of non-contact liquid handling methods, alongside additive manufacturing principles, in order to facilitate the deposition of cellular material.

2.3 Bioprinting Technologies

Bioprinting is a methodology used to co-process cells and biomaterials to generate 3D structures. Bioprinting techniques are commonly applied within the evolving field of biofabrication in order to generate a range of tissue models and cell-based therapies. A considerable overlap exists between the fields of biofabrication, tissue engineering and regenerative medicine as depicted in Figure 2.11.

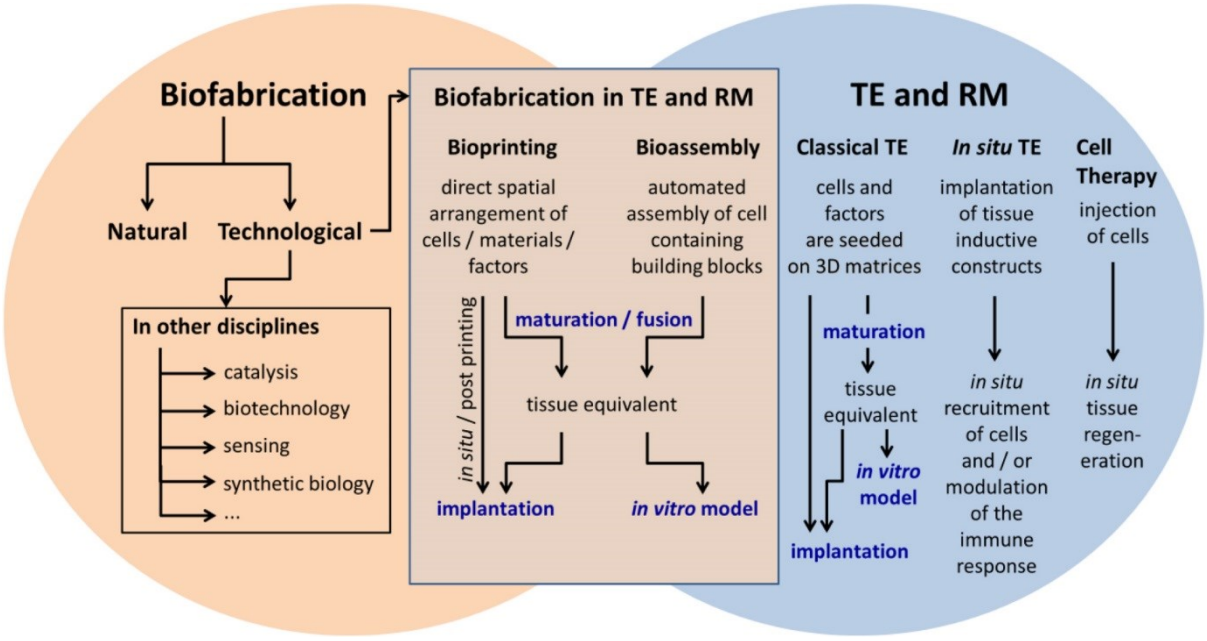

Figure 2.11 – Overlap between the fields of biofabrication and tissue engineering (TE) and regenerative medicine (RM). Reproduced from (Groll et al., 2016).

2.3.1 Overview of Common Bioprinting Processes

Bioprinting systems encompass a wide range of additive manufacturing technologies for tissue engineering applications. This includes material extrusion, material jetting and laser-based techniques as shown in Figure 2.12.

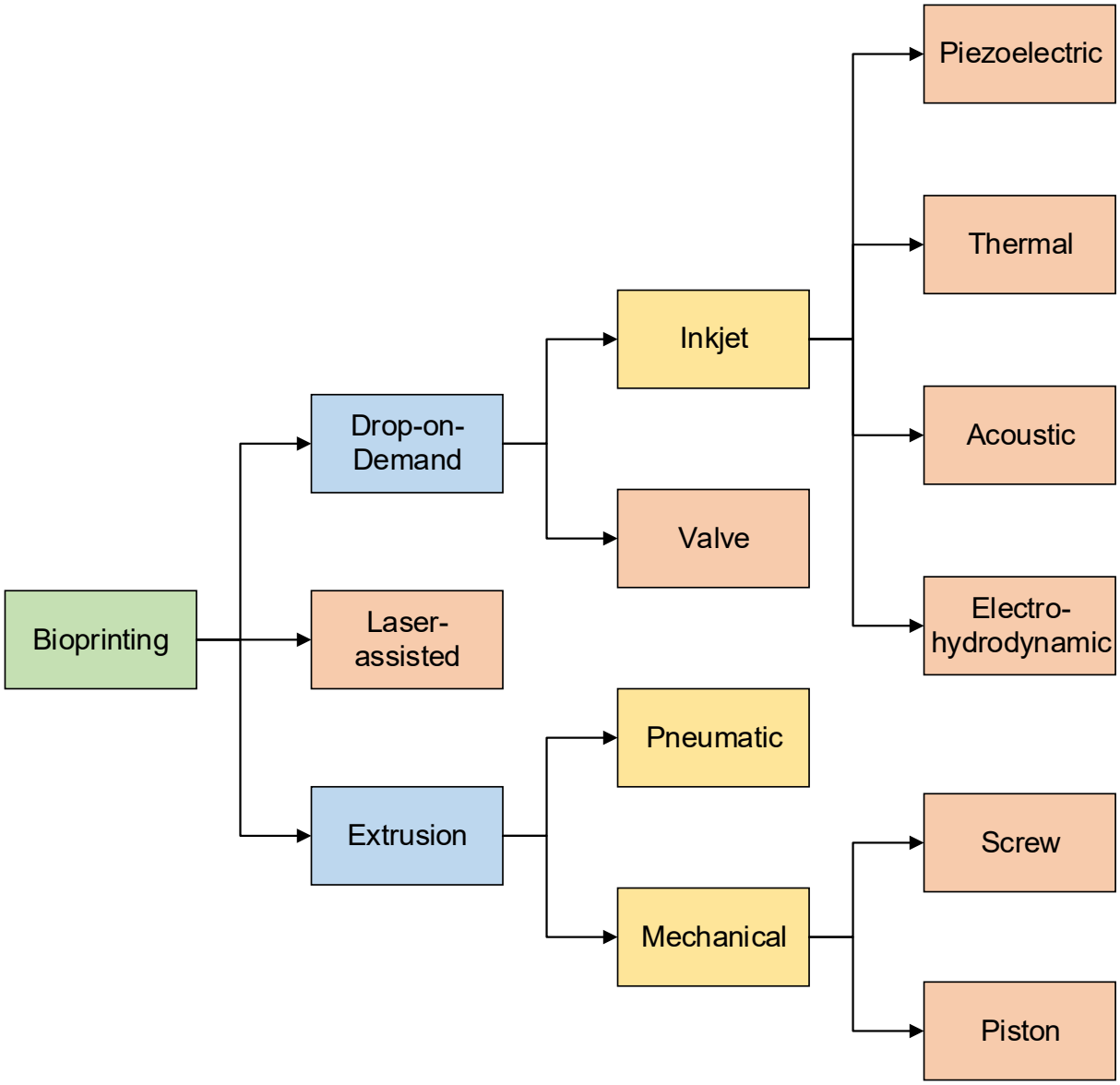

Figure 2.12 – Flow diagram showing the range of printing processes that have been explored for bioprinting applications. Adapted from (Gudapati, Dey and Ozbolat, 2016).

In order to generate a tissue structure using bioprinting, a range of design, optimisation and manufacturing tasks must be completed. These are summarised in the pathway displayed in Figure 2.13.

1. Product Design

- Collection of scan data - computed tomography, magnetic resonance imaging, X-ray
- Image segmentation, compression and stacking into 3D
- Conversion of data and optimisation within computer aided design package
- Generation of printer compatible stereolithography file format with suitable print-specific metadata

2. Material Selection

- Cells - autologous, primary, cell line
- Biomaterials - natural polymers, synthetic polymers, extracellular matrix
- External liquid nutrient supplies, oxygen permeability barriers, suspension and carrier liquids

3. Fabrication of Construct

- Extrusion bioprinting
- Material jetting
- Laser-assisted bioprinting

4. Post-Processing

- Cell culture media supplementation or nutrient and waste transfer
- Cytokine or mechanical stimulation
- Monitoring and assessment of biological and mechanical functionality

5. Functionalisation or Implantation

- Activation of target cellular behaviour and device functionality
- Implantation into patient or activation in laboratory environment
- Monitoring of functionality *in vivo* or *in vitro*

Figure 2.13 – Step-by-step process from conceptualisation to functionalisation of a bioprinted product for tissue engineering applications. Adapted from (Murphy and Atala, 2014).

The first stage of production involves the development of a computer aided design file using medical scan data or digital design software to represent the product requiring manufacture. The file is then converted into a printer-readable stereolithography file format and loaded onto the machine, alongside configuration settings in order to initiate the build. Post-processing is sometimes required following construction in order to achieve specific manufacturing properties or remove supporting structures. A nutrient and gaseous support system is also required to maintain cellular viability and functionality.

It is crucial to select an appropriate bioprinting technology for the intended tissue engineering application in order to maximise the efficiency, reliability and accuracy of the

bioprinting process. Each bioprinting technology possesses specific advantages and disadvantages and is capable of generating an end product with unique properties. It is therefore necessary to match the desired product properties to a specific manufacturing technique in order to most accurately replicate the intended design attributes within the printed product. Due to current process limitations, a design is often modified in accordance with the selected manufacturing technique to enhance compatibility and improve manufacturing outcomes. A breakdown of the most commonly researched bioprinting technologies for tissue engineering applications are outlined in Table 2.2.

	Printing Technique			
	Material Jetting	**Microextrusion**	**Laser-assisted**	**References**
Cell Viability	> 85 %	40 - 80 %	> 95 %	(Hopp *et al.*, 2005; Xu *et al.*, 2005, 2006; Chang, Nam and Sun, 2008; Koch *et al.*, 2018)
Cell Density	Low (10^6 - 10^7 cells per ml)	High	Medium (10^8 cells per ml)	(Xu *et al.*, 2005; Guillotin *et al.*, 2010; Mironov, Kasyanov and Markwald, 2011; Marga *et al.*, 2012; Da Conceicao Ribeiro *et al.*, 2019)
Material Viscosity	3.5-12 mPa/s	30mPa/s to > 6 x 10^7 mPa/s	1- 300 mPa/s	(Guillemot *et al.*, 2010; Kim *et al.*, 2010; Chang *et al.*, 2011; Guillotin and Guillemot, 2011)
Scalability	High	Medium	Low	(Roshanghias, Krivec and Baumgart, 2017; Kačarević *et al.*, 2018; Da Conceicao Ribeiro *et al.*, 2019)
Resolution	Picolitre to nanolitre range	5 µm to millimetre track width	Microscale	(Smith *et al.*, 2004; Campbell *et al.*, 2005; Phillippi *et al.*, 2008; Guillotin *et al.*, 2010; Faulkner-Jones *et al.*, 2013)
Cost	Low	Medium	High	(Kartmann *et al.*, 2015; Kačarević *et al.*, 2018; Kahl *et al.*, 2019)
Gelation Methods	Chemical, Photo-crosslinking	Chemical, Photo-crosslinking, sheer thinning, temperature	Chemical, Photo-crosslinking	(Smith *et al.*, 2007; Koch *et al.*, 2010; Michael *et al.*, 2013; Murphy, Skardal and Atala, 2013; Da Conceicao Ribeiro *et al.*, 2019)

Table 2.2 – Comparison between the key bioprinting processes that are commonly used within the field of biofabrication. Adapted from (Murphy and Atala, 2014).

Material jetting technology is ideal for the construction of tissue models due the high accuracy and deposition speed associated with this process. In addition, a wide range of previous literature is available reporting its use within cell deposition applications. Systems based upon material jetting technology are also comparatively low cost in both construction and operation. A diagram representing a typical material jetting system layout is presented in Figure 2.14.

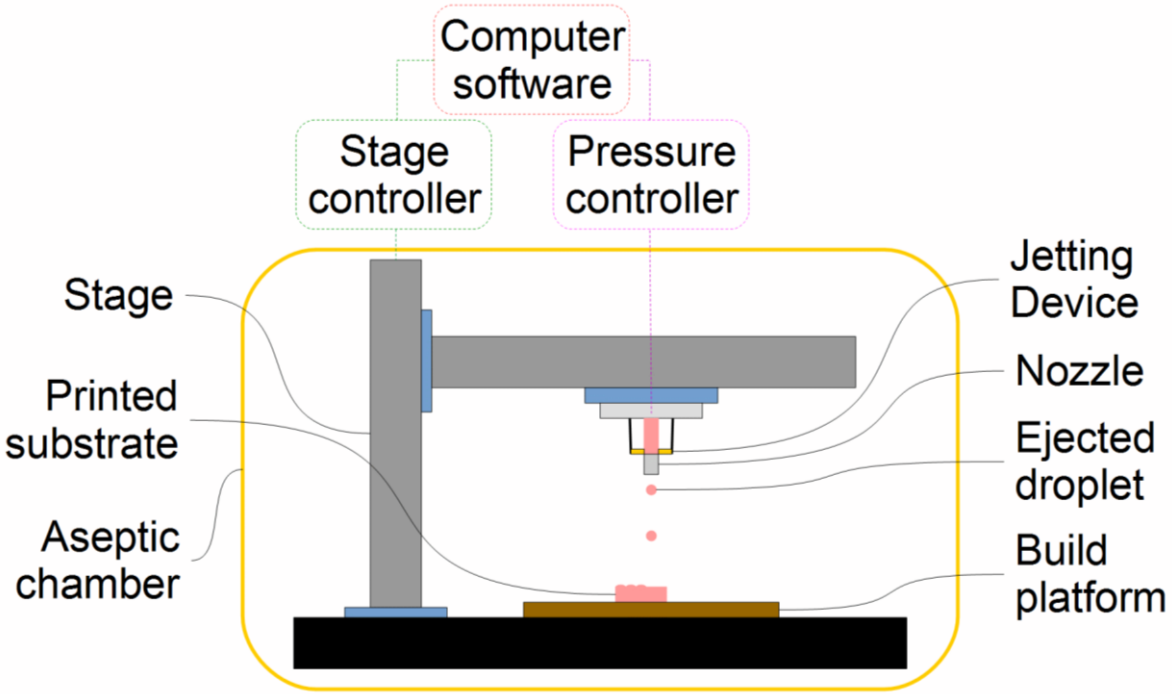

Figure 2.14 – Diagram depicting the various components of a typical material jetting printing platform.

The inherent similarities between material jetting technologies, commercial graphics printing and surface lamination treatment processes is also advantageous in terms of prior research. A significant volume of process and ink optimisation research exists detailing methods to maximise jetting performance, thus providing potentially transferrable solutions to current bioprinting challenges (Wijshoff, 2018).

Material jetting processes include both inkjet and valve-based printing equipment. Each actuation system can be operated in a continuous jetting (CJ) or drop-on-demand (DoD) configuration in order to deposit material onto a substrate.

2.3.2 Inkjet Printing

Inkjet printing systems encompass a range of different actuation techniques to generate pressure waves that propagate through ink contained within the printer nozzle. This includes acoustic, electrostatic, thermal and piezoelectric actuation methods (Xu *et al.*, 2005; Kim *et al.*, 2008; Khalate *et al.*, 2012; Hadimioglu, Stearns and Ellson, 2016).

Inkjet printing systems have been used across a wide variety of applications including graphics production, printed electronics, solder dispensing, additive manufacturing, display and solar panel production, pharmaceuticals, microarray and ELISA construction (Pierik *et al.*, 2008; Khan *et al.*, 2012; Joh *et al.*, 2017; Sturgess *et al.*, 2017; Xiong *et al.*, 2017;

Wijshoff, 2018; C *et al.*, 2019; Cader *et al.*, 2019; Ganesan *et al.*, 2019; Yus *et al.*, 2019). Research into the use of inkjet printing techniques for cell printing applications most commonly uses thermal or piezoelectric methods.

Continuous jetting approaches pump ink from the printer reservoir through an open-ended capillary tube to produce a stream of liquid. The liquid then separates into droplets as a result of Rayleigh instability, a process describing the break-up of a falling stream of fluid into droplets, thus minimising liquid surface area. A piezoelectric actuation device is used to vibrate the capillary, enabling modulation of the break-up of the fluid stream. An electrostatic field is then applied between the capillary and substrate, with an additional set of electrostatic deflection plates used to direct the positioning of each falling droplet. When printing is not required, the droplets are directed into a waste feed for recycling into the printer reservoir. Although such systems are widely used in a commercial setting, few bioprinting applications exist due to the high ink recycling rate required for printing. The requirement to continually recycle material increases the risk of contamination or cellular and material degradation during extended printing periods (Wheeler *et al.*, 2014).

With a DoD process, an actuation signal is selectively applied to generate single droplets on command. Ink is retained within the nozzle between print jobs due to a combination of surface tension effects at the nozzle tip and the application of low pressure within the ink reservoir. For thermally actuated devices, an electrical pulse is applied to activate a heating element within the nozzle of the printer. As this heat is transferred into the ink, a small quantity of material is vaporised, causing bubble formation and a subsequent change in pressure. This pressure pulse leads to droplet ejection from the nozzle, and subsequent collapse of the bubble provides a negative pressure to pull in additional ink from the printer reservoir.

Within piezoelectric DoD processes, an electrical pulse is applied to piezoelectric material surrounding the capillary of the inkjet nozzle as indicated in Figure 2.15. This causes a change in shape of the material, resulting in the expansion and contraction of the attached capillary. The volume changes within the capillary generate pressure propagations within the fluid that leads to droplet ejection and subsequent refilling of the nozzle.

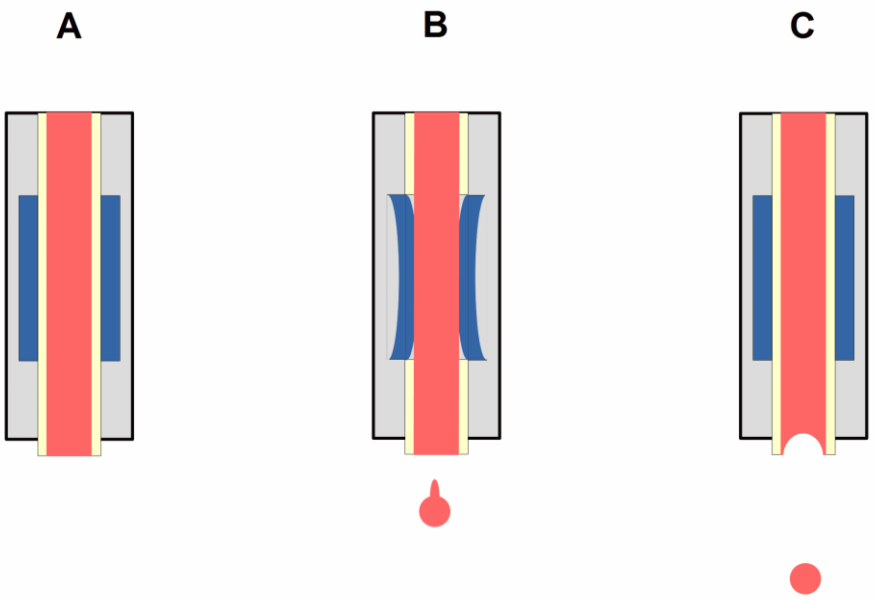

Figure 2.15 – Actuation cycle of a piezoelectric inkjet device under a push-pull configuration. (A) Resting state. (B) Piezoelectric material activation leading to droplet ejection through an increase in liquid pressure. (C) Retraction of piezoelectric material following ejection resulting in a negative pressure.

The waveform applied to a material jetting device represents the intensity, duration and polarity of the electrical signal applied to the actuator. It is important to consider both the rheological properties of the ink as well as the waveform parameters applied in order to achieve maximum printing performance. Previous research has demonstrated the impact of these characteristics on jetting performance for a wide variety of printing applications. In 2013, Woo *et al.* investigated the relationship between inkjet printability and ink rheology when jetting silver nanoparticle conductive ink solutions to demonstrate the effect of various ink formulations on droplet ejection behaviour and positional accuracy. This research highlights the significant impact of ink composition on jetting characteristics (Woo *et al.*, 2013).

Research by Kwon highlights a potential methodology for optimising the waveform design of a piezoelectric dispensing device through monitoring the meniscus motion. Within this research, custom software is developed to monitor the camera feed displaying the meniscus location at the tip of the jetting device nozzle. Data was generated on the meniscus motion in response to changes in the dwell time, velocity and polarity of the waveform applied to the printing device, which was then used to predict jetting performance, enabling subsequent algorithmic waveform optimisation. Results from this study demonstrated that the meniscus monitoring software methodology used is able to identify and optimise the

performance of jetting waveforms. This work identifies a potential method to preliminarily screen and optimise an efficient waveform without requiring extensive jetting studies (Kwon, 2010).

Wu and Hwang researched the effect of echo time on jetting performance when using a bipolar waveform design to deposit solder droplets. Here, a range of different echo times were applied and the properties of droplets deposited assessed and compared with simulated models of droplet formation. In combination, these methods were used to highlight the importance of echo time on droplet formation characteristics, as well as provide an optimised configuration for depositing solder droplets. This research highlights the complexity associated with waveform design, as well as the value of performing optimisation to achieve stable droplet formation (Wu and Hwang, 2015).

Initial research into the application of inkjet printing technology within the fields of tissue engineering and biofabrication focused on the deposition of biocompatible materials.

A review paper by Lemmo *et al.* in 1998 provides an early example of where the potential for using inkjet printing systems within high-throughput applications was considered. Early applications of this technology focussed on the deposition of proteins and genomic material, whereby much lower quantities could be dispensed when compared to conventional techniques (Lemmo, Rose and Tisone, 1998).

Research by Roth *et al.* in 2004 explored the use of a commercially available thermal inkjet printing system for the deposition of collagen. Patterns of collagen were generated on the surface of a material repellent to cellular attachment using inkjet printing. Smooth muscle cells were then deposited manually onto the surface of the material and cultured over a 16 day period. Cellular attachment was observed amongst surfaces where collagen had been deposited, allowing for the selective creation of cell patterns through the use of low cost printing equipment. This research provided an early indication of the potential of inkjet printing systems for tissue engineering applications (Roth *et al.*, 2004).

In regards to cell printing, Wilson and Boland provide an early example of where a thermal inkjet printing system was successfully used to deposit endothelial and smooth muscle cells. The selective deposition of cells and biomaterials was successfully demonstrated, with cells deposited at a concentration of 10^5 cells per mL in cell culture media. An average cell density of approximately 1.5 cells per droplet was reported, with cells deposited within 1 minute

following loading into the printer. A Live / Dead® cell viability assay was performed and a cell viability of 75 % was reported immediately following printing. This important research demonstrated the possibility of using inkjet printing systems to successfully deposit viable cells, whilst highlighting the potential implications of such technology for HTS applications and 3D tissue assembly *in vitro* (Wilson and Boland, 2003). As an additional output of this research, the nozzle head modifications developed by Wilson and Boland were patented for cell printing applications (Boland, Wilson and Xu, 2006). Further research into the applications of inkjet cell printing were then performed by Boland *et al.* to introduce the use of thermosensitive materials for multi-layered cell printing. This research used the same printing equipment combined with thermosensitive gels and bovine aortal endothelial cells. Multi-layered printing was demonstrated, with droplet stacking of individual gel layers to enable the construction of 3D structures. This research provides an early demonstration of the potential for combining cells and gels in order to construct 3D structures. It also represents an early example of where the potential impact of the cell and gel combination for tissue and organ construction was explored (Boland *et al.*, 2003).

In 2005, Xu *et al.* demonstrated that it was possible to jet Chinese hamster ovary cells using a modified thermal inkjet printer and corresponding cartridge system that had been commercially sourced from Hewlett Packard. These cells were suspended within phosphate buffered saline and printed onto a soy agar and collagen gel membrane at a concentration of 2-5 million cells per mL. A high cell viability was observed, with less than 8 % of cells lysed during the printing process, demonstrating the potential for using low-cost, commercially available technology in a modified form to process living cells (Xu *et al.*, 2005).

More recent work by Xu *et al.* has combined multiple manufacturing processes in order to produce a single cell scaffold. This consists of electrospun polycaprolactone fibres in combination with inkjet-printed rabbit elastic chondrocytes, suspended within a fibrin-collagen hydrogel. The resulting 5 layer tissue had a depth of approximately 1 mm, with cellular viability within the tissue reported to exceed 80 % following printing. This work indicates the potential of combining multiple manufacturing processes, each with specific advantages and limitations, in order to generate a single cell-laden structure with properties that would be difficult to achieve when utilising a single manufacturing technology (Atala *et al.*, 2012).

The effect of waveform parameters on cell printing performance was evaluated by Yamaguchi *et al.* in 2012. Using Sf9 insect cells, cells were deposited using a custom elliptical inkjet nozzle at a density of one cell per droplet in saline solution. Polymer beads were also independently deposited whilst the nozzle was simultaneously imaged to determine the positioning of each bead within the capillary in response to modifications to the jetting cycle. This research concluded that push-pull piezoelectric waveform designs provide superior cell jetting performance to pull-push methods, providing valuable information for future work where the optimisation of cell jetting waveform designs are required (Yamaguchi *et al.*, 2012).

Research by Park *et al.* has also examined the precision and accuracy of a piezoelectric inkjet printing platform for the construction of complex cellular arrays and patterns. Within this work, the effect of the printing process on cellular viability and proliferation was assessed, with printed cells exhibiting no significant differences when compared to manually deposited samples. Positional accuracy data of cell printing performance was also presented in response to printing parameter modifications in order to determine an optimal printing configuration. A complex array of cells labelled with different dyes was generated, demonstrating the precision of the printing process for the creation of small-scale co-culture models. This research provides validation of the inkjet printing process for the precise deposition of an array of different cellular materials (J. A. Park *et al.*, 2017).

Research by Lorber *et al.* highlights the feasibility of using piezoelectric inkjet printing technology to jet a liquid medium, here containing adult rat ganglion cells, onto a substrate. In their 2014 publication, the authors use droplet analysis tests to determine droplet ejection characteristics of the cell-containing ink solution. Furthermore, high cell viability was reported following deposition, providing further evidence of the potential for using inkjet dispensing for cell deposition. This work also highlights some of the key limitations of using jetting technologies to process cells by reporting complications such as cells settling within suspension, adherence to the internal surfaces of the reservoir, and nozzle blockages during printing that were observed during the experiments performed (Lorber *et al.*, 2014).

These effects are a recognised limitation of the material jetting process and are commonly observed when applying this technology within bioprinting applications, despite the lack of reporting within subject literature (Chahal, Ahmadi and Cheung, 2012). Nozzle blockages are particularly problematic within material jetting processes due to the small aperture

requirements of the nozzle to achieve high jetting accuracy. This can occur as a result of unfiltered solids within a suspension, crystallisation of ink components, cell adherence to the internal surface of the nozzle, and aggregation of cells into clumps. Collection of material on the outer surface of the nozzle can also impede droplet ejection and result in blockages or reduced jetting performance. These limitations occur alongside the more widely reported limitations surrounding ink viscosity and surface tension requirements to achieve stable droplet formation (Jang, Kim and Moon, 2009; McIlroy, Harlen and Morrison, 2013; Woo *et al.*, 2013).

2.3.3 Valve Printing

In valve-driven systems, a solenoid activated by an electrical signal generates a magnetic field: this magnetic field then opens and closes the valve mechanism to control material flow. This is most commonly achieved through the movement of a plunger to block and unblock the path of fluid flow through the device in response to actuation signals from the printer controller as shown in Figure 2.16. A positive pressure is continually applied behind the valve to drive material through the device when opened.

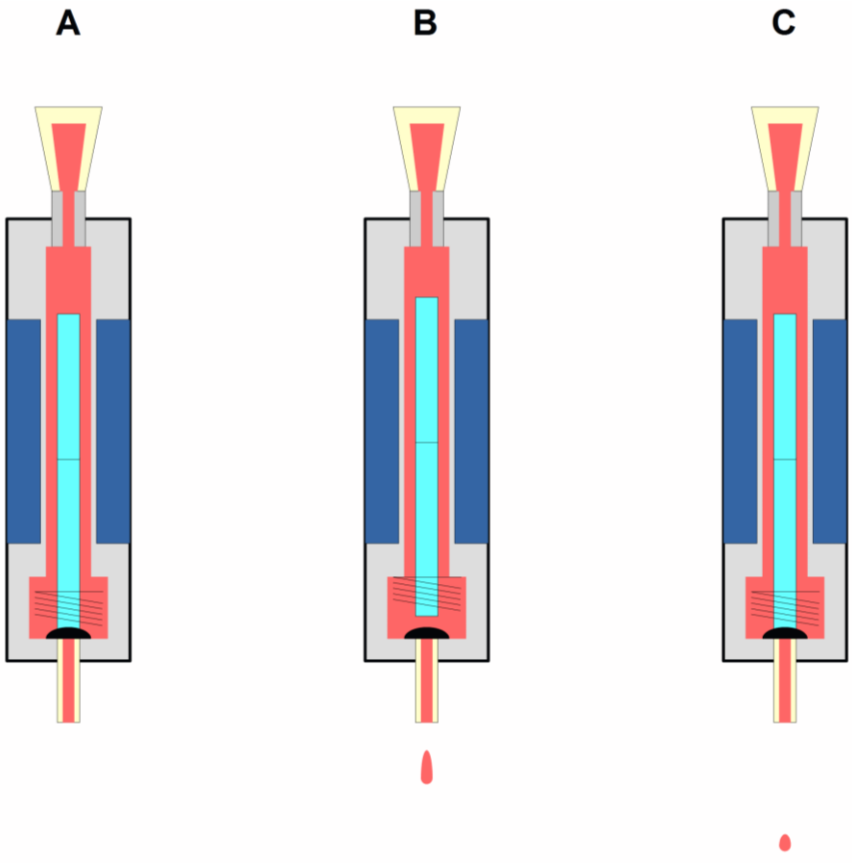

Figure 2.16 – Actuation cycle of a solenoid valve dispensing device under a drop-on-demand configuration. (A) Resting state. (B) Valve opening leading to droplet ejection. (C) Closure of orifice following actuation cycle.

Continuous jetting approaches hold the valve in the open position during printing until the desired volume of liquid has been dispensed at a single coordinate. This approach reduces mechanical wear on the actuator and maximises the rate of material deposition. As a consequence, a continuous stream of material is deposited towards the substrate.

Within a DoD configuration, the valve is sequentially opened and closed to repeatedly generate individual droplets of a consistent volume. A target volume is achieved through repeated deposition of droplets of a defined volume onto the substrate. This approach requires operating the valve under a higher duty cycle than CJ methods, and throughput is limited by the maximum actuation frequency of the valve. The deposition of individual droplets increases the precision of material delivery and has been previously combined with droplet impingement and reactive jetting processes to successfully generate 3D structures (Da Conceicao Ribeiro *et al.*, 2019).

Solenoid valves have been used across a wide range of engineering applications including pneumatic and hydraulic control as well as material dispensing (Razban and Davies, 1991; Moseler and Straky, 2000; Ahn and Yokota, 2005). More recent research has applied solenoid valve dispensing systems for liquid handling applications within biomedical research (Niles and Coassin, 2005; Bammesberger *et al.*, 2013). This includes the application of valve deposition systems to the field of biofabrication for the deposition of cellular materials.

A critical advantage of valve-based processes over inkjet printing technologies is the range of ink cell concentrations that can be deposited. Previous research by Ribeiro *et al.* used a solenoid valve in a DoD configuration to deposit MSCs at a concentration of up to 40 million cells per mL. Cells were deposited using a reactive jet impingement process, whereby two opposing valves directed a reactive mixture of collagen, alginate, fibrinogen, thrombin and cells contained within droplets at one another, to meet and react in mid-air, thus enabling the production of 3D gels. This research provides evidence of the flexibility of valve actuators to deposit high cell density solutions, as well as reporting a novel multi-jet configuration to enable *in situ* reactive printing for the production of 3D structures (Da Conceicao Ribeiro *et al.*, 2019).

Previous examples of where valve printing processes have been used to construct tissue models include research published in 2013 by Faulkner-Jones *et al*. Within this project, a solenoid valve dispensing device was retrofitted to a commercially available fused filament

fabrication printer, enabling the deposition of cellular material at a density of approximately 5 cells per droplet. This printing device was then applied for the construction of embryonic stem cell aggregates via a hanging droplet cell culture method. Cellular viability was retained following printing and throughout the aggregate culture period. This research provides new evidence for the semi-automated production of size-controlled micro tissues (Faulkner-Jones *et al.*, 2013).

A printed human skin model was generated by Lee *et al.* in 2014 using a solenoid valve actuation system operating under a CJ configuration. The system was used to sequentially dispense layers of collagen, fibroblasts and keratinocytes onto a Transwell® membrane insert, with subsequent tissue organisation induced using an air-liquid-interface culture technique. Biological analysis revealed that cell viability was maintained following the printing process, with distinct epidermal and dermal tissue layers retained throughout the 14 day culture period. This research provides a working example of where valve printing technology has been successfully applied for the production of an insert-based tissue model (Lee *et al.*, 2014).

In 2015, research by Ling *et al.* demonstrated the potential for using a custom solenoid valve-based printer to selectively deposit MCF-7 breast cancer cells for the manufacture of cell aggregates. Deposition volume was adjusted through modulating dispensing pressure and actuation pulse duration. Within this project, a gravimetric approach was applied to induce cell aggregation following deposition onto a printed concave gelatin microarray. Maintenance of cell viability following printing was confirmed using a Live / Dead® assay, with aggregate structure monitored over 7 days using microscopy. This research provides a further demonstration of the potential for using valve printing processes to scale up the manufacture of tissue aggregates (Ling *et al.*, 2015).

Work by Horvath *et al.* in 2015 applied valve printing technology for the fabrication of air-blood barriers. Within this research, a commercial bioprinter was used to deposit a proprietary ECM substitute onto Millicell® insert membranes, followed by the sequential addition of endothelial, ECM and epithelial cells. Maintenance of cellular viability was reported following printing through quantitative evaluation of cellular proliferation and lactate dehydrogenase release. Bioprinted tissues displayed a flatter morphology than manually deposited samples when assessed using histological staining techniques, thus providing a more physiologically replicative model of alveolar tissue. This research highlights

the versatility of valve printing techniques for the construction of tissue models that are comprised of a range of different cell types (Horvath *et al.*, 2015).

Further research by Min *et al.* in 2018 provides yet another example of bioprinted skin using a CJ valve deposition system in combination with sequential fibroblast, melanocyte, keratinocyte and collagen layering. A similar Transwell® membrane and air-liquid-interface was applied to promote and retain structural organisation of printed cells. Histological examination of the printed constructs was presented, demonstrating that the developed protocol was capable of generating skin tissue with clearly defined epidermal and dermal regions. Skin pigmentation as a result of melanocyte activity was also observed, further demonstrating the potential of valve printing processes for the production of *in vitro* tissue models (Min *et al.*, 2018).

2.3.4 Ink Composition

The performance of each material jetting process is heavily influenced by the fluid properties of the ink being dispensed. A number of dimensionless quantities within the field of fluid mechanics have been used to predict fluid behaviour within a material jetting system.

The Reynolds number is defined as being the ratio of inertial to viscous forces within a fluid and is used to predict fluid flow under different conditions.

$$Re = \frac{\rho u L}{\mu} = \frac{u L}{v}$$

Where:

$Re =$ Reynolds number
$\rho =$ Density of fluid
$u =$ Velocity of fluid with respect to object
$L =$ Characteristic linear dimension
$\mu =$ Dynamic viscosity of fluid
$v =$ Kinematic viscosity of fluid

Equation 2.1 – Definition of Reynolds number used to predict fluid flow under different conditions.

The Weber number is used to analyse fluid flow in the presence of an interface between two different fluids. It is used to characterise the ratio of surface to inertial forces within a fluid.

$$We = \frac{\rho v^2 L}{\sigma}$$

Where:

$\sigma =$ Surface tension
$We =$ Weber number

Equation 2.2 – Definition of Weber number used to characterise the ratio of surface to inertial forces within a fluid.

The Ohnesorge number is used to describe the significance of viscous forces within a fluid to inertial surface tension effects.

$$Oh = \frac{\mu}{\sqrt{\rho \sigma L}} = \frac{\sqrt{We}}{Re}$$

Where:

$Oh =$ Ohnesorge number

Equation 2.3 – Definition of Ohnesorge number used to describe the significance of viscous forces within a fluid to inertial surface tension effects.

The inverse of the Ohnesorge number (Z) has been used to define ink printability within DoD configurations (McKinley and Renardy, 2011). Initial research indicated that the Z factor of an ink must exceed 2 in order to achieve stable droplet formation (Fromm, 1984). More recent research has redefined the printable range as between 2 and 20 for practical ink designs through a combination of theoretical and practical experimental techniques (Reis and Derby, 2000; Jang, Kim and Moon, 2009; Liu and Derby, 2019). This research provides a marker for defining new ink properties in order to retain sufficient jetting performance.

It is also important to consider the influence of ink composition, droplet ejection characteristics and substrate properties on droplet-substrate and droplet-droplet interactions, due to the recognised impact that they have on substrate splashing and subsequent printing accuracy (Stow and Hadfield, 1981; Perelaer *et al.*, 2009; Jung, 2011; Yokoi, 2011; Staat, 2016).

Previous research by Derby in 2010 constructed the parameter space shown in Figure 2.17 to define ink printability within DoD systems by using the dimensionless quantities previously described.

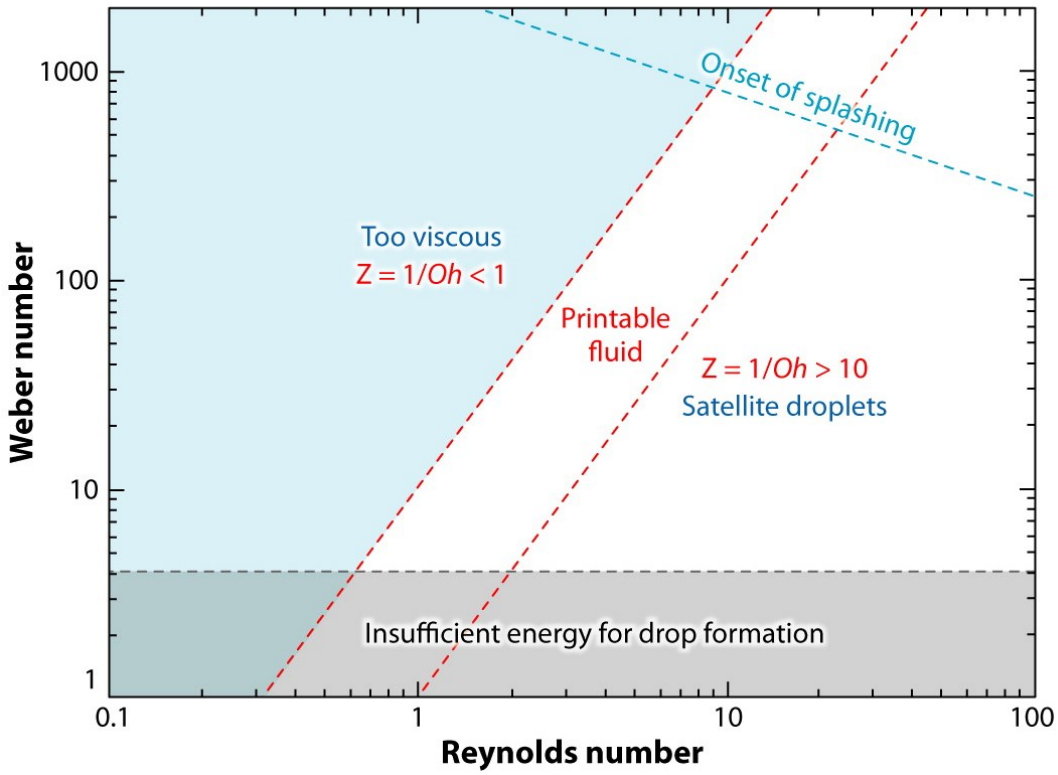

Figure 2.17 – Printability of inks plotted as a function of the Reynolds and Weber number for drop-on-demand printing processes. Reproduced from (Derby, 2010).

Ink design therefore requires careful consideration of the impact of potential constituent materials on fluid rheology in order to maintain jetting performance. Traditionally, such designs have employed the use of specific chemicals that act as humectants, defoamers, surfactants or rheology modifiers to improve the stability and printability of ink solutions, as well as the properties of printed material (Hutchinson, 1978; Ramirez and Tumolva, 2018).

Despite this, many materials commonly used to optimise the rheological properties of inks for commercial printing applications are not biocompatible with cellular material. This places greater restrictions on the level of ink optimisation that can be performed prior to printing. It is also important to consider the impact of solid cellular material suspended within a liquid ink on its overall printability. The distribution of suspended cells, individual cell size, and propensity of the cell type to aggregate can impact cell printing performance. Finally, the sensitivity of cells to shear forces induced by the jetting nozzle and potential reactivity of biological materials during printing must also be considered to determine the suitability of

the printing process with each cell and material combination. A range of research has been published on various methods to minimise nozzle blocking and subsequently improve the performance of the material jetting process when depositing cell-containing solutions. This includes modifications to the printing devices and bioink composition used for cell dispensing.

One example of a study into such effects is research by Parsa *et al.* in 2010 which evaluated the effect of using a combination of surfactants and stir-bar agitation on piezoelectric inkjet printing performance. Here, the authors use Pluronic® F68 at a concentration of 0.05 %, added to cell culture media to resuspend HepG2 hepatocyte cells at a density of 500,000 cells per mL. Cells were loaded into a custom reservoir containing a stir-bar and corresponding external mixer circuit. Cells were then deposited with the stir-bar intermittently activated for approximately 5 seconds at 2 minute intervals over a 10 minute printing period to determine the impact of the stir-bar and surfactant on cell viability and metabolic activity. The addition of surfactant was not reported to have any significant impact on cell viability, with improvements in droplet ejection characteristics attributed to the differences in ink rheology. Stir-bar agitation was reported to reduce cell sedimentation, however inconsistencies in cell printing performance were still observed as a result of continual cell aggregation. This study therefore provides further evidence of the issues surrounding cellular aggregation and sedimentation when performing cell printing, requiring further research to evaluate additional methods to improve printing performance (Parsa *et al.*, 2010).

Chahal *et al*. carried out research into methods to reduce the effect of cell sedimentation and aggregation during the printing process. Within this work, Ficoll-PM 400® and Pluronic F127® were added to cell culture media at a concentration of 0 - 20 % and 0.25 % respectively to reduce the rate of cell sedimentation and ink surface tension. Cells were then resuspended in the ink at a concentration of 500,000 cells per mL and deposited using a piezoelectric inkjet dispensing device. Sedimentation velocity analysis revealed that increasing the ink Ficoll® concentration reduced the rate of cellular sedimentation. Cell deposition performance was also assessed over a 90 minute period by dispensing 30,000 drops into individual wells of a 96 well plate. A significant reduction in variability of counted cells per well was reported in samples containing 5 or 10 % Ficoll® solution when compared to the control ink. In addition, the frequency of nozzle clogging was also reported to be

reduced. The presence of Ficoll® was not found to have a significant impact on cellular metabolic activity when compared with untreated samples. This work provides a potential method to improve jetting performance through the inclusion of media additives that reduce cellular sedimentation and aggregation. Further research is required to evaluate the effects of the ink formulation on cellular viability and function to assess its suitability for bioink applications (Chahal, Ahmadi and Cheung, 2012).

Research reported in a thesis by Tse in 2015 provides further evidence of the effect of cell sedimentation and aggregation on inkjet printing performance. Within this research, NG108 mouse neuronal cells were sequentially deposited over a period of 100 minutes. A rapid reduction in the number of cells deposited was reported within the first 10 minutes of printing, with further deterioration in performance over a subsequent 40 minutes. Further printing resulted in negligible numbers of cells being deposited when compared with the earlier time points. The study was then repeated with the addition of intermittent gaseous aspiration cycles to the printer reservoir, with a small increase in printing performance reported following each aspiration cycle. This study highlights the difficulty in maintaining cell printing performance over extended printing periods when using inkjet printing technology. It also provides an early evaluation of the use of gaseous aspiration techniques to reduce cell sedimentation during printing. Although the aspiration protocol used was shown to have an initial effect on cell printing performance, this was not sufficient to fully restore initial performance. Additional issues were also reported surrounding droplet instability caused by the pressure changes induced as a result of the aspiration process. Further work is therefore required to assess the use of alternative techniques to reduce cell sedimentation during printing (Tse, 2015).

Poly-l-lysine (PLL) is a polycation that is commonly used to coat cell culture plasticware in order to improve cellular adherence by ionically interacting with the negative charge of cell membranes. It has also previously been shown to promote chondrogenic differentiation of chondroprogenitor MSCs (San Antonio and Tuan, 1986; Woodward and Tuan, 1999). As a result, PLL has been studied as a potential material for the construction of hydrogels for cartilage tissue engineering applications (Clark *et al.*, 2016). It has also been combined with other materials such as alginate for the production of cell encapsulation systems (Wilson *et al.*, 2014).

Previous research by Ribeiro *et al.* employed PLL for the development of a temporary single cell coating process to reduce the cell agglomeration-induced nozzle blockages associated with material jetting technologies. The effect of the coating process was assessed on three cell types; neonatal human dermal fibroblasts, osteosarcoma cells and Ewing's sarcoma cells across a concentration range of 10 - 100 µg / mL. A cell viability of 70 % was reported following coating at a PLL concentration of 10 µg / mL, with additional analysis performed to define the endocytic pathways involved in subsequent polymer internalisation. The effect of the coating process on cellular agglomeration was assessed via a combination of microscopy and cell printing approaches. Printing performance for the coated osteosarcoma cell samples was maintained over a 1 hour assessment period, with uncoated samples resulting in a rapid deterioration in jetting performance within a 20 minute period. This work highlights a potential method to improve the jetting performance of bioinks through temporary modification of the cell surface charge. Possibilities for future research include characterising the effects of the coating process on cellular functionality and agglomeration across additional cell types (Ribeiro *et al.*, 2017).

Taken as a whole, further research is therefore required to assess the potential of novel processing techniques such as those previously described, to improve material jetting performance when processing cell-containing solutions.

Chapter 3. Methodology

3.1 Cell Culture

Y201 hTERT immortalised human Mesenchymal Stromal Cells (MSCs) (kindly donated by Professor Paul Genever, University of York) were obtained from passage 73, and cultured in high glucose (4.5 g / L) Dulbecco's Modified Eagle Medium (DMEM) (Thermo Fisher Scientific, USA) supplemented with 10 % foetal bovine serum (Thermo Fisher Scientific), 5000 U / mL Penicillin / Streptomycin (Sigma-Aldrich, UK) and 2 mM L-Glutamine (Sigma-Aldrich).

TC28a2 human chondrocyte cells (Merck, USA) were obtained at passage 22, and were cultured in high glucose (4.5 g / L) DMEM / Ham's F12 mix 1:1 v / v (Thermo Fisher Scientific) supplemented with 10 % foetal bovine serum (Thermo Fisher Scientific), 5000 U/mL Penicillin / Streptomycin (Sigma-Aldrich) and 2 mM L-Glutamine (Sigma-Aldrich).

Cells were incubated at 37 °C, 5 % CO_2 in a humidified atmosphere and passaged at ~70 % confluency through aspiration of media and washing with Phosphate Buffered Saline (PBS) (Sigma-Aldrich) (2.5 mL / 25 cm^2) to remove residual serum. Trypsin-ethylenediaminetetraacetic acid (0.05 %) (Sigma-Aldrich) (0.5 mL / 25 cm^2) was added to the flask and incubated at 37 °C, 5 % CO_2 until cells had detached from the flask surface. Cell culture media was added to the flask (> 1.0 mL / 25 cm^2) to inactivate the trypsin and the suspension transferred to a centrifuge tube. The solution was centrifuged at 200 g for 5 minutes and the resulting supernatant removed. The cell pellet was then re-suspended in 1 mL of fresh cell culture media for cell counting. The volume of the cell-containing solution was adjusted accordingly with cell culture media to achieve the desired final concentration for reseeding into cell culture flasks.

3.1.1 Cell Counting

A trypan blue exclusion test was performed to determine the viable cell number during cell counting. Trypan blue dye is only able to stain cells with a disrupted cell membrane, causing the cytoplasm of non-viable cells to appear blue during examination.

To perform a cell count a 20 µL aliquot of cell-containing solution was combined with an equal volume of 0.4 % trypan blue staining solution (Sigma-Aldrich). The viable cell number was determined by counting the number of unstained cells using a 0.1mm depth Neubauer chamber haemocytometer (Hawksley, UK).

3.1.2 Cryopreservation

Cells were trypsinised at ~70 % confluency using the procedures previously described and re-suspended in a volume of freezing medium consisting of 10 % v / v dimethyl sulfoxide (Sigma-Aldrich) in foetal bovine serum to achieve a final concentration of 10^6 cells per mL.

Cell suspension was then aliquoted into 1 mL cryopreservation tubes (Corning, USA) and placed in a dedicated freezing chamber (Thermo Fisher Scientific). The chamber was placed in a -80 °C freezer for 2-3 days to control the rate of cell freezing. Cryopreservation tubes were then transferred into liquid nitrogen for long-term storage at -196 °C.

Samples were thawed via suspension of the cryogenic storage tube in a water bath at 37 °C until partially thawed. The sample was then immediately resuspended into a minimum of 10 mL of cold fresh cell culture media and centrifuged at 200 *g* for 5 minutes. The supernatant was discarded and the pellet resuspended in cell culture media at the desired density for seeding into a cell culture flask.

3.2 Metabolic Activity Assays

Cells were seeded into the wells of a 96-well plate at a density of approximately 5,000 cells per well and incubated at 37 °C, 5 % CO_2 for a minimum of 12 hours to facilitate cell attachment.

3.2.1 MTT Assay

Following treatment in desired experimental conditions, the cell supernatant from each well was removed and replaced with 100 µL of freshly prepared MTT (Sigma-Aldrich) working solution (0.5 mg / mL) in phenol-red free cell culture media (Thermo Fisher Scientific). Plates were incubated for a further 4 hours until formazan crystals had been produced. Supernatant was then removed from each well and replaced with 100 µL of propan-2-ol detergent solution (Fisher Scientific, USA). The plate was agitated for 30 minutes to solubilise the formazan crystals. The absorbance values for each well were then obtained using an ELx800 microplate reader (Biotek, USA) at 570 nm with a 630 nm reference wavelength recorded for normalisation.

3.2.2 PrestoBlue® Assay

Following treatment in desired experimental conditions, the cell supernatant from each well was removed and replaced with 100 µL of PrestoBlue® (Thermo Fisher Scientific) working solution previously prepared from the addition of 10 % v / v PrestoBlue® reagent to phenol-red free cell culture media. Plates were incubated for a further 4 hours. Fluorescence values

for each plate were obtained using a FLUOstar® Omega microplate reader (BMG Labtech, Germany) using an excitation and emission filter of 544 nm and 620 nm respectively.

3.3 Cell Viability Assay

Cellular viability was assessed in response to different treatment conditions via the use of a Live / Dead® cell viability assay (Thermo Fisher Scientific). This assay contains a non-fluorescent calcein acetoxymethyl compound that enters the cell membrane and is readily converted into a green fluorescent calcein dye via esterase enzymatic activity within living cells. Ethidium homodimer-1 is also contained within the assay and enters cells with damaged membranes. This compound binds to nucleic acids within the cell leading to a red fluorescence upon exposure to light.

To perform the assay, each of the stock solutions were warmed to room temperature and diluted in PBS to produce a 2 µM calcein acetoxymethyl and 4 µM ethidium homodimer-1 working solution. Adherent cells were washed extensively with PBS prior to the application of Live / Dead® working solution. The samples were then incubated for a period of 30 minutes in a humidified atmosphere at 37 °C, 5 % CO_2 prior to imaging.

Imaging was performed using a DMLB fluorescence microscope (Leica Biosystems, Germany) at 10x magnification and images captured using a SPOT Advanced CMOS camera (Spot Imaging Solutions, USA) and corresponding microscopy software. A fluorescein filter was used to image the calcein fluorescence and Texas red filter for ethidium homodimer-1.

3.4 Cell Imaging

3.4.1 2D Sample Preparation

For adherent cells grown in monolayer culture, three PBS washes were performed prior to fixation for 15 minutes in 4 % paraformaldehyde solution (Thermo Fisher Scientific). Fixed cells were then washed three times in PBS and stored at 4 °C in PBS prior to staining.

3.4.2 3D Sample Preparation

At several time points, samples were embedded in Tissue-Tek® optimal cutting temperature compound (Sakura Finetek, USA) and were snap frozen in liquid nitrogen. Samples were kept at -80 °C until use. Samples were cryosectioned by Xin Xu of the Newcastle Central Biobank using a CM1900 cryostat (Leica Biosystems, Germany) and sectioned at a thickness of 10 µm. Slides were kept frozen until analysis, where they were dried, sections restricted with a PAP pen (Sigma-Aldrich), washed in PBS and fixed for 30 minutes in 4 % paraformaldehyde solution (Thermo Fisher Scientific).

3.4.3 Haematoxylin and Eosin Staining

Optimal cutting temperature compound embedded sections were immersed in PBS for approximately 1 minute prior to staining. Samples were incubated in Mayer's haematoxylin (Sigma-Aldrich) for 5 minutes prior to rinsing in running tap water for 2 minutes to blue haematoxylin stained nuclei. Samples were dehydrated through incubation in ethanol solutions of increasing concentration prior to immersion in eosin solution (Sigma-Aldrich) for 30 seconds. Samples were further dehydrated and incubated in Histo-Clear® II (National Diagnostics, USA) for 5 minutes before being mounted in DPX (Sigma-Aldrich). Samples were imaged using an Axio Imager® (Carl Zeiss AG, Germany) upright microscope at 20x magnification.

3.4.4 DAPI and Phalloidin Staining

A combination of phalloidin–tetramethylrhodamine B isothiocyanate (Sigma-Aldrich) and mounting medium containing 4',6-diamidino-2-phenylindole (DAPI, Sigma-Aldrich) were used to visualise the filamentous actin (F-actin) present within the cytoskeleton and cell nucleus respectively. Fixed cells were washed extensively in PBS prior to the addition of 1 µg / mL phalloidin working solution prepared in PBS. Cells were then incubated for a period of 20 minutes at room temperature prior to three washes in PBS.

Coverslips were mounted to glass slides following the addition of mounting media containing DAPI and incubated for a further 5 minutes before imaging. Imaging was performed using an LSM800 point scanning confocal microscope (Carl Zeiss AG) at 20x magnification.

3.4.5 Indirect Immunofluorescence Staining

Fixed samples were permeabilised in 0.1 % Triton X (Merck) and washed in PBS 3 times for 5 minute intervals. Samples were then blocked with an incubation of 2 % bovine serum albumin (Merck) for 30 minutes. Excess bovine serum albumin was removed and replaced with primary antibody solution. Primary antibodies were diluted in PBS to achieve a final concentration of 1/200 for Collagen II (ab34712, Abcam, UK) and 1/50 for Aggrecan (ab3778, Abcam). Samples were incubated for 2 hours at room temperature in the antibody solution before being washed 3 times for 5 minutes in PBS. Secondary antibody solution was then prepared using Alexa Fluor® 488 or 594 (Thermo Fisher Scientific) at a concentration of 1/500 and added to the samples for a further 1 hour incubation. Samples were washed 3 times in PBS and mounted in mounting medium containing DAPI. Imaging was performed using an LSM800 point scanning confocal microscope (Carl Zeiss AG) at 20x magnification.

3.5 Bioprinting

3.5.1 System Configuration

All printing experiments were performed using a JetLab® 4 XL (MicroFab, USA) printing work station combined with the JetDrive® printer drive electronics unit. Droplet ejection characteristics were assessed via the on-board stroboscopic camera in responses to printing parameter modifications.

The device was cleaned by flushing 1 % v / v Micro-90 cleaning solution (Cole-Parmer, USA) followed by 70 % v / v ethanol (Fisher Scientific) through the reservoir, tubing and jetting device for a minimum of 10 minutes to remove potential sources of contamination prior to and following each use. The device was extensively flushed with sterile filtered de-ionised water immediately prior to use to remove any residual cleaning agents.

3.5.2 Reservoir Configuration

An in-house developed reservoir design and accompanying agitation system were utilised for all cell printing experiments. Two different systems were employed for printing experiments with each design incorporating a MINSTAC® 062 thread (the Lee Company, USA) to maintain compatibility with both the inkjet and valve actuation devices used. A continuous voltage of 1.5 V was applied to the motor of either device via an external power supply unit (Elenco Electronics, USA) following ink loading to prevent cell sedimentation prior to or during printing.

The initial design, referred to as ‘Agitator A’, incorporated a shaft-driven axial-flow impeller attached to an electric motor to minimise cell sedimentation within the 2 mL capacity ink reservoir shown in Figure 3.1. Ink loading was performed through the decoupling of the agitator and reservoir components. During printing, ink was fed directly into the actuation device via a small orifice at the base of the reservoir.

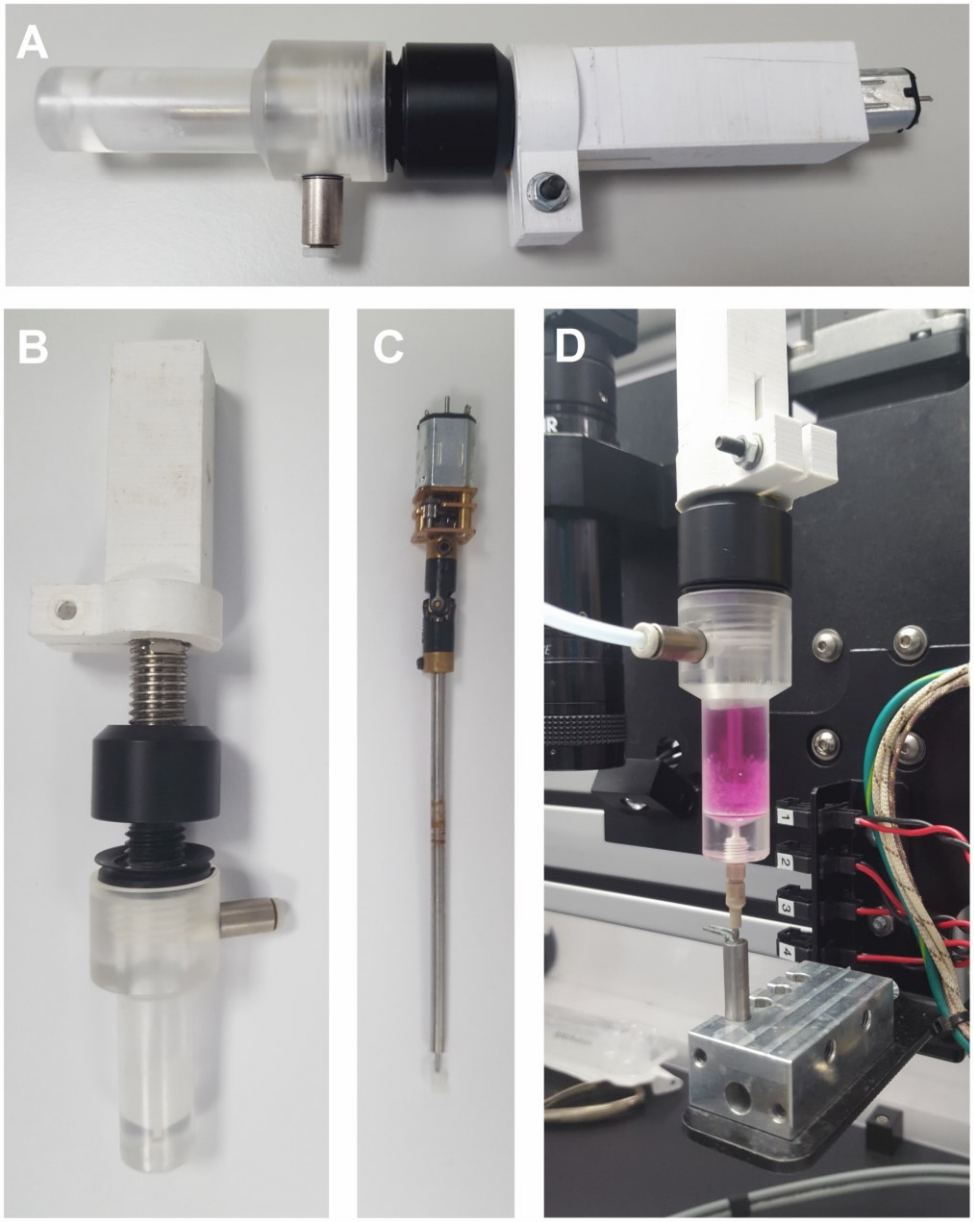

Figure 3.1 – Reservoir and agitator design 'A' used to minimise cellular aggregation during printing. (A) Reservoir and agitator following coupling. (B) View of threaded coupling between agitator and reservoir. (C) Motor, gearbox, driveshaft and impellor assembly. (D) Mounted reservoir and agitation system for printing.

A revised design referred to as 'Agitator B' comprised of a 5 mL capacity reservoir shown in Figure 3.2. Agitation was achieved through the rotation of a gold-plated cylindrical neodymium magnet mounted to the inside of the reservoir. Movement was induced via an electrical motor coupled to an additional magnet external to the reservoir. This design reduced the minimum size of the agitator and isolated the reservoir contents in a sealed container during operation. Ink loading was performed via the removal of the clamped reservoir lid. Ink was fed into the actuation device via an orifice at the base of the reservoir and through an s-shaped cut-out within the reservoir housing.

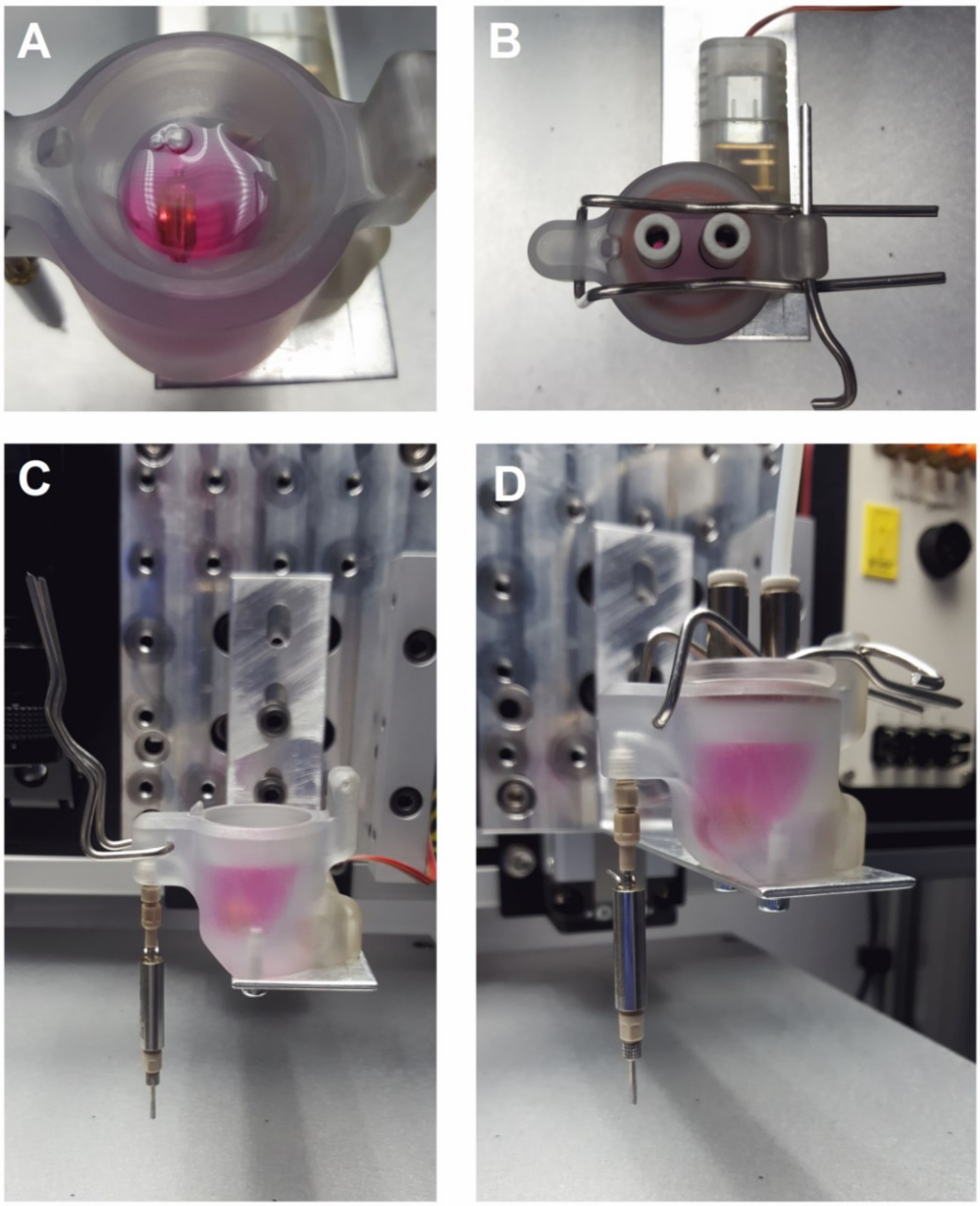

Figure 3.2 – Reservoir and agitator design 'B' used to minimise cellular aggregation during printing. (A) View of gold-plated magnet suspended within reservoir. (B) External motor housing, lid clamping mechanism and pneumatic tubing connectors used to pressurise reservoir during printing. (C) Open reservoir configuration to allow for ink refilling. (D) Closed reservoir configuration for printing.

3.5.3 Ink Preparation

Cell culture medium was used as the bioink in each of the bioprinting experiments. The solution was heated to 37 °C and filtered using a 0.22 µm filter (Merck) prior to use. Cell pellets were then re-suspended within the culture media formulation and transferred to the reservoir for printing.

3.5.4 Jetting Commands

A range of different scripted command sets were produced in order to control the positioning stage, pressure output, drive waveform and image capture systems. All plate-based cell printing experiments were performed using point-by-point, coordinate driven controls as shown in Figure 3.3.

```
moveall 0 0 -35
(move stage <X> <Y> <Z>)

set zpos -35
(Set printer movement height <Z>)

set well on -38
(Set lowered dispensing position height <State> <Z>)

begin
(Start printing)

-0 0 1 10 0
(<X> <Y> <Jet Number> <Droplet Number> <Bidirectional Flag>)

End
(Finish printing)
```

Figure 3.3 – Typical script layout for depositing material on a point-by-point basis using JetLab® printer control software.

3.6 Statistical Analysis

Data presented shows mean values ± standard deviation. All data were analysed using Prism® 8 statistical analysis software (GraphPad Software, USA) using two-way analysis of variance in combination with Tukey or Šídák multiple comparison tests. The Shapiro-Wilk test was used to assess normality prior to statistical analysis.

Linear regression analysis was performed to identify trends within standard curve data and enable interpolation from unknown values.

Cell proliferation assays were assessed via nonlinear regression analysis using an exponential (Malthusian) population growth model defined by the equation:

$$Y = Y_0 \times e^{kx}$$

Where:

Y_0 = Starting population
k = Rate constant
x = Population doubling time

Equation 3.1 – Assessment of cell proliferation using the exponential (Malthusian) population growth model.

An extra sum-of-squares F test was performed to compare the rate constant value of each sample group.

Levels of statistical significance were defined using $P \leq 0.05$ (*), $P \leq 0.01$ (**) and $P \leq 0.001$ (***).

Chapter 4. Single Cell Printing

4.1 Introduction

The aim of this chapter is to assess the suitability of an inkjet printing platform for the selective deposition of single cells.

Within this chapter, the printing performance of a piezoelectric drop-on-demand inkjet printing device is characterised in response to critical printing parameters such as waveform design, signal dwell time and voltage and device backpressure.

The biological effects of the inkjet printing process are characterised using mesenchymal stromal cell and chondrocyte cells, with the effects of this process determined by cell viability and function assessments.

Single cell printing performance data is presented to demonstrate the suitability of the technique for high resolution bioprinting applications.

Additional to this, an in-house developed poly-l-lysine cell coating protocol and reservoir agitation system are benchmarked to enhance inkjet cell printing performance over extended printing periods.

4.2 Methodology

4.2.1 Inkjet Printing Configuration

MJ-AT-01 (standard) and MJ-ATP-01 (protected) threaded low temperature single-orifice piezoelectric jetting devices (MicroFab, USA) were used to deposit material from the printing work station as shown in Figure 4.1, with 40, 60 and 80 μm orifice diameters tested.

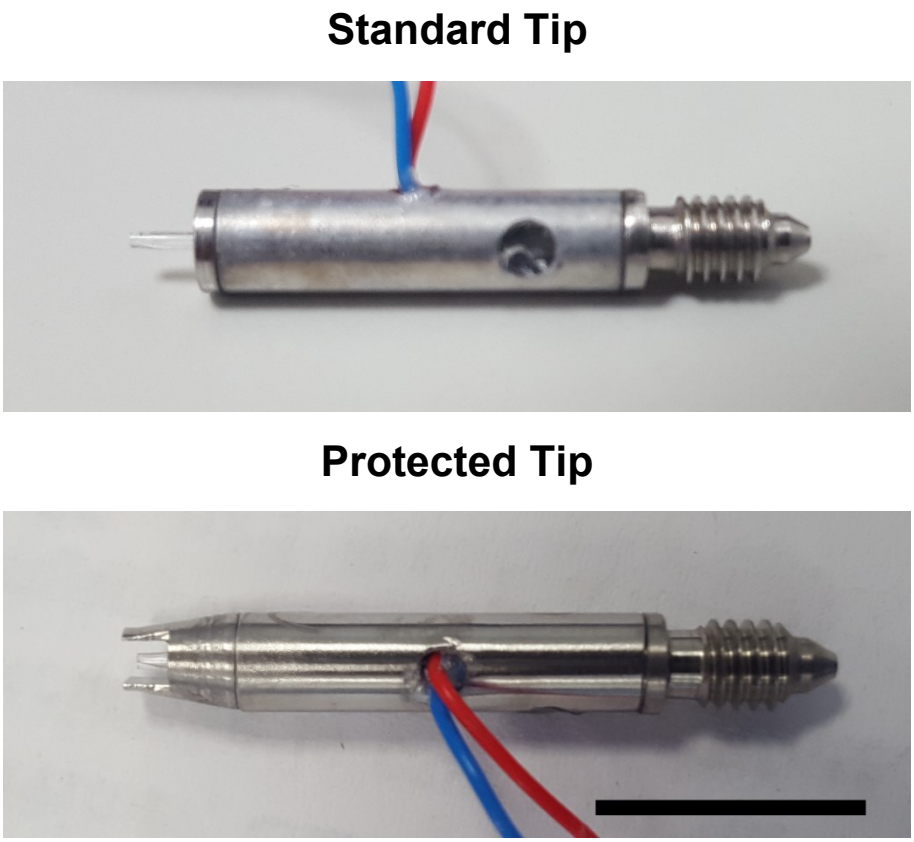

Figure 4.1 – MJ-AT series piezoelectric inkjet actuation device configurations. Scale bar = 10mm.

The on-board pneumatic regulator was controlled via the JetDrive® control software to provide a negative backpressure of between -0.1 and -0.3 psi at the reservoir, depending upon ink levels present during printing. The pressure level was adjusted prior to each print job to ensure that the ink meniscus at the nozzle tip remained flush with the orifice. This was required to maximise jetting performance and prevent fluid leakage or impeded droplet ejection, as shown in Figure 4.2.

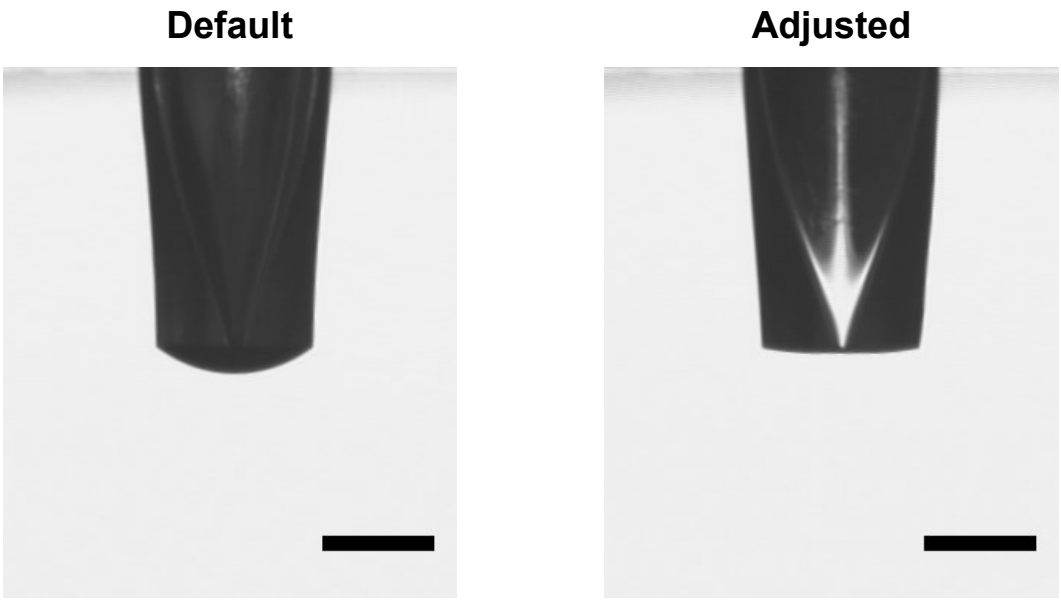

Figure 4.2 – Inkjet nozzle prior to and following backpressure adjustment. Scale bar = 400 µm.

A range of different waveform designs were assessed in order to maximise the jetting performance of various bioink solutions. The function of these designs was to modify the actuation voltage intensity, polarity and duration applied to the piezoelectric actuator within the nozzle to modify droplet ejection.

- A positive unipolar waveform configuration was developed that utilised a short ramp up period followed by a period of sustained applied voltage and equal ramp down period.
- A bipolar waveform was developed that incorporated a positive trapezoid pulse similar to that of the unipolar waveform, followed immediately by a negative trapezoid pulse.
- A tripolar waveform was developed that incorporated a similar pulse pattern to that of the bipolar waveform with the addition of a second trapezoid shaped positive pulse at the final stage of the waveform.

All waveforms were developed with a resting voltage of 0 V and maximum positive voltage of 70 V. A jetting frequency of 1000 Hz was selected for all printing experiments. These parameters were selected to maximise printing throughput whilst adhering to manufacturer recommendations to minimise piezoelectric depoling during extended periods of operation. Figure 4.3 provides a superimposed representation of each waveform design.

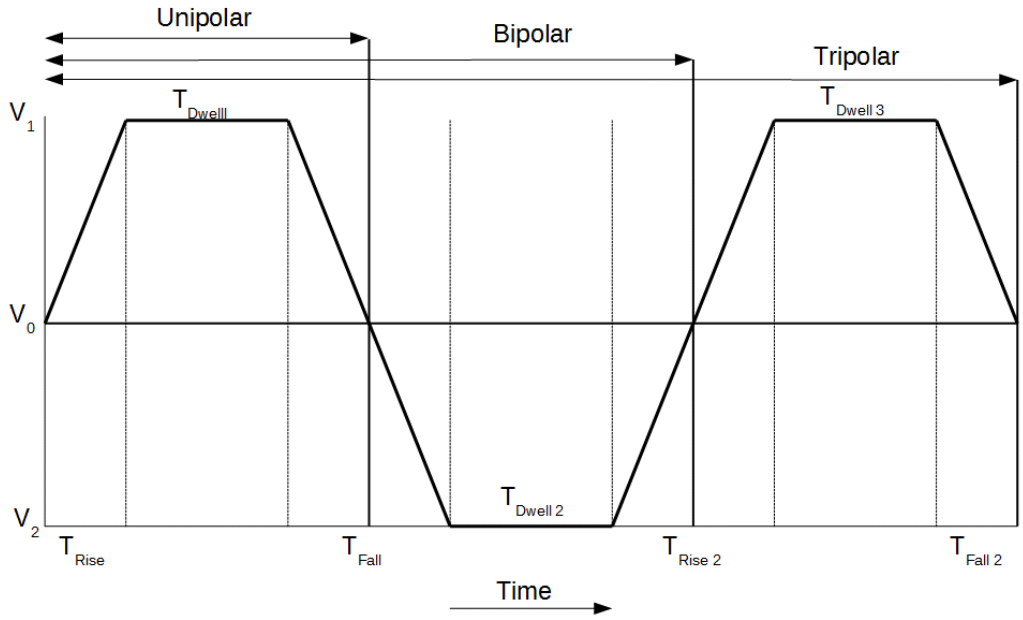

Figure 4.3 – Diagram of superimposed unipolar, bipolar and tripolar waveform designs used to apply an actuation signal to the piezoelectric inkjet actuation device.

4.2.2 Characterisation of Printing Performance

Droplet size and volume were calculated using the on-board stroboscopic camera in combination with the Aphelion® image processing software (ADCIS, France) incorporated within the JetDrive® printer control program. Droplets were dispensed from the inkjet nozzle and images captured using the stroboscopic camera following a strobe pulse generated synchronously with inkjet actuation. Adjustment of the timing delay of the strobe pulse following inkjet actuation enabled viewing of each stage of droplet ejection in response to different waveform configurations. Aphelion® image processing software was then used to identify the outline of the droplet across a series of sequential images. Droplet circumference, volume and velocity were calculated relative to the camera view scale and positional changes across the series of images.

Cell printing performance was determined by depositing 50 droplets per coordinate onto a glass slide and normalising the total cell count to droplet number. Single cell printing performance was characterised by manually counting the number of cells contained within single droplets sequentially deposited onto a glass slide. Cells were counted immediately following printing using a DMLB microscope (Leica Biosystems, Germany).

4.2.3 Polymeric Cell Coating

Single cell coating was performed using the polycationic polymer poly-l-lysine (PLL) hydrobromide (M_w =15-30 kDa) (Sigma-Aldrich, UK) across a range of concentrations.

Fluorescein isothiocyanate (FITC) labelled PLL (Sigma-Aldrich, UK) of an equal molecular weight was used for cell coating studies. PLL was dialysed for 2 days using a cellulose membrane (Sigma-Aldrich) with a molecular weight cut-off of 14 kDa. PBS dissolution was then performed to achieve a stock concentration of 1 mg / mL. The solutions were sterilised through filtration with a 0.22 µm pore size polyethersulfone filter (Sigma-Aldrich) and diluted to a desired final concentration using Hank's balanced salt solution. PLL-coated cell imaging was performed using an LSM800 point scanning confocal microscope (Carl Zeiss AG, Germany) at 40x magnification.

A PrestoBlue® assay was performed to assess the impact of PLL concentration on cellular metabolic activity. Mesenchymal stromal cells and chondrocyte cells were seeded at a density of 5,000 cells per well into a 96 well plate and incubated overnight to facilitate attachment. The media was then aspirated and replaced with media containing PLL at each specified concentration. Samples were incubated for a period of 15 minutes prior to washing with Hank's balanced salt solution (Sigma-Aldrich). Cell culture media was added to each well and the cells incubated for the desired time points before performing a PrestoBlue® metabolic activity assay as previously described.

To PLL coat the cells, a 200 µL cell suspension was prepared at a cell density of 10^7 cells per mL and the required concentration of coating solution added to achieve a final volume of 1 mL. As shown in Figure 4.4, the solution was agitated and incubated for 15 minutes at 37 °C, 5 % CO_2 to allow for cell coating. The coated cells were centrifuged at 200 *g* for 5 minutes and re-suspended in Hank's balanced salt solution twice to remove unattached polymer within the solution. Cells were re-suspended in cell culture media to achieve the desired density for cell seeding.

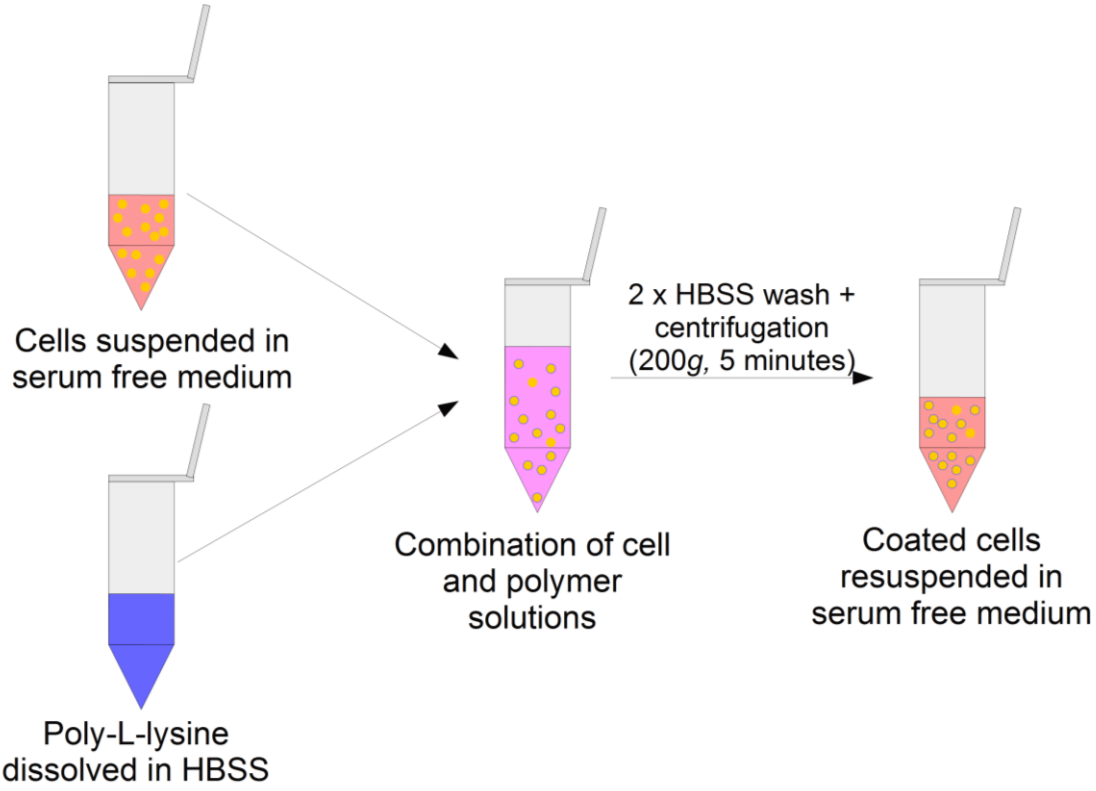

Figure 4.4 – Diagram depicting the stages of an in-house developed poly-l-lysine cell coating protocol developed to reduce cellular agglomeration.

4.3 Results

4.3.1 Waveform Optimisation

An initial series of experiments were performed in order to evaluate the performance of the inkjet printing device for depositing cell culture media. The first experiment compared the effect of a range of different waveform designs on droplet formation characteristics using the on-board stroboscopic camera. Figure 4.5 displays the droplet ejection behaviour resulting from each of the three waveform designs assessed.

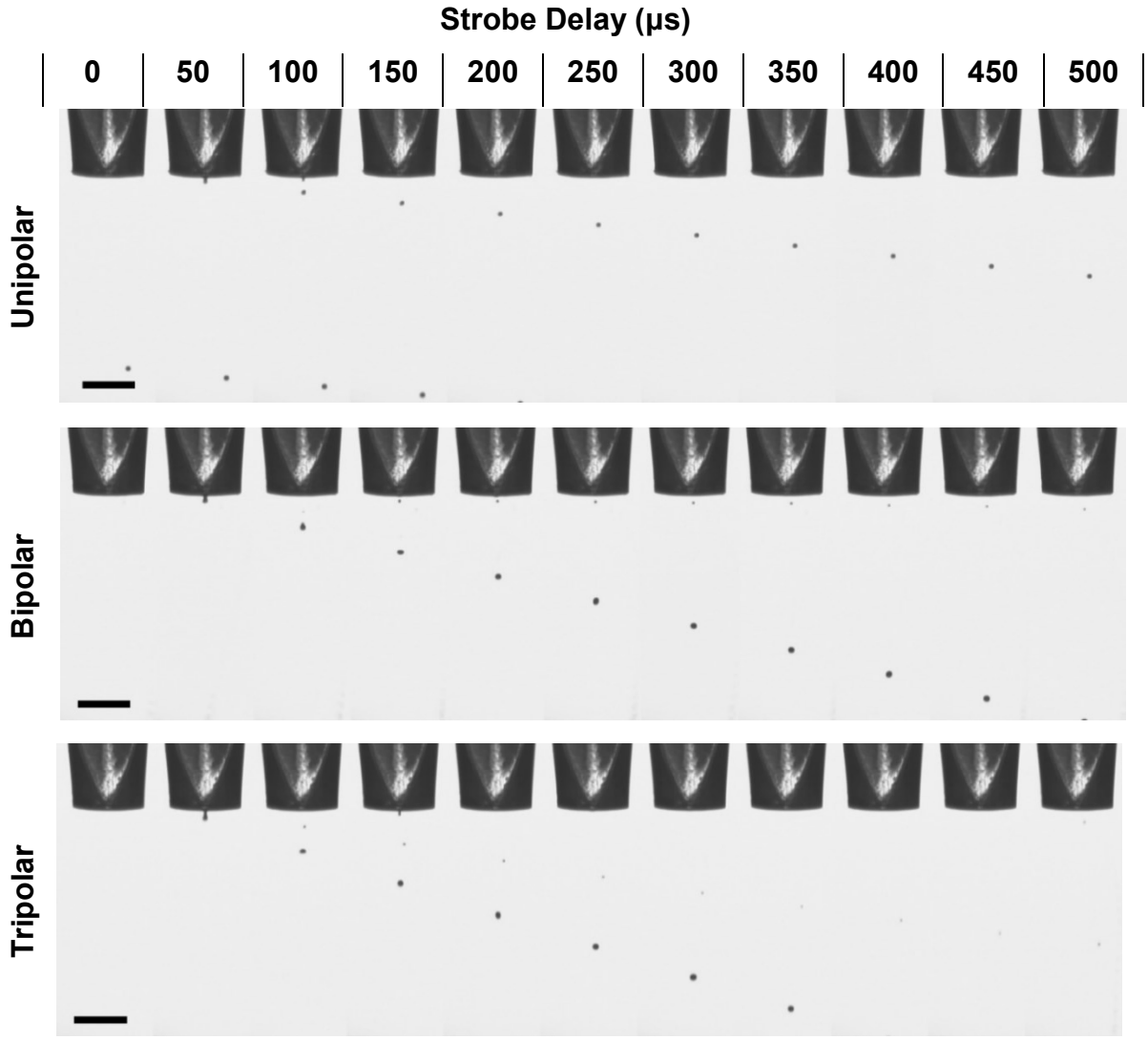

Figure 4.5 – Sequential droplet ejection images for each waveform design captured using the JetLab® on-board stroboscopic camera using an incremental strobe delay of 50 µs. Cell culture media was deposited at a jetting frequency of 1000 Hz and actuation voltage of 20 V. Scale bar = 400 µm.

All three waveforms were found to be capable of ejecting droplets of cell media under normal conditions. The tripolar configuration was found to be the least versatile, with jetting only achievable over a narrow voltage and dwell time range. Droplet ejection velocity was

reduced when using a unipolar waveform design, irrespective of other waveform parameters.

Droplet ejection performance was found to be highly dependent upon waveform design, with tripolar waveform configurations particularly susceptible to jetting instability. Ink accumulation around the nozzle orifice as well as air ingestion and entrapment within the nozzle was observed during extended jetting periods, resulting in jetting failure as depicted in Figure 4.6.

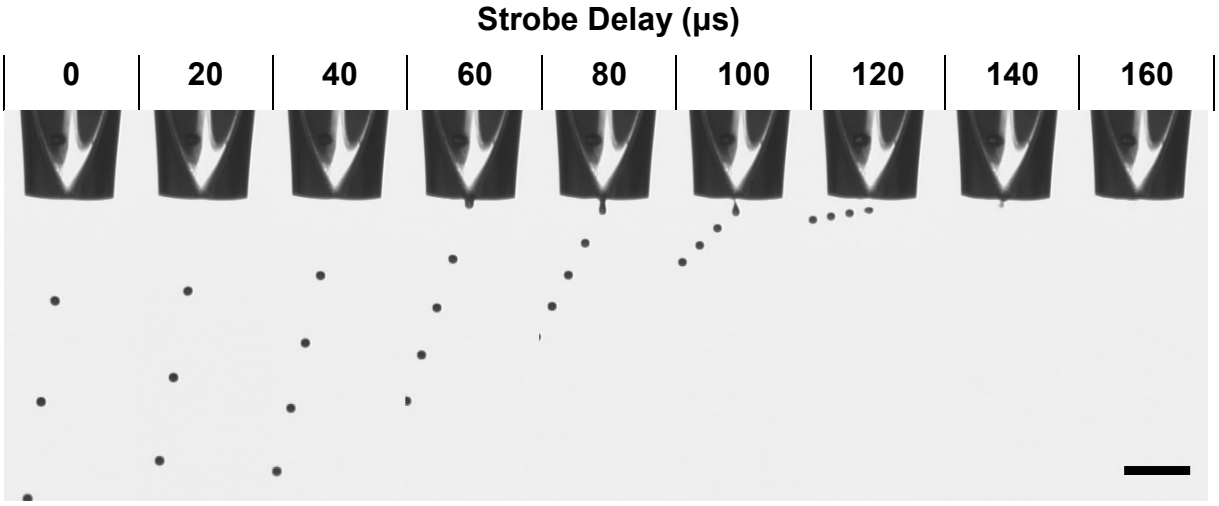

Figure 4.6 – Sequential droplet ejection images captured using the JetLab® on-board stroboscopic camera using an incremental strobe delay of 20 µs. Cell culture media was deposited at a jetting frequency of 1000 Hz and actuation voltage of 20 V. Scale bar = 400 µm.

Further assessment of the impact of voltage and dwell time on droplet formation characteristics was performed using the unipolar and bipolar waveform designs. An approximate minimum voltage of 20 V and dwell time of 4 µs was required to achieve droplet ejection across both unipolar and bipolar waveform designs as shown in Figure 4.7. Unipolar droplet ejection characteristics exhibited two discrete regions of stable droplet formation. Bipolar droplet ejection characteristics exhibited a single region of stable droplet formation with a correlation observed between dwell time and voltage application.

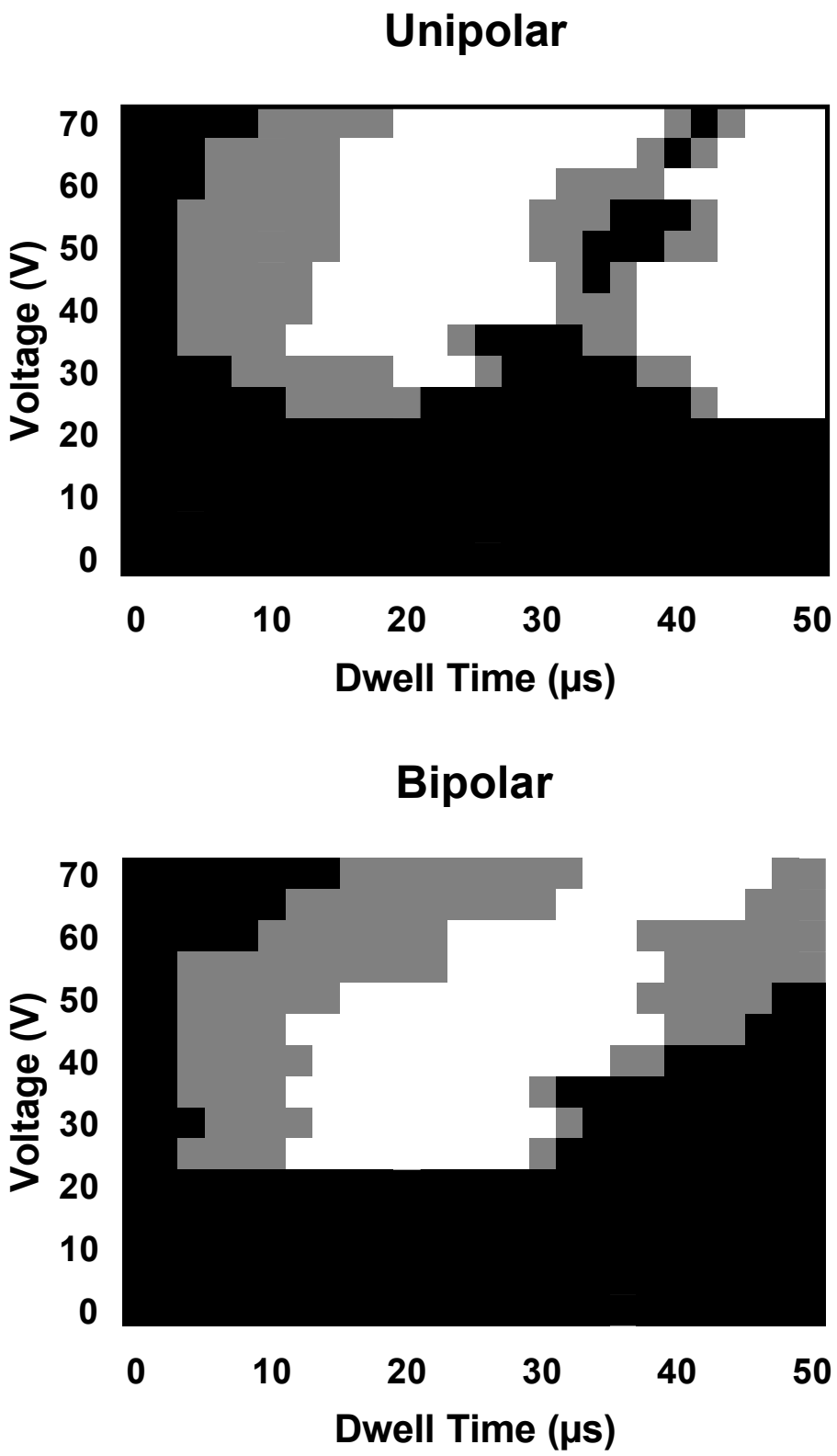

Figure 4.7 – Heat map showing the effect of jetting parameters on droplet ejection characteristics when dispensing cell culture media. ▱ = Stable droplet formation. ▰ = Unstable droplet formation. ▰ = No droplet ejection.

Figure 4.8 highlights the impact of each waveform design on droplet formation characteristics. Droplet volume and velocity were quantified using the on-board image analysis software.

The bipolar waveform design was observed to generate droplets of a higher velocity and volume in comparison to the unipolar design, irrespective of the dwell time applied to the actuation signal. An optimal dwell time configuration was determined to be 18 µs for the unipolar waveform and 30 µs for the bipolar waveform to consistently generate single droplets at a high ejection velocity and volume.

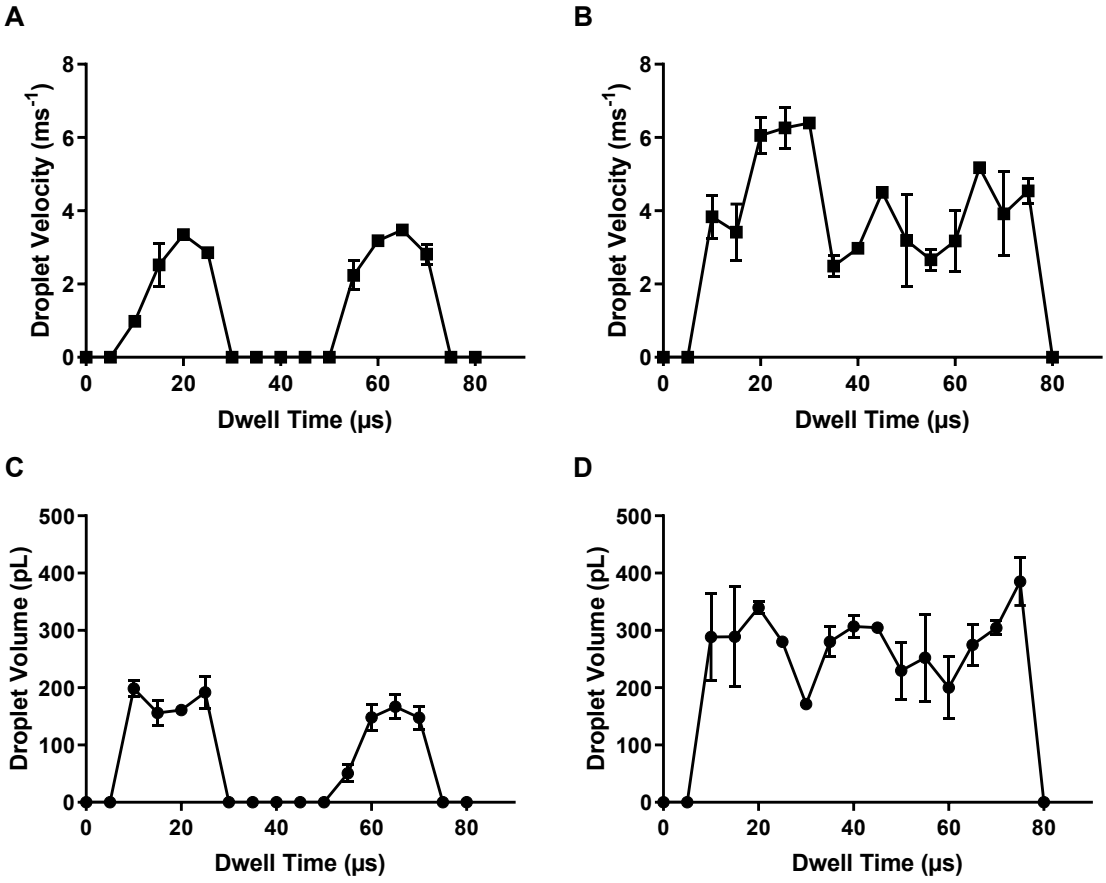

Figure 4.8 – Influence of dwell time on primary droplet ejection properties for unipolar and bipolar waveform designs at an actuation voltage of 40 V / -40 V. (A) Unipolar droplet ejection velocity. (B) Bipolar droplet ejection velocity. (C) Unipolar droplet ejection volume. (D) Bipolar droplet ejection volume. Data represents mean values ± SD. N=3.

Further comparison between the unipolar and bipolar waveform designs under the defined dwell time parameters highlighted a correlation between actuation voltage and droplet velocity, irrespective of waveform design. Figure 4.9 indicates that the bipolar waveform was capable of generating droplets with a higher ejection velocity than the unipolar waveform

configuration across each voltage configuration assessed. Droplet volume remained stable across a larger voltage range for the bipolar waveform design.

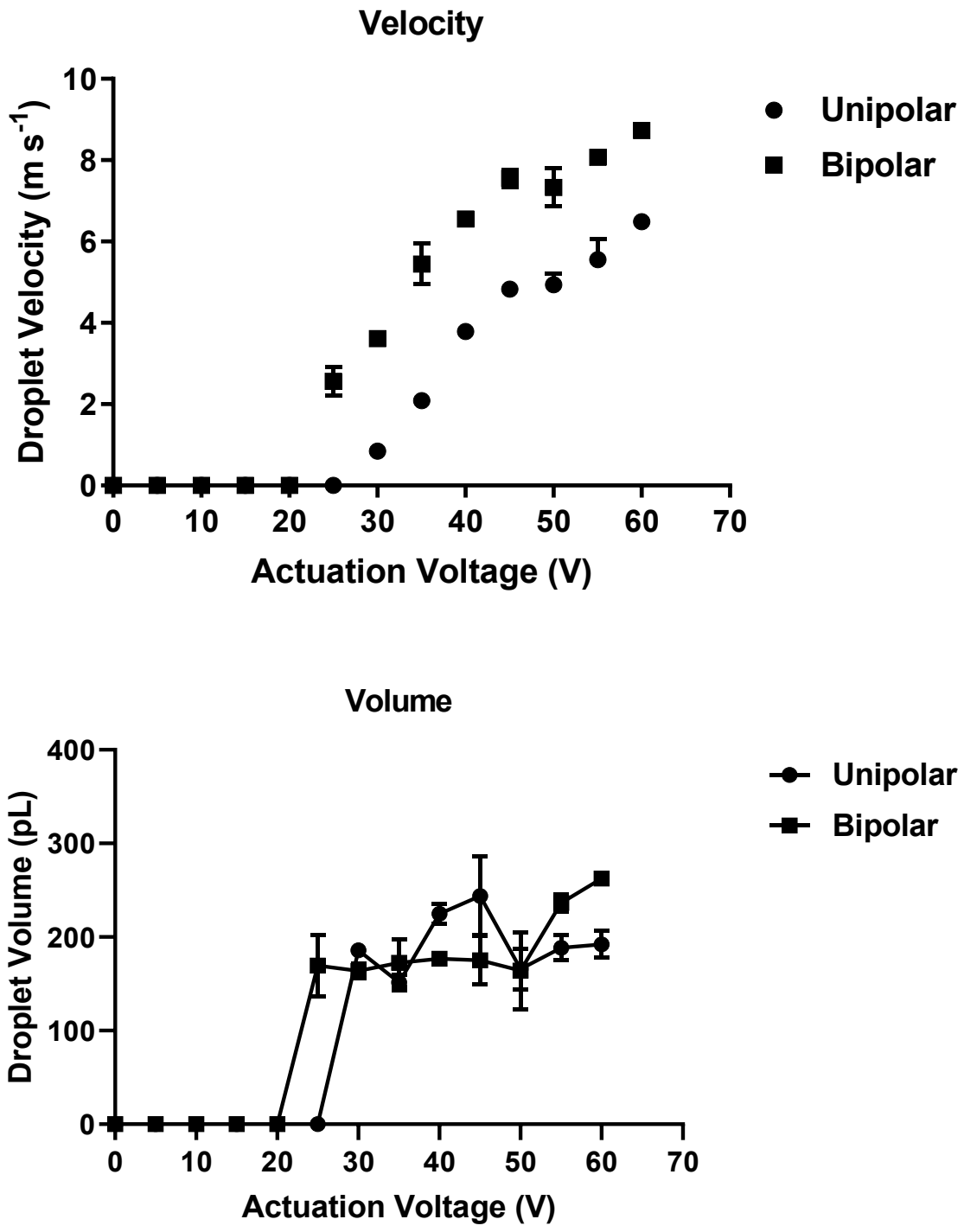

Figure 4.9 – Effect of actuation voltage on primary droplet ejection velocity and volume for unipolar and bipolar waveform designs at a dwell time of 18 and 30 µs respectively. Data represents mean values ± SD. N=3.

An additional study was performed to assess the influence of inkjet nozzle orifice size on droplet ejection characteristics. Data within Figure 4.10 displays a negative correlation between nozzle size and droplet velocity across the three nozzle diameters tested. Droplet volume was shown to increase in response to increases in the nozzle orifice diameter.

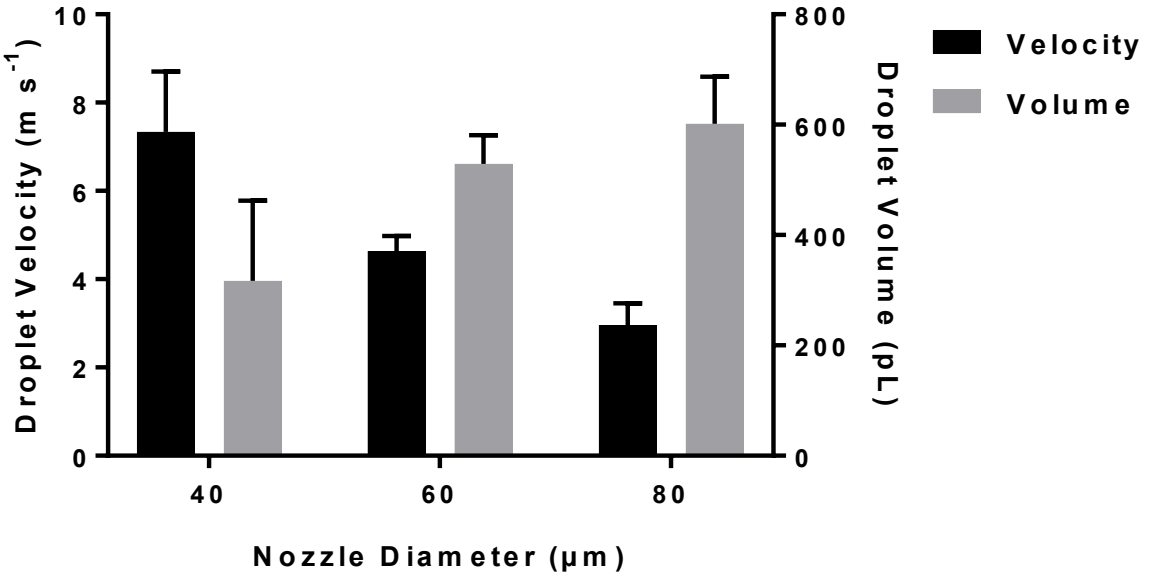

Figure 4.10 – Influence of nozzle orifice diameter on droplet ejection characteristics when depositing cell culture medium using a bipolar waveform design at an actuation voltage of 70 / -70 V and dwell time of 30 µs. Data represents mean values ± SD. N=6.

4.3.2 Cell Deposition Performance

Following material jetting characterisation, a range of further characterisation steps were performed to compare the effect of unipolar and bipolar waveform designs on cell printing performance. For these studies it was necessary to increase the minimum actuation voltage applied to the jetting device to 40 V in order to maintain printing performance.

The data in Figure 4.11 highlights the impact of waveform design on cell printing performance. The bipolar waveform design was shown to deposit approximately 0.5 cells per droplet across the three dwell times assessed. The unipolar waveform design failed to eject any material outside of the 20 µs dwell time range applied, resulting in no cells being deposited.

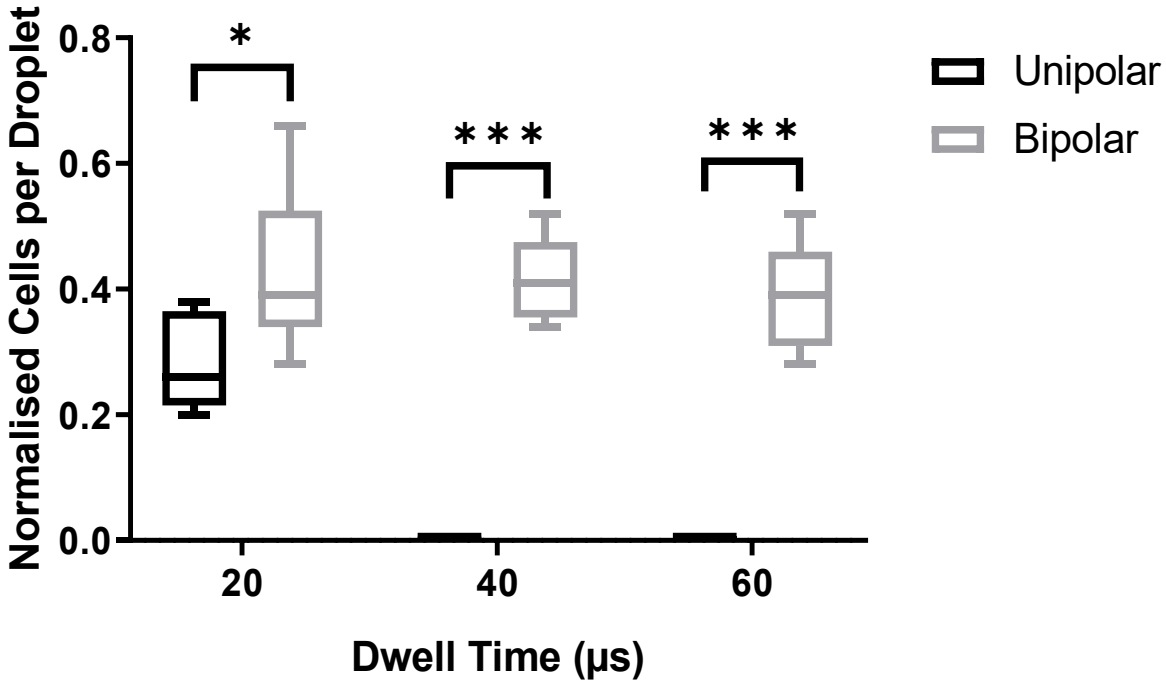

Figure 4.11 – Effect of waveform design and dwell time on inkjet cell printing performance when depositing MSCs at a concentration of 10^6 cells per mL. Data represents quartile values ± min / max values. N=6.

The impact of cell ink concentration was also assessed across each dwell time configuration for the bipolar waveform design as shown in Figure 4.12. The cell density per droplet was shown to increase as expected in response to increases in the cell ink concentration loaded into the printer. An increase in variability was also observed in response to an increase in cell ink concentration, irrespective of the applied dwell time.

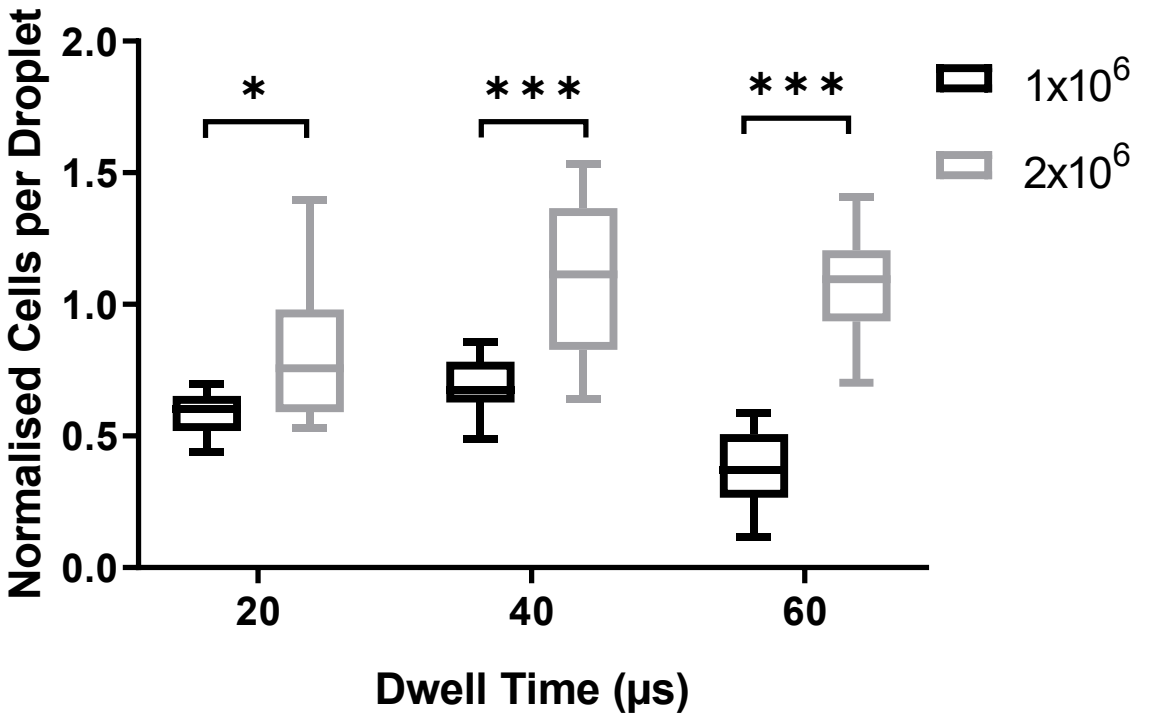

Figure 4.12 – Effect of cell concentration on inkjet printing performance across a range of different bipolar waveform dwell times. MSCs were deposited at a concentration of 10^6 cells per mL. Data represents quartile values ± min/max values. N=6.

An important consideration when studying the cell printing performance of the inkjet actuation device was the period in which the device had been inactive prior to commencing printing. A significant increase in cell density was temporarily observed following periods of inactivity where cells had been retained within the reservoir of the printing system.

The data presented in Figure 4.13 provides a quantification of this effect through comparing the cell printing performance of the inkjet system immediately following a purging cycle versus a sustained resting period. Cell density per printed droplet was observed to remain relatively stable over the course of a series of 10 subsequent actuation cycles where previous actuation immediately prior to the printing command had taken place. However, a temporary increase in cell density per droplet was observed where the printer had been inactive for a period in excess of 1 minute.

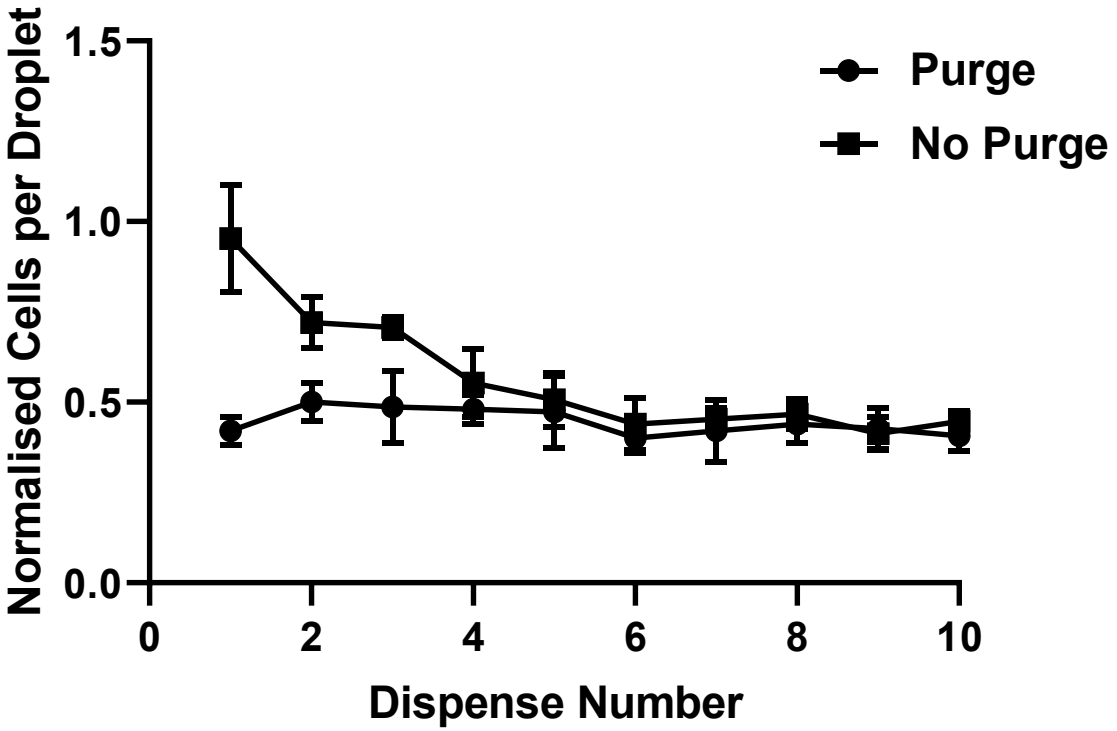

Figure 4.13 – Impact of nozzle purging on cell printing performance immediately prior to dispensing. Data represents mean values ± SD. N=3.

To determine the maximum possible resolution of the inkjet printing platform, a further experiment was performed using the previously defined printing parameters.

The sequential droplet deposition data displayed in Figure 4.14 highlights the frequency of achieving 1 cell per droplet for the MSC and chondrocyte cell types at ink concentrations of 1 and 2 million cells per mL.

At an ink concentration of 1 million cells per mL, a similar number of droplets contained either a single cell or none. Less than 10 per cent of droplets ejected contained more than a single cell for either cell type. At a concentration of 2 million cells per mL, an approximate cell density per droplet of 1 was achieved in the highest proportion of droplets assessed, with a smaller proportion of additional droplets containing either no cells or multiple cells, correlating with a Poisson probability distribution. No significant difference in cell density per droplet was observed when comparing the jetting performance of MSC and chondrocyte cell types. A cell density equivalent to approximately 1 cell per droplet was achieved at an ink concentration of 2 million cells per mL.

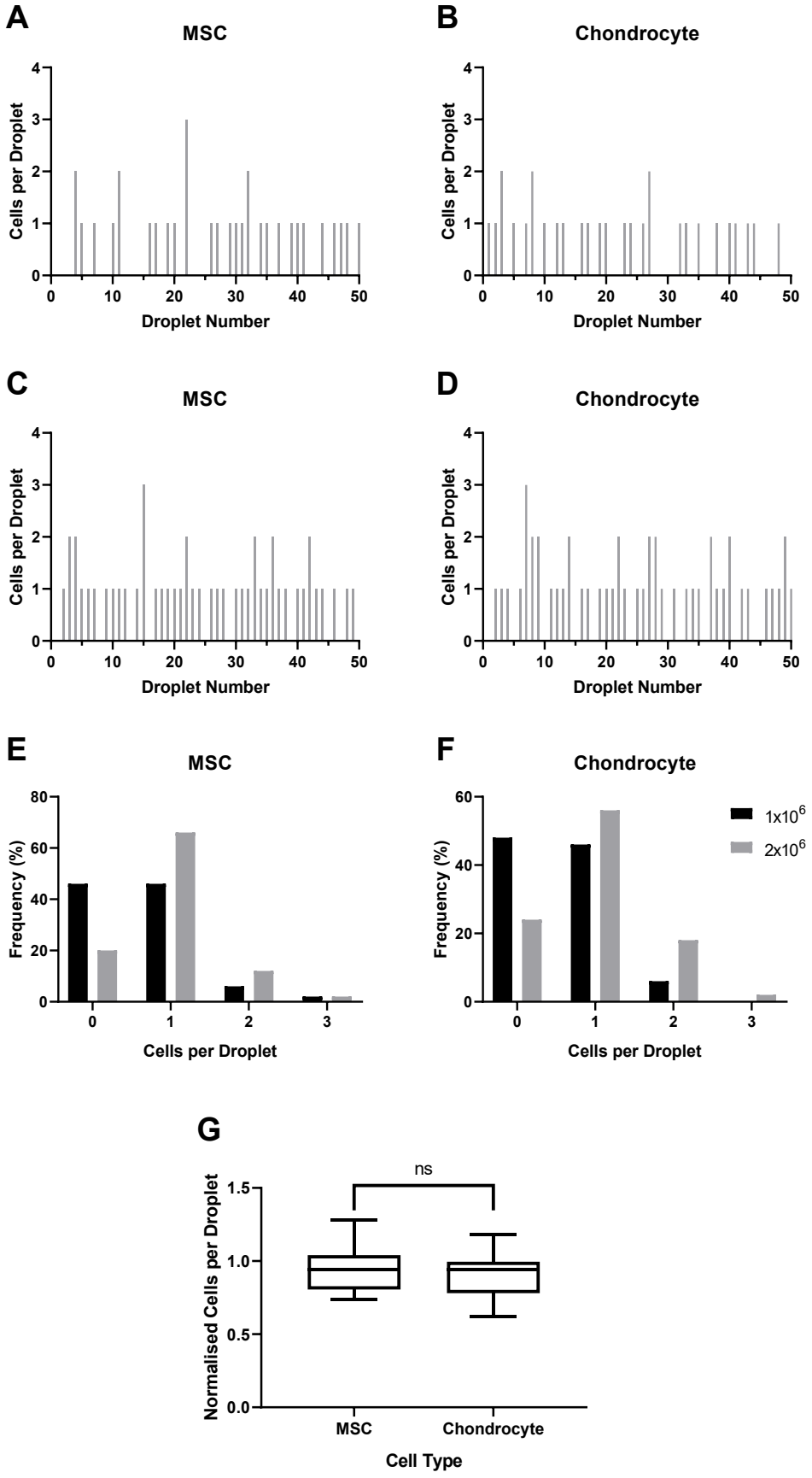

Figure 4.14 – Inkjet cell dispensing performance using an optimised bipolar waveform. Cell density per droplet for the MSCs (A) and chondrocytes (B) at an ink concentration of 1

million cells per mL. Cell density per droplet for the MSCs (C) and chondrocytes (D) at an ink concentration of 2 million cells per mL. Frequency distribution graphs showing the percentage of droplets containing different MSC (E) and chondrocyte (F) concentrations. (G) Normalised cell density per droplet for each cell type. N=50.

Figure 4.15 provides a sequential droplet ejection image array of cells deposited using the bipolar waveform design. A single primary droplet was ejected from the nozzle orifice with minimal ligand formation, preventing the formation of additional satellite droplets.

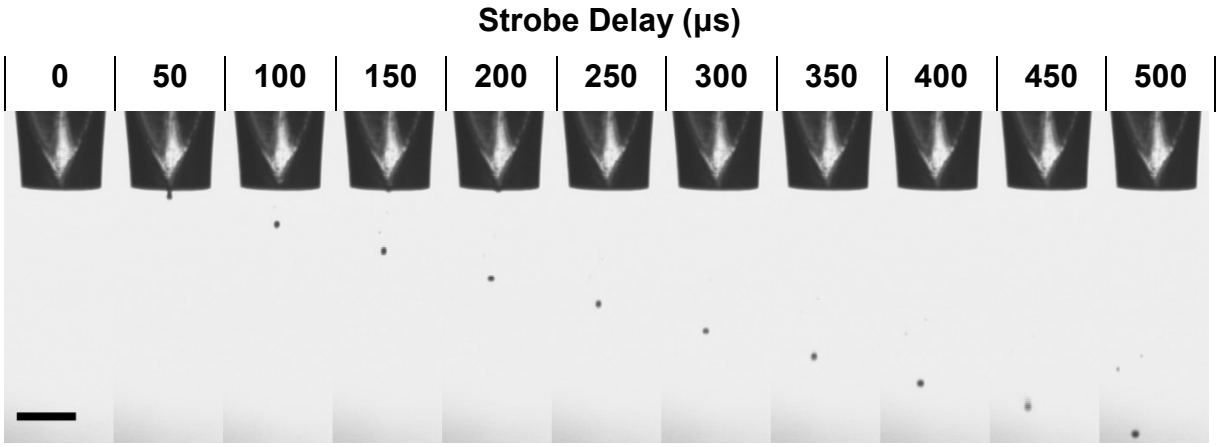

Figure 4.15 – Deposition of MSCs at a concentration of 10^6 cells per mL in cell culture media using a bipolar waveform design. Images were captured using a sequential strobe delay of 50 µs. Scale bar = 400 µm.

4.3.3 Biological Impact Assessment

Following assessment of cell deposition performance, it was necessary to characterise the effects of the printing process on cellular viability and function. A combination of morphological analysis and cell viability, proliferation and metabolic activity assays were used to characterise the cellular effects of the printing process.

Figure 4.16 displays the results of the Live/Dead® cell viability assay performed on cell samples deposited via the inkjet printing process versus manually pipetted controls. The ratio of live to dead cells, labelled green and red respectively, was maintained between manually seeded control samples and printed cells both immediately following and 24 hours after printing for both cell types. Cells appear smaller whilst in suspension immediately following printing, with cell adherence to the culture vessel surface and subsequent cell spreading occurring within a 24 hour period.

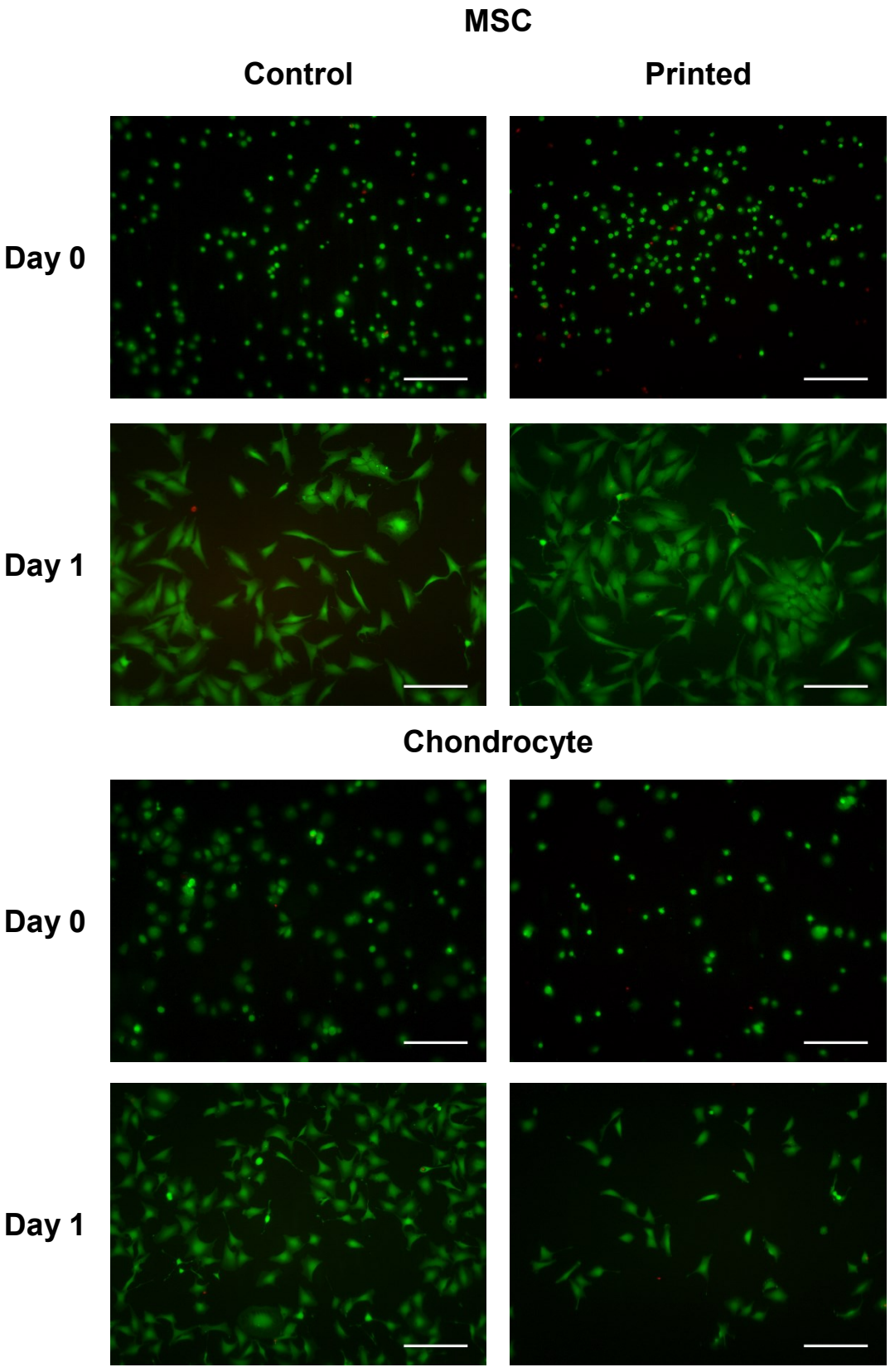

Figure 4.16 – Live / Dead® microscopy images displaying the viability of cells processed using the inkjet actuation device relative to manually pipetted control samples immediately following and 24 hours after printing. Scale bar = 200 µm.

An MTT metabolic activity assay was performed to assess the impact of the printing process on the overall metabolic activity of each cell type following seeding. No significant difference in metabolic activity was observed between printed and manually seeded cells at each time point for the MSC or chondrocyte cell lines, as displayed in Figure 4.17.

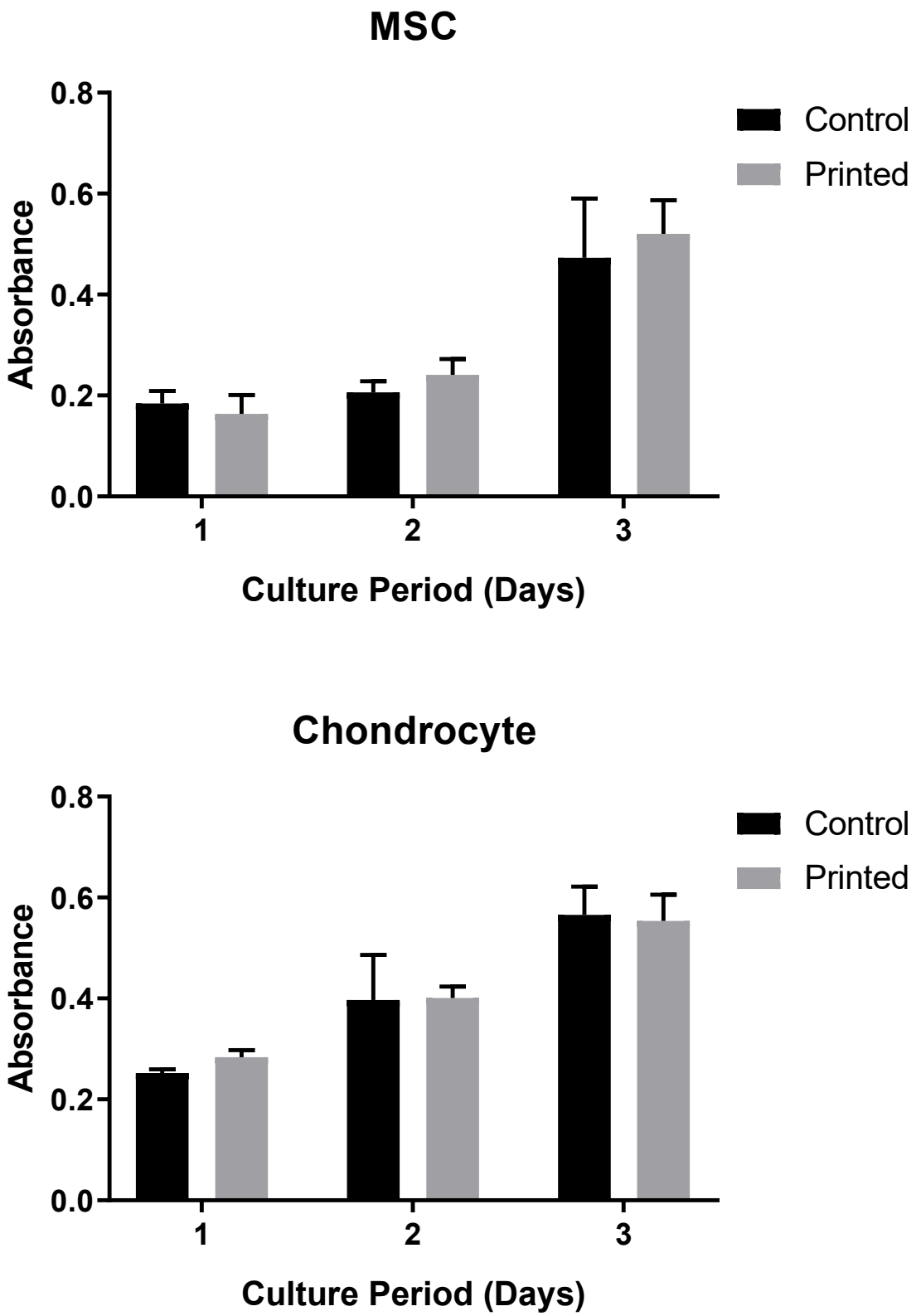

Figure 4.17 – MTT metabolic activity assay displaying the effect of the inkjet printing process on cellular metabolic activity when compared with manually seeded cells over a 3 day period for MSC and chondrocyte cell types. Data represents mean values ± SD. N=6.

Confocal microscopy was used to assess the morphology of each cell type prior to and following printing. The fluorescence microscopy data presented in Figure 4.18 and Figure 4.19 compares the effect of the printing process on cell morphology immediately after printing and after a subsequent incubation period. No discernible difference in cell morphology or adherence rate was observed for either cell line when compared with manually seeded samples.

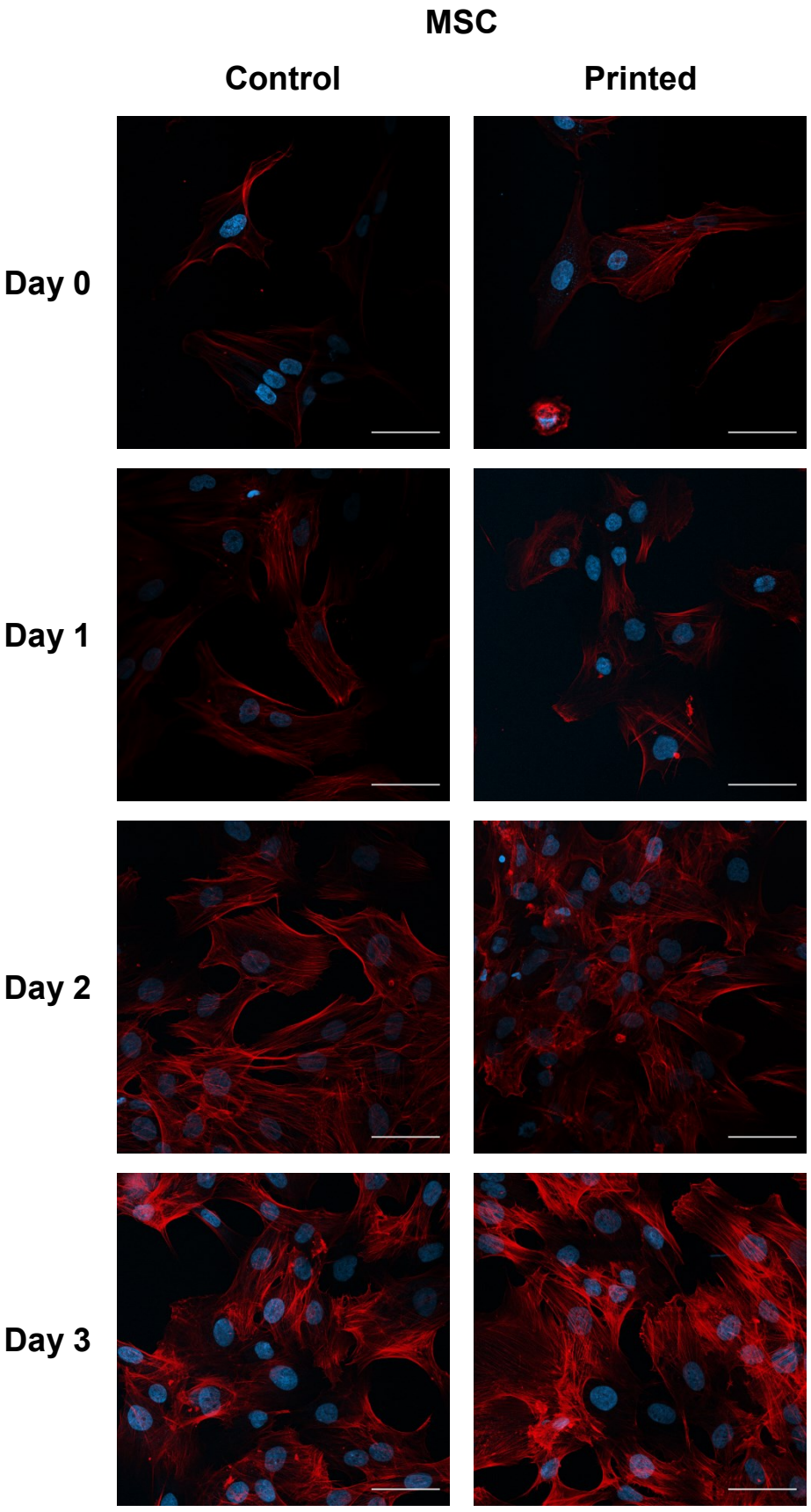

Figure 4.18 – Influence of inkjet printing process on cell morphology for the MSC line. Cell nuclei were visualised using DAPI (blue) and F-actin using phalloidin (red) staining. Scale bar = 50 µm.

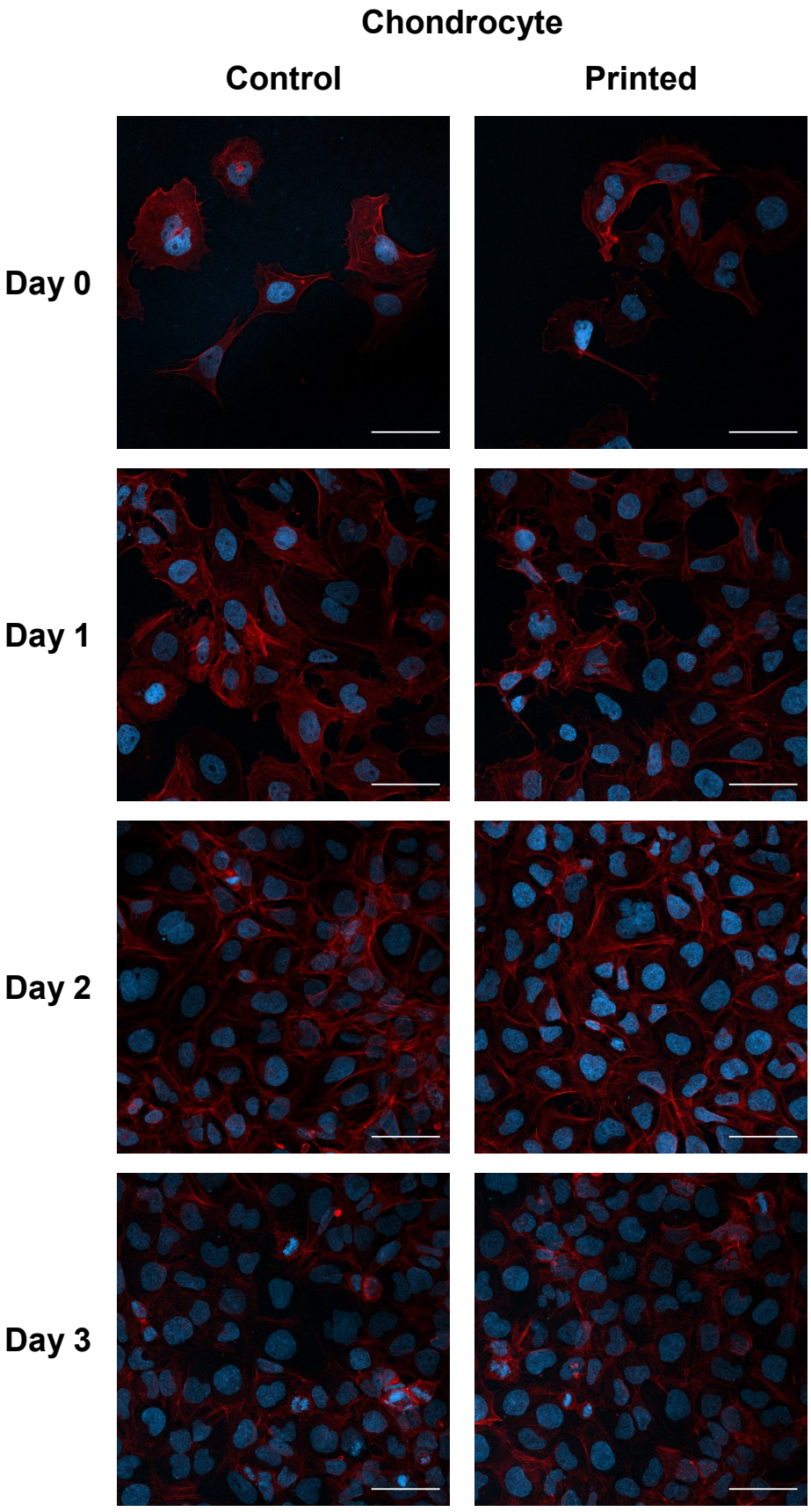

Figure 4.19 – Influence of inkjet printing process on cell morphology for the chondrocyte cell line. Cell nuclei were visualised using DAPI (blue) and F-actin using phalloidin (red) staining. Scale bar = 50 µm.

An additional study was performed to further analyse the effect of the inkjet printing process on cell viability through monitoring the rate of cell growth following printing. The data in Figure 4.20 displays the population growth rate and cell viability of MSC and chondrocyte cell types subjected to the inkjet printing process. No significant difference in population doubling time was observed when comparing samples of cells deposited via manual and inkjet printing techniques.

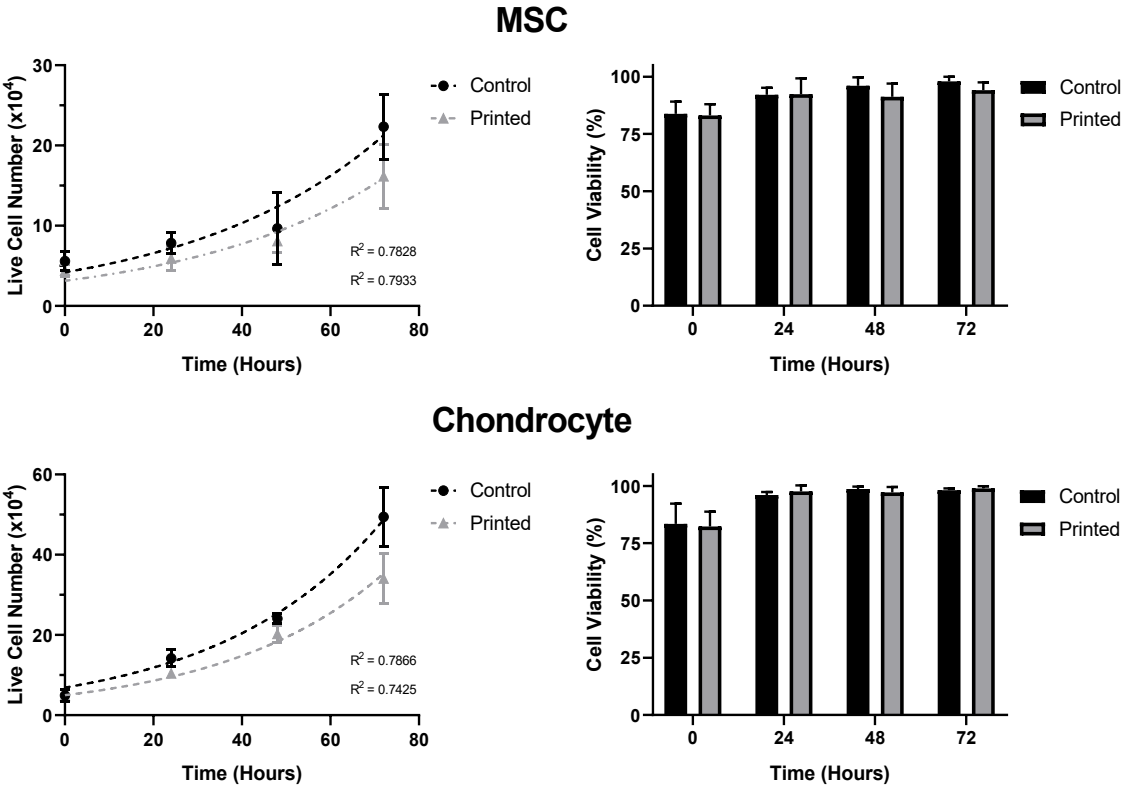

	MSC		Chondrocyte	
	Control	**Printed**	**Control**	**Printed**
Y0 (x10^4)	3.97	3.43	6.26	5.87
K (Hours^{-1})	0.023	0.021	0.029	0.025
Doubling Time (Hours)	29.58	32.87	24.17	28.17

Figure 4.20 – Effect of inkjet printing process on the proliferation rate of MSC and chondrocyte cell lines in comparison to manually seeded cells. (Left) Live cell number assessed via a trypan blue exclusion test. (Right) Percentage of live cells counted at each time point. (Bottom) Parameters obtained from nonlinear regression analysis using an exponential growth model of cell proliferation data. Data represents mean values ± SD. N=6.

4.3.4 Cell Aggregation

A deterioration in printing performance was observed when jetting cellular material for extended periods of time. This resulted in failed print jobs, and in some cases required full disassembly and cleaning of the printing device. This was despite the production of droplets of uniform consistency using the optimised printing parameters previously defined.

The deterioration in performance was caused by the agglomeration of cells within the printer reservoir leading to blockage of the nozzle orifice. Figure 4.21 displays the nozzle prior to, during and following extended periods of jetting. The accumulation of cells within the nozzle was observed via the on-board camera, which showed the progressive blocking of the orifice over the course of the print. Microscopic analysis following printing showed the presence of large agglomerates of cells within the nozzle orifice, preventing further material flow from the nozzle.

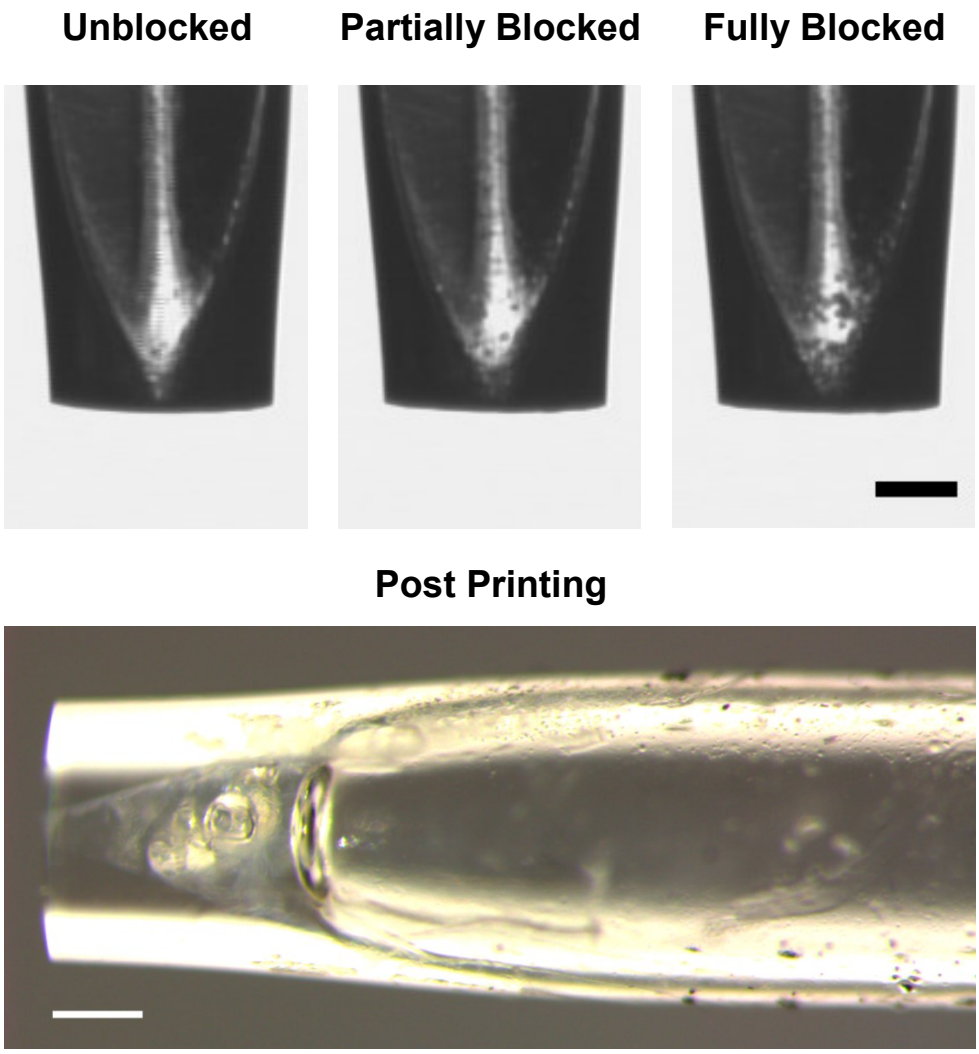

Figure 4.21 – Nozzle blockage and cell sedimentation captured using the JetLab® on-board stroboscopic camera (top) and via a microscope (bottom) when depositing cells at a concentration of 10^6 cells per mL in cell culture media. Scale bar = 200 µm.

It was therefore necessary to assess potential modifications to the printing process in order to reduce the rate of cellular agglomeration and minimise the possibility of nozzle blockages occurring. This included the use of agitation systems to minimise the rate of cell sedimentation during extended periods of printing, as well as the coating of cell membranes with poly-l-lysine to prevent cellular agglomeration.

4.3.5 Polymeric Cell Coating

The effect of the cell coating process on cellular viability and metabolic activity was assessed in order to determine the most appropriate poly-l-lysine concentration for cell coating.

Fluorescence microscopy images from the Live / Dead® assay shown in Figure 4.22 indicate an equal proportion of live to dead cells across both cell lines up to a PLL concentration of 50 µg / mL. A significant reduction in live cell number immediately following and 24 hours after the coating process was observed across samples exposed to PLL concentrations of 50 and 100 µg / mL.

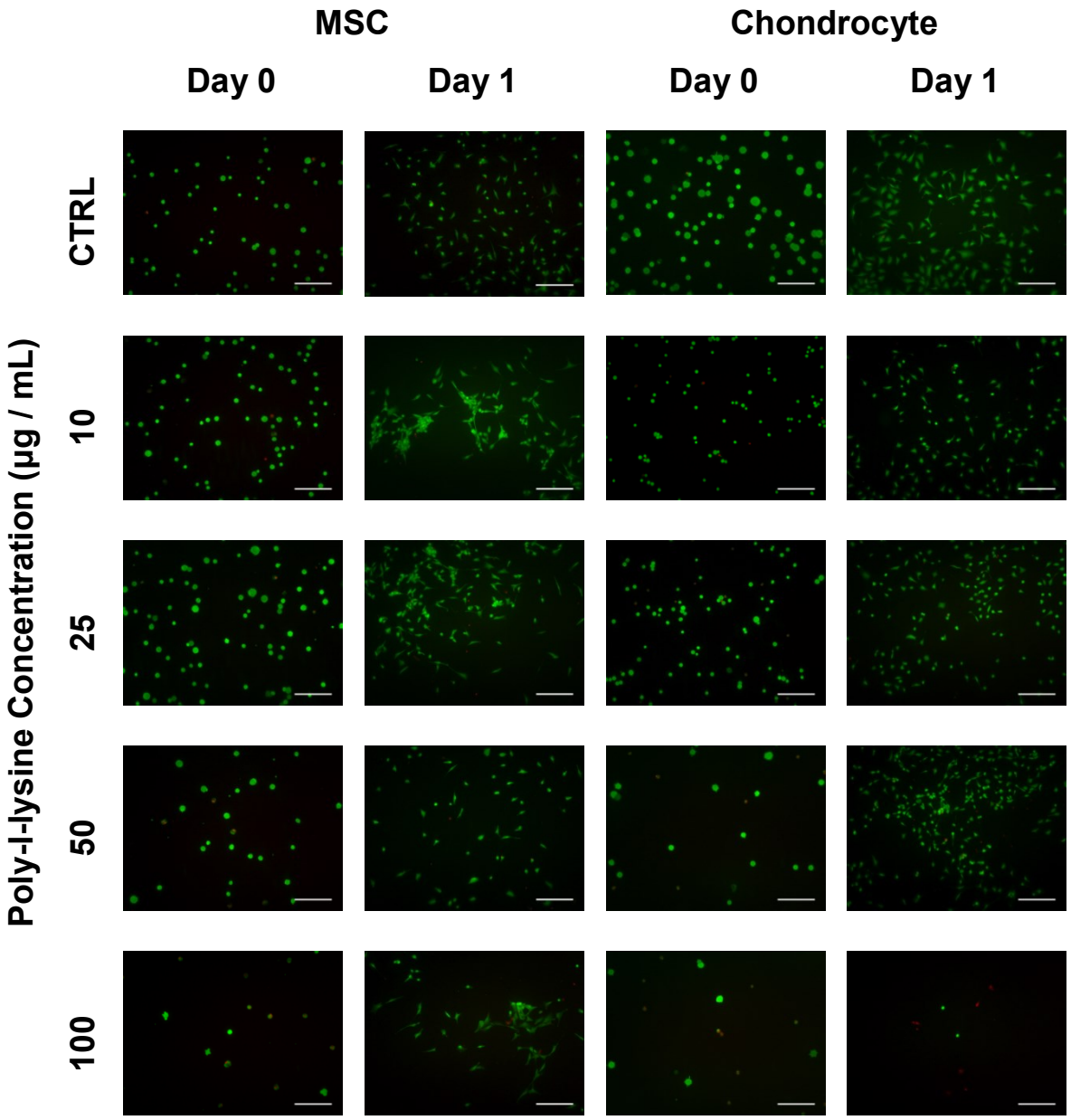

Figure 4.22 – Effect of PLL coating concentration on cellular viability of the MSC and chondrocyte cell lines immediately following and 24 hours after coating. Scale bar = 200 µm.

Metabolic activity data displayed in Figure 4.23 quantifies the effect of PLL coating concentration on cellular metabolic activity across a range of time points. A significant initial reduction in metabolic activity was observed for the MSC and chondrocyte cell lines in response to polymer concentrations in excess of 25 µg / mL. Although metabolic activity was shown to increase over the 72 hour incubation period, this was not sufficient to match the activity of untreated MSCs. A partial recovery in metabolic activity over 72 hours was observed for chondrocyte cells exposed to a PLL concentration of 50 µg / mL or greater. Below this concentration, no significant difference in metabolic activity was observed between PLL coated and untreated cells at the final time points.

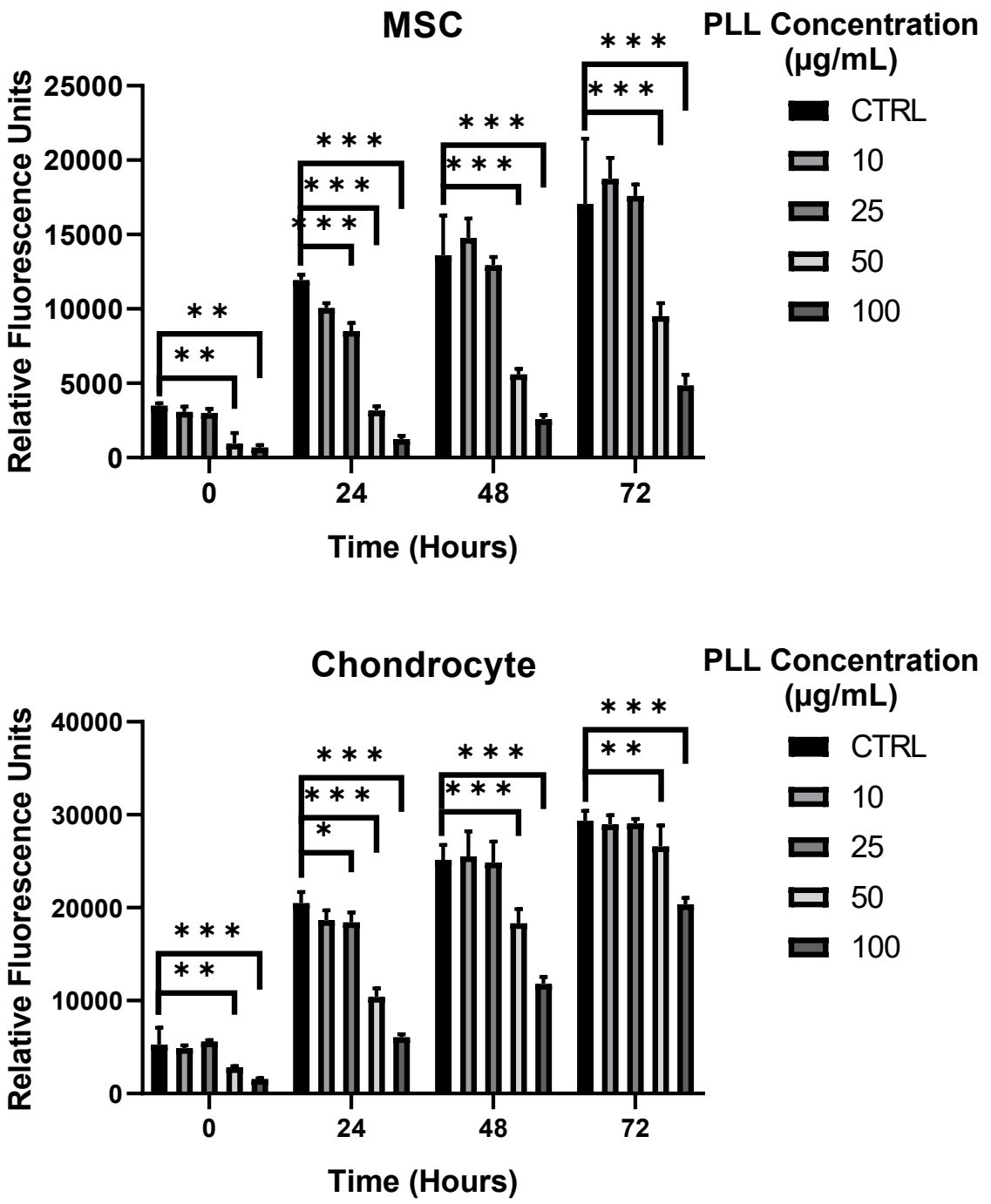

Figure 4.23 – Effect of PLL coating concentration on cellular metabolic activity for the MSC and chondrocyte cell lines. Data represents mean values ± SD. N=6.

Confocal microscopy was performed on samples coated with FITC-conjugated PLL to identify the efficiency and stability of the single cell coating process, as well as its subsequent degradation and internalisation. FITC-PLL fluorescence intensity and coating efficiency was shown to increase in response to increasing PLL concentration, with full cell coating achieved

at concentrations of 50 µg / mL or higher in the MSCs, as shown in Figure 4.24. At lower concentrations, speckling of FITC-PLL was visible on the cell surface. Following a 24 hour incubation period all cells displayed speckled areas of PLL.

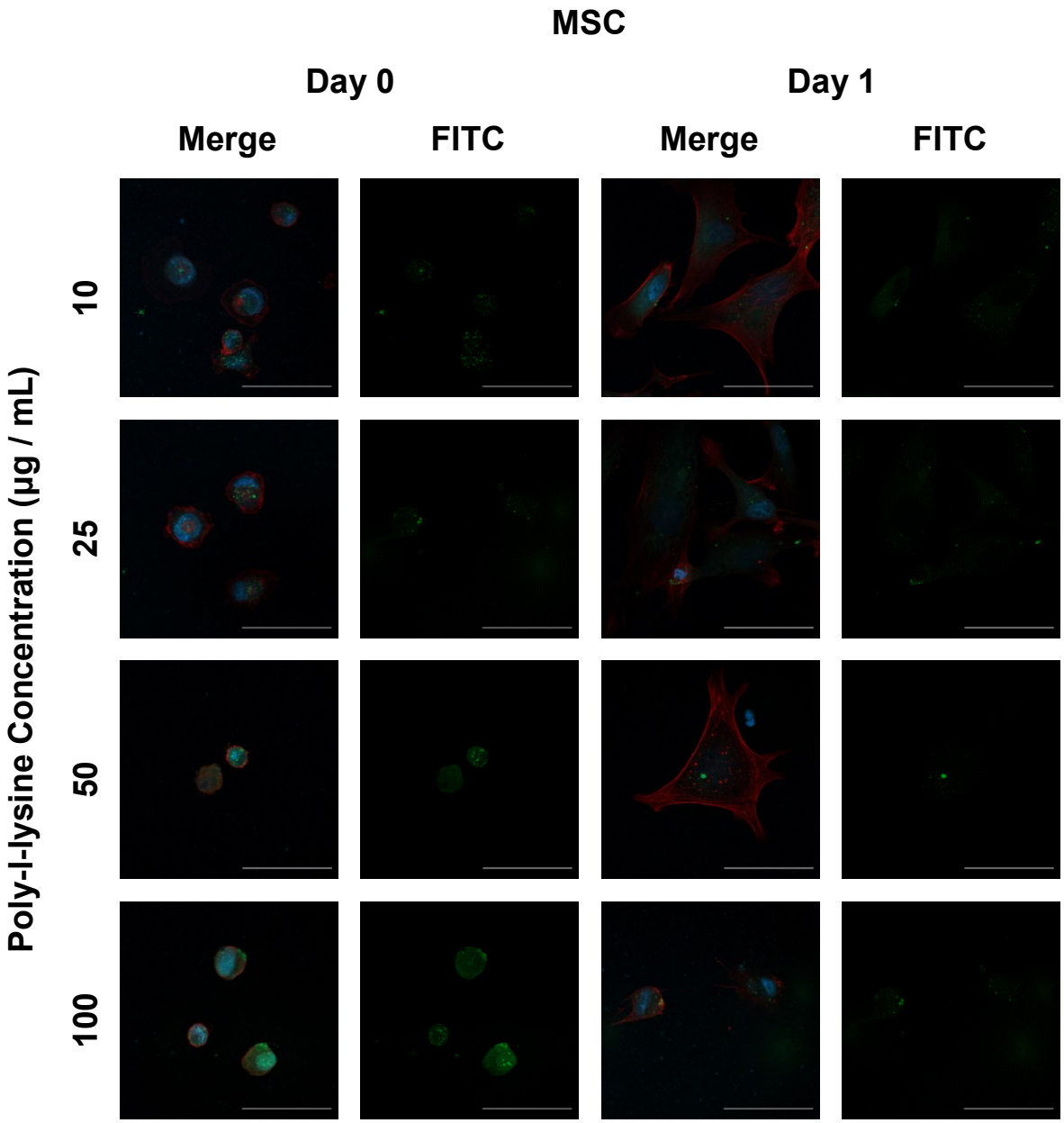

Figure 4.24 – Cell coating efficiency of FITC-conjugated PLL (green) at various concentrations for the MSC line. Cells were imaged immediately following and 24 hours after coating. Cell nuclei were visualised using DAPI (blue) and F-actin using phalloidin (red) staining. Scale bar = 50 µm.

Chondrocyte cells exposed to the coating process demonstrated speckling across the full concentration range assessed, with none of the tested concentrations sufficient to fully coat the cell membrane, as shown in Figure 4.25. Evaluation of the cells 24 hours following coating revealed a similar reduction in speckling intensity to results obtained for the MSCs.

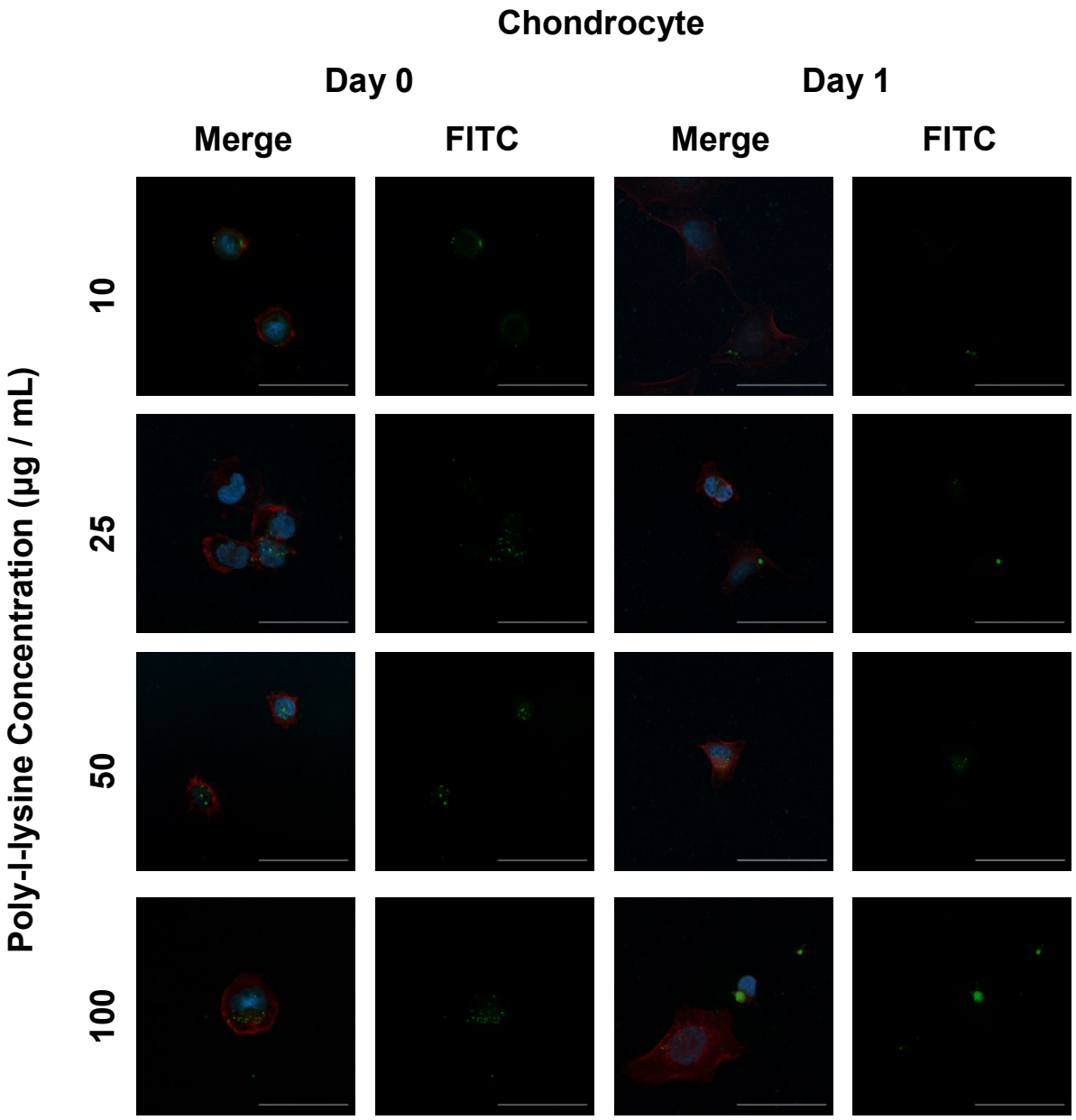

Figure 4.25 – Cell coating efficiency of FITC-conjugated PLL (green) at various concentrations for the chondrocyte cell line. Cells were imaged immediately following and 24 hours after coating. Cell nuclei were visualised using DAPI (blue) and F-actin using phalloidin (red) staining. Scale bar = 50 µm.

4.3.6 Printer Reservoir Agitation

The performance of two separate agitation systems was assessed in terms of both the level of cellular dispersion retained within the reservoir over time as well as cellular function in response to the agitation process.

Figure 4.26 demonstrates the impact of sedimentation on cellular dispersion across each continually agitated reservoir design in comparison to both non-agitated samples and those agitated manually using a pipette. A rapid reduction in cellular dispersion was observed in the non-agitated control condition within the first 30 minutes of the 2 hour incubation

period assessed. Cellular dispersion remained stable across the full time course where agitation within the reservoir was employed, irrespective of agitator design.

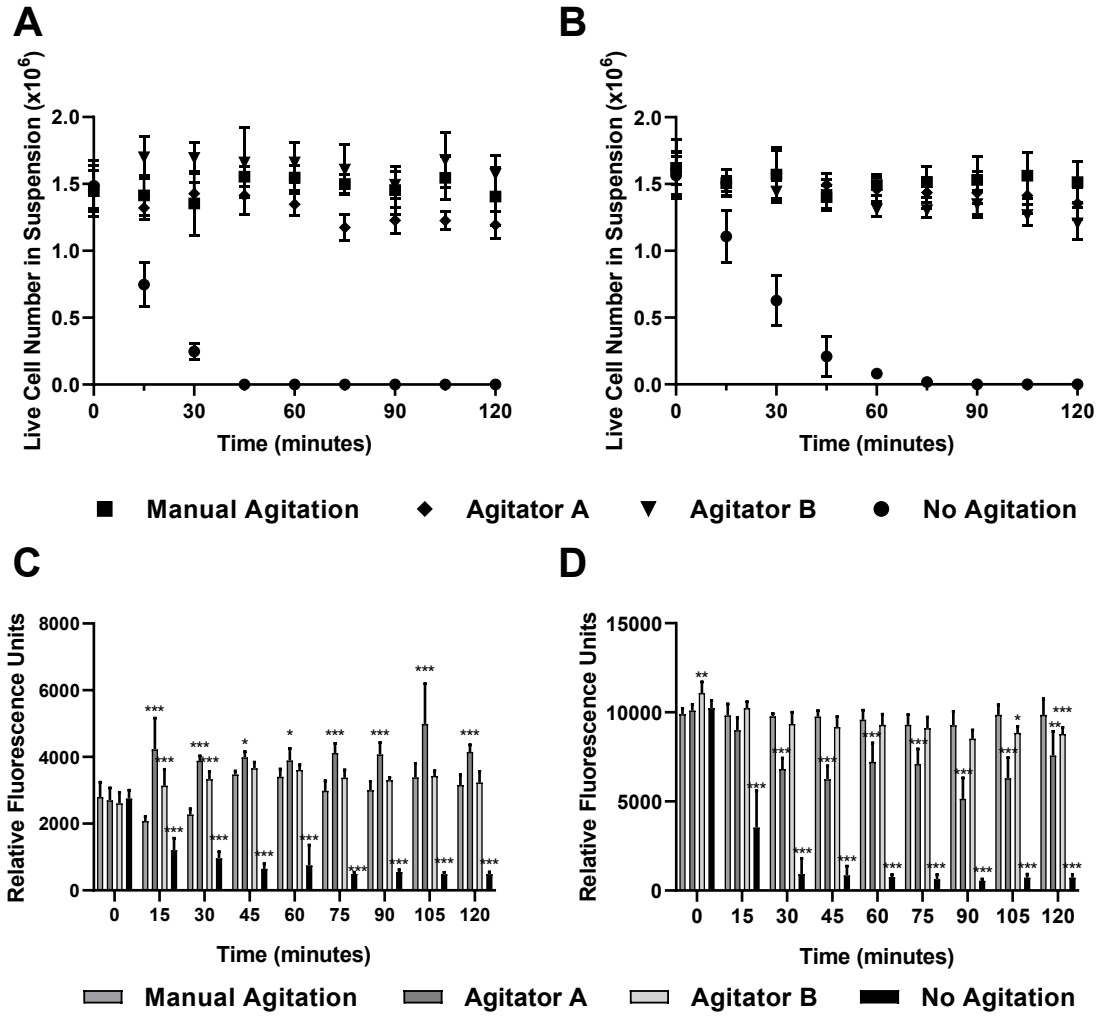

Figure 4.26 – Effect of continuous reservoir agitation on cellular dispersion and metabolic activity at a concentration of 10^6 cells per mL. (A) MSC count. (B) Chondrocyte cell count. (C) MSC metabolic activity. (D) Chondrocyte metabolic activity. Data represents mean values ± SD. N=6.

Assessment of cell metabolic activity for each sample revealed a significant reduction in the metabolic activity of non-agitated samples within the first 30 minutes of incubation across each cell type assessed. A greater metabolic activity range was recorded for agitator A when compared with manually agitated samples. Agitator B was shown to provide a minimal impact on metabolic activity when compared with manually agitated samples.

A minimum agitator ink volume of approximately 1.5 mL was required for agitator B to function. This was caused by the movement of the magnetic stirrer in and out of liquid volumes below this range leading to the formation of bubbles as shown in Figure 4.27.

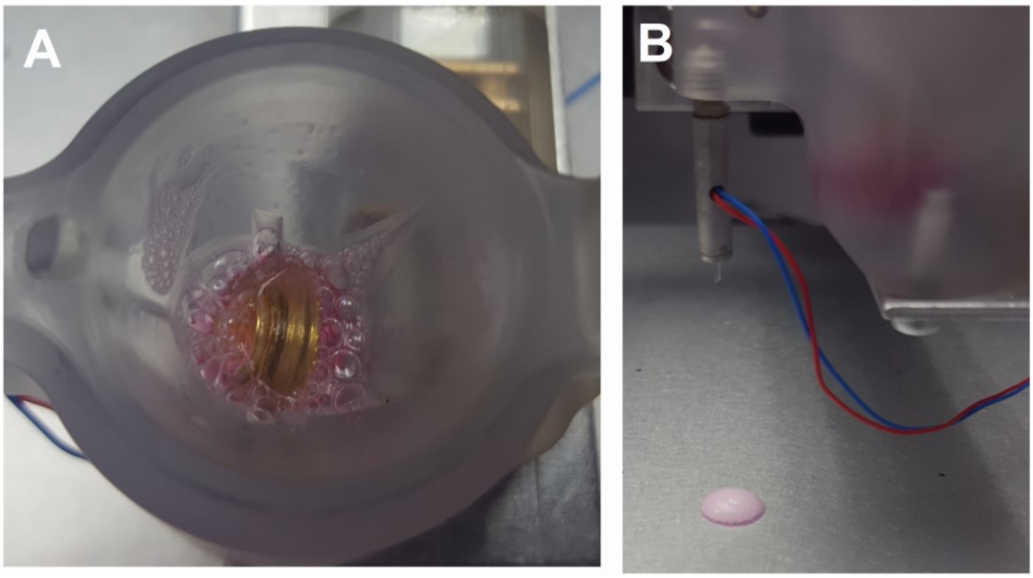

Figure 4.27 – Bubble formation in Agitator B. (A) Foam generated within reservoir during agitation under low ink volumes. (B) Foam in ejected material following jetting.

An additional experiment was performed to determine the impact of the reservoir agitation system on cell printing performance. Figure 4.28 compares the printing performance of the inkjet system under agitated and non-agitated conditions. A gradual reduction in cell number deposited per droplet was observed under non-agitated conditions over the first 60 minutes of printing followed by a nozzle blockage preventing further deposition. Consistent deposition performance was maintained within the agitated sample group throughout the 2 hour assessment period.

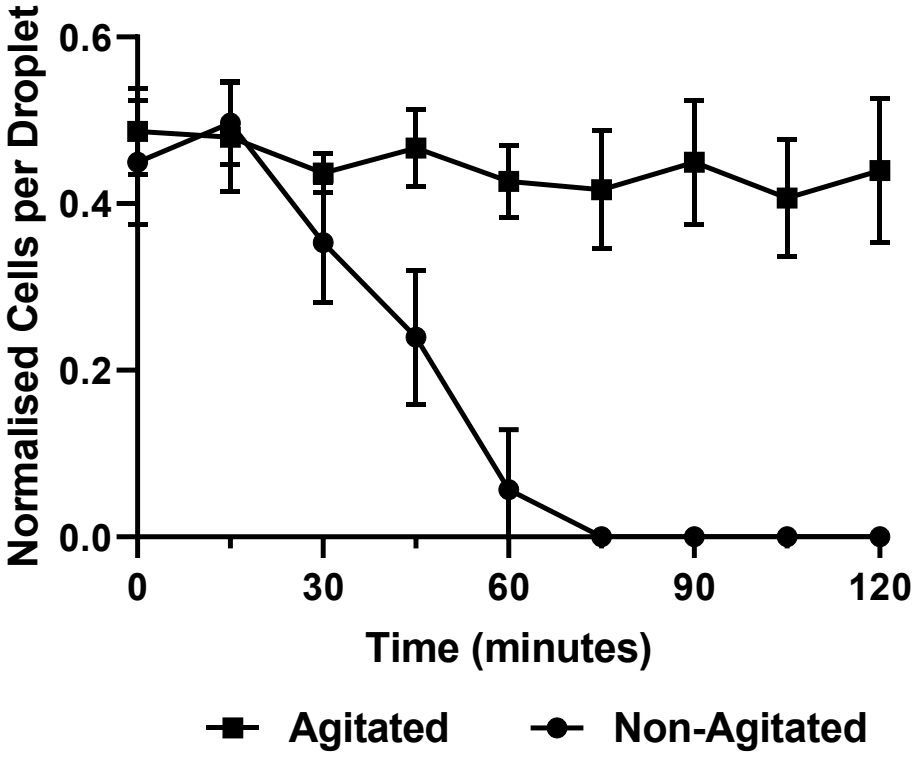

Figure 4.28 – Effect of agitation system on inkjet dispense performance over time when depositing MSCs. Data represents mean values ± SD. N=6.

4.4 Discussion

4.4.1 Waveform Optimisation

Initial experimentation with the inkjet actuation device highlighted the importance of developing printing parameters optimised to the ink's rheological properties. Significant variation in droplet velocity, volume and directionality occurred in cases where droplet ejection characteristics varied as a result of satellite formation or the sequential ejection of multiple droplets per actuation pulse. These effects negatively implicated both the accuracy and printing resolution that could be achieved. As a consequence, partially ejected material accumulated around the tip of the nozzle, leading to a further reduction in printing accuracy and a progressive deterioration in jetting performance. Additionally, minor variations within the manufacturing tolerances of the piezoelectric element, orifice diameter or glass capillary length also affected the pressure oscillations and subsequent jetting performance of each inkjet device. It was therefore necessary to tailor the waveform design and printing parameters to both each jetting device and the bioink composition used in order to maximise process reliability.

Cell culture media has a high surface tension and low viscosity, resulting in a theoretically low degree of printability when defined through fluid properties (Wasan and Papoutsakis, 1995; Jang, Kim and Moon, 2009). A significant amount of energy was therefore required during printing to overcome the surface tension forces and initiate droplet ejection from the ink volume contained within the nozzle. Due to the comparatively low viscosity, once droplet ejection had been initiated a reduced trailing ligand was generated following the ejection of the primary droplet, with the high surface tension reducing droplet ejection velocity. This resulted in a reduced operational range for actuation voltage intensity and waveform dwell time settings. Ejected droplets also displayed a less stable trajectory, resulting in reduced depositional accuracy when impacting the substrate.

It was therefore necessary to experiment with a range of custom waveforms in order to improve droplet formation and ink deposition. It was possible to reduce the jetting frequency down to 100Hz for material deposition. Although droplet ejection characteristics could be further improved at reduced jetting frequencies, printing speed was substantially reduced, resulting in an excessively compromised jetting throughput.

A jetting frequency of 1000Hz was selected for printing experiments in order to maximise the inkjet deposition rate whilst adhering to the operational range of the actuation device used. Jetting frequencies beyond 1000Hz increase the risk of damage to the piezoelectric actuator within the nozzle and provide a reduced total waveform duration between actuations, further limiting potential configuration options.

Waveforms were developed that utilised the lowest possible voltage in order to achieve stable droplet ejection. A consistent voltage and jetting frequency was used across each of the waveform designs assessed to allow for direct comparisons to be made solely on the effects of the waveform dwell time and signal polarity.

Images in Figure 4.5 outline the sequential droplet deposition images captured when employing unipolar, bipolar and tripolar waveforms. This study was performed to identify the most robust and reliable configuration for material deposition. Considerable ink accumulation and air ingestion was observed when using a tripolar waveform, resulting in jetting failure as shown in Figure 4.6.

Quantification of the effect of unipolar and bipolar waveform designs on droplet ejection performance was reported in Figure 4.7 and Figure 4.8. Bipolar waveform designs were

shown to generate droplets of a higher velocity and volume when compared with unipolar waveform designs, alongside operating across a greater parameter range. An optimal dwell time for each waveform was defined as 18 μs and 30 μs for the unipolar and bipolar waveforms respectively to maximise droplet velocity and volume. Further characterisation data presented in Figure 4.9 demonstrated that the bipolar waveform design was capable of achieving a higher droplet ejection velocity than the unipolar design, alongside reduced variability in ejection volume where actuated under the optimal dwell time previously defined.

In combination, these results indicate that the bipolar waveform design is most suitable for depositing cell culture media, through operating across the widest parameter range and ejecting droplets of a higher velocity and volume when compared to unipolar and tripolar configurations. These observations reinforce previous findings within the literature whereby waveform designs were compared for the ejection of material using a similar piezoelectric inkjet printing device (Kwon, 2009).

The effect of nozzle orifice diameter on printing performance was also assessed, with droplet volume positively correlating with nozzle diameter in response to a reduced ejection velocity, as shown in Figure 4.10. This reinforces prior research recognising the relationship between orifice diameter and printing performance (Miers and Zhou, 2017).

4.4.2 Cell Deposition Performance

The inclusion of cells within the liquid ink solution produced a colloidal dispersion, which altered the rheological properties of the ink and led to variations in inkjet printing performance.

The minimum actuation voltage required to successfully deposit material was higher when jetting solutions containing cells than when jetting cell culture media alone, irrespective of waveform design. In addition, droplet ejection characteristics were found to be more sensitive to dwell time adjustments where cell-based inks were used. It was therefore necessary to further evaluate the parameters previously defined in order to maximise cell deposition performance.

The bipolar waveform design was shown to be more robust when depositing cell-containing ink solutions, reinforcing previous observations when jetting cell culture media alone. This

was demonstrated in Figure 4.11 when assessing the cell density of dispensed material in response to changes in dwell time for each of the waveform designs.

A target cell density of 1 cell per droplet was achieved following further optimisation of the ink concentration and dwell time configuration. A significant increase in cell density per droplet was observed in response to increasing the ink concentration from 1 to 2 million cells per mL, as shown in Figure 4.12. Variability in cell density per droplet was found to increase in response to an increase in the cell concentration within the ink, representing a trade-off between deposition density and resolution when using the inkjet printing process.

Idle time between print jobs was also found to have a significant impact on inkjet cell deposition performance. The use of purge cycles immediately prior to printing was shown in Figure 4.13 to reduce the variability in cell density per droplet obtained, as well as providing a mechanism to clear partial nozzle blockages. These findings reflect previous observations in other fields where inkjet printing techniques have been extensively studied for high-volume material printing applications (Lund and Ward, 1998; Pawlowski and Childers, 2001; Park, 2013). They also provide a valuable mechanism that can be employed to reduce the performance issues commonly associated with inkjet printing platforms.

The efficiency of the single cell printing configuration was also demonstrated via the sequential deposition of individual droplets. The majority of droplets printed were found to contain single cells, with a minority containing 0, 2 or 3 cells. The frequency distribution of cells per droplet, displayed in Figure 4.14, correlated with Poisson distribution probability modelling. These observations reflected previous research exploring the potential for single cell printing via inkjet deposition technologies, whereby a similar distribution of ejected cells per droplet was observed (Liberski, Delaney and Schubert, 2011; Moon *et al.*, 2011; Yusof *et al.*, 2011).

4.4.3 Biological Impact Assessment

The biological impacts of the inkjet printing process were characterised using a combination of cell viability, metabolic activity and proliferation assays, as well as morphological analysis. The Live / Dead® assay data reported in Figure 4.16 showed no significant difference in the ratio of live to dead cells between manually seeded and printed samples for both cell types studied. This result indicated that the inkjet printing process does not induce any immediate detrimental effects on cellular viability.

The data presented in Figure 4.17 compared the metabolic activity of cells printed using the inkjet printing platform with manually seeded cell controls using an MTT assay. No significant differences in metabolic activity were observed for the MSC or chondrocyte cell lines when comparing manually deposited and inkjet printed samples. These results provide evidence of the suitability of the inkjet printing process for cell deposition applications.

The morphology of cells processed using the inkjet printing technique were compared with manually seeded cells in Figure 4.18 and Figure 4.19 for the MSC and chondrocyte cell lines respectively. Cell adherence and growth was shown to be similar for both seeding techniques, with no discernible differences in cell morphology observed over the assessment period.

Proliferation studies comparing the growth rate of manually seeded and printed MSC and chondrocyte cells displayed a similar percentage of viable cells at each time point, with a small variation in the number of cells counted immediately following seeding. No significant difference in the rate of population growth following seeding was observed between printed and manually seeded cells, as reported in Figure 4.20, indicating that the cell printing process had no significant effect on cell growth kinetics following seeding.

Taken together, these findings indicate that the inkjet printing process can be used to deposit MSC and chondrocyte cells without significantly affecting cellular viability or function, highlighting the biocompatibility of the printing process for cell deposition applications. These findings provide further evidence of previous observations within the literature that examined the impact of inkjet printing on cellular viability and function using alternative cell types (Saunders, Gough and Derby, 2008; Cui *et al.*, 2010).

4.4.4 Cell Aggregation

Nozzle blockages previously reported within the literature were observed when printing for extended periods of time, as shown in Figure 4.21 (Chahal, Ahmadi and Cheung, 2012; Tse, 2015; Tse *et al.*, 2016). This significantly reduced the reliability of the printing process by regularly interrupting the printing job. It was not possible to alleviate this issue through modifications to the jetting parameters used, or the use of alternative nozzles with a larger orifice diameter. The passage of cellular clumps through the nozzle was also found to impair the flow of material through the nozzle chamber during actuation-induced pressure oscillations. This resulted in a reduction in jetting performance and droplet ejection stability

when compared with the ejection characteristics observed when depositing cell culture media.

These effects had a considerable impact on the scale at which cell printing could be performed when using inkjet dispensing devices. Two separate techniques were researched as potential methods to reduce cellular agglomeration and improve process reliability. This included both the use of an agitation system within the reservoir compartment of the printer, as well as the process of coating individual cells with a polycation prior to printing.

4.4.5 Polymeric Cell Coating

The effect of the poly-l-lysine cell coating process on cellular viability and metabolic activity was studied to identify an optimal concentration range for cell printing applications.

The Live / Dead® assay data reported in Figure 4.22 displayed a significant reduction in cell viability in response to concentrations exceeding 50 µg / mL for both the MSC and chondrocyte cell lines. Analysis of the metabolic activity of each cell type following coating revealed a significant reduction in metabolic activity across samples exposed to PLL concentrations exceeding 25 µg / mL for the MSCs, and 50 µg / mL for the chondrocyte cell line, as shown in Figure 4.23.

The efficiency of the PLL cell coating process was assessed by fluorescence microscopy, as shown in Figure 4.24 and Figure 4.25 for the MSC and chondrocyte cell lines respectively. FITC-conjugated PLL cell coating efficiency was shown to increase with PLL concentration for the MSC cell line, with a minimum concentration of 50 µg / mL required to fully coat the membrane of the cells. PLL coating efficacy was reduced in the chondrocyte cell line, with speckled coating observed across the full concentration range assessed. A reduction in FITC-PLL signal intensity following a 24 hour incubation period indicated that the PLL was internalised within the cell over time. The reduction in speckling area and increased point intensity of the fluorophore highlighted potential polymer consolidation by internal cellular processes.

In combination, this data provides evidence of a dose-dependent response to the PLL concentration used for cell coating. This reflects the observations of previous research whereby low PLL concentrations were found to have a negligible impact on the viability of other cell types, with higher concentrations reducing cellular viability and function (Ribeiro *et al.*, 2017). As a consequence, PLL coating procedures could only be considered for

applications to reduce cellular agglomeration where a low polymer concentration was used. Further research is required to characterise the biocompatibility of the PLL coating process on additional cell lines, as well as benchmark its impact on inkjet printing performance.

4.4.6 Printer Reservoir Agitation

A combination of two in-house agitation systems were developed and evaluated to reduce the rate of cell sedimentation and agglomeration during extended printing periods. Gravity-induced cell sedimentation occurred during printing, leading to cell sedimentation at the base of the reservoir. Subsequent cell agglomeration and attachment to the interior surfaces reduced the concentration of cells within suspension, leading to a reduction in printing performance irrespective of reservoir outflow positioning.

The data reported in Figure 4.26 indicated that both designs were capable of greatly reducing the rate of cellular sedimentation within the reservoir chamber when assessed over a 120 minute incubation period, providing agitation performance comparable to that of manually agitated samples. This represented a significant improvement over the use of a regular reservoir design during cell printing experiments. When comparing each agitator design against manually agitated cells, agitator design B was shown to provide the smallest variation in metabolic activity for each cell type. Despite this, it was important to consider the working volume of each agitation system due to the bubble formation that occurred during operation at low volumes, as depicted in Figure 4.27. These effects were not observed within agitator design A, making this design more suitable for low volume applications.

The impact of the agitation system on inkjet printing performance was also benchmarked in Figure 4.28. Agitated samples were shown to prevent a deterioration in printing performance over a 120 minute testing duration. This contrasted with the results obtained for the non-agitated samples printed, whereby a significant deterioration in performance occurred over the first 60 minutes of printing, leading to the blockage of the inkjet nozzle. Although nozzle blockages still occurred during normal use when using the agitated reservoir system, the frequency of blockages was significantly reduced. This data highlights the value of employing an agitation system in order to reduce cellular sedimentation and agglomeration, thus providing a mechanism to improve the reliability of the inkjet printing process. These findings have important implications within the field of biofabrication to maximise the potential applications of inkjet printing techniques.

4.5 Conclusions

Within this chapter, an inkjet printing process was explored for the selective deposition of biological material for high-accuracy bioprinting applications.

- A bipolar waveform design was developed to enable the deposition of biological material at the picolitre-scale
- Single cell printing was achieved, with the cell density per droplet correlating with a Poisson probability distribution
- The inkjet process was shown to not have any significant effect on cellular viability, metabolic activity, morphology or proliferation rate when assessed using the MSC and chondrocyte cell types, demonstrating its suitability for cell printing applications
- A novel polycationic cell coating system was benchmarked, with a PLL concentration of up to 25 µg / mL shown to not affect cellular viability or metabolic activity
- A custom reservoir agitation system and purging process was successfully demonstrated to reduce the rate of cellular sedimentation and subsequent performance issues during printing

Chapter 5. Aggregate Construction using Valve-based Bioprinting

5.1 Introduction

The aim of this chapter is to investigate the application of a valve-actuated bioprinting process for the production of 3D cell aggregates. The material jetting performance of a drop-on-demand valve-based printer is characterised through evaluation of the effect of various actuation parameters, such as waveform and backpressure, on printing accuracy, resolution, throughput and reliability.

Cell printing performance is also assessed, with additional studies conducted to determine the biocompatibility of the printing process with mesenchymal stromal cell and chondrocyte cell lines.

A combination of 3D aggregate culture methods are utilised to construct tissue models of each cell type using the valve printing technique. Biological characterisation is performed to determine the impact of the printing process on model morphology, cellular organisation and phenotypic marker expression.

5.2 Methodology

5.2.1 Valve Printing Configuration

Lee VHS Series 24 V solenoid valves, connected via a 0.62 MINSTAC® fitting to a 0.25 mm jewelled orifice dispensing nozzle (The Lee Company, USA), were used to deposit material for all valve-based bioprinting experiments, as shown in Figure 5.1. An adjustable spike-and-hold driver (The Lee Company) was used to convert the JetDrive® waveform output into a valve-compatible signal to control device actuation. An external power supply (ISO-Tech, UK) was connected to the spike-and-hold driver to provide the additional power source required for actuation. This setup provided a continuous 24 V supply to the spike driver terminal and 5 V supply via a separate channel to the hold driver terminal.

VHS Series Valve

Spike-and-Hold Driver

Figure 5.1 – VHS series valve actuator with 0.25 mm diameter jewelled orifice nozzle and accompanying spike-and-hold driver. Scale bar = 10 mm.

The MicroFab CT-PT4 standalone pneumatics controller box was used to generate a backpressure of between 100 and 400 mmHg at the reservoir, depending upon ink levels present during printing. The pressure level was manually adjusted to achieve accurate and reliable material ejection characteristics. An external pneumatics system was required due to the limited pressure output capability of the on-board pneumatics system designed for use with inkjet devices.

A simple trapezoid shaped unipolar waveform, shown in Figure 5.2, was used to provide a 5 V actuation signal and 0 V resting signal to the external spike-and-hold driver using the JetDrive® control software. A dwell time of 200 µs and actuation signal frequency of 500 Hz was applied to the valve for the majority of printing experiments.

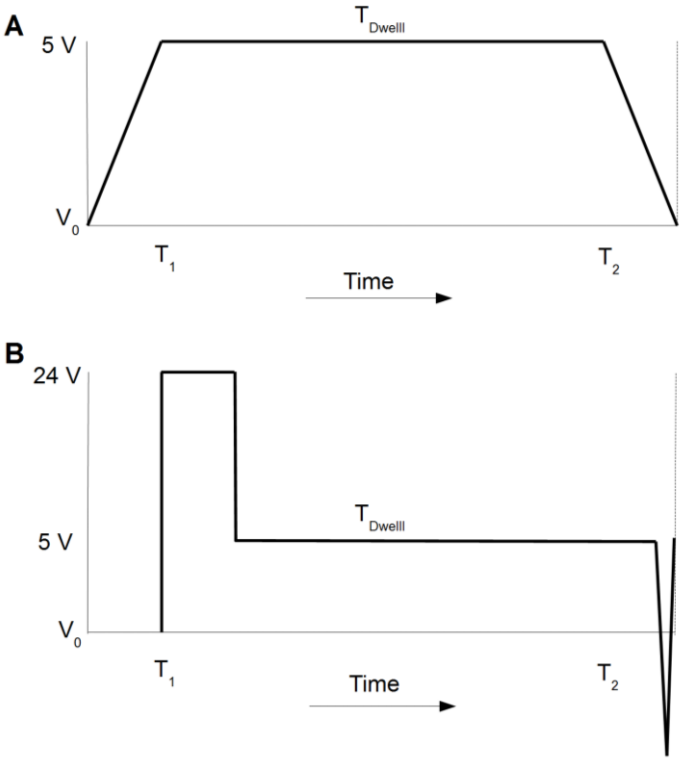

Figure 5.2 – Diagram of actuation signal waveform generated to operate the valve via an intermediary spike-and-hold controller. (A) Unipolar waveform of drive signal applied to spike-and-hold controller. (B) Spike-and-hold controller output signal applied to valve.

5.2.2 Characterisation of Printing Performance

Characterisation of droplet volume via gravimetric methods was performed by selectively depositing material onto a substrate in response to changes in total droplet number or printing parameters. The substrate mass was then immediately measured using an Explorer® analytical balance (Ohaus, USA).

Droplet volume was determined via the following equation:

$$Droplet\ Volume\ (nL) = \frac{Liquid\ Mass\ (g) \times Density\ of\ Cell\ Culture\ Media \times 10^6}{Number\ of\ Droplets}$$

Equation 5.1 – Determination of mean droplet volume using the liquid mass, density of cell culture media and printed droplet number.

Fluorometric characterisation of droplet volume was performed using fluorescein sodium salt (Sigma-Aldrich, UK) prepared to a stock concentration of 1 M in PBS. A 100 µM fluorescein working solution was prepared in PBS for the generation of standard curves and for dispensing within valve performance tests. Fluorescence values for each plate were obtained using a FLUOstar® Omega (BMG Labtech, Germany) microplate reader using an

excitation and emission filter of 485 nm and 520 nm respectively. Droplet volume was interpolated from standard curve data.

For low ink cell density studies, the cell printing performance was characterised by manually counting the number of cells contained within single droplets sequentially deposited onto a glass slide. Cells were counted immediately following printing using a DMLB microscope (Leica Biosystems, Germany).

For high ink cell density studies, a volume of material was deposited into the individual wells of a multi-well plate and a 10 µL aliquot transferred to a 0.1 mm depth Neubauer chamber haemocytometer (Hawksley, UK) for cell counting. Cell concentration was calculated by normalising the cell count to the calculated droplet volume previously determined.

5.2.3 Hanging Droplet Aggregate Culture

Mesenchymal stromal cells and chondrocyte cells were seeded via either manual dispensing or valve deposition onto the inside surface of petri dish lids (Corning, USA) across a range of densities. The lids were then carefully rotated and placed onto the petri dish base. The base of the petri dish was partially filled with PBS to provide an additional source of humidity during incubation at 37 °C, 5 % CO_2. Gravity-induced cell aggregation occurred within 24 hours of culture and a partial media change was performed every 2 days to minimise aggregate disruption.

5.2.4 In-Well Aggregate Culture

Mesenchymal stromal cells and chondrocyte cells were seeded at varying densities via either manual dispensing or valve deposition into individual wells of non-adherent U-bottomed 96-well plates (Fisher Scientific, USA) in medium containing 0.25 % methyl cellulose (Sigma-Aldrich). Cells self-aggregated within 12 hours and a partial media change was performed every 2-3 days to minimise aggregate disruption.

5.2.5 Aggregate Imaging

Aggregate size and morphology was assessed using a Leica DMLB bright-field microscope at 5x magnification and images captured using a SPOT Advanced CMOS camera (Spot Imaging Solutions, USA) and corresponding microscopy software. Aggregate size was measured manually using ImageJ image analysis software (National Institutes of Health, USA).

5.2.6 Conditioned Media Formulation

A differentiation-inducing media formulation was prepared for the MSC aggregates via the addition of supplements to basal cell culture media prepared as previously described. A breakdown of the composition of the media formulation is shown in Table 5.1.

Supplement	**Manufacturer**	**Concentration**
L-Ascorbic acid-2-phosphate	Merck	50 µg / ml
Dexamethasone	Merck	100 nM
L-Proline	Merck	40 µg / ml
ITS^{+}1	Merck	1 %
TGF-ß3	Thermo Fisher Scientific	10 ng / ml

Table 5.1 – Chondrogenic conditioned media formulation for MSCs.

5.3 Results

5.3.1 Material Deposition Performance

An initial study was performed to determine the impact of waveform dwell time and backpressure on the deposition performance of the valve actuation device when dispensing cell culture media. Figure 5.3 displays the gravimetric assessment of valve ejection volume across a range of printing parameters. The volume of media dispensed was shown to positively correlate with the waveform dwell time applied. Pressure behind the valve was shown to have a minimal impact on dispense volume per actuation cycle at lower dwell times with greater variation observed above 300 µs. Droplet ejection was not achieved below a dwell time of 150 µs. A dwell time of 200 µs at a pressure of 200 mmHg was shown to dispense droplets with a total volume of approximately 50 nL.

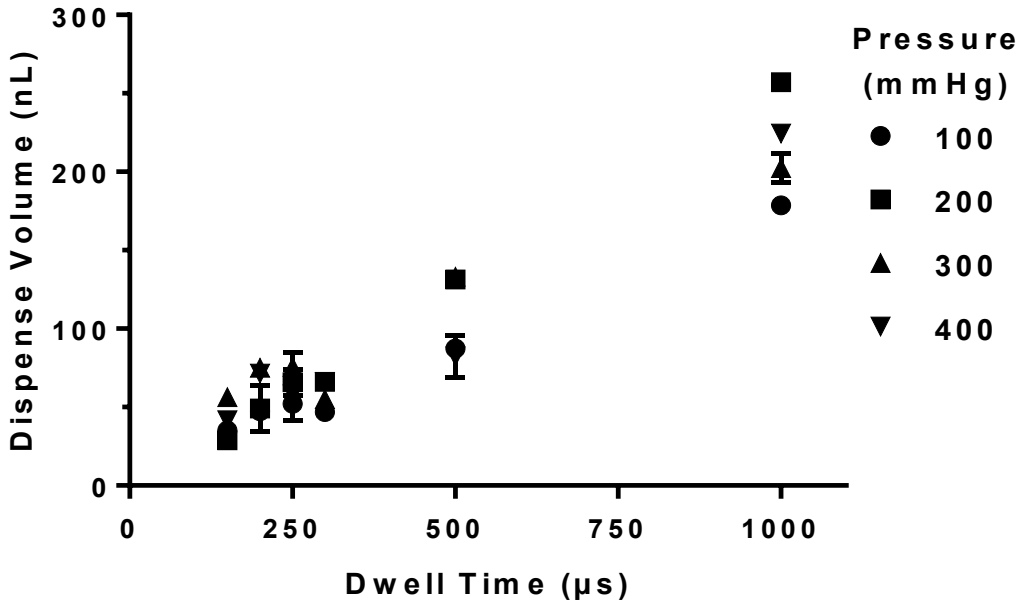

Figure 5.3 – Influence of waveform dwell time and backpressure applied to the valve on dispense volume when printing cell culture media. Data represents mean values ± SD. N=3.

Fluid ejection characteristics for the valve were observed using the on-board stroboscopic camera. Sequential ejection images displayed in Figure 5.4 show a significant droplet generated within the actuation cycle followed by a tailing ligand. Satellite and ligand formation were observed irrespective of the applied printing parameters.

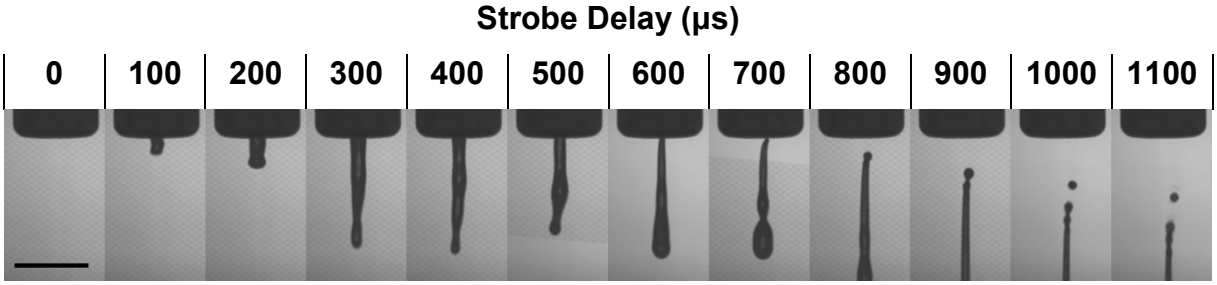

Figure 5.4 – Sequential droplet ejection images captured using the JetLab® on-board stroboscopic camera at an incremental strobe delay of 100 µs. The valve was used to dispense cell culture media at a dwell time of 200 µs and backpressure of 200 mmHg. Scale bar = 1 mm.

An additional study was conducted to assess the impact of actuation cycle number on material ejection volume. Figure 5.5 shows a high degree of linearity between ejection volume and actuation cycle number. Linear regression analysis revealed a droplet volume of 61 nL, identified via the gradient of the line of best fit across the actuation cycle range assessed. The percentage coefficient of variation was calculated for each actuation cycle number assessed and ranged from 2 % to 11 %.

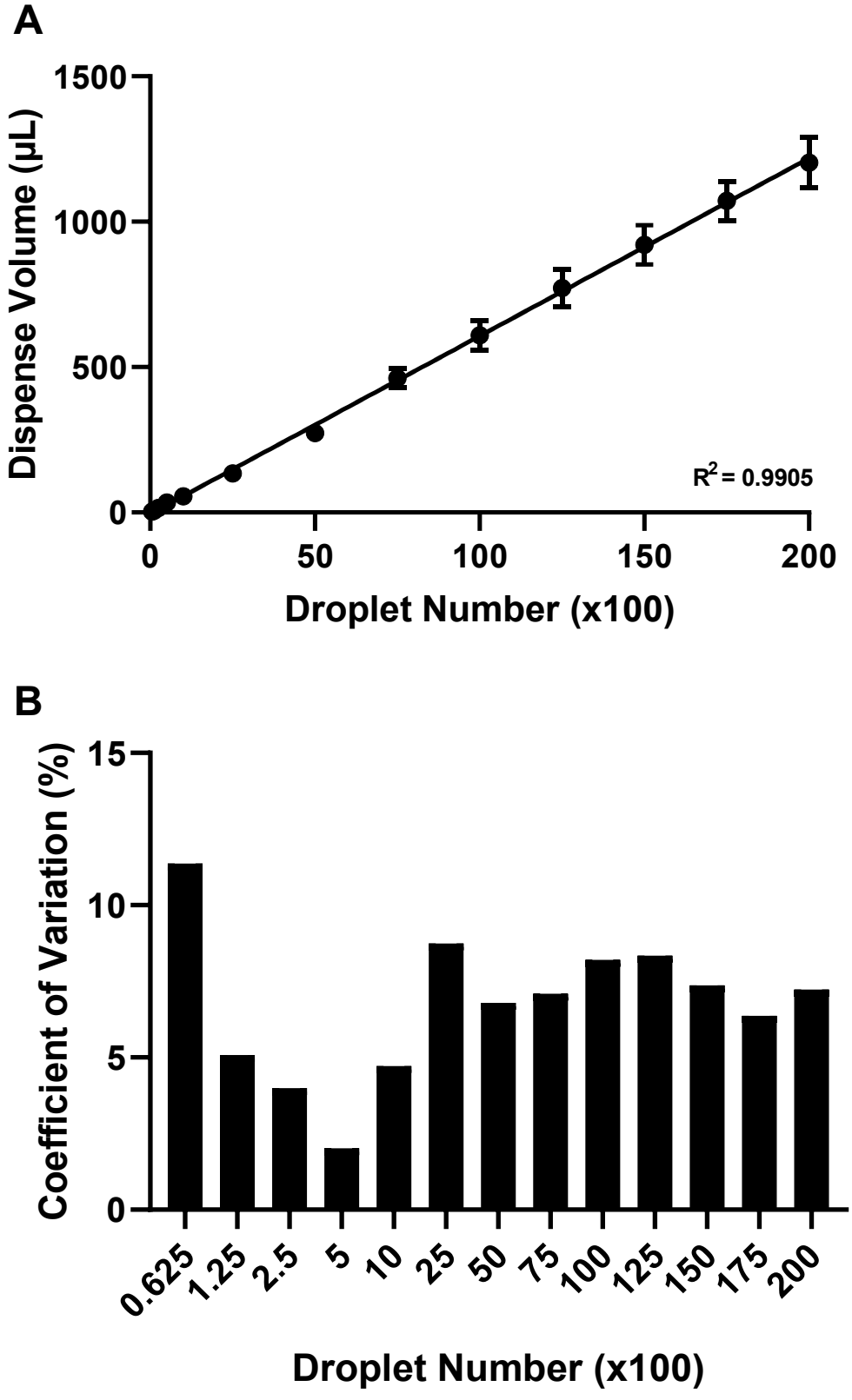

Figure 5.5 – Linearity of material ejection when printing cell culture media at a dwell time of 200 µs and pressure of 200 mmHg. (A) Dispense volume per droplet was calculated via the measurement of dispensed material mass. The gradient of the linear regression trend line corresponds to a droplet volume of 61 nL. (B) Coefficient of variation data calculated for each actuation cycle request. Data represents mean values ± SD. N=6.

Further characterisation of valve dispense performance was performed using a fluorometric method as shown in Figure 5.6. A calibration standard curve (A) was prepared across a wide concentration range to determine a suitable working concentration range of fluorescein solution. A linear range was identified (B) for experimental work below a fluorescein concentration of 6 µM.

A high degree of linearity was observed between the fluorescence values of the samples and the number of droplets of fluorescent material added to each sample (C). Percentage coefficient of variation calculations across each sample group demonstrated a volume dispensing precision of below 9 % (D).

Droplet volume calculated for each droplet deposition number was shown to be stable across the range of 1-20 drops assessed, with an average droplet volume of approximately 54 nL achieved (E).

Comparisons between the fluorescence intensity of material deposited using the valve printing processes versus manual pipetting across a range of target volumes revealed a variation in the level of dispersion between samples (F). Samples generated using the valve printing process displayed a reduced degree of fluorescence intensity variation when compared with those generated using a pipette. A significant difference in fluorescence intensity between valve deposited and manually pipetted samples was observed at the highest deposition volume assessed.

The effect of sample positioning within the valve printing script was also assessed using normalised fluorometric data (G). An elevated Z-score was observed at the first deposition coordinate followed by a period with minimal variation. A reduction in Z-score was observed at the final deposition coordinate for each print run.

Comparisons between the dispense performance of two independent valve actuators displayed an increasing variation in the fluorescence intensity of dispensed samples in response to increases in the droplet number dispensed (H).

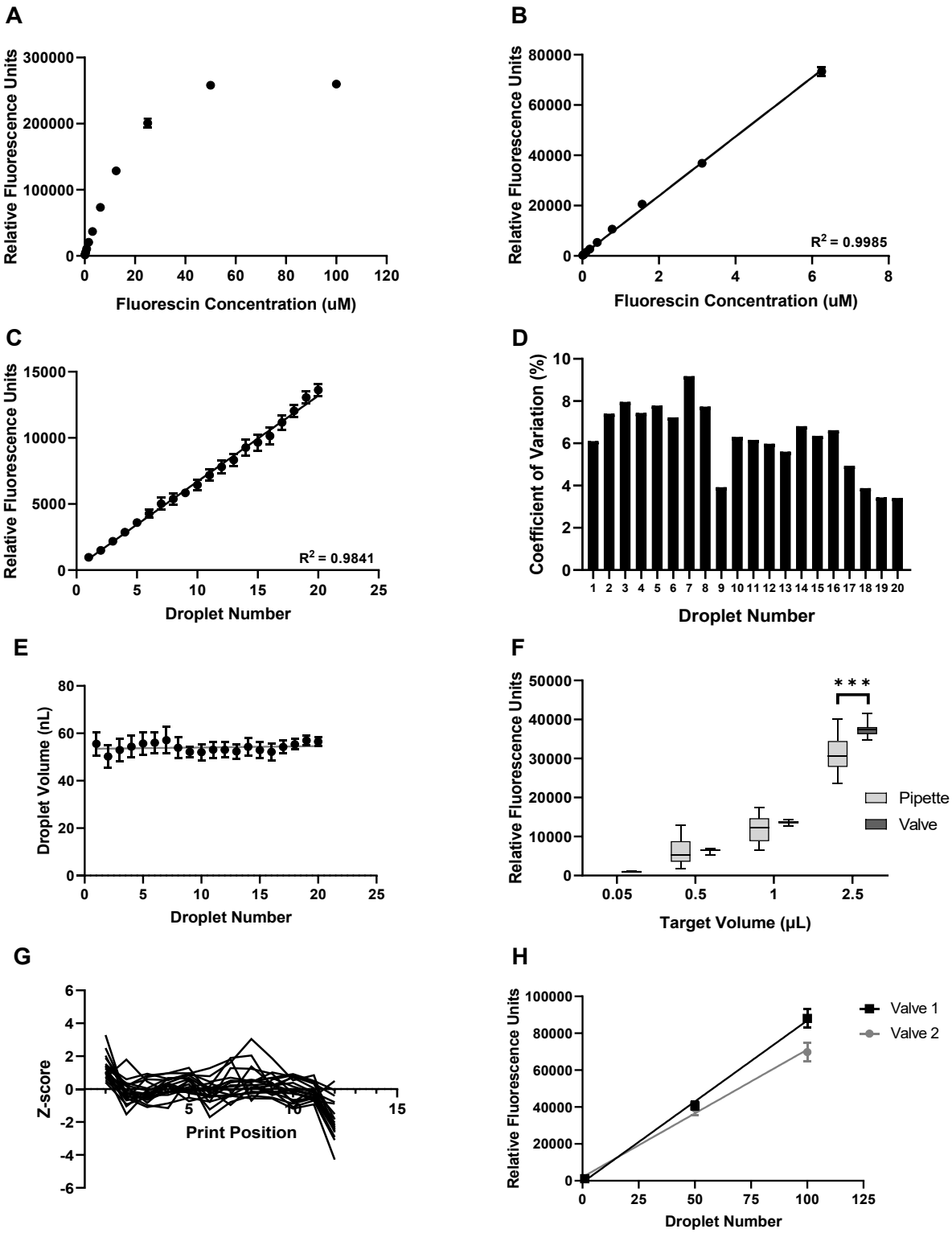

Figure 5.6 – Fluorometric evaluation of valve deposition performance. (A) Fluorescein standard curve data of serial dilution from 100 µM. (B) Linear region of standard curve data displaying a linear regression trend line. (C) Linearity of droplet ejection from the valve measured via the fluorescence intensity of ejected material. (D) Percentage coefficient of variation calculations for replicates of samples at each droplet dispense number. (E) Calculated per droplet volume deposited from the valve across a droplet deposition range of 1-20 droplets displaying a linear regression trend line. (F) Comparison

between fluorescence values obtained from samples dispensed using a pipette and valve across a range of target volumes. (G) Z-score of normalised valve printing data showing well positioning bias amongst replicates within each volume request. (H) Comparison between jetting performance of 2 independent valves. Data represents mean values ± SD. N=12.

5.3.2 Cell Deposition Performance

The effect of each printing parameter on cell deposition performance was assessed when dispensing MSC and chondrocyte cells. An increase in cell density per droplet was observed in Figure 5.7 for both cell lines in response to increases in the dwell time applied to the actuation signal. This effect was diminished beyond a dwell time of 500 µs. A minimum dwell time of 200 µs and 150 µs was required in order to deposit cellular material for the MSC and chondrocyte cell lines respectively, irrespective of the applied backpressure.

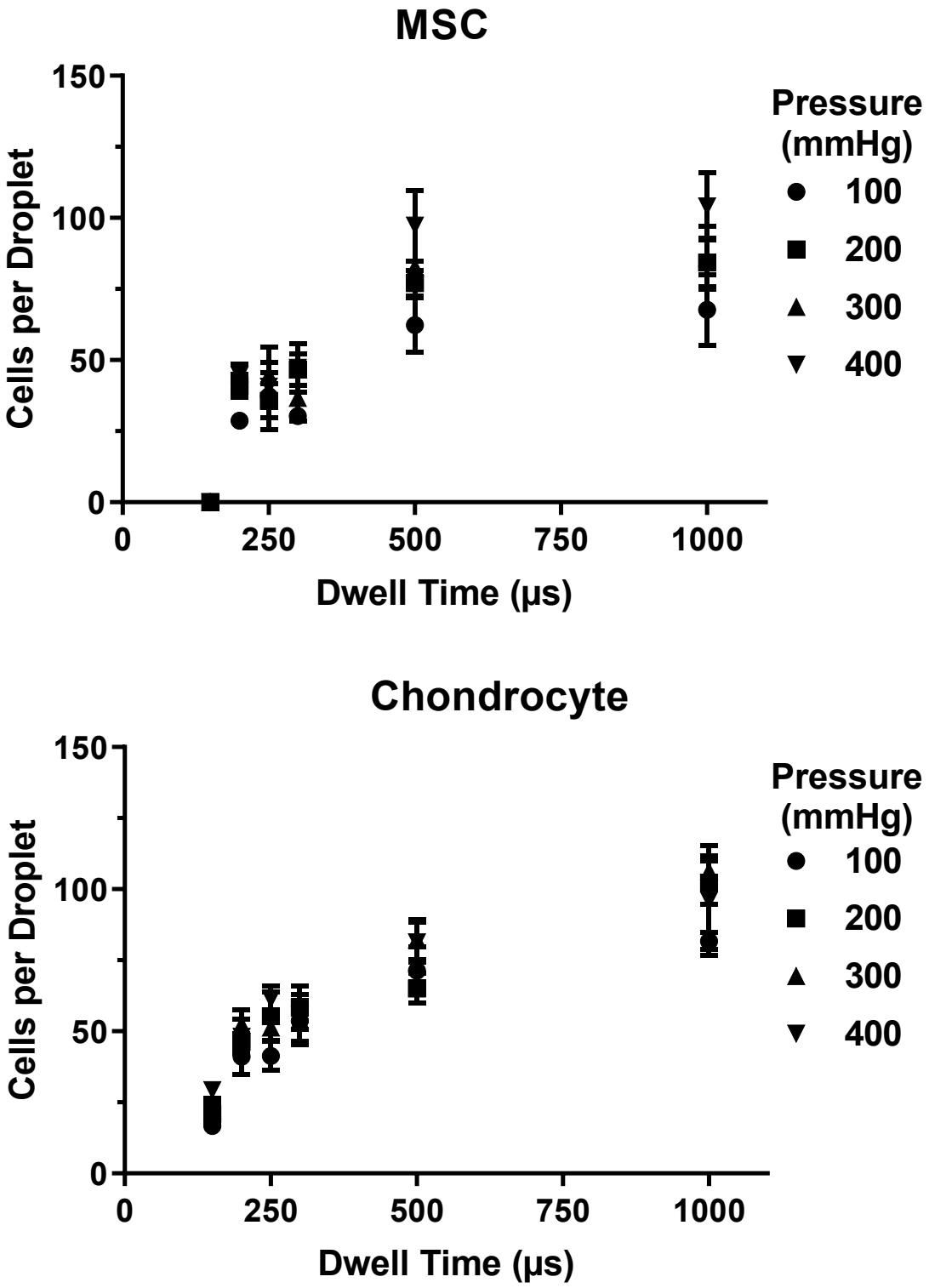

Figure 5.7 – Influence of waveform dwell time and backpressure applied to valve on cell density per droplet when printing MSC and chondrocyte cell lines at a concentration of 10^6 cells per mL. Data represents mean values ± SD. N=3.

Significant cell sedimentation was observed within the actuation device and device-reservoir coupling during extended printing periods. A further study presented in Figure 5.8 was performed to quantify the effect of applying a purge cycle prior to printing on cell density per sequentially dispensed droplet. A rapid initial reduction in the cell density per droplet was observed for the non-purged sample until stable printing performance was achieved. The addition of a purge cycle immediately prior to printing was shown to reduce the variability in cell density during printing by replacing stationary material within the nozzle with ink contained within the reservoir.

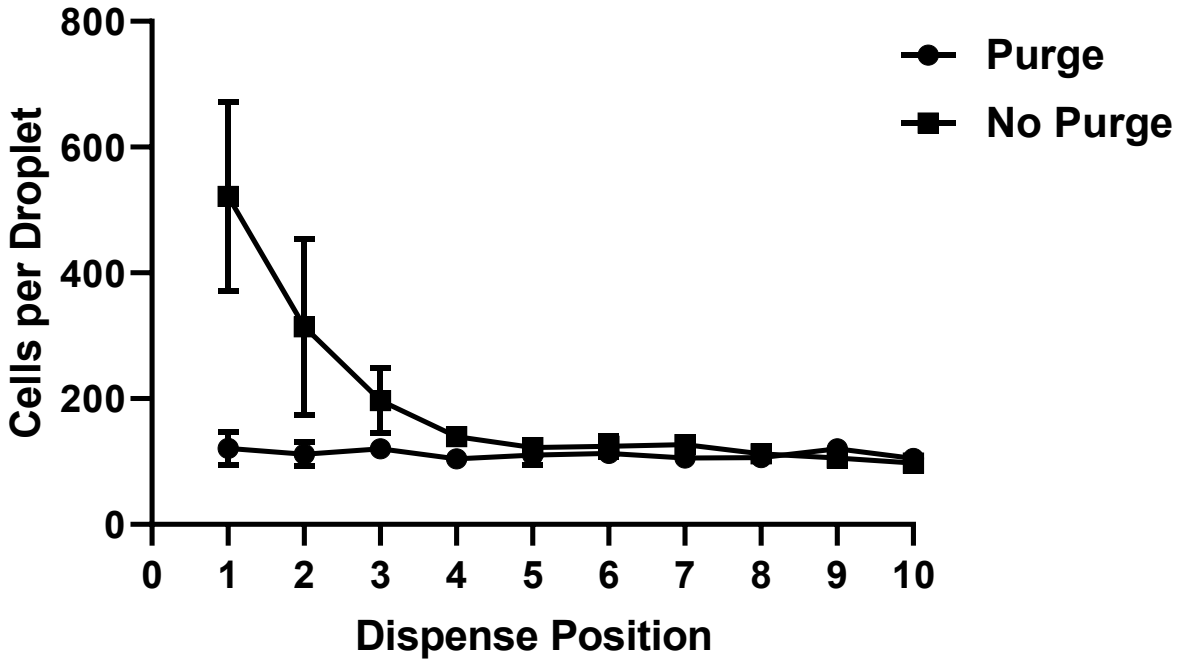

Figure 5.8 – Cell density of sequentially dispensed single droplets with and without the addition of a purge cycle prior to printing. Data represents mean values ± SD. N=3.

The performance of a custom reservoir agitation system was benchmarked in Figure 5.9 for the valve printing process. Printing performance in the absence of an agitation device was shown to deteriorate over a 60 minute printing period resulting in printing failure. The incorporation of an agitation system within the reservoir was shown to prevent a deterioration in printing performance with a stable cell density per droplet observed over the full 2 hour assessment period.

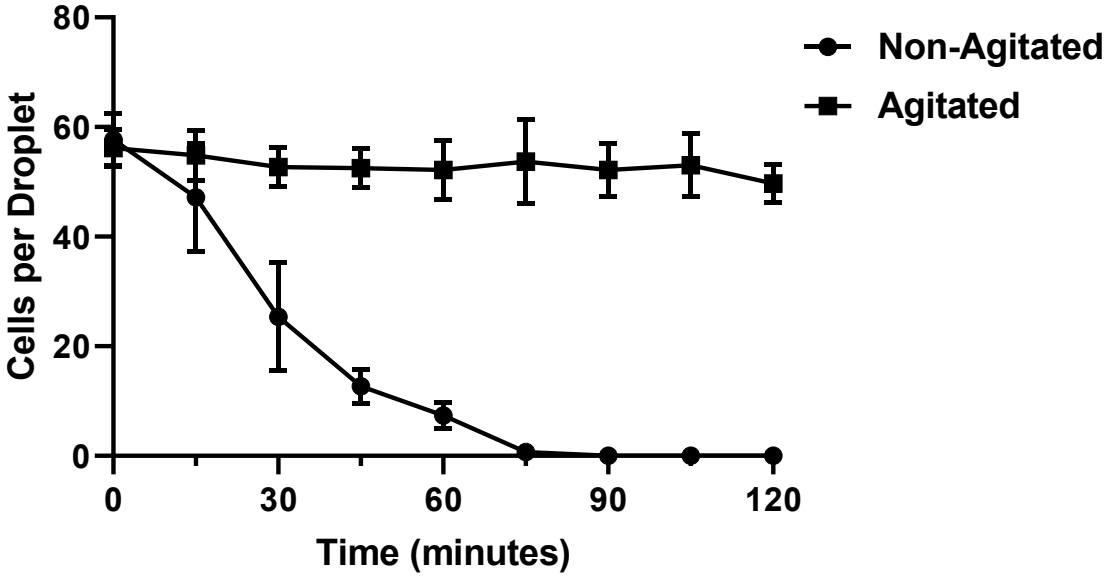

Figure 5.9 – Effect of a reservoir agitation system on valve cell printing performance over time. Data represents mean values ± SD. N=6.

An assessment of the impact of ink cell density on printing performance was performed to determine the operational range of the valve printing process. Figure 5.10 displays the impact of ink cell concentration on the cell printing performance for MSCs over a 30 minute period. A positive correlation was observed between the ink cell concentration and cell density per droplet. Total printing period was shown to have an increasing impact on cell printing performance over time at higher ink cell concentrations.

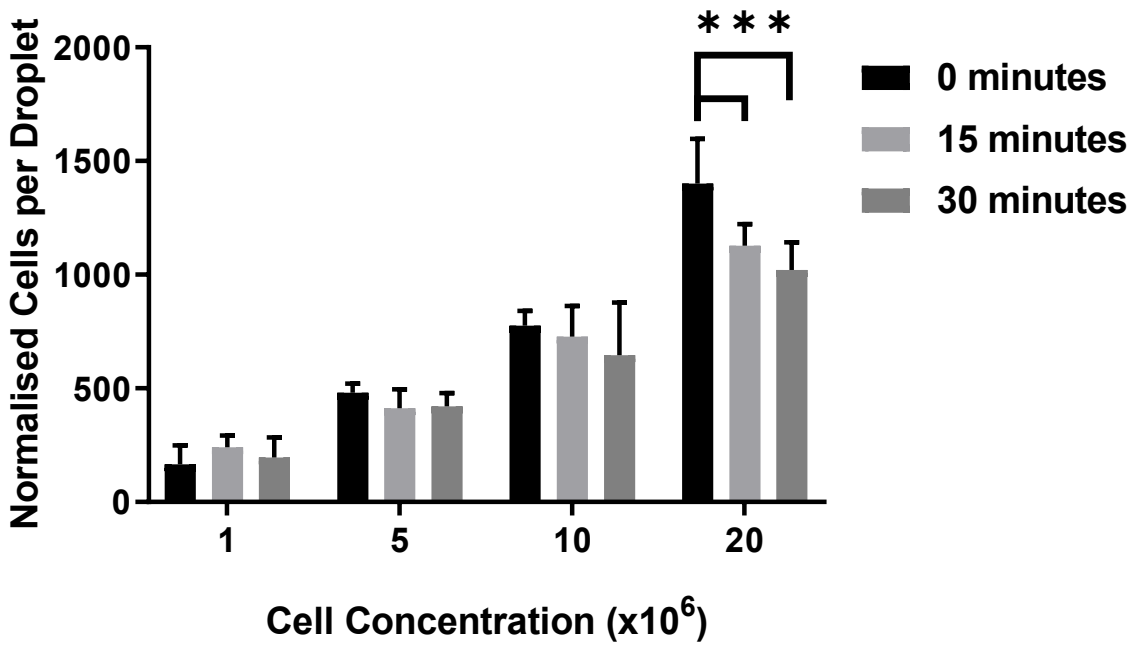

Figure 5.10 – Influence of ink cell concentration on cell deposition performance over a 30 minute period. The valve was configured to operate with a dwell time of 200 µs and backpressure of 200 mmHg. Data represents mean values ± SD. N=6.

Data in Figure 5.11 provides a comparison between the printing performance of the MSC and chondrocyte cell lines across a range of ink cell concentrations. A linear relationship between cell concentration and printing density was observed for both cell lines, with an increasing variation in cell density per droplet observed at higher ink cell concentrations. Cell type was shown to have an increasing influence on the reliability of the printing process at higher ink densities.

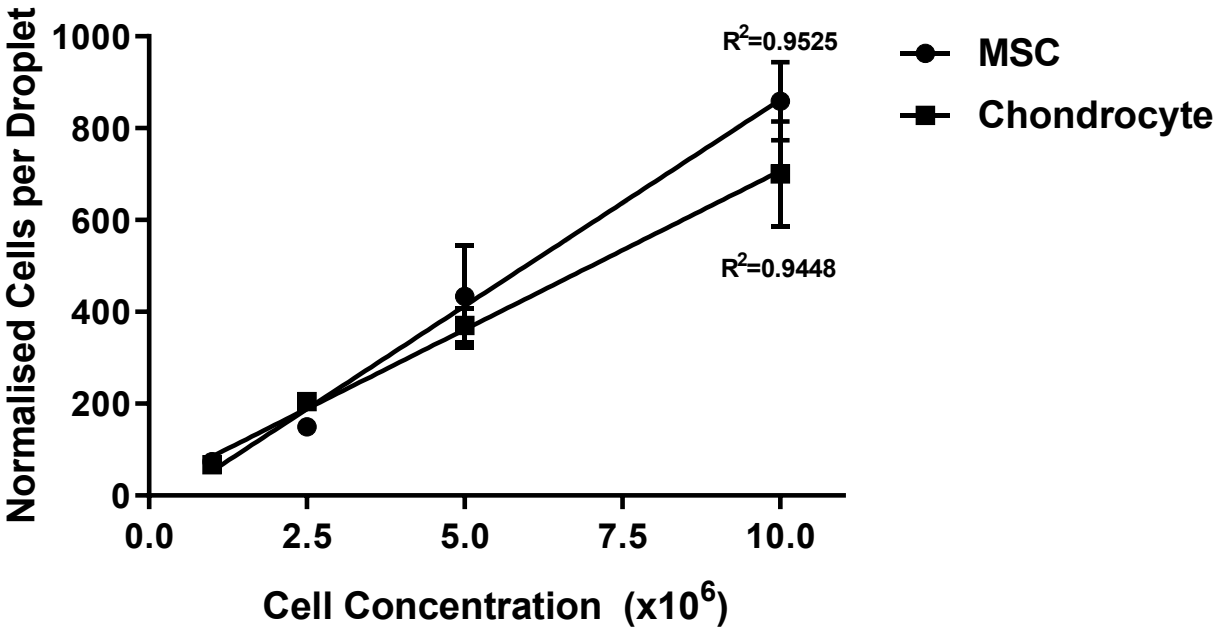

Figure 5.11 – Effect of ink cell concentration on cell deposition performance for MSC and chondrocyte cells printed in cell culture media at a dwell time of 200 µs and backpressure of 200 mmHg. Cell number per sample was normalised to a mean droplet volume of 54 nL. Data represents mean values ± SD. N=6.

5.3.3 Biological Impact Assessment

A range of experiments were conducted to determine the impact of the valve deposition process on cellular viability and function for the MSC and chondrocyte cell lines.

Data presented in Figure 5.12 displays the results of a Live / Dead® cell viability assay comparing the samples deposited via the valve printing process versus manual pipetting. A similar ratio of live to dead cells is observed across both cell lines in either sample group immediately following printing. An increase in cell number is observed at day 1 across both sample groups, with cells readily adhering to the substrate and maintaining viability. Cells appear smaller whilst in suspension immediately following printing, with cell adherence to the culture vessel surface and subsequent cell spreading occurring within a 24 hour period.

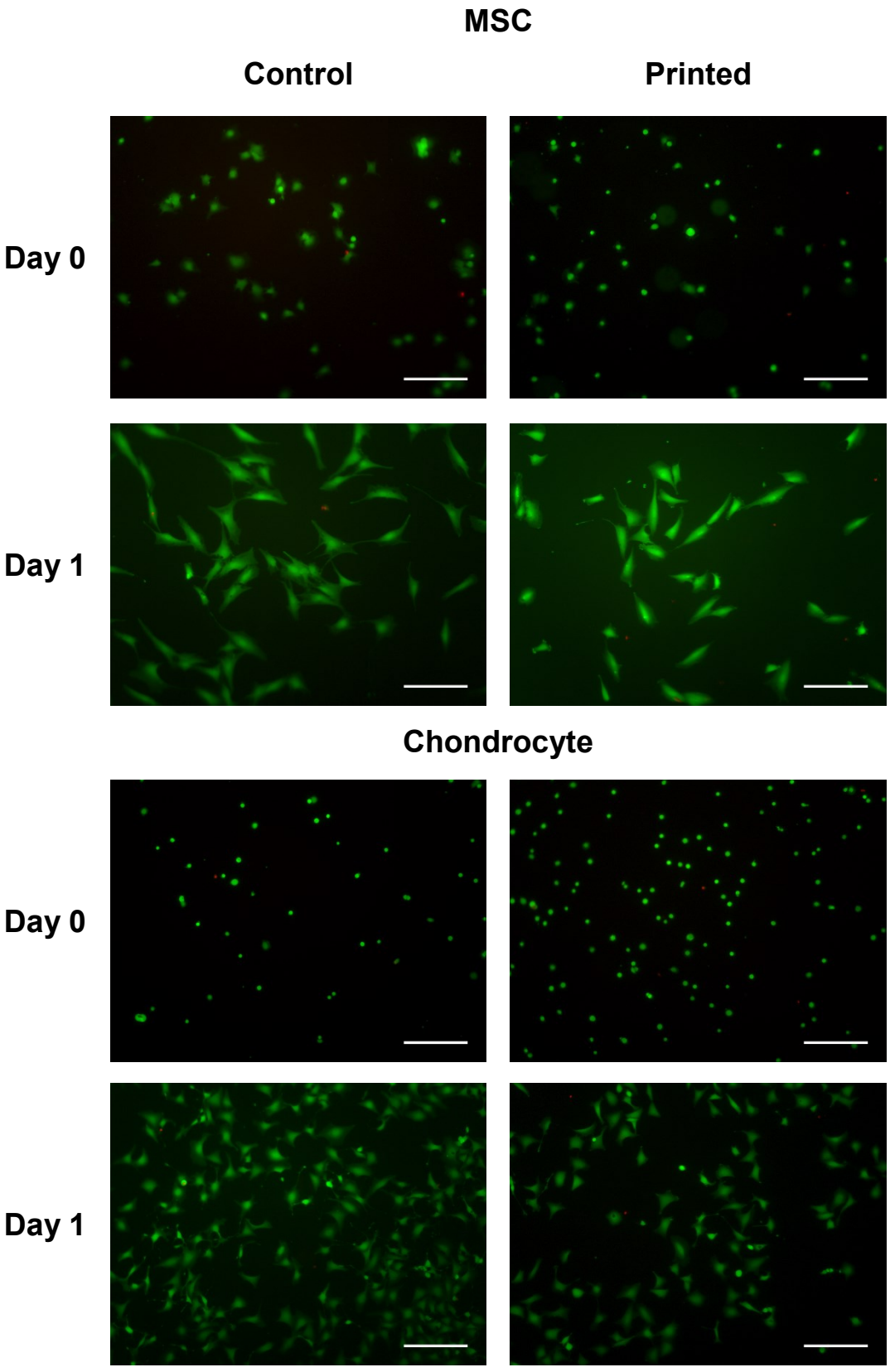

Figure 5.12 – Live / Dead® microscopy images displaying the viability of cells deposited using the valve printer relative to manually pipetted control samples immediately following and 24 hours after printing. Scale bar = 200 µm.

PrestoBlue® metabolic activity data presented in Figure 5.13 displays the impact of the valve printing process on cell metabolism when compared to manual pipetting techniques. No initial effect on the metabolic activity of either cell line was observed across each sample group immediately following seeding. A significant difference between manually seeded and printed samples was observed for both cell lines 24 hours following printing, however this effect was not observed throughout later time points.

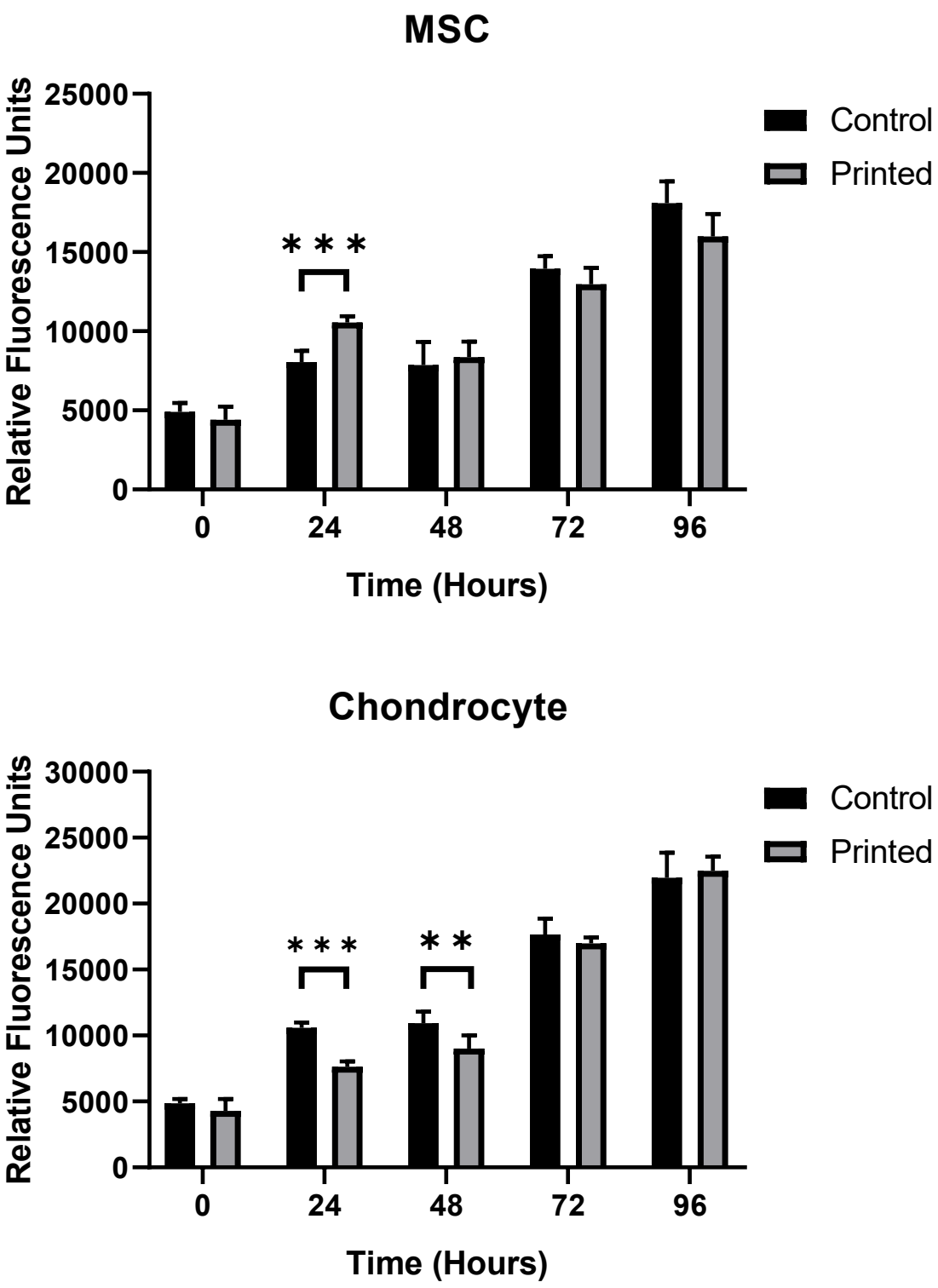

Figure 5.13 – PrestoBlue® metabolic activity assay comparing the metabolic activity of MSC and chondrocyte cell types following printing versus manually pipetted control samples. Data represents mean values ± SD. N=6.

Fluorescence microscopy was used to compare the morphology of cells deposited using the valve printing process with manually seeded cells. No discernible differences in cell adherence rate or morphology were observed for either cell line displayed in Figure 5.14 and Figure 5.15, when compared to manually seeded control cells. Cell confluency was shown to increase in response to increasing incubation period, irrespective of cell seeding method.

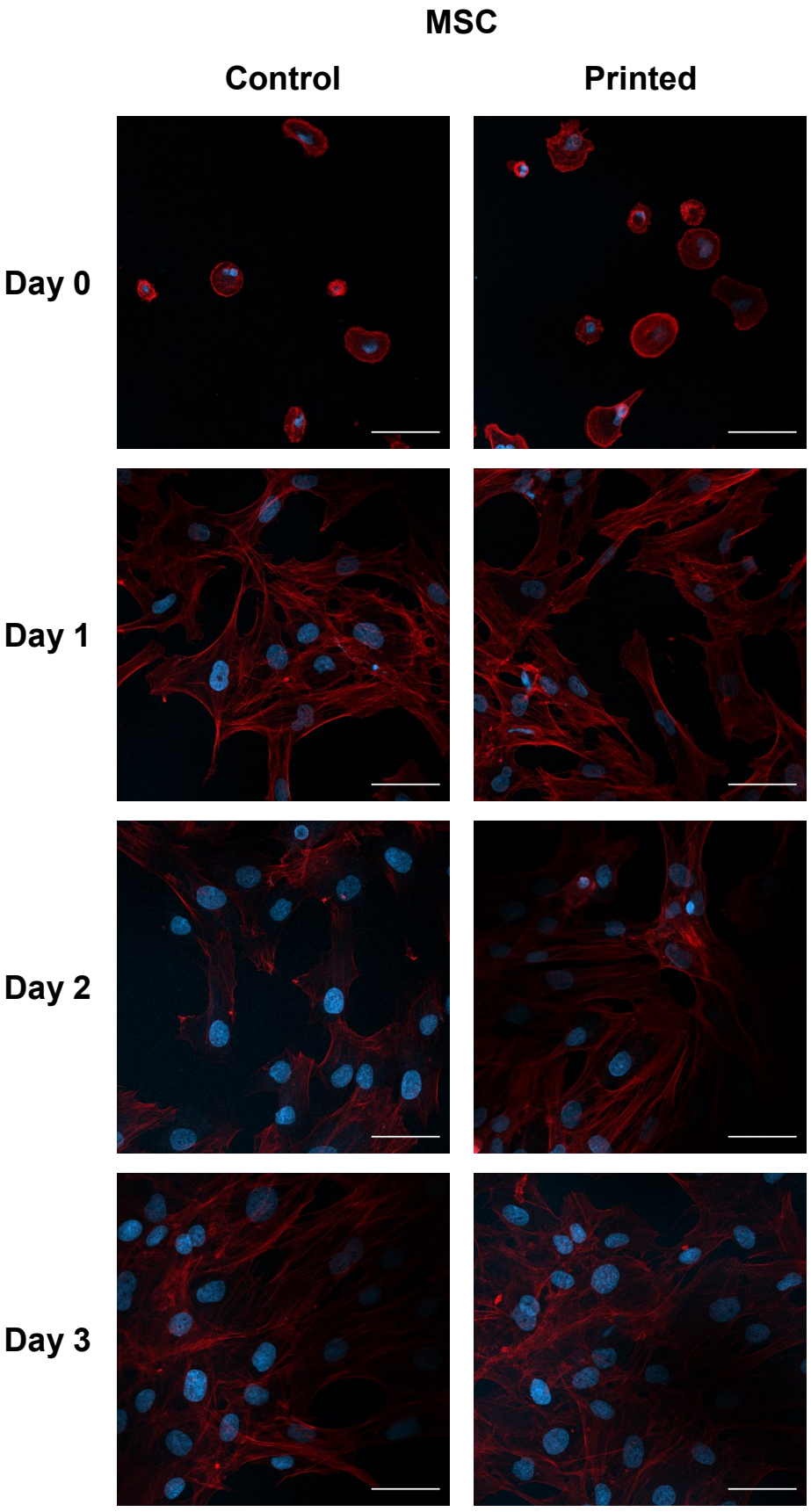

Figure 5.14 – Influence of valve printing process on cell morphology for the MSC line. Cell nuclei were visualised using DAPI (blue) and F-actin using phalloidin (red) staining. Scale bar = 50 µm.

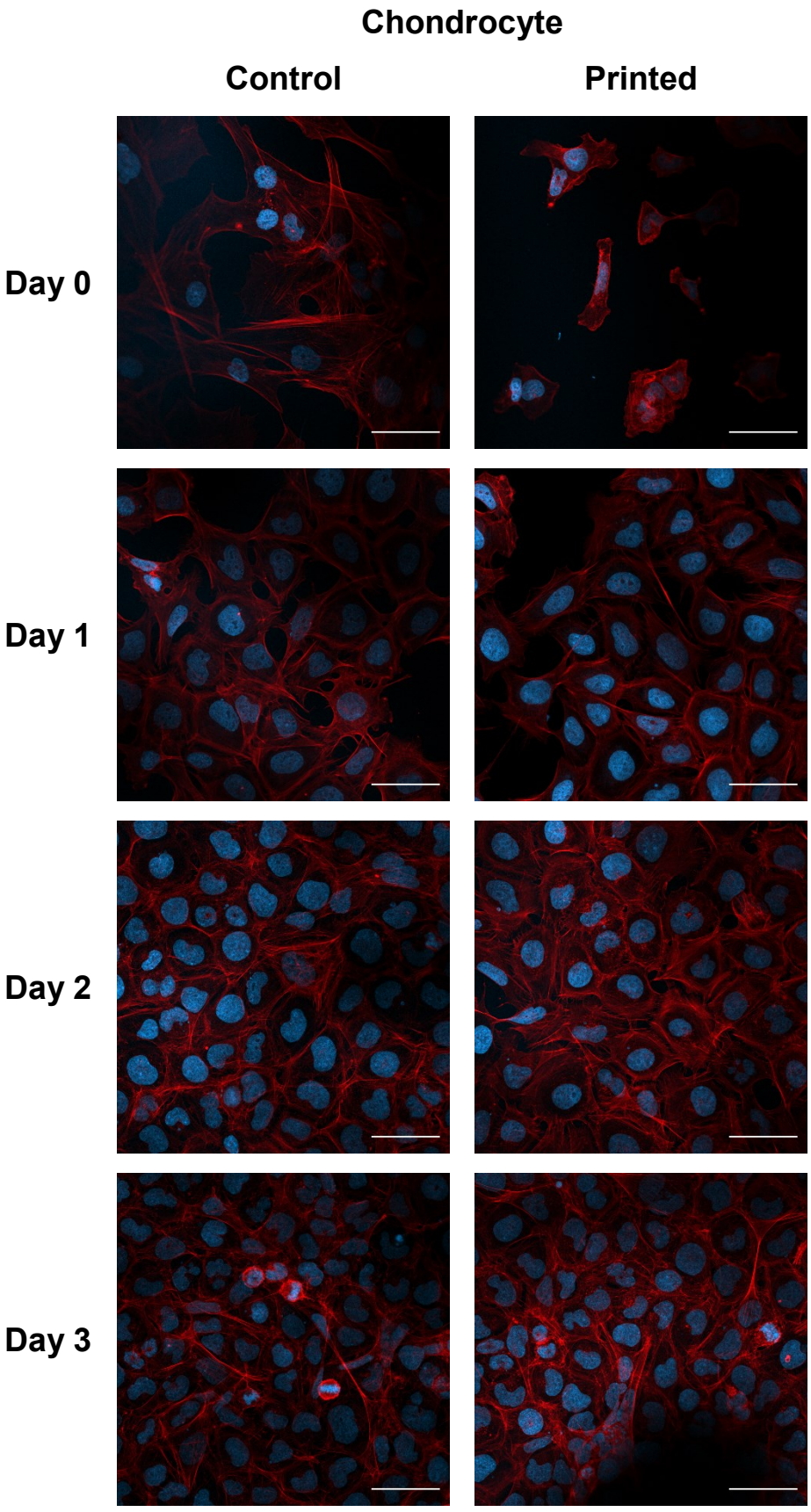

Figure 5.15 – Influence of valve printing process on cell morphology for the chondrocyte cell line. Cell nuclei were visualised using DAPI (blue) and F-actin using phalloidin (red) staining. Scale bar = 50 µm.

A comparison between the proliferation rates of cell seeded using the valve printing process versus manual seeding techniques is shown in Figure 5.16. No significant difference in cell viability or proliferation rate was observed for cells seeded via each technique.

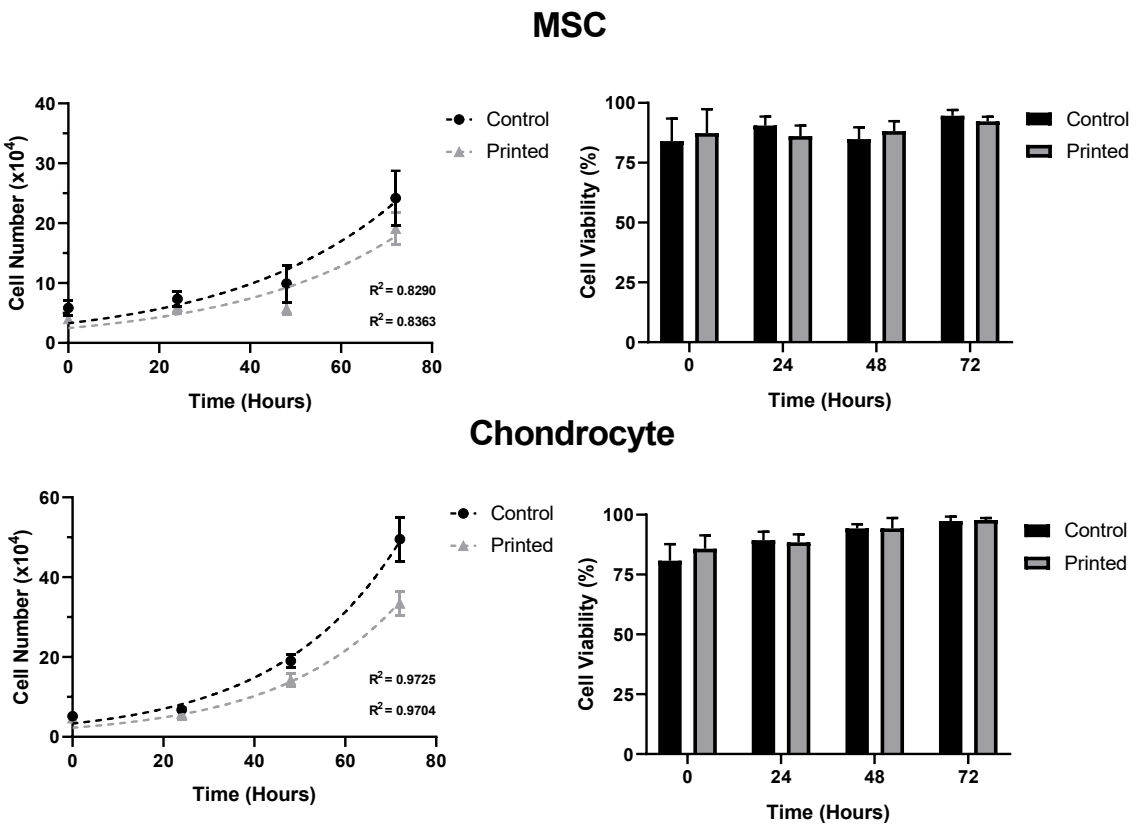

	MSC		Chondrocyte	
	Control	**Printed**	**Control**	**Printed**
Y0 (x10^4)	3.61	2.05	2.98	2.88
K (Hours^{-1})	0.026	0.030	0.039	0.034
Doubling Time (Hours)	26.74	22.84	17.77	20.40

Figure 5.16 – Effect of valve printing process on the proliferation rate of MSC and chondrocyte cell lines in comparison to manually seeded cells. (Left) Live cell number assessed via a trypan blue exclusion test. (Right) Percentage of live cells counted at each time point. (Bottom) Parameters obtained from nonlinear regression analysis using an exponential growth model of cell proliferation data. Data represents mean values ± SD. N=6.

An investigation was performed to assess the potential for using the valve printing process to seed cells for the production of cell aggregates. The suitability of the valve printing process was assessed by comparing the aggregate formation of printed MSC and chondrocyte cells with aggregates generated via manual seeding techniques.

5.3.4 Hanging Droplet Aggregate Culture

The hanging droplet culture technique was initially employed for the production of cellular aggregates across a range of cell seeding densities over a 9 day incubation period.

MSC aggregates were successfully generated across the cell seeding density range assessed in both manually deposited and printed samples within the first 24 hours of culture, as shown in Figure 5.17. Aggregates remained intact throughout the 9 day incubation period with subsequent cellular outgrowth and debris accumulation occurring during the later time points. Secondary aggregate formation was observed in the printed samples, reducing the compactness and sphericity of the primary aggregates generated.

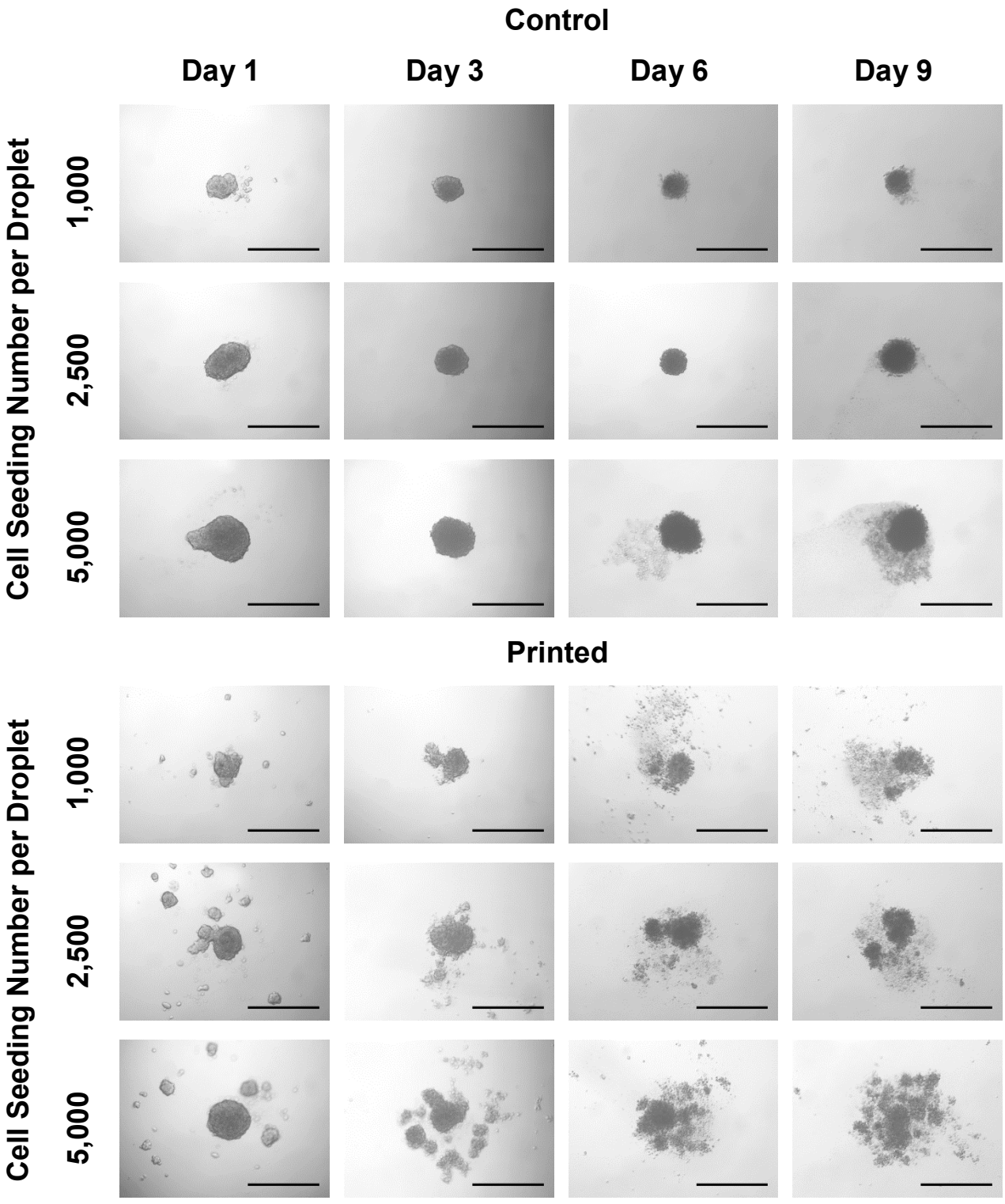

Figure 5.17 – Comparison between MSC aggregates seeded via manual pipetting and valve-based deposition when using the hanging droplet culture method. Cells were seeded across a range of cell seeding densities and imaged over a 9 day incubation period. Scale bar = 400 µm.

Chondrocyte hanging droplet aggregate formation was observed in Figure 5.18 across all samples, however aggregate compactness and stability was significantly reduced when compared to MSC cultures. Extensive secondary aggregate formation was observed within

the first 24 hours of culture, alongside a reduction in primary aggregate density over the course of the incubation period. Progressive cellular outgrowth and a reduced degree of aggregation were also observed across both manually seeded and valve printed samples, irrespective of the initiating cell seeding density. These effects were most significant at the highest cell seeding density of 5,000 cells per hanging droplet.

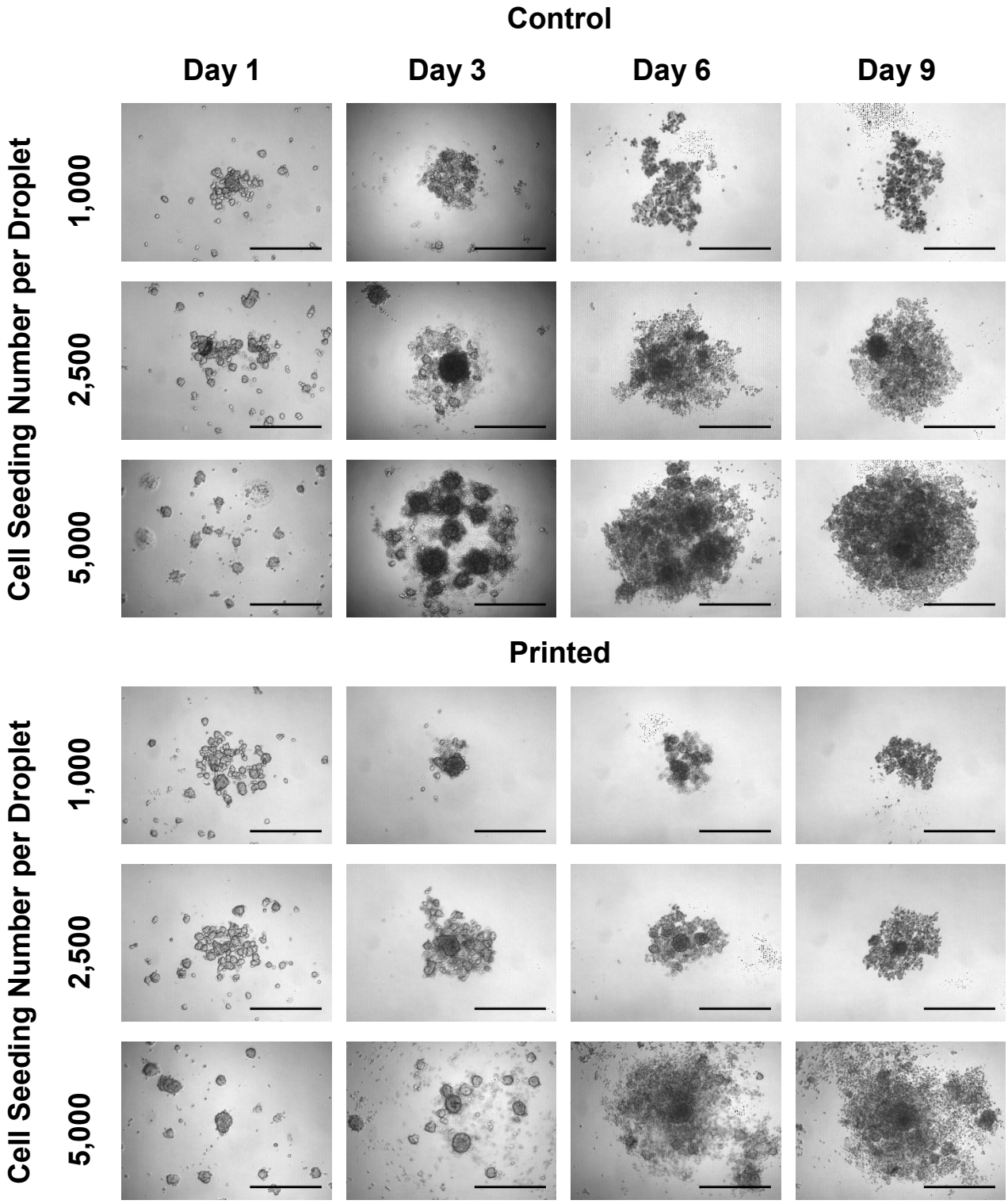

Figure 5.18 – Comparison between chondrocyte aggregates seeded via manual pipetting and valve-based deposition when using the hanging droplet culture method. Cells were

seeded across a range of cell seeding densities and imaged over a 9 day incubation period. Scale bar = 400 µm.

Bubble formation was observed in samples generated using the printing technique due to the air gap between the jetting device and substrate during printing. This is highlighted in the image in Figure 5.19 taken immediately following the seeding of hanging droplets.

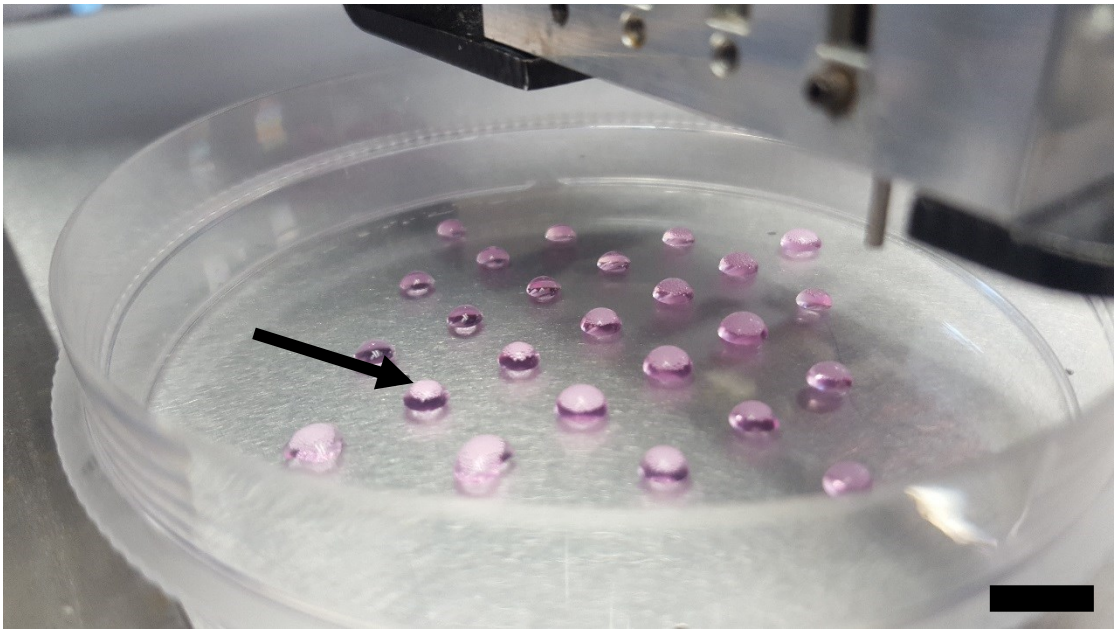

Figure 5.19 – Bubble formation within valve printed hanging droplet arrays. MSCs were deposited at a concentration of 10^6 cells per mL in cell culture media. Scale bar = 1 cm.

Figure 5.20 displays images of arrays of hanging droplets printed across a range of valve backpressures. An increase in pressure applied to the valve was shown to increase the degree of droplet splashing, resulting in additional bubble formation and irregular droplet volumes. The removal of foetal bovine serum from the cell culture media altered the surface tension of the ink, thus reducing the rate of bubble formation during printing.

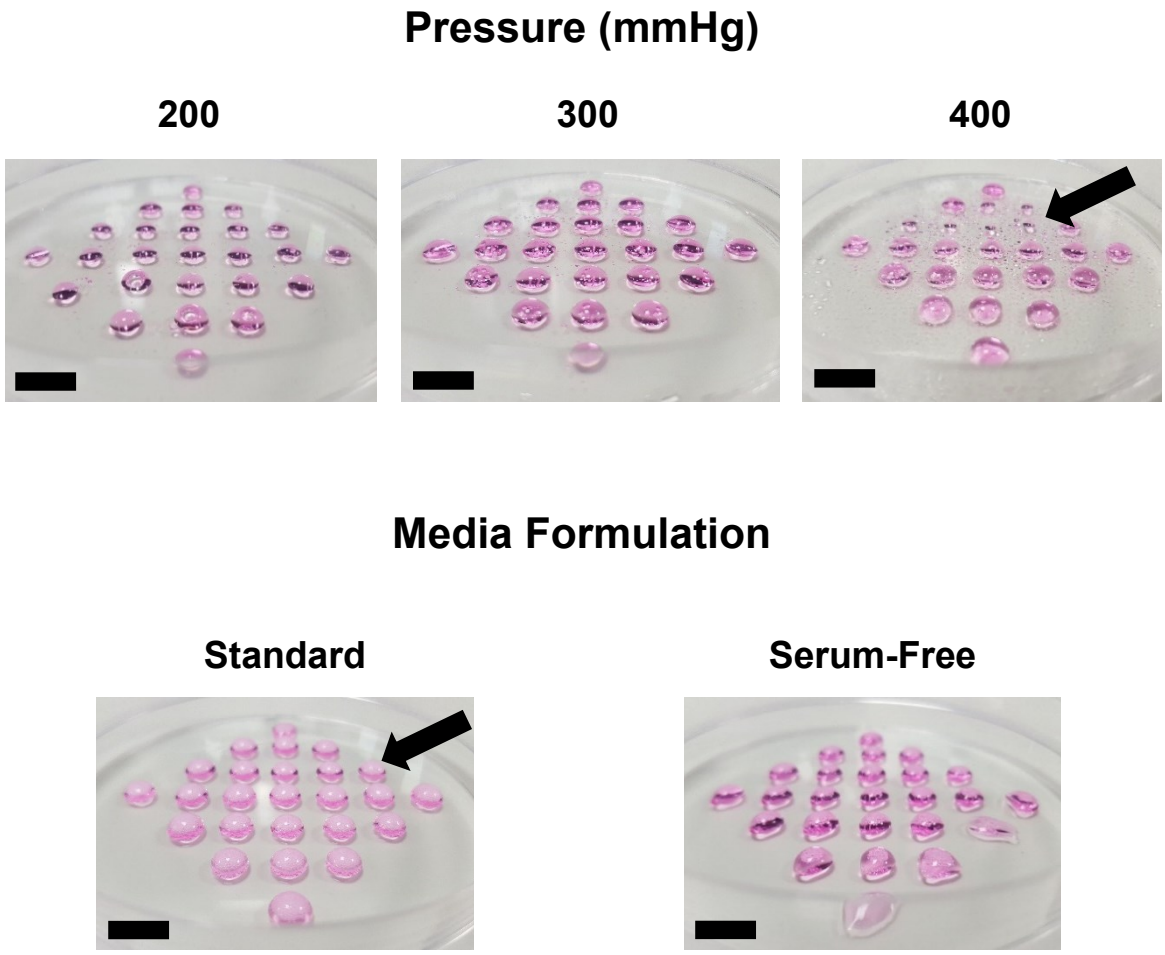

Figure 5.20 – Effect of backpressure applied to the valve and media composition on bubble formation within printed droplets of cell culture media. Arrows indicate droplet splattering and foam formation respectively. Scale bar = 1 cm.

5.3.5 In-Well Aggregate Culture

An in-well gravimetric culture technique was also assessed for the production of MSC and chondrocyte aggregates across a higher cell seeding density range.

Images in Figure 5.21 display the morphology of aggregates generated by seeding MSCs using the valve printing process versus manual seeding techniques. MSC aggregates were formed within the first 24 hours of seeding for both manually seeded and printed samples across the full range of cell seeding densities assessed. Cells further condensed over the remainder of the time course, with minimal cell outgrowth or secondary aggregate formation observed.

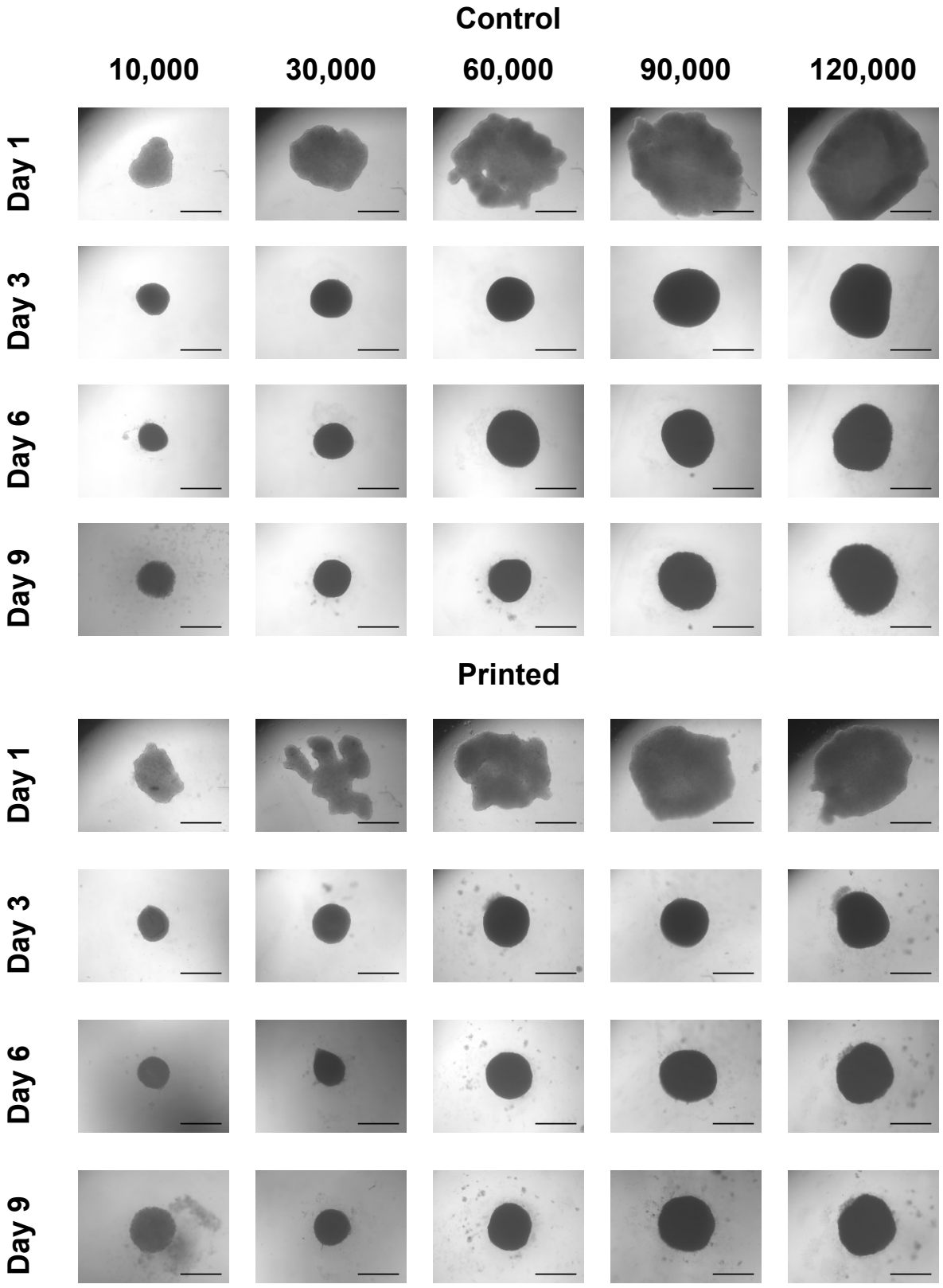

Figure 5.21 – MSC aggregates generated using the in-well aggregate culture technique across a range of cell seeding densities. Scale bar = 400 µm.

Quantification of aggregate diameter in Figure 5.22 revealed a reduction in aggregate diameter over the first 3 days of culture as cells condensed, with no further change in aggregate diameter observed across each condition. Cell seeding density was shown to

positively correlate with aggregate size throughout the 9-day incubation period. No significant difference in aggregate size was observed between manually seeded and printed aggregates in each cell seeding density sample group.

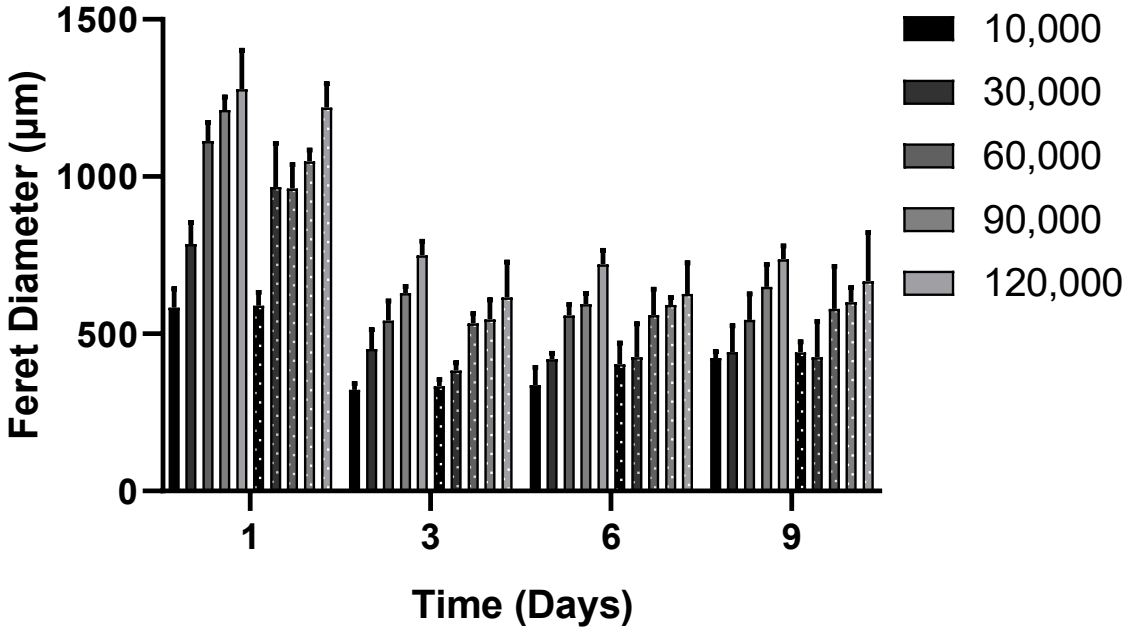

Figure 5.22 – MSC aggregate diameter measurements generated using the in-well aggregate culture technique across a range of cell seeding densities. Cells were seeded using either manual (solid lines) or printed (dotted lines) methods. Data represents mean values ± SD. N=3.

Figure 5.23 displays the morphology of chondrocyte aggregates generated using the valve deposition technique. Cells aggregated within the first 24 hours of culture across each of the cell seeding densities assessed, irrespective of seeding method. Cellular debris was observed from day 3 and was most pronounced in samples with a higher cell seeding density. This resulted in a reduction in aggregate sphericity and density.

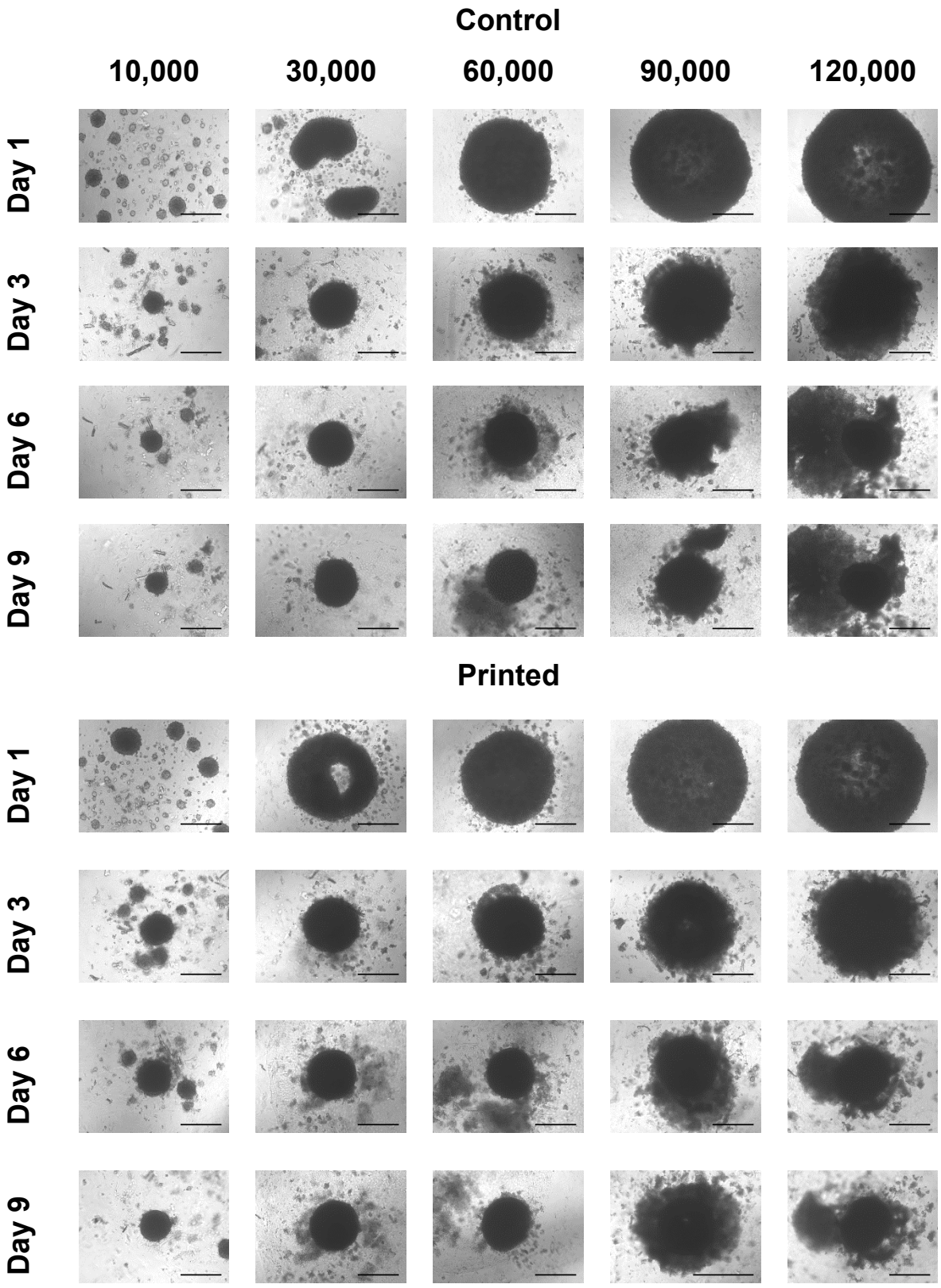

Figure 5.23 – Chondrocyte aggregates generated using the in-well aggregate culture technique across a range of cell seeding densities. Scale bar = 400 µm.

Quantification of aggregate diameter in Figure 5.24 displayed a similar pattern of cell condensation over the first 3 days of culture via a reduction in aggregate diameter. Cell seeding density was shown to correlate with aggregate size alongside a further reduction in

the diameter of aggregates seeded at 10,000 cells per well. A statistically significant difference in the size of printed versus manually seeded aggregates was observed at day 1 when seeding cells at a density of 30,000 cells per well. Cell seeding technique was not observed to significantly impact aggregate size across other time points or cell seeding densities.

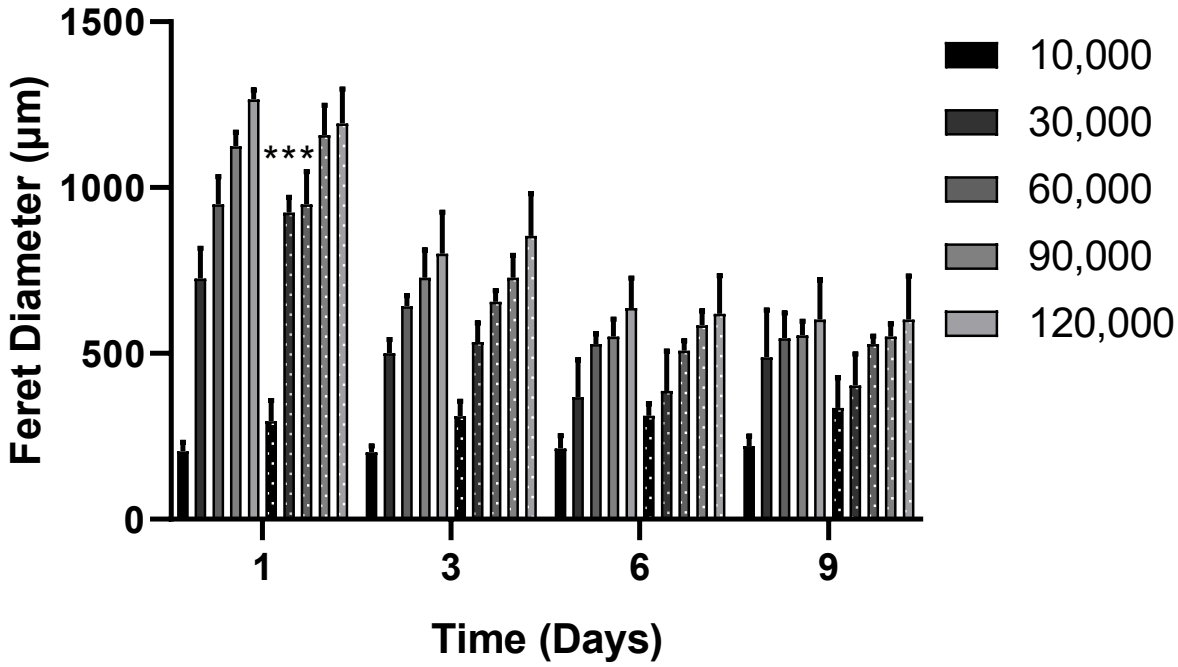

Figure 5.24 – Chondrocyte aggregate diameter measurements generated using the in-well aggregate culture technique across a range of cell seeding densities. Cells were seeded using either manual (solid lines) or printed (dotted lines) methods. Data represents mean values ± SD. N=6.

An additional set of experiments were performed to assess the stability and biological properties of the aggregates generated over an extended culture period.

Figure 5.25 shows the morphology and diameter measurements of chondrocyte aggregates generated at a cell seeding density of 60,000 cells per well. Aggregate size remained stable following an initial cell condensation period within the first 7 days. A significant amount of cellular debris accumulated within the base of the wells surrounding each aggregate during extended culture. No significant difference in aggregate morphology or diameter was observed between the manually seeded and printed samples at each time point.

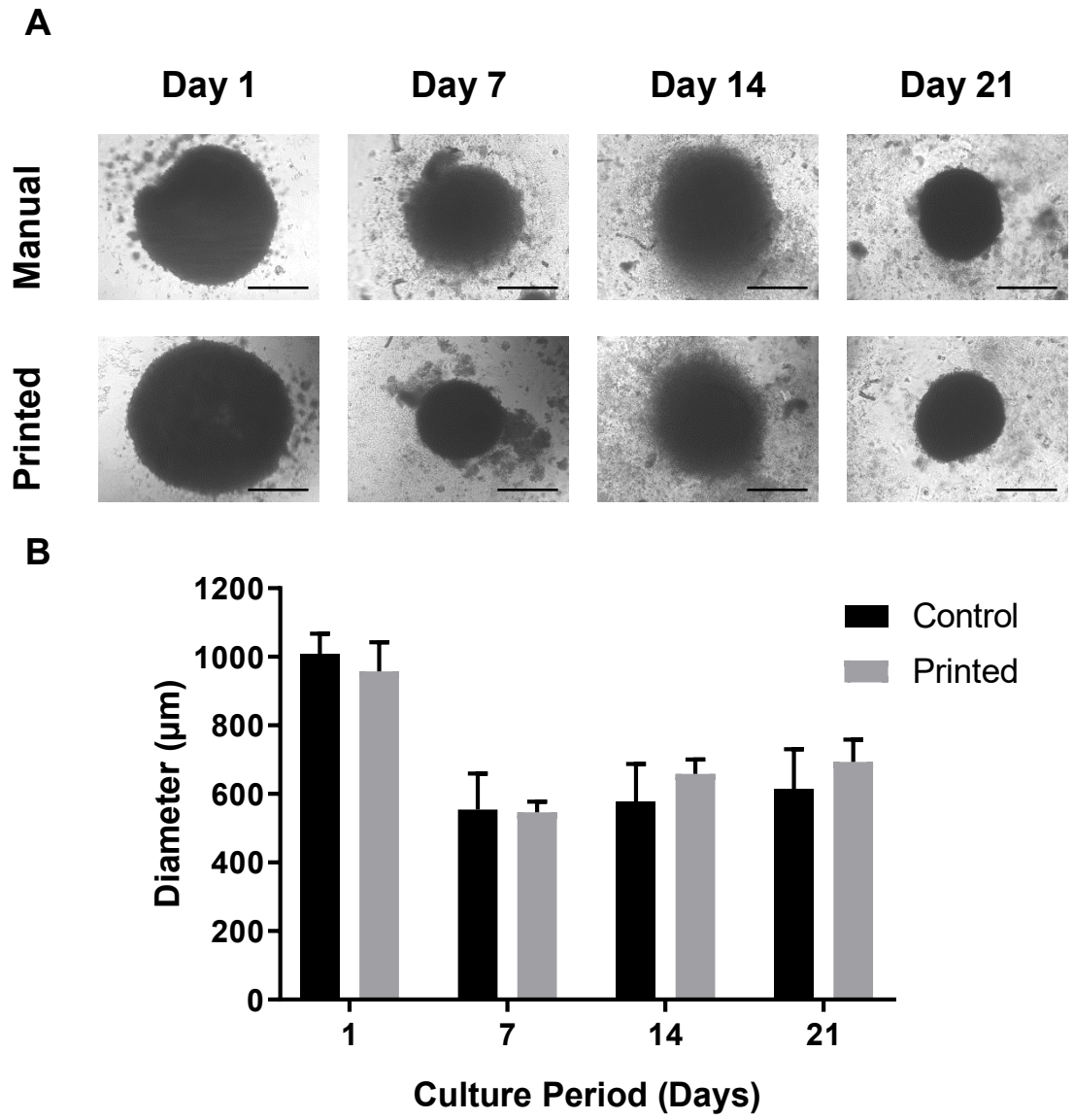

Figure 5.25 – Comparison between chondrocyte aggregates seeded via manual pipetting and valve-based deposition when using the in-well culture method. Cells were seeded at a density of 60,000 cells per well and incubated over a 21-day period. (A) Bright-field microscopy images showing aggregate morphology during culture. Scale bar = 400 am. (B) Quantification of aggregate diameter. Data represents mean values ± SD. N=6.

A combination of histological and indirect immunofluorescence staining was employed to biologically characterise the aggregates generated.

Haematoxylin and eosin staining of sectioned aggregates displayed in Figure 5.26 revealed no significant differences in tissue morphology or cellular organisation as a result of the printing process. An increase in eosinophilic staining was observed within the central region of each aggregate. Sample degradation was observed as a result of the sectioning process.

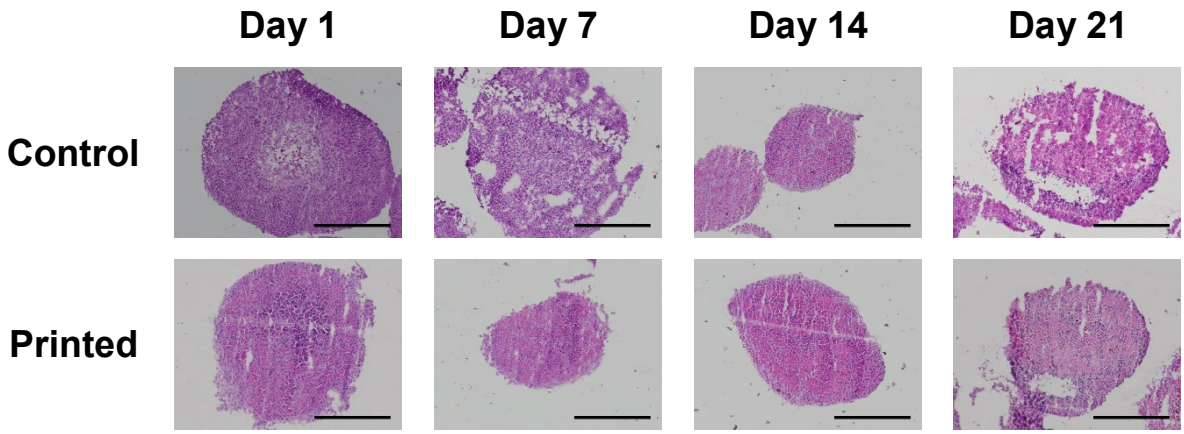

Figure 5.26 – Haematoxylin and eosin staining of chondrocyte cell aggregates generated using the valve printing process versus manually seeded controls. Cells were cultured in DMEM / F12 media over a 21-day culture period. Scale bar = 500 µm.

Indirect immunofluorescence microscopy data shown in Figure 5.27 displays no discernible variations in collagen II or aggrecan expression between aggregates seeded using the valve printing technique and manual methods. A low level of marker expression was observed throughout the 21-day assessment period.

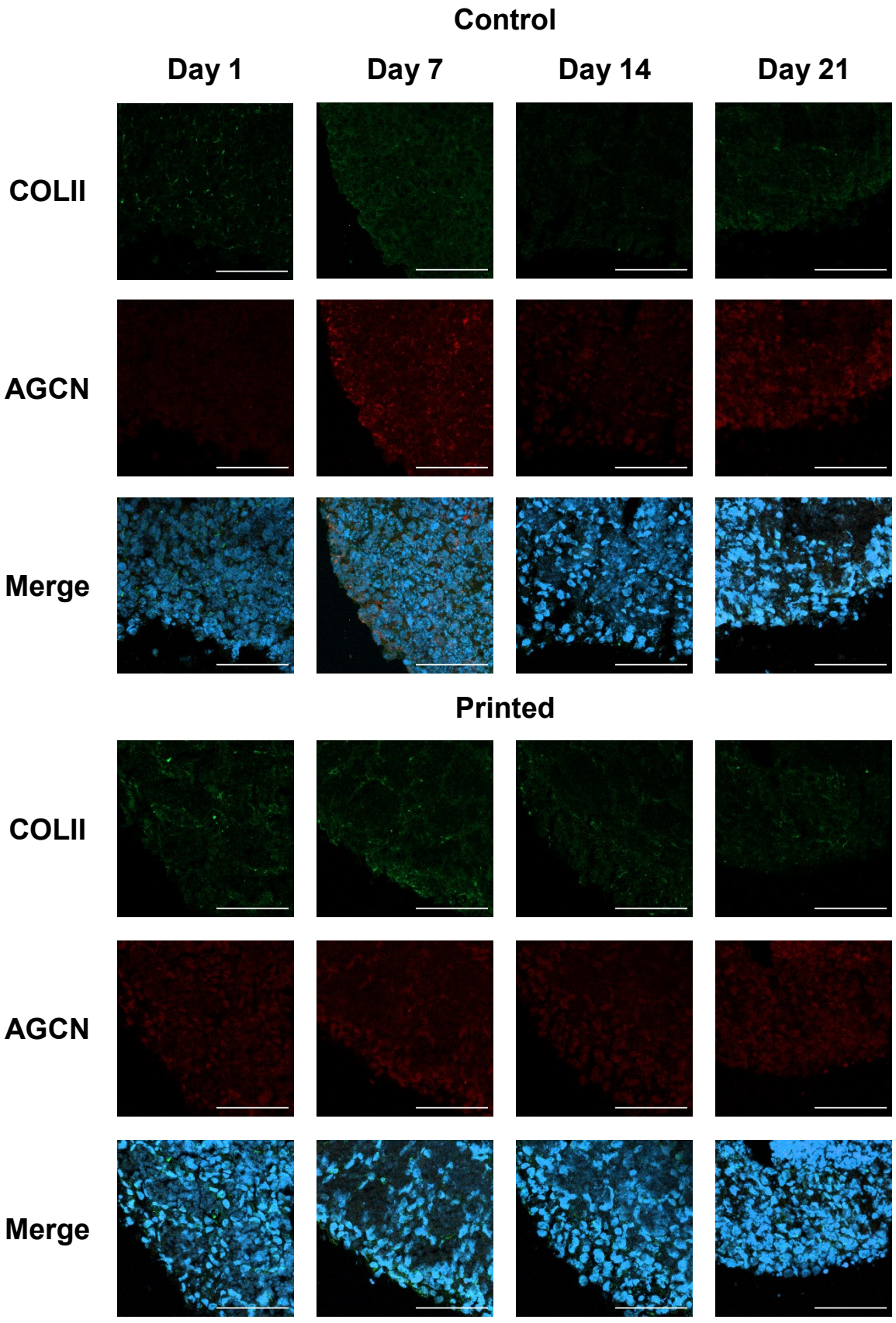

Figure 5.27 – Immunostaining data comparing the collagen II (COLII, green) and aggrecan (AGCN, red) content of chondrocyte cell aggregates generated using the valve printing process versus manually seeded controls. Cells were cultured in DMEM / F12 media over a 21-day culture period. Cell nuclei were visualised using DAPI (blue) staining. Scale bar = 100 µm.

Figure 5.28 presents the aggregates generated from MSCs seeded at a density of 60,000 cells per well over a 21-day incubation period. Cells were treated with both basal and chondrogenic media formulations to evaluate the influence of differentiation-inducing media on cell phenotype within the aggregate culture format. A similar pattern of cell condensation was observed within aggregates during the first 7 days of culture, with aggregate size remaining stable throughout the remaining time points. Secondary aggregate formation was also observed during extended periods of culture. No significant differences were observed in aggregate size or morphology between printed and manually seeded cells under basal media formulations. Chondrogenic media formulations were shown to have a significant effect on aggregate size in both manually seeded and valve printed samples.

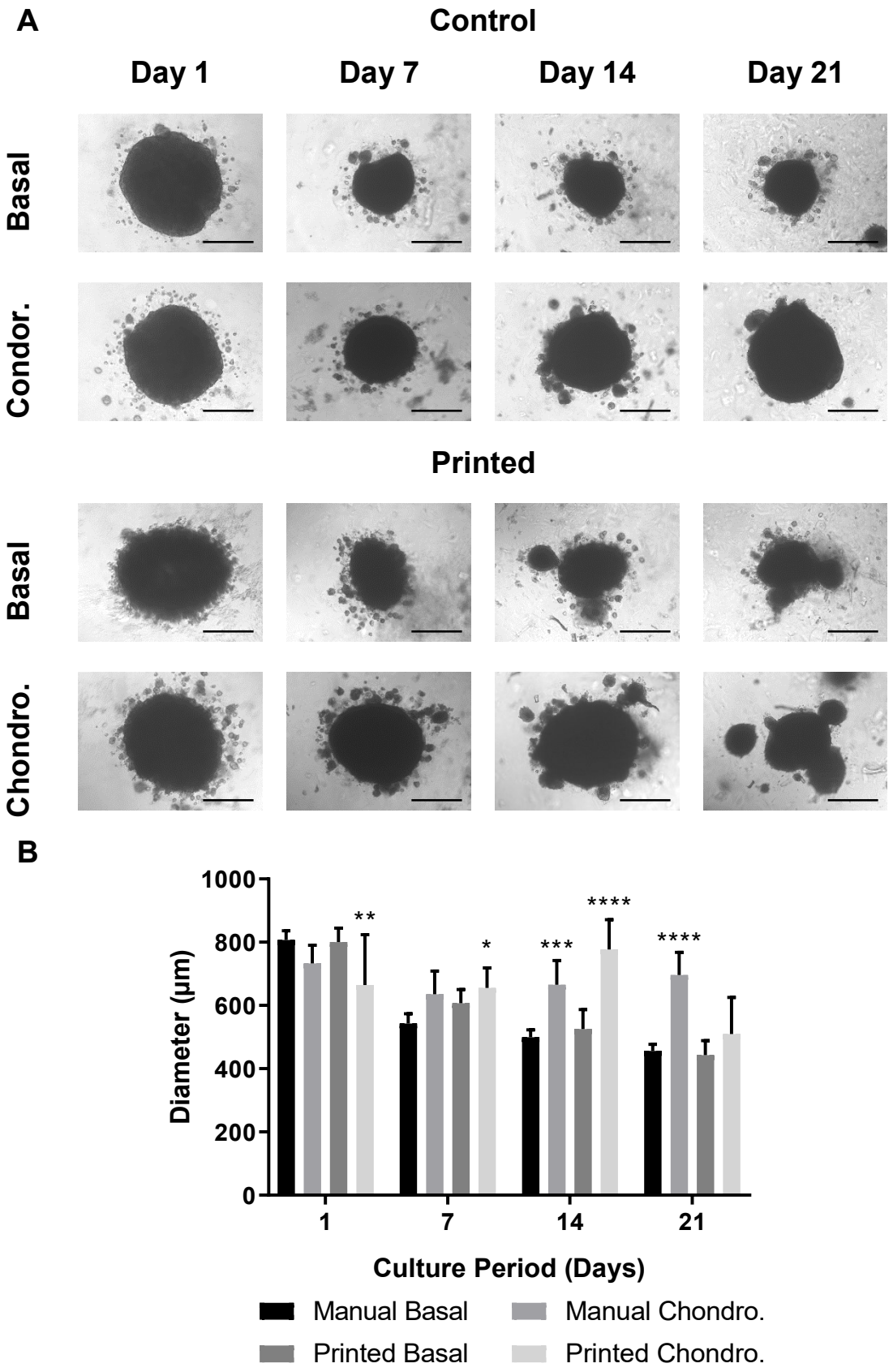

Figure 5.28 – Comparison between MSC aggregates seeded via manual pipetting and valve-based deposition when using the in-well culture method. Cells were seeded at a density of 60,000 cells per well and incubated in basal and chondrogenic media formulations over a 21-day period. (A) Bright-field microscopy images showing aggregate

morphology during culture. Scale bar = 400 µm. (B) Quantification of aggregate diameter. Data represents mean values ± SD. N=6.

Haematoxylin and eosin staining of the sectioned MSC aggregates in Figure 5.29 revealed no significant differences in tissue structure in response to the cell seeding method. A similar pattern of sample degradation was observed in response to the sectioning process with variations in section size caused by section positioning within the tissue.

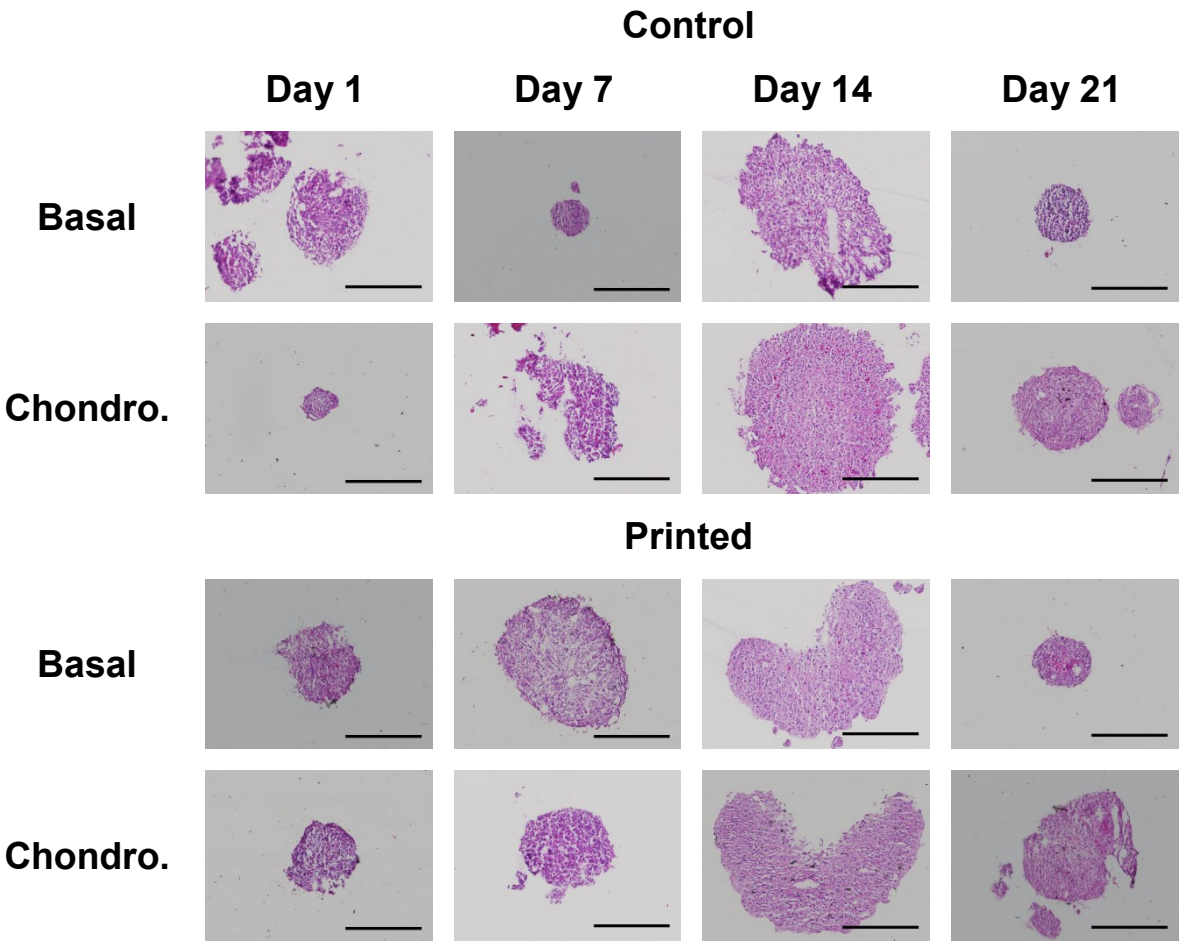

Figure 5.29 – Haematoxylin and eosin staining of MSC aggregates generated using the valve printing process versus manually seeded controls over a 21 day culture period in basal and chondrogenic media formulations. Scale bar = 500 µm.

Indirect immunofluorescence staining was performed on the MSC aggregates displayed in Figure 5.30 and Figure 5.31 for basal and chondrogenic media formulations respectively. No discernible difference in collagen II or aggrecan protein expression was observed between the printed and manually seeded aggregates under either media formulation. An elevation in aggrecan expression was observed at 21 days for samples exposed to basal media formulations and 7 days for samples exposed to chondrogenic media formulations. Basal media formulations displayed peak collagen II expression at 21 days of culture, with cells

exposed to chondrogenic media formulations displaying peak collagen II expression within the first 7 days of culture.

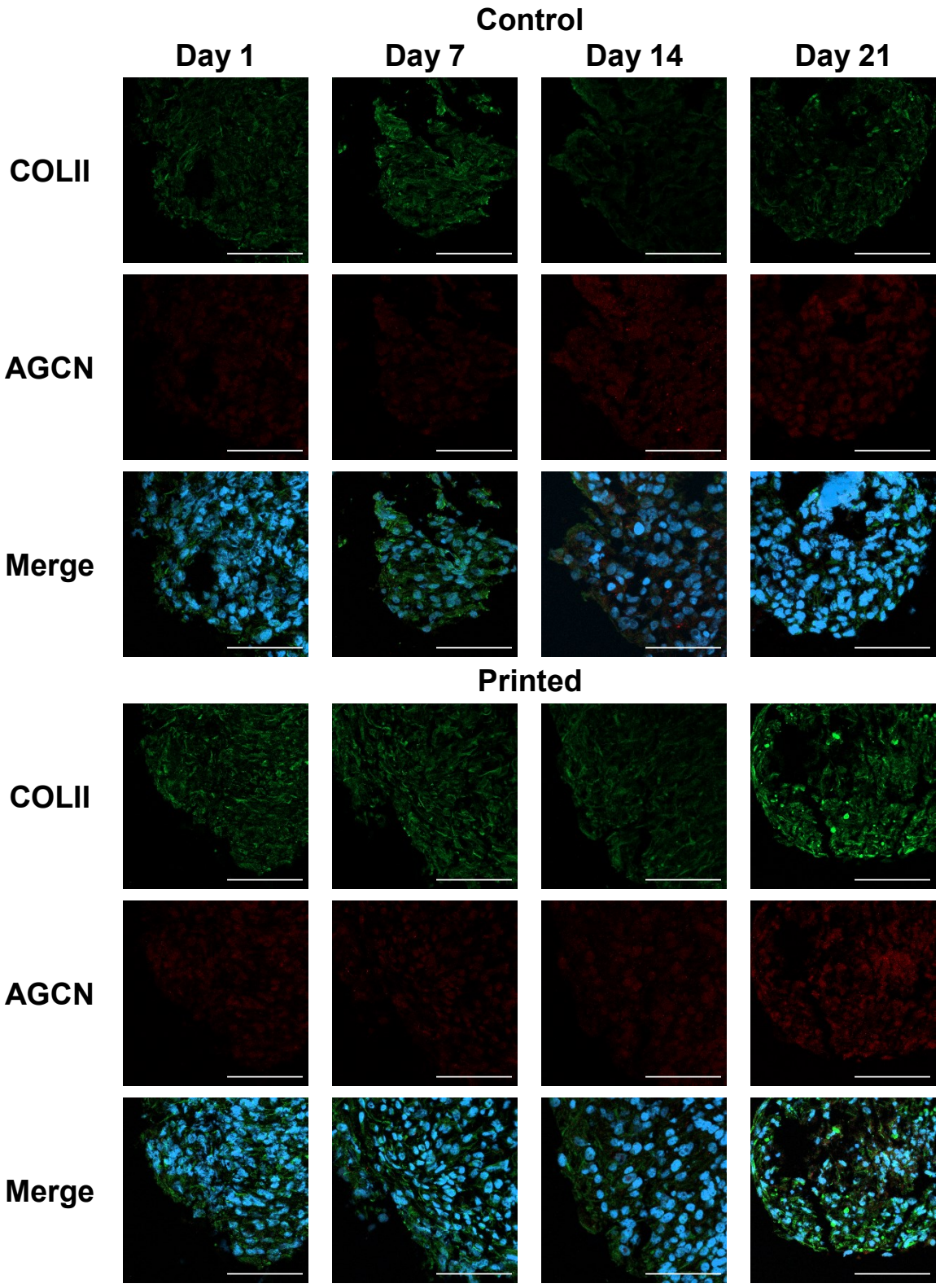

Figure 5.30 – Immunostaining data comparing the collagen II (COLII, green) and aggrecan (AGCN, red) content of MSC aggregates generated using the valve printing process versus manually seeded controls over a 21 day culture period in basal media. Cell nuclei were visualised using DAPI (blue) staining. Scale bar = 100 µm.

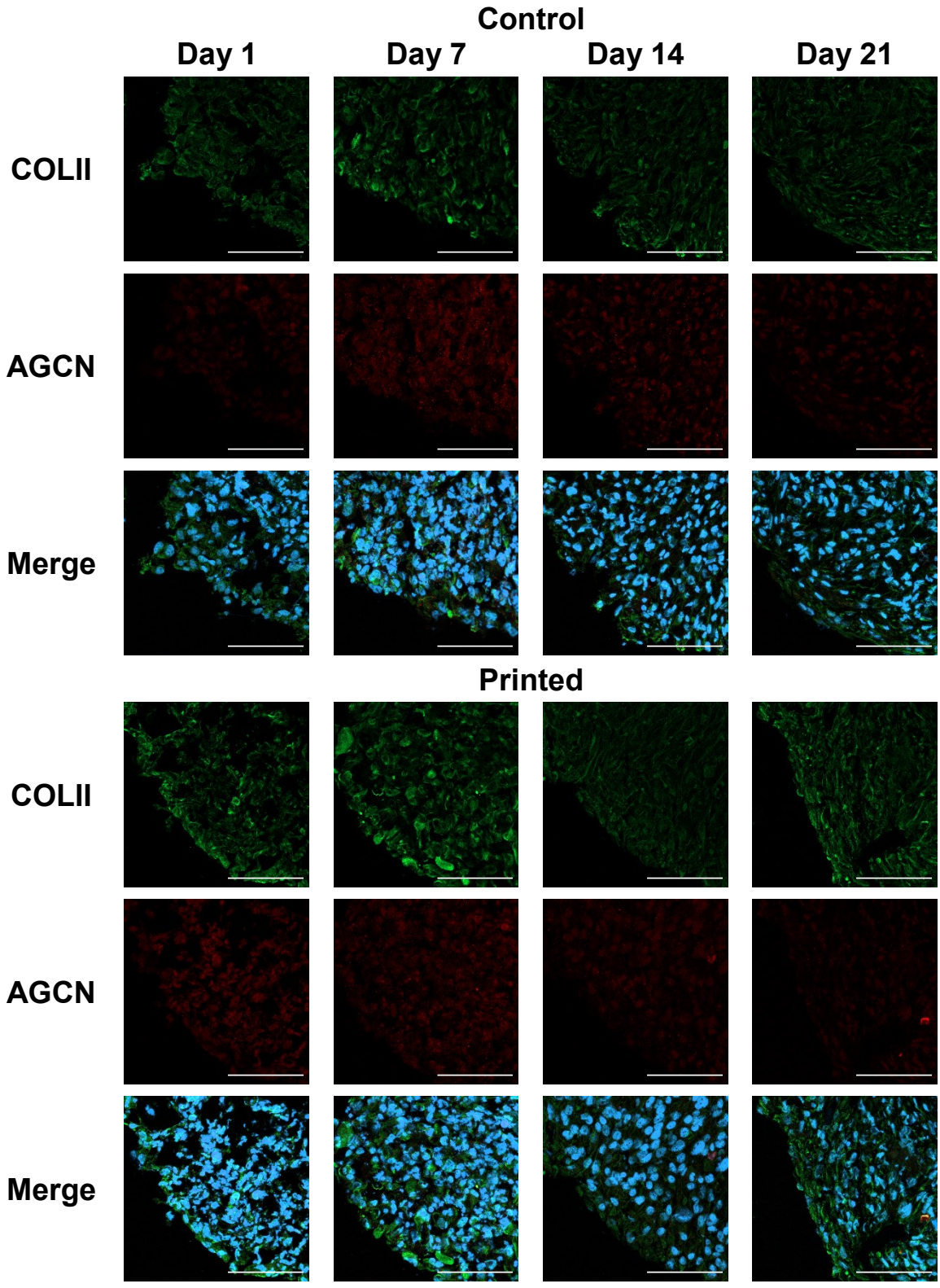

Figure 5.31 – Immunostaining data comparing the collagen II (COLII, green) and aggrecan (AGCN, red) content of MSC aggregates generated using the valve printing process versus manually seeded controls over a 21 day culture period in chondrogenic media. Cell nuclei were visualised using DAPI (blue) staining. Scale bar = 100 µm.

5.4 Discussion

5.4.1 Material Deposition Performance

An initial investigation was performed to assess the impact of various printing parameters on valve deposition performance. A gravimetric approach was used to determine droplet volume via the measurement of material mass following deposition.

Experimental research displayed in Figure 5.3 showed a strong correlation between the waveform dwell time applied to the valve and the volume of material dispensed per actuation cycle. A minimum operational dwell time of 150 µs was required in order to achieve droplet ejection, with a dwell time of 200 µs required to prevent material build-up on the nozzle during printing. Backpressure applied to the valve during jetting was shown to have a minimal effect on material ejection characteristics under shorter dwell time configurations, with 200 mmHg providing the greatest linearity in dispense performance over the dwell time range assessed. A low pressure range was assessed within this research to minimise potential pressure related damage to cellular material during bioprinting experiments. It is possible that this range was insufficient to cause substantial variations in material ejection volume per valve actuation cycle due to the considerably larger range of operational pressures that the valve was designed to function across.

A pressure of 200 mmHg and dwell time of 200 µs was selected in order to maximise the resolution of the valve printing process whilst maintaining printer reliability. Under this configuration, a droplet volume of approximately 50 nL was achieved.

Observation of the fluid ejection characteristics from the valve displayed the ejection of a large droplet volume with a substantial tailing ligand, as shown in Figure 5.4. Partial ligand recombination was observed during droplet flight, with a small number of satellite droplets forming as a result of ligand destabilisation. A lack of granularity in the control of droplet ejection characteristics was observed when comparing the valve printing process to previous research using inkjet printing devices. This was due to the limited waveform modifications that could be achieved when employing a spike-and-hold driver and ‘ON/OFF’ actuator versus the dynamically adjustable piezoelectric actuator within an inkjet system. As a result, it was not possible to further adjust droplet volume or prevent satellite formation, limiting the accuracy and maximum resolution of the printing process.

Figure 5.5 displayed the correlation between actuation cycle number and total dispensed volume for the valve under previously defined parameters. As anticipated, a high degree of

linearity was observed between dispense volume and the total number of droplet ejections requested. A droplet volume of approximately 61 nL was defined for the printing configuration assessed, based upon linear regression analysis. A coefficient of variation percentage (CV) was calculated for measurements at each droplet ejection cycle number to determine the precision of the printing process across different target volumes. The CV ranged from 2-11 %, with the highest variation in dispense volume occurring at the lowest dispensed volume. A CV of below 7 % was calculated across droplet volumes above the minimum dispense volume. The precision of the valve printing system corroborated with the literature values reported for state-of-the-art liquid handling systems when dispensing similar fluids under a gravimetric calibration methodology (Taylor *et al.*, 2002; Stangegaard *et al.*, 2011; Bessemans *et al.*, 2016). This data demonstrates the precision of the valve dispensing device in a DoD configuration to deposit material across a wide volume range.

A recognised limitation of the gravimetric measurement technique is the high minimum droplet mass required for measurements using a conventional microbalance. Due to the low per actuation cycle volume dispensed by the valve, it was necessary to deposit a large number of droplets and divide the final mass by this number to identify an average droplet mass. As a consequence, this approach prevented comparisons from being made between the volumes of individual droplets dispensed. In addition, material lost as a result of splashing or evaporation was not accounted for within droplet measurements, and all measurements were dependent upon the accuracy and precision of the balance used. It is hypothesised that these effects contributed to the increased CV observed when depositing a low number of droplets. Despite these limitations, gravimetric methods remain a common standard for the calibration of printing devices and liquid handling systems (Faulkner-Jones *et al.*, 2013; Bessemans *et al.*, 2016).

An additional experiment was performed, as shown in Figure 5.6, to determine the volume of individual droplets based upon the detection of printed fluorescent material. This technique required interpolation of material volume via fluorescent readings from a standard curve, having been previously validated within the literature to assess the dispensing performance of liquid handling systems at the nanolitre-scale (Rodríguez-Puente, Linacero-Blanco and Guasch, 2013). Data was obtained on the printing performance of the valve when dispensing material across a lower volume range than the gravimetric method.

A droplet volume of approximately 54 nL was identified using the fluorometric approach. This technique enabled the calculation of dispense volumes down to the single droplet scale, providing further characterisation of the deposition process. A high degree of linearity was observed when depositing 1-20 droplets per well, indicating that the sequential actuation of the valve had no significant effect on per droplet volume. In addition, CV calculations for each sample group revealed a consistent dispensing precision of below 9 %. This data contrasts with the findings of earlier gravimetric studies by indicating that the precision of the valve dispensing system remained stable across the low droplet cycle range. This finding represented a critical factor for the operation of the valve printing processes in a DoD configuration, whereby variations in actuation cycle represent the primary method to adjust dispense volume. Retaining the DoD approach was considered essential in the optimisation of the printing process to maximise compatibility with 3D bioprinting applications, where structures are generated from the sequential stacking of individual droplets at a specified coordinate (Da Conceicao Ribeiro *et al.*, 2019).

These results corroborate with research conducted by Bammesberger *et al.* to compare the performance of commercial non-contact valve and positive displacement micro dispensing systems using fluorometric detection methods. The jetting performance of state-of-the-art valve dispensing devices was assessed across a target droplet volume range of 50 nL to 1 µL under a continuous jetting mode, whereby total dispense volume was controlled through adjusting the dwell time of the actuation signal. Jetting precision and volume working range of the system benchmarked within this research was shown to remain competitive with the commercial systems assessed, whilst retaining a DoD printing approach. The precision and accuracy of the DoD valve printing device was also shown to be superior to the results reported for positive displacement systems (Bammesberger *et al.*, 2013).

Comparisons between the dispensing performances of the valve actuator versus a conventional manual pipette demonstrated that the valve was capable of reproducibly dispensing larger volumes across the 0.5-2.5 µL range. A reduced variability in fluorescence intensity across samples at each target range demonstrated the high degree of precision that could be achieved when using the valve printer to dispense liquids in a DoD configuration. At the highest deposition volume, a significant difference in fluorescent intensity of samples generated using each seeding technique was observed. Due to the nature of the DoD jetting configuration, small variations between the theoretical and actual volume of dispensed

droplets significantly impact total dispensed volume where a large number of actuation cycles are requested. It is hypothesised that this variation in deposition performance was caused by the cumulative error associated with droplet volume calculations when performing large numbers of actuation cycles, representing an inherent limitation of the DoD valve actuation approach. Potential approaches to control such errors within future work include the independent calibration of DoD dispensing devices across separate working volume ranges. This would ensure that printing performance is retained for both high accuracy and high volume jetting applications.

Assessment of the intra-well fluorescence revealed a positive and negative bias towards the first and last coordinates within a print job respectively, indicating that additional fluorescent material was deposited at the first coordinate and reduced material at the final coordinate. There are a number of potential causes for such effects, including jetting hardware associated errors and plate edge effects. Multi-well plate edge effects are commonly associated with fluorometric assays due to variations in the temperature and evaporation rate between regions of the multi-well plate (Lundholt, Scudder and Pagliaro, 2003). In addition, variations in fluorescence intensity readings across the plate or inaccuracies in plate reading hardware can cause placement-related variation in well readings. A range of potential methods are available to reduce such effects, and further work will be required to determine the cause of this observation due to the significant reduction in calculated valve precision when comparing datasets inclusive of edge wells (Jean-Philippe *et al.*, 2012; Chen *et al.*, 2017; Shterev *et al.*, 2018).

Additional research highlighted the intra-valve variability between two identical actuation devices. Due to the DoD nature of this process, small variations in droplet volume between printing devices can lead to substantial variations in total dispensed volume where high numbers of actuation cycles are employed. This data emphasises the importance of independently calibrating printing protocols to each jetting device used due to inherent variations in actuator performance. This is of particular importance where multi-valve systems are employed to increase printing throughput (Faulkner-Jones, 2015; Da Conceicao Ribeiro *et al.*, 2019). These results reinforce previous studies within the literature highlighting the high variability in printing precision amongst independent actuators within a single printing platform (Bammesberger *et al.*, 2013).

In combination, this data demonstrates the suitability of using the valve in a drop-on-demand configuration to selectively and reliably deposit material across a wide volume range by solely adjusting the actuation cycle number applied during printing.

5.4.2 Cell Deposition Performance

Analysis of the effect of valve printing parameters on cell deposition performance was shown for the MSC and chondrocyte cell lines in Figure 5.7. Pressure was observed to have a minimal impact on cell density per droplet, reinforcing previous observations in Figure 5.3 where material deposition performance was characterised. Increases in dwell time were shown to have a diminishing effect on cell dispense performance beyond a dwell time of 500 µs. It was hypothesised that the changes in ejection behaviour under higher dwell times could have been caused by sedimentation or material flow effects through the valve, where larger volume displacements were requested.

An additional experiment was performed to characterise this effect by comparing the cell density of sequentially deposited droplets in the presence or absence of a valve purging process immediately prior to printing. Data in Figure 5.8 displayed a rapid reduction in cell density per droplet in response to each sequential ejection cycle until a stable droplet density was achieved. Stable cell density per droplet was maintained where a purge cycle was employed immediately prior to printing, reflecting previous observations in Figure 4.13 for the inkjet printing platform. This data highlights the importance of using purge cycles when depositing cellular material contained within a liquid suspension to maximise process precision.

A deterioration in jetting performance was observed in response to extended printing periods. Data presented in Figure 5.9 provides a comparison between the cell printing performances of the valve using a standard reservoir configuration versus a custom reservoir agitation system. The incorporation of a custom agitation system was shown to minimise degradative effects by maintaining cell printing performance over a 2-hour assessment period. This reflects previous research presented in Figure 4.26 which compared the printing performance of an inkjet actuator with and without the use of a reservoir agitation system.

In combination, these results signify the importance of maintaining adequate processes to account for the presence of cell suspensions within DoD bioprinting techniques in order to maximise cell jetting reliability. This research demonstrated that the valve printing process

could be used to precisely and reliably print cells using a DoD dispensing method under appropriately optimised jetting parameters.

Additional experiments were performed to determine the impact of ink cell density on valve printing performance. Data shown in Figure 5.10 compared the printing performance of the valve across a cell density range of 1-20 million cells per mL at 0, 15 and 30 minute increments. Cell density per droplet was shown to correlate with increasing ink cell concentration as anticipated, with a greater variation in cell density per droplet observed at higher ink cell concentrations. Printing period was also shown to have a significant impact on cell density per droplet at the higher cell concentrations, indicating a deterioration in jetting performance.

These results corroborate with previous observations within the literature whereby cell printing at concentrations of up to 40 million cells per mL have been reported using valve printing processes (Da Conceicao Ribeiro *et al.*, 2019). The ability to process high cell densities using valve printing techniques represents a major advantage over alternative DoD processes, whereby greater limitations are placed on the ink properties and maximum cell density that can be reliably printed (Cui *et al.*, 2010; Parsa *et al.*, 2010; Chahal, Ahmadi and Cheung, 2012).

Data in Figure 5.11 compared the valve printing performance when depositing MSC and chondrocyte cell lines across a concentration range of 1-10 million cells per mL. An increasing variation in cell density per droplet was observed in response to increases in the ink cell concentration, with the cell type having a greater influence on cell density per droplet at higher concentrations. It is hypothesised that the trade-off between printing reliability and ink cell concentration could be caused by the changing rheological characteristics of the ink, leading to variations in valve ejection volumes per actuation cycle. Additional considerations for further research include the effect of cell size and concentration on the rheological properties of the fluid, as well as quantification of the error associated with calculating and processing high cell density solutions using standard tissue culture techniques.

5.4.3 Biological Impact Assessment

A crucial factor when considering different bioprinting technologies or printing parameters is the impact of the printing process on cellular viability and function. A range of different

assays were employed to determine the biological effects of the valve printing process on the MSC and chondrocyte cell types.

A Live / Dead® assay was performed to compare the ratio of live to dead cells in printed and manually seeded samples. Cellular viability was maintained immediately following and 24 hours following printing for both cell lines, as indicated in Figure 5.12, demonstrating that the printing process had no significant effect on membrane integrity or cellular viability.

Characterisation of the impact of the printing process on the metabolic activity of each cell type was performed using a PrestoBlue® assay as shown in Figure 5.13. A significant difference in metabolic activity was observed 24 hours following cell seeding for both cell lines, indicating potential short-term changes in cell metabolism in response to the deposition process. No significant difference in metabolic activity was observed immediately following cell seeding or after an extended incubation period for either cell line. This data indicates that the valve printing process induces a temporary variation in cellular metabolism as a result of the associated mechanical forces during deposition, however recovery and function is restored following a short period of culture.

Morphological analysis was performed over a range of time points following printing to identify any potential effects on cell adherence or morphology. Comparisons between manually pipetted and valve printed samples, shown in Figure 5.14 and Figure 5.15, revealed no visible differences in the rate of cell adherence or subsequent morphology for either cell line. A progressive increase in cell confluency was observed over the 72 hour culture period irrespective of seeding method, indicating the suitability of the valve printing process for cell seeding applications.

A cell proliferation study, shown in Figure 5.16, was conducted to quantitatively compare the rate of growth between valve printed and manually seeded MSC and chondrocyte cells. No significant differences were observed between the population growth rate of manually seeded and valve printed cell samples, indicating that the valve deposition process did not significantly impact cellular growth kinetics following seeding. In addition, no significant differences were observed between the percentage cell viability of manually deposited and printed cells for either cell line at each time point.

In combination, these findings indicate that the valve deposition process is highly suitable for the deposition of MSC and chondrocyte cell lines. No significant effects on cellular

morphology, viability, metabolic activity or cell proliferation over extended culture periods were observed as a result of the printing process. These findings strengthen previous observations within the literature that demonstrate the biocompatibility of the valve deposition process with a range of cell types, enabling the production of hepatic and breast cancer aggregates alongside skin and alveolar tissue models (Lee *et al.*, 2014; Faulkner-Jones *et al.*, 2015; Horvath *et al.*, 2015; Ling *et al.*, 2015).

The application of 3D cell culture techniques for *in vitro* research has become increasingly common due to the more replicative cellular environment that is induced when compared to traditional monolayer culture (McMurtrey, 2016; Nath and Devi, 2016; Melissaridou *et al.*, 2019). In addition, advancements within the field of cellular therapies has enabled the development of aggregate-based surgical procedures to treat diseases such as osteoarthritis (National Institute for Health and Care Excellence, 2017; Ong *et al.*, 2018). The suitability of the valve printing process for the production of MSC and chondrocyte tissue aggregates was assessed using a combination of gravity-induced aggregate culture techniques.

5.4.4 Hanging Droplet Aggregate Culture

A hanging droplet aggregate culture technique was assessed for the production of MSC aggregates. Data presented in Figure 5.17 revealed outgrowth of aggregates produced via manual pipetting during later time points. This was most pronounced in aggregates seeded at higher cell densities. These observations were hypothesised to have been caused by cell proliferation following aggregate formation and condensation, resulting in a loss of model stability.

Aggregates generated using the valve printing process were shown to be less stable in culture than manually seeded cells, with a significant reduction in aggregate density accompanied by increased cellular debris over the 9-day incubation period. In addition, a considerable number of secondary aggregates were observed shortly following cell seeding.

Subsequent analysis of the technique using chondrocytes in Figure 5.18 revealed a low rate of cell aggregation for both manually seeded and valve deposited samples, leading to the formation of secondary aggregates. Poor aggregate stability was also observed, with a considerable amount of cell outgrowth occurring throughout the course of the incubation period. One potential cause for the increased rate of cellular outgrowth when compared with the MSC aggregates is the more rapid rate of cell proliferation that is characteristic of the chondrocyte cell line.

A combination of factors inherent to the valve deposition process could have contributed to the poor rate of cellular aggregation within the printed samples. This includes bubble formation, shown in Figure 5.19, which occurred as a result of the air-liquid-interface present during printing, as well as the greater dispersion of cells within the liquid substrate when dispensed from above versus directly within the droplet.

The effect of pressure and media formulation on bubble formation within the printed droplets was assessed in Figure 5.20. An increase in backpressure resulted in an increase in bubble formation alongside droplet splattering on substrate impact. These effects further reduced the resolution of the printing process and increased the variability in droplet volume within printed arrays. The removal of foetal bovine serum from the media formulation was shown to reduce the number of bubbles generated during printing. This was due to the recognised effects of protein concentration on the surface tension and subsequent bubble formation within liquids (Zhang, Handa-Corrigan and Spier, 1992). It was not feasible to further reduce the backpressure of the valve whilst maintaining reliable printing performance. In addition, changes to the protein composition of the media would negatively influence cellular growth and function due to the critical role that proteins play in cellular processes.

Further limitations of this technique were observed during culture. This includes challenges surrounding media exchange when using conventional and automated liquid handling methods, as well as model sensitivity to mechanical shocks. These limitations have been previously been reported within the literature (Breslin and O'Driscoll, 2013; Joshi and Lee, 2015).

It was therefore necessary to assess the suitability of an alternative in-well aggregate culture technique for the production of MSC and chondrocyte aggregates.

5.4.5 In-Well Aggregate Culture

An in-well aggregate culture technique was selected due to its compatibility with well-plate based biological analysis techniques. In addition, the well-plate format provided a high sample density to culture large numbers of aggregates for high-throughput applications.

Data presented in Figure 5.21 displayed microscopy images of aggregates generated across a range of cell seeding densities via both manual pipetting and valve deposition processes. Aggregates were consistently generated across the full cell seeding density range assessed

within 24 hours, irrespective of the seeding method employed. No visible differences in the size, shape or stability of aggregates were observed when comparing the manually seeded and valve deposited samples over the 9-day culture period. Quantification data presented in Figure 5.22 revealed no significant differences between the sizes of aggregates generated using either seeding method, with cell seeding density correlating with aggregate size as anticipated. A gradual reduction in aggregate size over the first 3 days of culture was observed indicating cell condensation. Cultures remained stable throughout the remaining time period, with minimal cell outgrowth or secondary aggregate formation. These results support previous research by Pennock *et al.,* who demonstrated the impact of cell seeding concentration on primary MSC aggregate size and density across a 7 day in-well culture (Pennock *et al.*, 2015). These findings demonstrate the suitability of the in-well culture technique for the production of MSC aggregates, as well as the compatibility of the culture format with the valve printing process.

Evaluation of the in-well aggregate culture methodology with chondrocyte cells, reported in Figure 5.23 and Figure 5.24, revealed a similar pattern of cell aggregation and condensation over the first 3 days of culture. No significant differences in the morphology or density of aggregates were observed between manual and valve seeded samples. A reduced aggregate size was observed within the lower cell seeding densities assessed leading to subsequent secondary aggregate formation. These observations indicate that a higher cell number is required for chondrocyte cells to reliably generate single aggregates. Aggregate outgrowth was observed irrespective of cell seeding density or technique. It is hypothesised that this was due to the more rapid rate of proliferation that is characteristic of the chondrocyte cell line, as indicated within previous experiments.

Both cell types were shown to be compatible with the in-well culture technique across a wide range of cell seeding densities. A seeding density of 60,000 cells per well was selected for further experiments to minimise the number of cells required, whilst retaining reliable aggregate formation.

Further research was performed to determine the impact of extended culture on the stability of the aggregate model for each cell type, alongside any potential biological effects of the printing process. Figure 5.25 displays the morphology of chondrocyte cells cultured using the in-well aggregate culture technique over a 21-day period. A similar pattern of

aggregate formation and condensation followed by a period of stable culture was observed, with cellular debris collecting within each well over the later time points.

Haematoxylin and eosin staining of sections, shown in Figure 5.26, displayed an increase in eosinophilic staining within the central region of the aggregate across all sample conditions, indicative of an upregulation in ECM production or reduction in cellular viability. A reduction in cell nuclei frequency within the central region of the aggregates was also observed. This is characteristic of literature observations reporting a necrotic core induced by localised hypoxia within the central zone of larger aggregates that are comprised of higher cell densities (Huang *et al.*, 2017; Riffle *et al.*, 2017).

Indirect immunofluorescence staining in Figure 5.27 displayed a low degree of aggrecan and collagen II protein expression amongst both manually seeded and printed samples across the time points assessed. No discernible differences in marker localisation or intensity was observed between printed and manually seeded aggregates. These results indicate that the printing process did not significantly affect the cellular phenotype or tissue structure of the aggregates generated.

Figure 5.28 displays the morphology of MSC aggregates maintained over a 21-day period. Aggregates were treated with both basal and chondrogenic media formulations to identify any differentiation inducing effects of the culture format on MSC phenotype when compared with cells differentiated using standardised protocols. The addition of pro-chondrogenic compounds to cell culture media resulted in an increased aggregate size following the initial cell condensation period, compared to samples incubated in a basal media formulation. It was hypothesised that this was caused by an elevation in the rate of MSC proliferation, or nuclear hypertrophy, in response to chondrogenic differentiation-inducing media stimuli. Previous research has indicated chondrogenic differentiation of MSCs induces an intermittent elevation in proliferation rate within a high density culture format, resulting in similar increases in aggregate size (Shimizu, Yokoyama and Asahara, 2007; Dexheimer, Frank and Richter, 2012).

Haematoxylin and eosin staining of sectioned MSC aggregates, presented in Figure 5.29, revealed no obvious differences in tissue structure between manually seeded and printed aggregate models under basal or chondrogenic media stimulation. Variations in aggregate size and shape were attributed to section positioning within the tissue, alongside sample

degradation during the cryosectioning process. These artifacts have been previously reported within the literature and are inherent of the sectioning process (Pampaloni, Ansari and Stelzer, 2013).

Indirect immunofluorescence of collagen II and aggrecan content was presented in Figure 5.30 and Figure 5.31 for the MSCs treated with basal and chondrogenic media formulations respectively. No visible differences in signal intensity or marker localisation were observed between manually seeded and printed aggregates under either media formulation. An increase in aggrecan and collagen II expression was observed over the 21-day culture period for cells exposed to basal media formulations, indicating potential chondrogenic differentiation of the MSCs as a result of the aggregate culture method. High density culture has been previously reported within the literature to promote chondrogenic differentiation of MSCs (Shimizu, Yokoyama and Asahara, 2007; James *et al.*, 2015; Lu *et al.*, 2017). Peak aggrecan and collagen II signal intensity was observed on day 7 within aggregates treated with the chondrogenic media formulation, indicating that the chondrogenic media supplements had a significant effect on MSC differentiation status, irrespective of the 3D culture format.

Both collagen II and aggrecan are extensively used within the literature as markers of the chondrogenic phenotype for chondrocyte and MSC cell types (Das *et al.*, 2008; Chen *et al.*, 2009; Karlsen, Shahdadfar and Brinchmann, 2011). Despite this, previous research has reported conflicting outcomes on their suitability as markers to monitor chondrogenesis (Mwale *et al.*, 2006; Karlsen, Shahdadfar and Brinchmann, 2011; Yeung *et al.*, 2018).

These findings present an opportunity to further research the influence of cell seeding density on the formation of a necrotic region within each aggregate, as well as the region's impact on cellular phenotype, using a more comprehensive range of chondrogenic markers and over a longer culture period.

In addition, advancements within the field of fluorescence microscopy provide an alternative method to assess cell marker expression and tissue organisation by using whole-mount microscopy techniques. Recent research has demonstrated the potential of using such techniques to study tissues of a similar size and shape to those generated within this research, thus avoiding the challenges in sample preparation and processing throughput associated with tissue sectioning processes (Marshall, Barnes and Genever, 2018). This

includes the use of light sheet fluorescence microscopy to enable whole-mount tissue imaging, whereby an illumination system excites fluorophores within a narrow focal plane. A detection lens is placed perpendicularly to the light sheet to reduce out-of-focus light, thus enabling the collection of high definition images within a single plane of tissue. Recent research has successfully applied this technology to study tissue architecture and drug penetration within aggregate culture formats (Smyrek and Stelzer, 2017; Lazzari *et al.*, 2019).

Nevertheless, this research has demonstrated the compatibility of the in-well aggregate culture technique with valve printing systems for scaling up the production of 3D aggregate tissues. This has applications for both *in vitro* osteoarthritis research and potential aggregate-based cellular therapies. These findings build upon previous research into other tissue types, whereby the compatibility of valve printing processes with in-well and hanging droplet aggregate culture techniques were assessed (Faulkner-Jones *et al.*, 2013; Ling *et al.*, 2015)

5.5 Conclusions

Within this chapter, the bioprinting performance of a valve-based DoD printing process was benchmarked to construct 3D aggregate tissue models.

- A combination of printing parameters were optimised to enable the reliable deposition of material at the nanolitre-scale
- Cell printing was demonstrated across an ink concentration range of 1-20 million cells per mL, through the sequential deposition of droplet volumes of approximately 54 nL
- The suitability of the valve process for cell printing applications was demonstrated through results which show no significant effects on cellular viability or function when compared to manual seeding techniques
- An in-well aggregate culture platform was successfully reproduced using the valve printing process, providing a method to automate the construction of 3D aggregate tissue cultures for *in vitro* OA research, as well as the development of novel cellular therapies

Chapter 6. Production of a Bioprinted Co-culture Model of Osteoarthritis

6.1 Introduction

The purpose of this chapter is to apply the valve printing process that was previously benchmarked in order to construct a co-culture model which could be used for osteoarthritis research.

Within this chapter, the valve printing process is used to sequentially deposit mesenchymal stromal cell and chondrocyte cell lines onto a microplate insert membrane. A range of biological tests are performed to characterise the impact of cell co-culture on tissue structure and organisation, versus single cell type cultures, over a 14-day incubation period. This includes cell proliferation and metabolic activity assays, cell tracking, histological staining and indirect immunofluorescence staining of phenotypic markers of chondrogenesis.

6.2 Methodology

6.2.1 Plate Configuration

The Transwell® 96-well plate permeable support system (Corning, USA) was selected for co-culturing MSCs and chondrocyte cell lines. This system featured 96 interconnected polycarbonate well inserts with a 0.4 μm pore size alongside a dedicated receiver plate. This platform was selected due to its robotics friendly design to maximise compatibility with the bioprinting equipment.

It was necessary to separate the Transwell® insert into smaller segments to enable the acquisition of each sample group from a single plate at each time point. A Laserscript® LS3020 laser cutting device and accompanying Lasercut® software (HPC Laser Limited, UK) was used to compartmentalise the Transwell® inserts prior to cell seeding to enable rapid collection and isolation of samples.

6.2.2 Cell Seeding

The Transwell® inserts were pre-soaked in cell culture media prior to cell printing to promote cell attachment. Each cell type was then sequentially seeded onto the base of each of the Transwell® inserts to achieve a cell seeding density equivalent to 1 million cells per cm^2 using the valve deposition parameters defined within the previous chapter. Co-culture samples were generated by seeding an equivalent number of chondrocytes, immediately followed by MSCs, onto the base of each well insert.

A target volume of 80 µL per insert well was maintained across all samples in accordance with the manufacturer's recommendations. Cells were cultured in high glucose DMEM / Ham's F12 mix 1:1 v / v supplemented with 10 % foetal bovine serum (Thermo Fisher Scientific, USA), 5000 U / mL Penicillin / Streptomycin (Sigma-Aldrich, UK) and 2 mM L-Glutamine (Sigma-Aldrich) using the Transwell® independent 96-well receiver plate.

Cell culture media was added to each isolated well of the Transwell® receiver plates to achieve a target volume of 235 µL. Media was changed daily using the well-specific feeder ports during culture.

The diagram in Figure 6.1 provides an overview of each step of the cell seeding and analysis process.

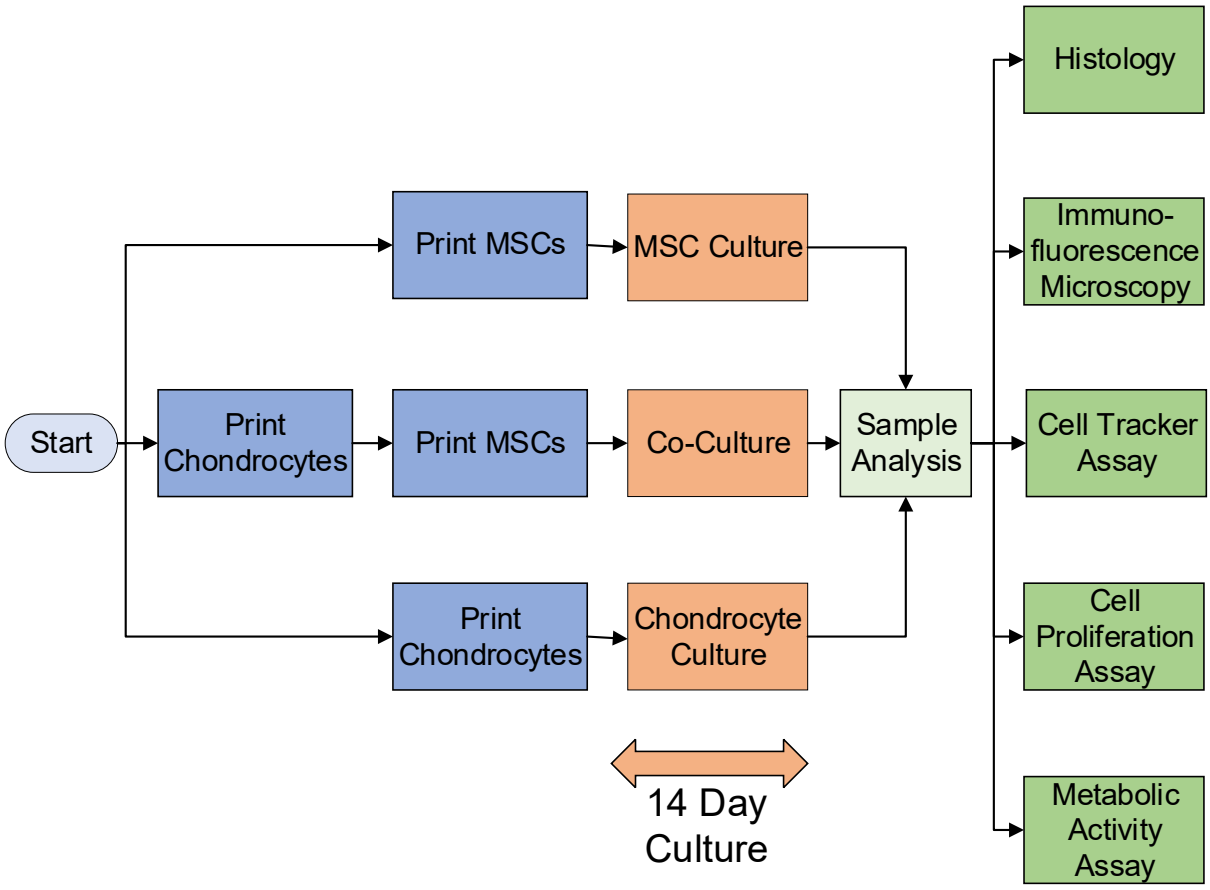

Figure 6.1 – Flow diagram displaying an overview of the cell printing, culture and analysis procedures for each model.

6.2.3 Sample Retrieval

Samples were isolated at each time point via removal of the insert from the Transwell® receiver plate. Membranes were separated from the insert using a scalpel and immediately snap-frozen according to previously described methodologies.

6.2.4 Cell Tracker Staining

CellTracker® Red and CellTracker® Green dyes (Thermo Fisher Scientific) were used to label MSC and chondrocyte cell samples respectively prior to printing. Cell tracker solutions were prepared to a final concentration of 25 µM in cell culture media. Pelleted cells were resuspended in the CellTracker® solutions and incubated for 45 minutes at 37 °C. Following centrifugation, the supernatant from each sample was removed and cells resuspended in cell culture media at the required density for printing. At the desired time points the Transwell® membranes were removed from the insert mounts, fixed for 30 minutes in 4 % paraformaldehyde solution (Thermo Fisher Scientific) and washed 3 times in PBS (Sigma-Aldrich). Whole samples were mounted onto glass slides using DPX (Sigma-Aldrich) prior to imaging. Imaging of samples labelled with CellTracker® dyes was performed using an LSM800 point scanning confocal microscope (Carl Zeiss AG, Germany) at 20x magnification.

6.2.5 Cell Proliferation Assay

Cell proliferation was assessed using the 5-ethynyl-2'-deoxyuridine (EdU)-Click 594 cell proliferation assay (Baseclick, Germany). Samples were seeded and cultured in media containing 10 µM EdU for 48 hours prior to processing at each time point. Day 1 samples were incubated in EdU for 24 hours. Transwell® inserts were then snap-frozen and sectioned as previous described. Sections were stained with the EDU-Click kit according to manufacturer's instructions and mounted in mounting medium containing DAPI nuclear counterstain (Sigma-Aldrich). Imaging was performed using an LSM800 point scanning confocal microscope (Carl Zeiss AG) at 20x magnification.

6.2.6 Metabolic Activity Assay

Following culture, the supernatant from each well was removed and replaced with 235 µL of PrestoBlue® working solution previously prepared via the addition of 10 % v / v PrestoBlue® reagent to phenol-red free cell culture media. Plates were incubated for 2 hours prior to the collection of supernatant. Fluorescence values were obtained using a FLUOstar® Omega microplate reader (BMG Labtech, Germany) using an excitation and emission filter of 544 nm and 620 nm respectively.

6.3 Results

6.3.1 Haematoxylin and Eosin Staining

Haematoxylin and eosin staining of the sectioned tissue models is displayed in Figure 6.2. Tissues comprising of multiple cell layers on the upper surface of the Transwell® insert membranes formed across each sample group within the first 24 hours of culture.

Separation of the membrane from the tissue structure was observed indiscriminately of sample conditions as a consequence of the sectioning process. A reduction in cell density was observed on the apical surface of each tissue, with the exception of the chondrocyte models and co-culture models at day 14. Co-culture sections displayed an overall increase in tissue thickness during culture when compared to single cell conditions. Distinct cell layering within the co-culture sample was observed at 14 days.

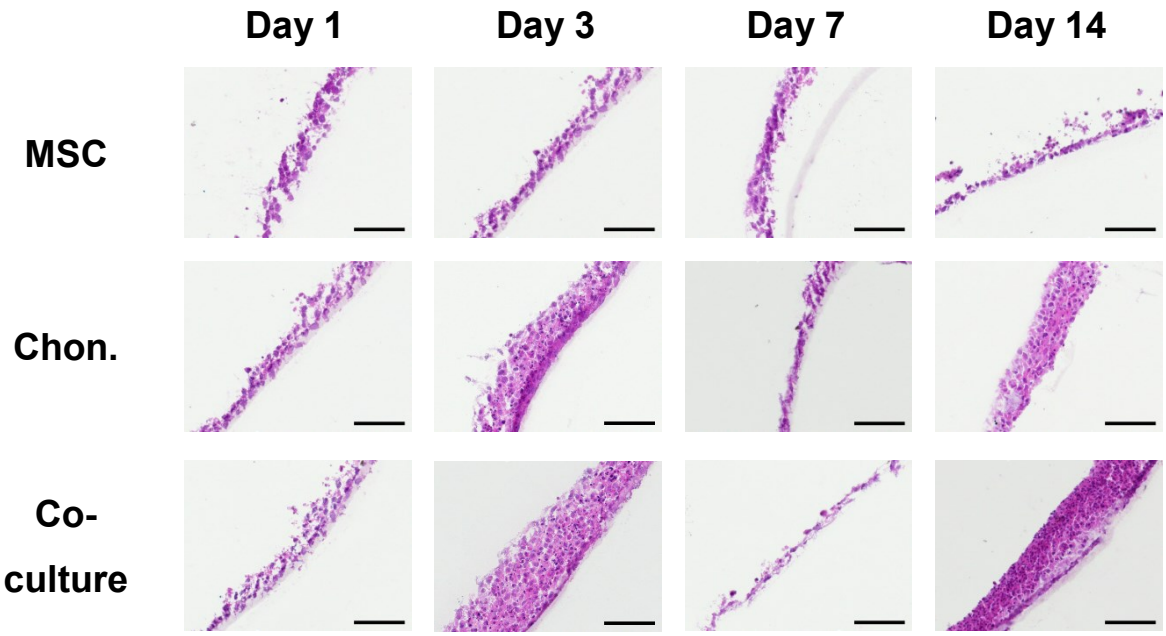

Figure 6.2 – Haematoxylin and Eosin staining of printed Transwell® insert cultures generated from MSC, chondrocyte and cell co-cultures over a 14 day culture period. Scale bar = 100 µm.

6.3.2 Indirect Immunofluorescence Staining

Indirect immunofluorescence staining of collagen II and aggrecan protein expression is presented in Figure 6.3, Figure 6.4 and Figure 6.5 for the MSC, chondrocyte and co-culture samples respectively. An increase in collagen II expression was observed within the chondrocyte and co-culture samples when compared to the tissue generated solely from MSCs, with a comparatively low expression of aggrecan observed across all samples. An increase in tissue thickness and cellular organisation was also observed within the chondrocyte and co-culture samples at day 3 and 14, corroborating with previous observations within Figure 6.2 of haematoxylin and eosin stained sections.

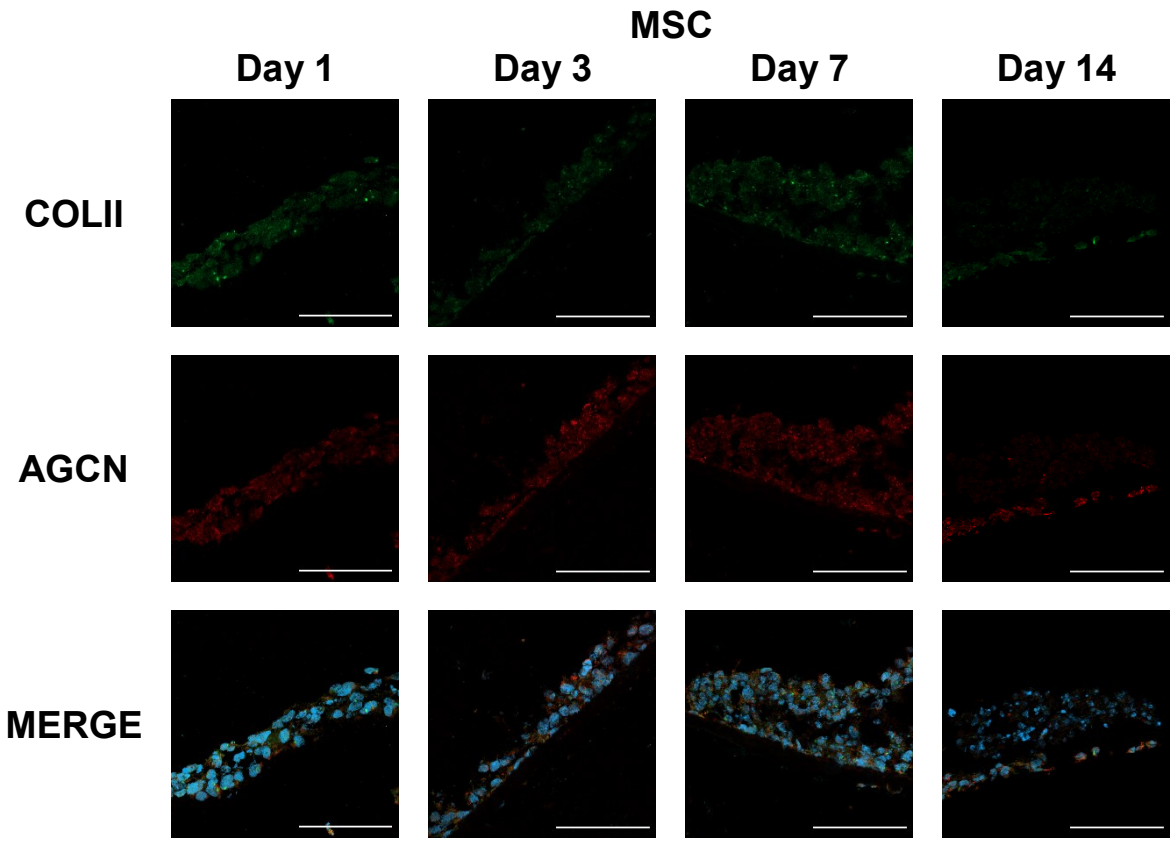

Figure 6.3 – Immunostaining data comparing the collagen II (COLII, green) and aggrecan (AGCN, red) content of MSCs printed onto the Transwell® inserts over a 14 day culture period. Cell nuclei were visualised using DAPI (blue) staining. Scale bar = 100 µm.

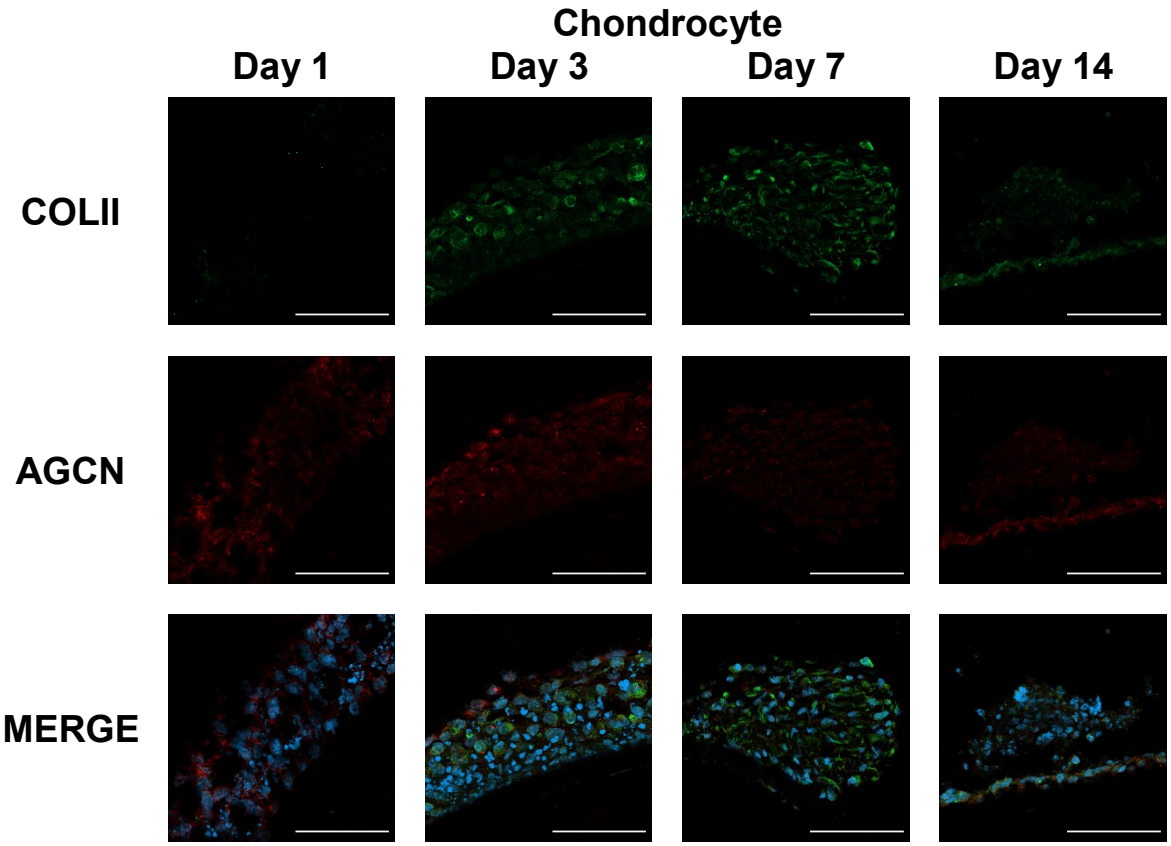

Figure 6.4 – Immunostaining data comparing the collagen II (COLII, green) and aggrecan (AGCN, red) content of chondrocyte cells printed onto the Transwell® inserts over a 14 day culture period. Cell nuclei were visualised using DAPI (blue) staining. Scale bar = 100 µm.

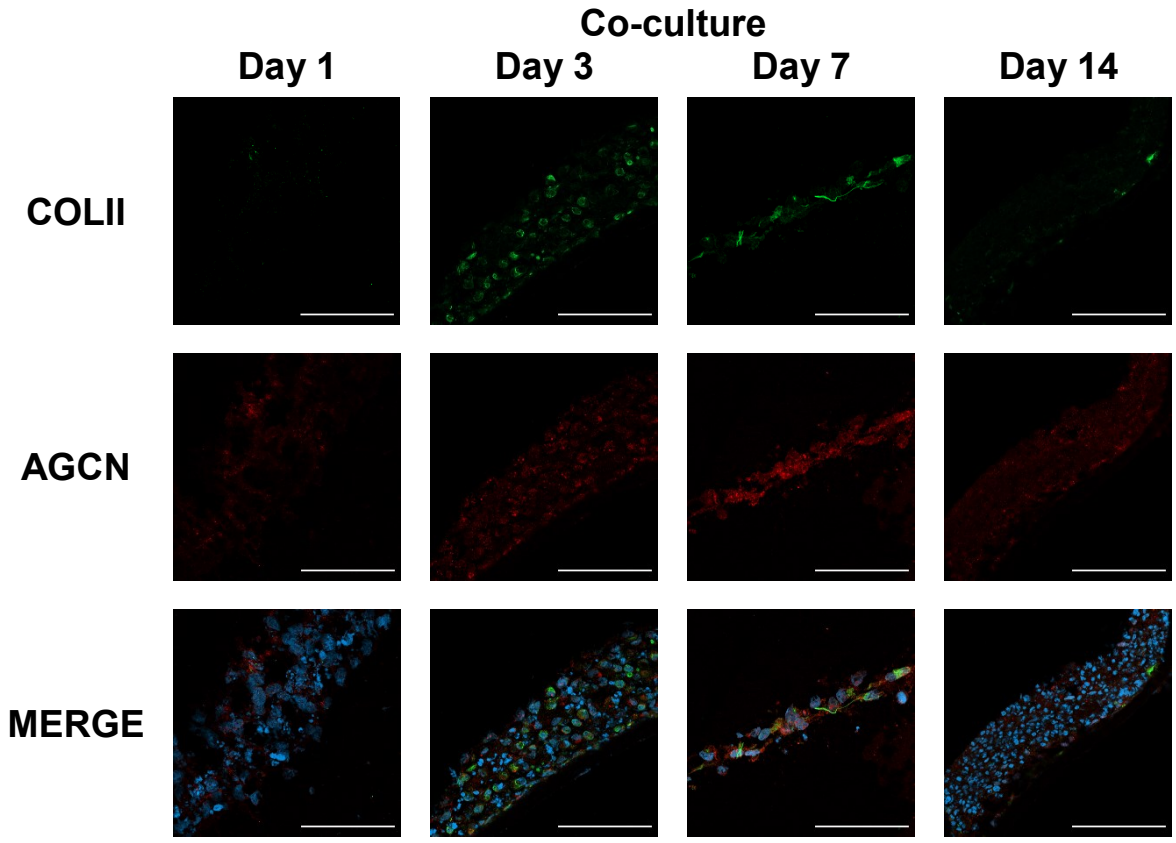

Figure 6.5 – Immunostaining data comparing the collagen II (COLII, green) and aggrecan (AGCN, red) content of the MSC and chondrocyte cell co-culture printed onto the Transwell® inserts over a 14 day culture period. Cell nuclei were visualised using DAPI (blue) staining. Scale bar = 100 µm.

6.3.3 Cell Tracker Staining

Analysis of the localisation of MSC and chondrocyte cell types on the surface of the co-culture model is displayed in Figure 6.6. Both MSCs and chondrocytes were retained throughout the 14 day culture period. A reduction in signal intensity for each cell line was observed over the first 3 days, with a subsequent increase in chondrocyte cell number and signal intensity over the remaining time points.

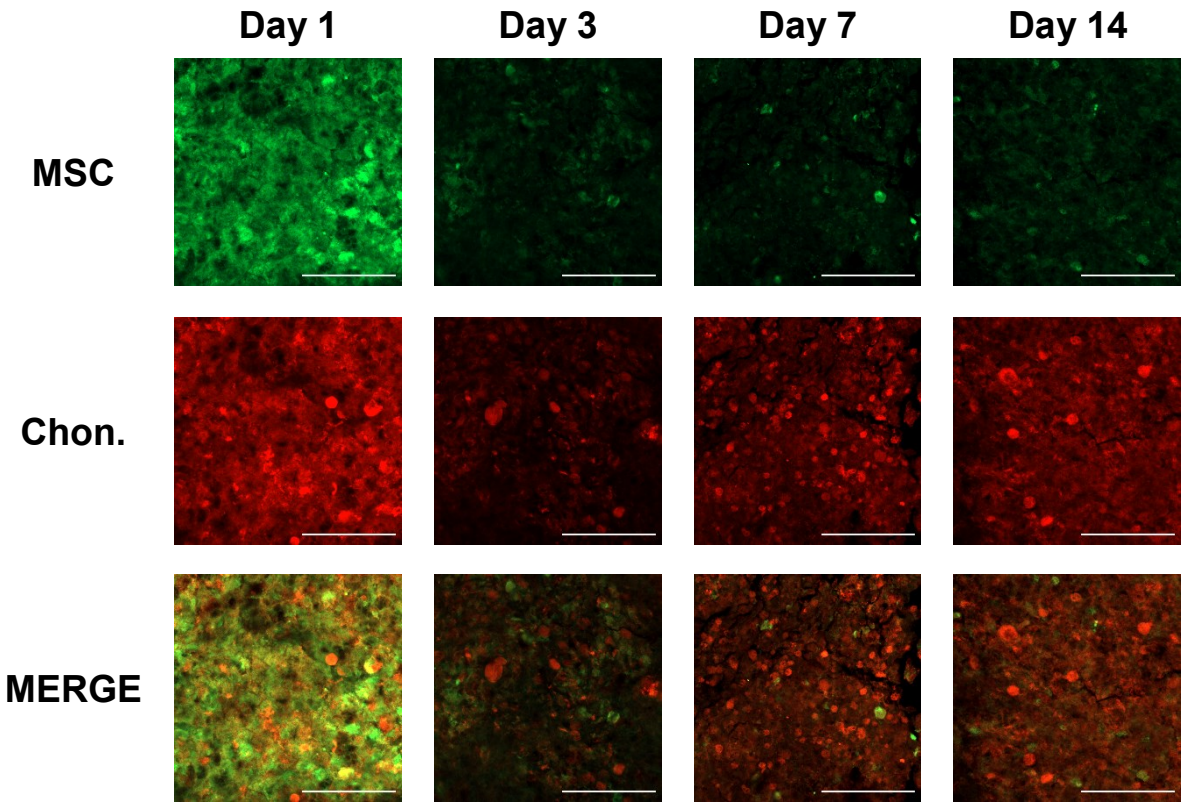

Figure 6.6 – Immunofluorescence microscopy of printed MSC (green) and chondrocyte (red) cells on the surface of the co-culture over a 14 day culture period. Cells were labelled using CellTracker® fluorescent dyes prior to printing. Scale bar = 100 µm.

6.3.4 Cell Proliferation Assay

An EdU cell proliferation assay was conducted to identify regions of proliferation within the insert-based tissues generated from MSC, chondrocyte and cell co-cultures. Indirect immunofluorescence data presented in Figure 6.7, Figure 6.8 and Figure 6.9 displays the proportion and location of proliferating cells within the MSC, chondrocyte and co-culture models respectively. Proliferation was maintained within all three models across the full 14 day culture period assessed. No discernible differences in the proportion of proliferating cells were observed between individually cultured and co-cultured cells. Proliferation was shown to be most prominent at the base of the tissue on the interface with the Transwell® insert membrane.

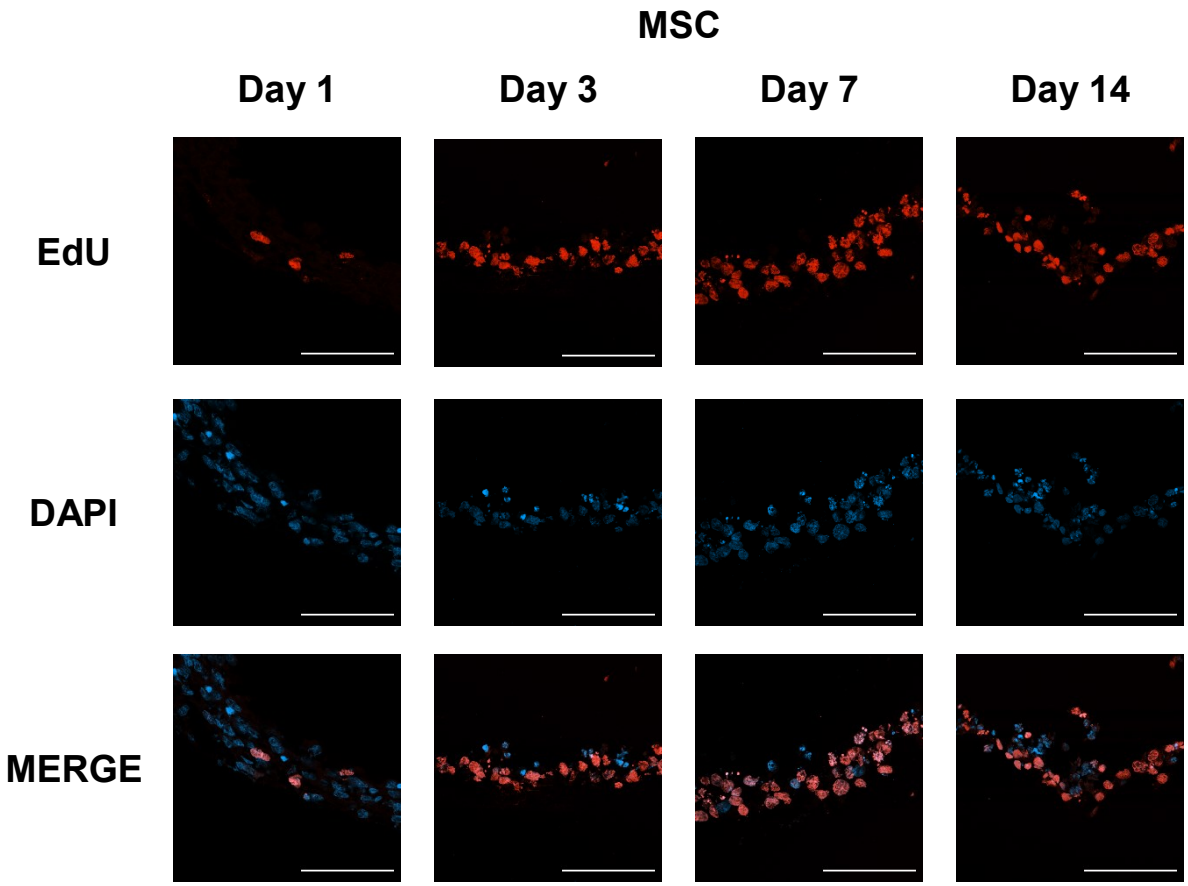

Figure 6.7 – Immunofluorescence detection of proliferating cells via EdU incorporation within MSCs printed onto the Transwell® inserts over a 14 day period. Cell nuclei were visualised using DAPI (blue) staining. Scale bar = 100 µm.

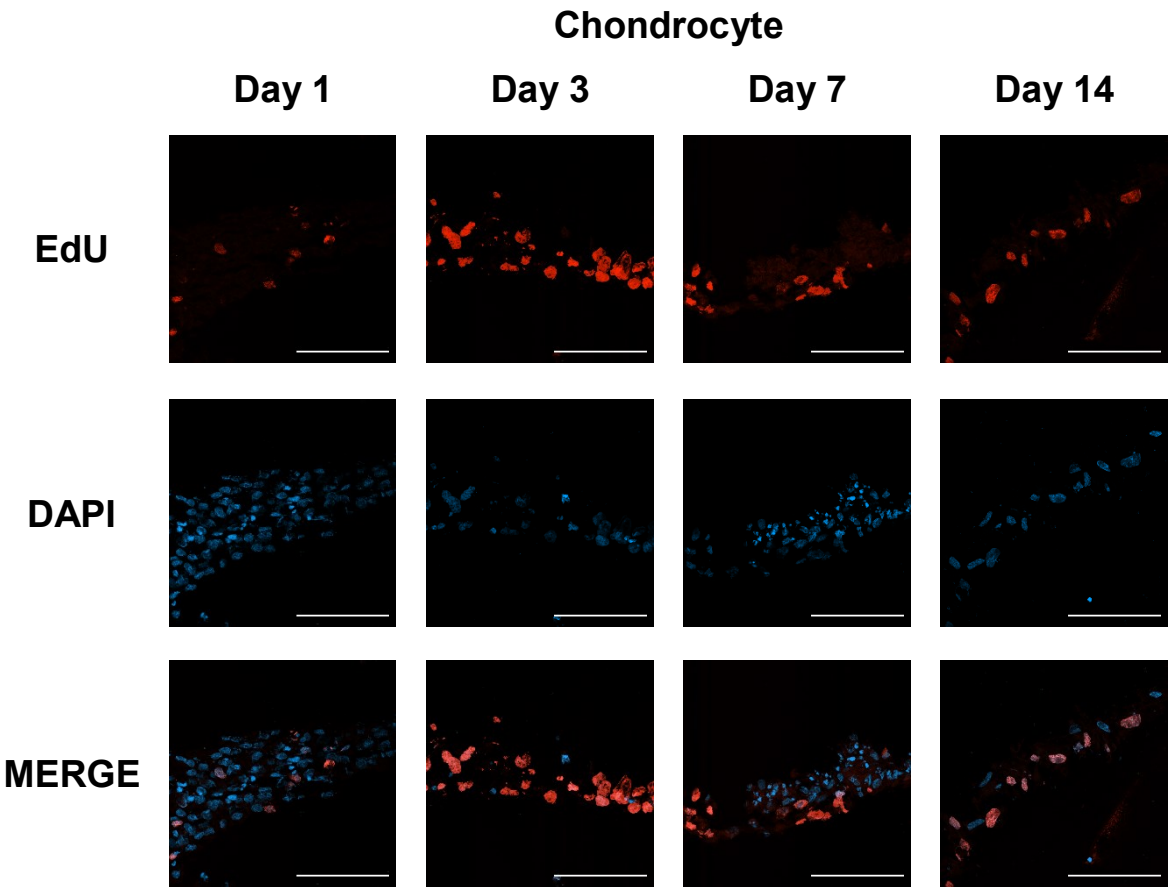

Figure 6.8 – Immunofluorescence detection of proliferating cells via EdU incorporation within chondrocyte cells printed onto the Transwell® inserts over a 14 day period. Cell nuclei were visualised using DAPI (blue) staining. Scale bar = 100 µm.

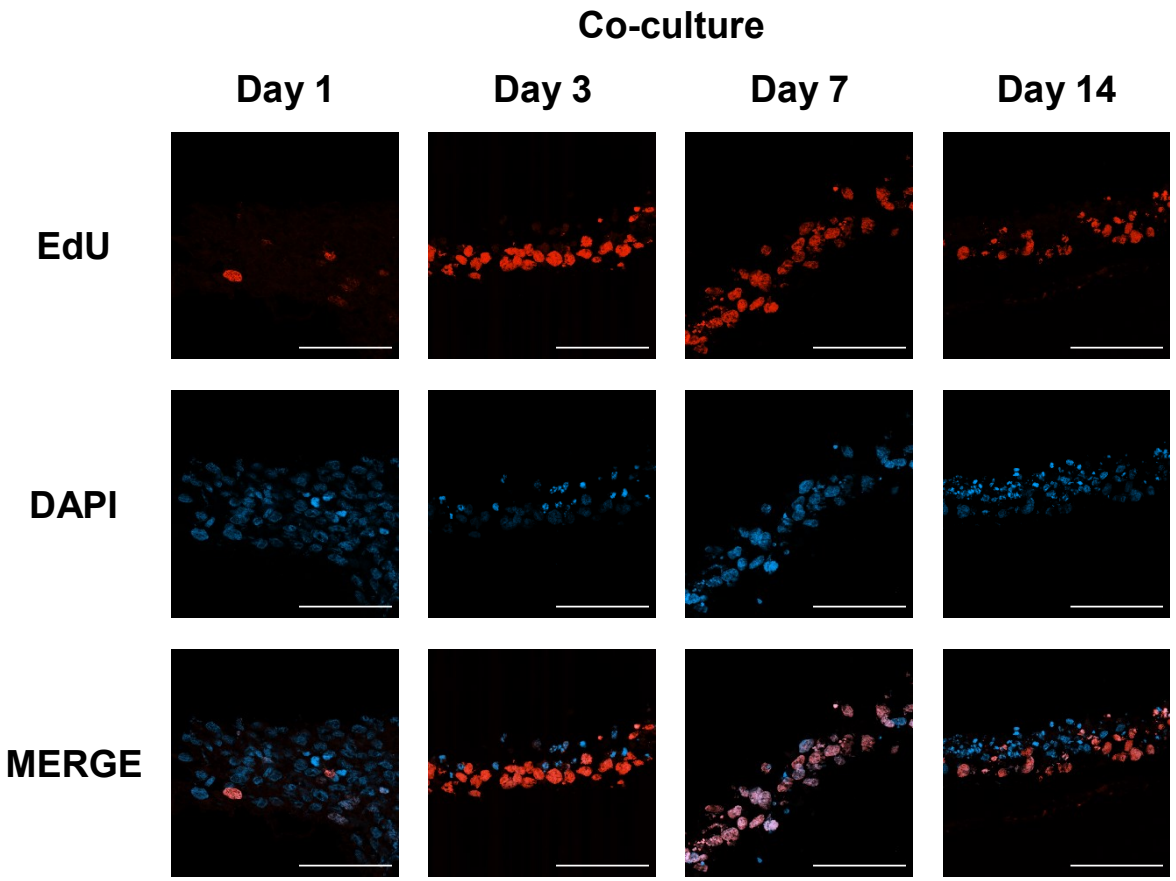

Figure 6.9 – Immunofluorescence detection of proliferating cells via EdU incorporation within MSC and chondrocyte co-cultures printed onto the Transwell® inserts over a 14 day period. Cell nuclei were visualised using DAPI (blue) staining. Scale bar = 100 µm.

6.3.5 Metabolic Activity Assay

A PrestoBlue® metabolic activity assay was performed to determine the metabolic activity of each cell line in comparison to the co-culture model over time. No significant difference in metabolic activity was observed between each cell culture condition at any of the time points assessed in Figure 6.10. A significant reduction in metabolic activity was observed over the first 7 days of the 14 day culture period.

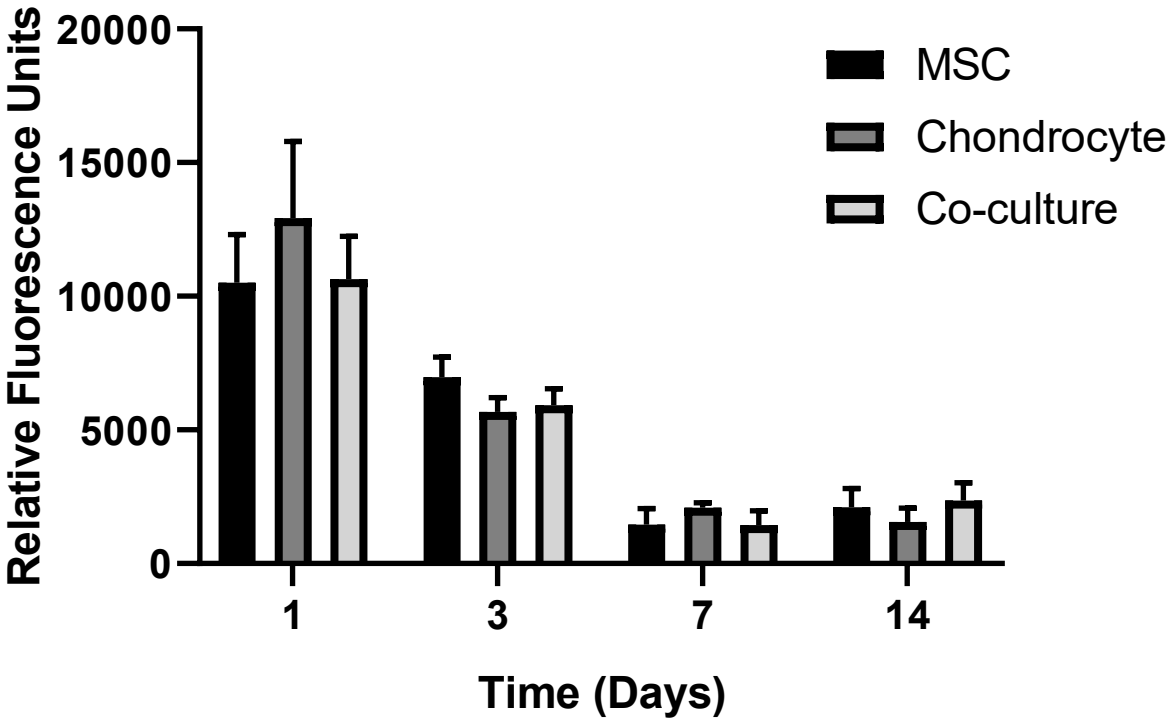

Figure 6.10 – PrestoBlue® metabolic activity assay for the printed MSC, chondrocyte and cell co-culture models over a 14 day incubation period. Data represents mean values ± SD. N=3.

6.4 Discussion

A bioprinted tissue model was constructed using the valve jetting process previously optimised in chapter 5. Tissues consisting of printed MSC, chondrocyte and MSC-chondrocyte cell co-cultures were generated and compared over a 14 day period.

A rapid reduction in the pH of cell culture media contained within each well was observed due to the combined high cell densities and low media volume of generated cultures. Although daily media exchange was performed, it is hypothesised that these effects significantly affected biological conditions within the culture.

Nutrient and waste diffusion gradients are of specific importance within 3D culture formats due to the recognised role that they play in cellular viability, activity and migration. Previous studies have demonstrated the significant effects of nutrient diffusion within high density 3D cultures on cellular activity (Bock and Mrowietz, 2001; Keenan and Folch, 2007; Knight, 2013; Sip, Bhattacharjee and Folch, 2014).

Current strategies reported within the literature to reduce such effects include seeding cells at lower densities, performing more frequent media exchanges and using high-volume well plates. These methods collectively increase the availability of nutrients within the media and reduce the rate of waste product build-up (Knight, 2013; Mikhailova *et al.*, 2014; Cozens *et al.*, 2018). Reducing the cell density of the culture for OA disease models provides limited usefulness due to the important contribution that high cell densities have on tissue formation, differentiation and subsequent *in vitro* replication of current OA cell-based surgical procedures (Foldager *et al.*, 2012; Mennan *et al.*, 2018; Armoiry *et al.*, 2019; Wang *et al.*, 2019). In addition, modifications to the frequency of media exchange or plate size reduce the maximum throughput and density of model cultures, limiting their value for commercial scale HTS applications.

Further research is therefore required to assess the suitability of novel methods to improve media exchange within high density culture environments. Exploratory research has investigated the potential for using active perfusion-based plate designs to allow for continual media exchange, thus avoiding the build-up of nutrient and waste gradients, as well as providing a continual source of material for real-time cell activity monitoring (Huang *et al.*, 2015; Ma *et al.*, 2018; Parrish *et al.*, 2018). Such systems are currently implemented at the expense of compatibility with standard tissue culture plasticware, as well as plate handling and analysis equipment. Research by Huang *et al.* proposes a novel 24-well culture platform with a custom microfluidic lid to circumvent such issues (Huang *et al.*, 2015).

6.4.1 Haematoxylin and Eosin Staining

Histological analysis of sectioned tissues was reported in Figure 6.2. Cells were shown to adhere to the membrane within the first 24 hours of culture, generating tissues consisting of multiple layers of cells. Over the remaining time points, an increase in tissue thickness and cell density was observed for the chondrocyte and cell co-cultures, with MSC tissues retaining a similar thickness. Additional tissue organisation at the final time point was observed in the co-culture, indicating the formation of multiple cell layers.

Variations in nuclei size were also observed within the chondrocyte and cell co-cultures following tissue formation. These changes are characteristic of nuclear blebbing, a process whereby structural changes such as chromatin condensation and fragmentation lead to the formation of distinct regions within the nucleus (Cataldi *et al.*, 1994). Nuclear blebbing was evenly distributed across samples comprised of chondrocytes from day 3 to day 14. Within

the co-culture, cells undergoing nuclear blebbing transitioned from being evenly dispersed within the tissue to becoming localised on the upper surface region. These results indicate that the co-culture of MSC and chondrocyte cell types promotes *in vivo* cellular differentiation and organisation when compared to single cell cultures of either cell type. These findings support a range of existing literature indicating a potential relationship between the co-culture of MSC and chondrocyte cell types versus single cell cultures for the production of cartilage tissues (Hwang *et al.*, 2011; Meretoja *et al.*, 2012, 2014; Yang, Lee and Barabino, 2012; Dahlin *et al.*, 2014; Li *et al.*, 2016). This has potentially significant implications on the cellular therapies under development for the treatment of OA (Richardson *et al.*, 2017; Wang *et al.*, 2019).

The process of cryosectioning was also observed to significantly impact the quality of the tissue yield. Insert membranes readily separated from the tissue upon thawing to room temperature, resulting in tissue tearing and inconsistencies in tissue thickness. Furthermore, small variations in blade cutting force, blade integrity, or adhesiveness of the tissue or polycarbonate membrane impacted sample quality and led to membrane separation. These challenges represent inherent limitations of the sectioning process and have been reported within the literature for similar insert-based cultures (Knight, 2013; Pampaloni, Ansari and Stelzer, 2013; Marx *et al.*, 2018).

Additionally, variations in cell seeding technique have also been shown to affect the distribution of tissue on the membrane surface, with dispersed versus concentrated pipetting techniques having been reported to effect tissue localisation (Knight, 2013). Due to the nature of the bioprinting process, material is deposited onto the membrane at a significant ejection velocity and within a specified region, potentially impacting tissue formation.

6.4.2 Indirect Immunofluorescence Staining

Indirect immunostaining microscopy comparing the protein expression of collagen II and aggrecan within the sectioned tissue models was displayed in Figure 6.3, Figure 6.4 and Figure 6.5 for the MSC, chondrocyte and cell co-culture samples respectively. An elevation in collagen II expression was observed within the chondrocyte and co-culture samples over time. Collagen represents the most abundant structural macromolecule within cartilage ECM, of which the majority is type II collagen (Sophia Fox, Bedi and Rodeo, 2009). These results provide evidence of the formation of ECM components within the chondrocyte and

co-culture models that would normally be found within cartilage tissue. An elevation in aggrecan expression was observed in MSC and co-culture tissues when compared to tissues comprised solely of chondrocyte cells.

These findings corroborate with data presented within the previous chapter, whereby the effect of aggregate culture on MSC and chondrocyte expression of collagen II and aggrecan was studied. An opportunity for further work is provided to study the biological effects of the co-culture using a wider range of cellular markers. This could include SOX9, a transcription factor upregulated during chondrogenesis, alongside markers previously discussed to define the MSC population within the model (Dominici *et al.*, 2006; Hino *et al.*, 2014; James *et al.*, 2015).

Additionally, a similar pattern of variations in nuclear size and shape was observed within indirect immunofluorescence stained samples that is characteristic of nuclear blebbing. This was visualised through DAPI nuclear binding within apoptotic cells, prior to the subsequent membrane damage and cell lysis that is characteristic of apoptosis (Eidet *et al.*, 2014). These findings support the previous observations within Figure 6.2 of haematoxylin and eosin stained tissue sections.

These results provide an opportunity for further research in a number of areas. This includes the use of whole-mount microscopy techniques to analyse tissue composition, the incorporation of a wider range of cellular makers to assess tissue changes, as well as an assessment of the effect of the different bioprinting protocols on tissue formation (Smyrek and Stelzer, 2017; Lazzari *et al.*, 2019).

6.4.3 Cell Tracker Staining

A combination of green and red CellTracker® fluorescent dyes were used to label MSC and chondrocyte cells respectively prior to printing. Cell tracking was performed to determine the ratio and localisation of each cell type within the co-culture model over time. Immunofluorescence images presented in Figure 6.6 confirmed the presence and maintenance of both cell types within the co-culture throughout the 14 day incubation period. A reduction in signal intensity was observed within the first 3 days, representing the degradation of the fluorophore and its reduced retention within proliferating cells.

An increase in chondrocyte cell number and subsequent signal intensity was observed throughout the remainder of the time points, indicative of rapid cellular proliferation, with a

smaller increase in signal intensity observed for the MSCs. It is hypothesised that the variations in proliferation rate that were previously quantified had resulted in a discernible change in the ratio of MSC to chondrocyte cells within the model. It is also possible that the presence of MSCs within the co-culture caused an elevation in the rate of chondrocyte proliferation. This is supported with previous findings whereby the presence of MSCs was shown to stimulate chondrocyte proliferation (Wu *et al.*, 2011). An opportunity for further validation work could include the application of techniques such as fluorescence-activated cell sorting to quantitatively assess the cellular composition of the co-culture tissue.

Additionally, a greater proportion of surface-level chondrocyte cells were present within the model when compared to MSCs. In combination with the layered tissue structure observed within Figure 6.2, this data indicates that the chondrocyte cell population formed a surface layer above the MSCs within the tissue models generated, contrasting the initial post-printing cellular organisation. This is supported by previous research indicating the organisational potential of MSCs when co-cultured with other cell types (Wu *et al.*, 2011; Marshall, Barnes and Genever, 2018). Further research is required to more comprehensively assess the changes in cellular localisation and composition using advanced microscopy techniques such as optical sectioning.

This data provides an important validation step to confirm the maintenance of a cell co-culture within the tissues generated, as well as indicating a time frame for the maintenance of a 50:50 ratio of MSC and chondrocyte cell types.

6.4.4 Cell Proliferation Assay

Immunofluorescence microscopy images indicating the regions of proliferation within the MSC, chondrocyte and co-culture models were presented in Figure 6.7, Figure 6.8 and Figure 6.9 respectively, via EdU incorporation within cellular DNA during replication.

Proliferation was shown to be maintained across all sample groups throughout the full 14 day assessment period, with cellular composition having no discernible effect on proliferation activity. Proliferating cells were shown to be localised towards the membrane side of the tissue. These results imply that the tissue was polarised, and actively proliferating from the membrane level, with non-proliferative cells transferred to the apical surface. This data corroborates with the histological staining previously presented in Figure 6.2, whereby a reduction in cell density was observed towards the upper layers of the tissue across each model.

Additionally, a distinct reduction in nuclei size and sphericity was observed towards the uppermost surface of the co-culture tissue at day 14, in combination with an increase in fluorophore intensity within localised nuclear regions, indicative of nuclear blebbing. These observations further support the hypothesis that cells were transferred from a proliferative region at the base of the tissue to the apical layer, whereby they underwent maturation and subsequent controlled cell death. These results indicate potential structural organisation of the micro-tissue into distinct layers based upon cellular density, size and maturation status, mimicking the structural variations of hyaline cartilage tissue outlined in Figure 2.3.

Previous research using insert-based 3D culture platforms has demonstrated that cellular migration through dense tissues or pore structures promotes the formation of nuclear blebbing and membrane rupture, indicating a possible mechano-regulatory role on cell cycle phase (Pfeifer *et al.*, 2018; Xia *et al.*, 2019). These findings provide evidence of physical changes to cellular structure and organisation in response to high density culture conditions, indicating a potential mechanism through which the nuclear blebbing observed was induced.

6.4.5 Metabolic Activity Assay

Data showing the results of a PrestoBlue® metabolic activity assay of each culture condition were presented in Figure 6.10. Cellular composition was not shown to significantly affect tissue metabolic activity, with a reduction in metabolic activity observed over the first 7 days of culture in all samples. These results contrast with the findings of previous research presented within this thesis, whereby a significant difference in metabolic activity was observed between the MSC and chondrocyte cell lines during routine 2D culture, as shown in Figure 4.17 and Figure 5.13.

A number of factors could have contributed to the overall reduction in cellular metabolic activity. This includes a reduction in cell number or viability due to increasing resource and space constraints. In addition, a reduction in cellular metabolic activity is commonly observed in response to a reduced rate of cellular proliferation or substrate adherence during culture (Liberio *et al.*, 2014). However, such effects would contrast with previous findings whereby the proliferation and adherence of each cell type was maintained throughout culture.

It is therefore likely that the metabolic activity assay selected provided poor compatibility with the 3D culture format. Previous research has demonstrated that a range of commonly used cell assays, previously optimised for 2D culture experiments, provide a poor

representation of cellular activity when applied to 3D culture conditions. This is due to the requirements for rapid diffusion, internalisation, conversion and subsequent externalisation and diffusion of reagents to provide an indicator of internal cellular processes (Mosmann, 1983; Quent *et al.*, 2010; Walzl *et al.*, 2014; Uzarski *et al.*, 2017).

Within a 3D culture platform, the rate of compound diffusion is rapidly reduced in response to increasing tissue thicknesses, with upper bounds placed on tissue thickness where vasculature networks are absent (Malda *et al.*, 2004; Zhou, Cui and Urban, 2008; Cai *et al.*, 2015; McMurtrey, 2016). This is further compounded within an insert-based model, whereby diffusion through the membrane is required to ensure that the full cellular composition is represented, with the porous membrane reducing compound diffusion rates (Bock and Mrowietz, 2001). Under normal conditions, a progressive increase in cell density and adherence onto the insert would be anticipated, further reducing its permeability for cell-based assays. These findings therefore provide an opportunity for further research to assess the effectiveness of commonly used cell-based assays within the 3D culture environment to identify the most appropriate biological markers. In addition, further research is needed to optimise assay protocols to 3D platforms in order to provide a more robust and reproducible system to monitor cellular changes during 3D tissue culture.

In combination, this research demonstrates the suitability of valve deposition processes for the construction of tissue models for *in vitro* OA research applications. These results complement wider literature in this area, whereby bioprinting technologies were successfully combined with insert culture formats to generate models of alternative tissue types (Horvath *et al.*, 2015; King *et al.*, 2017; Min *et al.*, 2018).

6.5 Conclusions

Within this chapter, a DoD valve printing process was applied for the construction of 3D tissue models.

- A combination of MSC, chondrocyte and cell co-cultures were successfully printed onto an insert-based platform using the valve printing process, providing a method to automate the manufacture of 3D tissue models
- Cellular proliferation and composition within each model was maintained across the 14 day culture period, with histological assessment demonstrating the formation of dense tissues within chondrocyte and co-culture models
- Further work is required to fully ascertain the effect of the cell co-culture on tissue formation when compared with tissues generated using a single cell type

Chapter 7. Discussion

7.1 Summary of Results

The research presented in this thesis focussed on the characterisation of piezoelectric inkjet and valve-based drop-on-demand printing technologies, alongside their application in the construction of 3D tissue models for osteoarthritis research.

7.1.1 Single Cell Printing

The jetting performance of a piezoelectric inkjet printing device was characterised in response to changes across a range of critical printing parameters. A printing configuration was defined to enable reliable material deposition at the picolitre-scale. Cell printing performance was evaluated under this configuration, with a resolution achieved to enable the selective deposition of biological material at the single cell level, whilst maintaining cellular viability.

Cellular agglomeration and nozzle blockages previously reported within the literature were observed when jetting cellular material for extended time periods. These effects reduced the reliability and performance of the printing process. Cell deposition performance was improved through the development and application of an in-house designed reservoir agitation system to maintain cellular dispersion within the ink solution. A poly-l-lysine cell coating protocol was also evaluated to reduce cellular agglomeration, with a working range of up to 25 µg / mL defined based upon compatibility with the MSC and chondrocyte cell types studied.

7.1.2 Valve Cell Printing

A solenoid valve dispensing system was evaluated under a drop-on-demand actuation configuration to deposit biological material at the nanolitre-scale. The impact of printing parameter effects on dispensing performance were quantified, using a combination of gravimetric and fluorometric analysis techniques, to determine an optimal configuration for reliable printing.

Cell printing performance was demonstrated with the dispensing process exhibiting no significant effects on cellular viability or biological activity. In addition, jetting was reliably achieved across a concentration range of 1-20 million cells per mL, demonstrating the versatility of the printing process for jetting a range of cell-containing ink solutions.

7.1.3 Tissue Model Production

The suitability of aggregate and insert-based 3D culture platforms were assessed for the construction of printed tissue models.

An in-well aggregate culture protocol was successfully replicated using the valve printing process to generate high density cultures of MSC and chondrocyte cell types. The model format was retained across a 21 day culture period, with biological analysis confirming that the printing process had no significant effect on aggregate morphology, size or cell protein expression of chondrogenic markers.

The insert-based culture platform was generated using the valve printing device to culture MSC, chondrocyte and MSC-chondrocyte co-cultures. Tissues were generated and retained over a 14 day culture period, exhibiting continual proliferation. Histological analysis revealed the formation of distinct cellular layers within the chondrocyte and co-culture samples, with both cell types retained within the model at 14 days.

In combination, these findings demonstrate the compatibility of the valve printing process with aggregate and insert-based 3D culture formats.

7.2 Implications of Research

7.2.1 Considerations for Cell Printing

A wide range of drop-on-demand bioprinting processes have been reported for cell printing applications within the literature. Most commonly, these publications have focussed on the biological applications of inkjet printing, where the authors have taken care to ensure the efficient modelling and optimisation of printing parameters to improve cell printing performance (Xu *et al.*, 2005; J. A. Park *et al.*, 2017). Yet despite this, limited research exists on the practical limitations of dispensing cellular material within a liquid solution (Kwon, 2009; Parsa *et al.*, 2010; Yusof *et al.*, 2011; Chahal, Ahmadi and Cheung, 2012; Tse, 2015).

Within this work, the effects of cellular materials on droplet ejection, printing density and jetting reliability have been investigated, and the implications these factors have on bioprinting systems have been reported. This includes challenges surrounding the maintenance of cellular suspensions within a reservoir, as well as the agglomeration of cellular material and subsequent nozzle blockages that occur during extended printing periods.

A combination of three independent methodologies have been assessed and presented as potential mechanisms to improve printing performance. This includes the use of purge cycling between print runs, the development of an in-house designed reservoir agitation system to reduce cell sedimentation, and benchmarking of a polycationic cell coating process to minimise cellular agglomeration. Each of these strategies provide a valuable alternative to current bioprinting approaches in order to maximise print performance, and alleviate the issues that are inherent when processing cell-containing solutions over extended periods of time. As a result, this research serves as an important reference when developing or refining novel bioprinting approaches to account for cell ink effects, thus maximising the potential applications of such techniques within the fields of tissue engineering and regenerative medicine.

7.2.2 Liquid Handling Applications of Valve Deposition Technology

The emergence of the fields of biofabrication and high-throughput screening have increased demand for reliable, low-volume dispensing apparatus for applications within tissue engineering and drug discovery research. Commercially available non-contact liquid handling systems are often designed to feature pneumatic actuation methods. These systems generally employ disposable tips to hold and transfer material between plates, making printing performance heavily dependent on tip-to-tip manufacturing tolerances. In addition, physical limitations are placed on the minimum volume that can be practically transferred per actuation cycle due to the considerable impact of surface tension, material viscosity and component mixing on dispensing performance.

A growing number of systems have begun to employ solenoid valve actuated dispensing devices to circumvent such issues and provide a significant improvement in minimum dispense resolution. Despite this, such systems commonly require the valve open time to be adjusted to change droplet volume. As a result, they offer less control over material ejection characteristics, generating a continual stream of material under large volume requests. These systems therefore provide a poor method to bioprint structures in 3D, where spatial control of material volume is required, and in many cases *in situ* contact or curing reactions are applied to generate layered structures (Sturgess *et al.*, 2017; Da Conceicao Ribeiro *et al.*, 2019; Zimmermann *et al.*, 2019).

In this thesis, the versatility of a valve deposition process for material and cell deposition applications was demonstrated to enable the reliable deposition of bioink solutions under a

drop-on-demand configuration. In addition, the ability to process cellular material across a wide concentration range represents a significant advantage over alternative techniques such as inkjet printing, whereby jetting performance is limited to lower cell concentrations (Cui *et al.*, 2010). The ability to process high cell ink concentrations is of particular importance for bioprinting applications within the field of tissue engineering due to the high cell density of natural tissues. Comparisons between gravimetric and fluorometric analysis techniques also highlighted the challenges associated with quantifying deposition performance at the nanolitre-scale to assess printing accuracy and reproducibility, as well as providing potential methods for circumvention.

These results provide an important validation step to ensure that valve printing performance can be maintained when using actuation cycle number to control total dispense volume. In addition, biological characterisation data demonstrated the biocompatibility of the valve deposition process to deposit MSC and chondrocyte cell types, without significantly implicating cellular viability or function.

7.2.3 Scaling Up Aggregate Production

The emergence of cellular therapies for the treatment of osteoarthritis provides a valuable alternative to conventional surgical procedures. Ongoing clinical trials have demonstrated the potential of such therapies across a range of implantation formats, of which aggregate culture and surgical implantation are being developed at the clinical and commercial scale (National Institute for Health and Care Excellence, 2018; Armoiry *et al.*, 2019; Wang *et al.*, 2019). In addition, aggregate culture has gained increased attention within recent literature due to the improved recapitulation of the 3D environment of living tissue, thus providing a more replicative environment when compared to the commonly employed monolayer culture techniques for *in vitro* research (McMurtrey, 2016; Nath and Devi, 2016).

Current methodologies to generate tissue aggregates are labour intensive, thus limiting the scale at which cultures can be generated (Foty, 2011; Leung *et al.*, 2015). Within this research, a valve-based dispensing system was successfully applied to generate 3D aggregates of MSC and chondrocyte cell types using a gravity-induced culture method. The printing process was shown to have no significant effect on aggregate size, morphology, or expression of key chondrogenic cell markers, when compared with manual seeding techniques using an in-well culture format. This approach therefore provides a potential methodology to scale-up the manufacture of tissue aggregates using bioprinting techniques,

whilst simultaneously reducing labour requirements. As a result, such technologies could provide improvements to the roll-out and cost-effectiveness of existing cellular therapies, alongside increasing the potential throughput of *in vitro* OA research platforms.

7.2.4 Bioprinting of Osteoarthritis Tissue Models

Recent strategies to improve the performance of emerging osteoarthritis cell therapies include the combination of MSC and chondrocyte cell types to promote cartilage formation on implantation. However, few studies exist to provide evidence of the potential impact of MSCs on chondrocyte tissue formation in both *in vitro* and *in vivo* formats (Li *et al.*, 2016; Kim *et al.*, 2019; Wang *et al.*, 2019). In addition, there is a growing demand for novel disease models that can be used for early-stage high-throughput screening applications due to the high costs and low success rates that are characteristic of the therapy development process (Dimitri, 2011; DiMasi, Grabowski and Hansen, 2016).

It is therefore imperative that *in vitro* platforms are developed to better model the cellular microenvironment within the joint, thus enabling improved early-stage testing of potential compounds or cellular therapies for the treatment of osteoarthritis. Within this research, a combination of MSC, chondrocyte and MSC-chondrocyte co-culture tissues were generated within an insert-based culture format to study cell-cell interactions and provide a platform for high-throughput screening. Models were constructed using a valve printing process in a 96-well plate format to maximise throughput and scalability. Biological characterisation data demonstrated that the model remained viable over the full 14 day assessment period through continual cell proliferation and the maintenance of both cell types, as well as elucidating a potential mechanism of cellular organisation within the co-cultured tissue.

This work provides a platform for assessing the effect of cell co-cultures on tissue formation, as well studying tissue responses to external pathological stimuli such as cytokines IL-1β and TNF-α, which are implicated in OA pathophysiology (Rahmati, Mobasheri and Mozafari, 2016). Following the induction of an OA phenotype, this model may also provide a platform to assess treatment response during the early stages of the drug discovery process.

7.3 Future Research

A number of areas for further research are highlighted within this work. This includes the scaling up of inkjet or valve-based actuation systems to enable simultaneous printing across multiple actuation channels. Such modifications could include the use of a microfluidic or manifold block to couple a series of actuation devices to a central reservoir. Alternatively,

separate reservoir systems could be designed to enable the simultaneous delivery of multiple different cell types within a single model. Further development of the drive electronics systems would be required to enable the application of independent actuation parameters to each device according to print and ink specifications. These modifications would increase the throughput of the device to match that of commercial non-contact dispensing systems, as well as enable the simultaneous deposition of multiple materials into each well of a multi-well plate. As a result, such changes would significantly improve the commercial applicability of the printing platform.

Further development of the printing platform could also include upgrades to the on-board image acquisition and analysis systems to integrate image-based automated cell counting. This would provide a rapid and automated method to calibrate and benchmark printing performance prior to each print job in order to ensure printing reliability.

In addition, the demonstration of single cell printing capabilities presented using the inkjet deposition system in chapter 4 provides a unique method to scale down the size of disease models, opening up new opportunities to research intercellular interactions and responses to external stimuli. Further research could incorporate this printing technology to deposit multiple cell types within a microfluidic chamber or culture format that is an order of magnitude smaller than conventional high density multi-well plates. Decreasing model size would confer increased model densities and subsequently higher-throughput platforms for *in vitro* research. It would also significantly reduce reagent and cell requirements, lowering associated development and maintenance expenses. When combined with appropriate analysis techniques, such models could provide an opportunity to study interactions at the single cell level, thus providing unique research opportunities that would be difficult to achieve at an equivalent scale and throughput when using conventional liquid handling processes.

Further research is also required to identify biomarkers and analysis techniques that could be used to study tissue models at a greater screening throughput. Within both the aggregate and insert-based models, a key challenge throughout the project has been the low throughput and complexity of conventional sectioning, staining and imaging processes. In addition, phenotypic markers of cellular differentiation have provided a limited understanding of cellular changes within the tissue. Culture formats were also primarily studied using destructive biological analysis techniques. As a consequence, large numbers of

samples were required to determine cellular changes over time with a reduced analytical throughput. Further research could incorporate whole-mount microscopy techniques, more comprehensive biomarker screening, or non-destructive supernatant analysis techniques, to provide an analysis methodology that is able to more comprehensively and rapidly monitor cellular changes within the tissue models.

The exchange of cell culture media represented a continual challenge when culturing high cell densities within high-throughput compatible culture formats. Due to the recognised role that nutrient and waste diffusion gradients have on cellular functionality, it is essential to select culture formats, media formulation and exchange procedures to minimise any variabilities in culture conditions. In addition, the collection and management of media exchange provides a valuable opportunity for further study, when coupled with the requirements to provide non-destructive sample analysis techniques such as supernatant analysis. Further research should be performed to explore the potential of using novel media exchange methods to automate the media exchange process, as well as to provide an additional sample stream for real-time analysis. This may incorporate modifications to well volumes, perfusion-based systems or microfluidic devices.

Finally, a number of additional areas of interest exist in relation to the specific 3D culture formats explored within this research. This includes the impact of initiating cell seeding densities and ratios on model stability and function, as well as methods to induce and monitor OA-like pathophysiological processes within the tissues generated. Such methods could include the use of cytokine induction within the cell culture media formulation, as well as mechanical methods to initiate tissue instability or damage, in order to recapitulate specific pathophysiological conditions that are characteristic of OA.

7.4 Conclusion

The research presented within this thesis has demonstrated the versatility of inkjet and valve-based drop-on-demand processes for cell printing applications. Each technique was characterised to determine the influence of jetting parameters on printing performance.

Single cell printing was achieved using the inkjet printing process, enabling the deposition of material at the picolitre-scale, thus providing unique opportunities for the development of small-scale cellular models.

Valve printing performance was demonstrated over a concentration range of 1-20 million cells per mL to enable the deposition of material at the nanolitre-scale, providing a versatile method to dispense high cell density solutions.

Both printing processes were successfully applied for the deposition of mesenchymal stromal and chondrocyte cell types without significantly affecting cellular viability or function, with a combination of intermittent nozzle purging, polycationic cell coating, and reservoir agitation systems presented to maximise cell jetting performance. These results demonstrate the suitability of drop-on-demand processes for bioprinting applications, as well as providing potential mechanisms to reduce cell printing performance issues that are inherent within droplet-based bioprinting processes.

Aggregate and insert-based 3D culture formats were then replicated using the valve printing technology to generate tissue models for *in vitro* osteoarthritis research applications. These models provide the first examples of DoD bioprinted platforms to study the underlying pathophysiological mechanisms of osteoarthritis, as well as evaluate the efficacy of novel therapies.

Chapter 8. References

Ahn, K. and Yokota, S. (2005) 'Intelligent switching control of pneumatic actuator using on/off solenoid valves', *Mechatronics*, 15(6), pp. 683–702. doi: 10.1016/j.mechatronics.2005.01.001.

Aijian, A. P. and Garrell, R. L. (2015) 'Digital Microfluidics for Automated Hanging Drop Cell Spheroid Culture', *Journal of Laboratory Automation*, 20(3), pp. 283–295. doi: 10.1177/2211068214562002.

Amin, A. K. *et al.* (2009) 'Chondrocyte survival in articular cartilage: The influence of subchondral bone in a bovine model', *Journal of Bone and Joint Surgery - Series B*, 91(5), pp. 691–699. doi: 10.1302/0301-620X.91B5.21544.

Anderson, G. D. *et al.* (1996) 'Selective Inhibition of Cyclooxygenase (COX)-2 Reverses Inflammation and Expression of COX-2 and Interleukin 6 in Rat Adjuvant Arthritis', *J. Clin. Invest*, 97(11), pp. 2672–2679.

Armoiry, X. *et al.* (2019) 'Autologous Chondrocyte Implantation with Chondrosphere for Treating Articular Cartilage Defects in the Knee: An Evidence Review Group Perspective of a NICE Single Technology Appraisal', *PharmacoEconomics*, 37(7), pp. 879–886. doi: 10.1007/s40273-018-0737-z.

Armstrong, S. J. *et al.* (1993) 'Moderate exercise exacerbates the osteoarthritic lesions produced in cartilage by meniscectomy: a morphological study', *Osteoarthritis and Cartilage*, 1(2), pp. 89–96. doi: 10.1016/S1063-4584(05)80023-8.

Astashkina, A., Mann, B. and Grainger, D. W. (2012) 'A critical evaluation of in vitro cell culture models for high-throughput drug screening and toxicity', *Pharmacology & Therapeutics*, 134(1), pp. 82–106. doi: 10.1016/j.pharmthera.2012.01.001.

Atala, A. *et al.* (2012) 'Hybrid printing of mechanically and biologically improved constructs for cartilage tissue engineering applications', *Biofabrication*. IOP Publishing, 5(1), p. 015001. doi: 10.1088/1758-5082/5/1/015001.

Bammesberger, S. *et al.* (2013) 'Quantitative characterization of non-contact microdispensing technologies for the sub-microliter range', *Drug Discovery Today*, 18. doi: 10.1016/j.drudis.2012.12.001.

Bartosh, T. J. *et al.* (2010) 'Aggregation of human mesenchymal stromal cells (MSCs) into 3D spheroids enhances their antiinflammatory properties', *Proceedings of the National Academy of Sciences of the United States of America*, 107(31), pp. 13724–13729. doi: 10.1073/pnas.1008117107.

Basso, N. and Heersche, J. N. M. (2006) 'Effects of hind limb unloading and reloading on nitric oxide synthase expression and apoptosis of osteocytes and chondrocytes', *Bone*, 39(4), pp. 807–814. doi: 10.1016/j.bone.2006.04.014.

Bay-Jensen, A. C. *et al.* (2016) 'Osteoarthritis year in review 2015: soluble biomarkers and the BIPED criteria', *Osteoarthritis and Cartilage*, 24(1), pp. 9–20. doi: 10.1016/j.joca.2015.10.014.

Bellido, M. *et al.* (2011) 'Improving subchondral bone integrity reduces progression of cartilage damage in experimental osteoarthritis preceded by osteoporosis', *Osteoarthritis and Cartilage*, 19(10), pp. 1228–1236. doi: 10.1016/j.joca.2011.07.003.

Berenbaum, F. (2013) 'Osteoarthritis as an inflammatory disease (osteoarthritis is not osteoarthrosis!).', *Osteoarthritis and cartilage / OARS, Osteoarthritis Research Society*. W.B. Saunders, 21(1), pp. 16–21. doi: 10.1016/j.joca.2012.11.012.

Bessemans, L. *et al.* (2016) 'Automated Gravimetric Calibration to Optimize the Accuracy and Precision of TECAN Freedom EVO Liquid Handler', *Journal of Laboratory Automation*, 21(5), pp. 693–705. doi: 10.1177/2211068216632349.

Bhadriraju, K. and Chen, C. S. (2002) 'Engineering cellular microenvironments to improve cell-based drug testing', *Drug Discovery Today*, 7(11), pp. 612–620. doi: 10.1016/S1359-6446(02)02273-0.

Bhosale, A. M. and Richardson, J. B. (2008) 'Articular cartilage: Structure, injuries and review of management', *British Medical Bulletin*, 87(1), pp. 77–95. doi: 10.1093/bmb/ldn025.

Birgersdotter, A., Sandberg, R. and Ernberg, I. (2005) 'Gene expression perturbation in vitro—A growing case for three-dimensional (3D) culture systems', *Seminars in Cancer Biology*, 15(5), pp. 405–412. doi: 10.1016/j.semcancer.2005.06.009.

Bock, O. and Mrowietz, U. (2001) 'Development of a new method of analysing chemotactic deactivation of human neutrophil granulocytes', *Journal of Biochemical and Biophysical*

Methods. Elsevier, 48(3), pp. 257–268. doi: 10.1016/S0165-022X(01)00157-9.

Boland, T. *et al.* (2003) 'Cell and organ printing 2: Fusion of cell aggregates in three-dimensional gels', *Anatomical Record - Part A Discoveries in Molecular, Cellular, and Evolutionary Biology*, 272(2), pp. 497–502. doi: 10.1002/ar.a.10059.

Boland, T., Wilson, W. and Xu, T. (2006) 'Ink-jet printing of viable cells'. United States: United States Patent and Trademark Office. Available at: https://patents.google.com/patent/US7051654B2/en.

Bondeson, J. *et al.* (2008) 'The regulation of the ADAMTS4 and ADAMTS5 aggrecanases in osteoarthritis: A review', *Clinical and Experimental Rheumatology*, 26(1), pp. 139–145. doi: 2261 [pii].

Boutros, M., Heigwer, F. and Laufer, C. (2015) 'Microscopy-Based High-Content Screening', *Cell*, 163(6), pp. 1314–1325. doi: 10.1016/j.cell.2015.11.007.

Breslin, S. and O'Driscoll, L. (2013) 'Three-dimensional cell culture: The missing link in drug discovery', *Drug Discovery Today*, 18(5–6), pp. 240–249. doi: 10.1016/j.drudis.2012.10.003.

Brew, K., Dinakarpandian, D. and Nagase, H. (2000) 'Tissue inhibitors of metalloproteinases: evolution, structure and function', *Biochimica et Biophysica Acta (BBA) - Protein Structure and Molecular Enzymology*, 1477(1), pp. 267–283. doi: 10.1016/S0167-4838(99)00279-4.

Brew, K. and Nagase, H. (2010) 'The tissue inhibitors of metalloproteinases (TIMPs): An ancient family with structural and functional diversity', *Biochimica et Biophysica Acta (BBA) - Molecular Cell Research*, 1803(1), pp. 55–71. doi: 10.1016/j.bbamcr.2010.01.003.

C, A. *et al.* (2019) 'Inkjet printing of thermally activated delayed fluorescence (TADF) dendrimer for OLEDs applications', *Organic Electronics: physics, materials, applications*. North-Holland, 74, pp. 218–227. doi: 10.1016/j.orgel.2019.07.011.

Cader, H. K. *et al.* (2019) 'Water-based 3D inkjet printing of an oral pharmaceutical dosage form', *International Journal of Pharmaceutics*. Elsevier, 564, pp. 359–368. doi: 10.1016/J.IJPHARM.2019.04.026.

Cai, Y. *et al.* (2015) 'Oxygen transport in a three-dimensional microvascular network incorporated with early tumour growth and preexisting vessel cooption: Numerical simulation study', *BioMed Research International*, 2015. doi: 10.1155/2015/476964.

Campbell, P. G. *et al.* (2005) 'Engineered spatial patterns of FGF-2 immobilized on fibrin direct cell organization', *Biomaterials*, 26(33), pp. 6762–6770. doi: 10.1016/j.biomaterials.2005.04.032.

Caplan, A. I. (2009) 'New Era of Cell-Based Orthopedic Therapies', *Tissue Engineering Part B: Reviews*, 15(2), pp. 195–200. doi: 10.1089/ten.teb.2008.0515.

Caplan, A. I. and Bruder, S. P. (2001) 'Mesenchymal stem cells: building blocks for molecular medicine in the 21st century', *Trends in Molecular Medicine*. Elsevier Current Trends, 7(6), pp. 259–264. doi: 10.1016/S1471-4914(01)02016-0.

Caron, M. M. J. *et al.* (2012) 'Redifferentiation of dedifferentiated human articular chondrocytes: comparison of 2D and 3D cultures', *Osteoarthritis and Cartilage*. W.B. Saunders, 20(10), pp. 1170–1178. Available at: https://www.sciencedirect.com/science/article/pii/S1063458412008710.

Castañeda, S. *et al.* (2012) 'Subchondral bone as a key target for osteoarthritis treatment', *Biochemical Pharmacology*, pp. 315–323. doi: 10.1016/j.bcp.2011.09.018.

Cataldi, A. *et al.* (1994) 'The behaviour of nuclear domains in the course of apoptosis', *Histochemistry*, 102(3), pp. 221–231. doi: 10.1007/BF00268899.

Cawston, T. E. and Wilson, A. J. (2006) 'Understanding the role of tissue degrading enzymes and their inhibitors in development and disease', *Best Practice & Research Clinical Rheumatology*, 20(5), pp. 983–1002. doi: 10.1016/j.berh.2006.06.007.

Chaganti, R. K. and Lane, N. E. (2011) 'Risk factors for incident osteoarthritis of the hip and knee', *Current Reviews in Musculoskeletal Medicine*, 4(3), pp. 99–104. doi: 10.1007/s12178-011-9088-5.

Chahal, D., Ahmadi, A. and Cheung, K. C. (2012) 'Improving piezoelectric cell printing accuracy and reliability through neutral buoyancy of suspensions', *Biotechnology and Bioengineering*, 109(11), pp. 2932–2940. doi: 10.1002/bit.24562.

Chang, C. C. *et al.* (2011) 'Direct-write bioprinting three-dimensional biohybrid systems for future regenerative therapies', *Journal of Biomedical Materials Research - Part B Applied Biomaterials*, pp. 160–170. doi: 10.1002/jbm.b.31831.

Chang, R., Nam, J. and Sun, W. (2008) 'Effects of dispensing pressure and nozzle diameter on

cell survival from solid freeform fabrication-based direct cell writing', *Tissue Engineering - Part A.* Mary Ann Liebert Inc., 14(1), pp. 41–48. doi: 10.1089/ten.a.2007.0004.

Chen, W. H. *et al.* (2009) 'In vitro stage-specific chondrogenesis of mesenchymal stem cells committed to chondrocytes', *Arthritis and Rheumatism*, 60(2), pp. 450–459. doi: 10.1002/art.24265.

Chen, Y. *et al.* (2017) 'Edge effect detection for real-time cellular analyzer using statistical analysis', *RSC Advances*, 7(34), pp. 20833–20839. doi: 10.1039/c6ra26375e.

Chevalier, X. *et al.* (2009) 'Intraarticular injection of anakinra in osteoarthritis of the knee: A multicenter, randomized, double-blind, placebo-controlled study', *Arthritis & Rheumatism*. Wiley Subscription Services, Inc., A Wiley Company, 61(3), pp. 344–352. doi: 10.1002/art.24096.

Choi, Y. Y. *et al.* (2010) 'Controlled-size embryoid body formation in concave microwell arrays', *Biomaterials*, 31(15), pp. 4296–4303. doi: 10.1016/j.biomaterials.2010.01.115.

Chowdhury, T. T. *et al.* (2008) 'Signal transduction pathways involving p38 MAPK, JNK, NFκB and AP-1 influences the response of chondrocytes cultured in agarose constructs to IL-1β and dynamic compression', *Inflammation Research*, 57(7), pp. 306–313. doi: 10.1007/s00011-007-7126-y.

Claassen, H. *et al.* (2011) 'C-28/I2 and T/C-28a2 chondrocytes as well as human primary articular chondrocytes express sex hormone and insulin receptors—Useful cells in study of cartilage metabolism', *Annals of Anatomy - Anatomischer Anzeiger*. Urban & Fischer, 193(1), pp. 23–29. doi: 10.1016/J.AANAT.2010.09.005.

Clark, E. C. *et al.* (2016) 'Evaluation of cell-laden polyelectrolyte hydrogels incorporating poly(l -Lysine) for applications in cartilage tissue engineering', *Biomaterials*, 83, pp. 332–346. doi: 10.1016/j.biomaterials.2016.01.020.

Clav, A. *et al.* (2016) 'Third-Generation Autologous Chondrocyte Implantation Versus Mosaicplasty for Knee Cartilage Injury: 2-Year Randomized Trial', *Journal of Orthopaedic Research*, 34(4), pp. 658–665. doi: 10.1002/jor.23152.

Clutterbuck, A. L. *et al.* (2011) 'High throughput proteomic analysis of the secretome in an explant model of articular cartilage inflammation.', *Journal of proteomics*. Elsevier, 74(5), pp.

704–15. doi: 10.1016/j.jprot.2011.02.017.

Da Conceicao Ribeiro, R. *et al.* (2019) 'Reactive jet impingement bioprinting of high cell density gels for bone microtissue fabrication', *Biofabrication*, 11(1). doi: 10.1088/1758-5090/aaf625.

Cova, M. and Toffanin, R. (2002) 'MR microscopy of hyaline cartilage: Current status', *European Radiology*, pp. 814–823. doi: 10.1007/s003300101128.

Cozens, D. *et al.* (2018) 'Development and optimization of a differentiated airway epithelial cell model of the bovine respiratory tract', *Scientific Reports*, 8(1), p. 853. doi: 10.1038/s41598-017-19079-y.

Cross, M. *et al.* (2014) 'The global burden of hip and knee osteoarthritis: estimates from the Global Burden of Disease 2010 study.', *Annals of the rheumatic diseases*, 73(7), pp. 1323–30. doi: 10.1136/annrheumdis-2013-204763.

Cui, X. *et al.* (2010) 'Cell damage evaluation of thermal inkjet printed chinese hamster ovary cells', *Biotechnology and Bioengineering*, 106(6), pp. 963–969. doi: 10.1002/bit.22762.

Dahlin, R. L. *et al.* (2014) 'TGF-β3-induced chondrogenesis in co-cultures of chondrocytes and mesenchymal stem cells on biodegradable scaffolds', *Biomaterials*, 35(1), pp. 123–132. doi: 10.1016/j.biomaterials.2013.09.086.

Das, R. H. J. *et al.* (2008) 'In vitro expansion affects the response of chondrocytes to mechanical stimulation', *Osteoarthritis and Cartilage*. W.B. Saunders, 16(3), pp. 385–391. doi: 10.1016/J.JOCA.2007.07.014.

Dehne, T. *et al.* (2010) 'Gene expression profiling of primary human articular chondrocytes in high-density micromasses reveals patterns of recovery, maintenance, re- and dedifferentiation', *Gene*, 462(1–2), pp. 8–17. doi: 10.1016/j.gene.2010.04.006.

Derby, B. (2010) 'Inkjet Printing of Functional and Structural Materials: Fluid Property Requirements, Feature Stability, and Resolution', *Annual Review of Materials Research*, 40(1), pp. 395–414. doi: 10.1146/annurev-matsci-070909-104502.

Dexheimer, V., Frank, S. and Richter, W. (2012) 'Proliferation as a requirement for in vitro chondrogenesis of human mesenchymal stem cells', *Stem Cells and Development*, 21(12), pp. 2160–2169. doi: 10.1089/scd.2011.0670.

Diaz-Romero, J. *et al.* (2005) 'Immunophenotypic analysis of human articular chondrocytes: Changes in surface markers associated with cell expansion in monolayer culture', *Journal of Cellular Physiology*, 202(3), pp. 731–742. doi: 10.1002/jcp.20164.

Dieppe, P. A. and Lohmander, L. S. (2005) 'Pathogenesis and management of pain in osteoarthritis', *Lancet*, 365(9463), pp. 965–973. doi: 10.1016/S0140-6736(05)71086-2.

DiMasi, J. A., Grabowski, H. G. and Hansen, R. W. (2016) 'Innovation in the pharmaceutical industry: New estimates of R&D costs', *Journal of Health Economics*, 47, pp. 20–33. doi: 10.1016/j.jhealeco.2016.01.012.

Dimitri, N. (2011) 'An assessment of R&D productivity in the pharmaceutical industry', *Trends in Pharmacological Sciences*, 32(12), pp. 683–685. doi: 10.1016/j.tips.2011.09.005.

Dobre, O. *et al.* (2018) 'An immortalised mesenchymal stem cell line maintains mechano-responsive behaviour and can be used as a reporter of substrate stiffness', *Scientific Reports*. Nature Publishing Group, 8(1), p. 8981. doi: 10.1038/s41598-018-27346-9.

Dominici, M. *et al.* (2006) 'Minimal criteria for defining multipotent mesenchymal stromal cells. The International Society for Cellular Therapy position statement.', *Cytotherapy*, 8(4), pp. 315–7. doi: 10.1080/14653240600855905.

Edmondson, R. *et al.* (2014) 'Three-dimensional cell culture systems and their applications in drug discovery and cell-based biosensors', *Assay and Drug Development Technologies*. Mary Ann Liebert, Inc., 12(4), pp. 207–218. doi: 10.1089/adt.2014.573.

Ehret, F., Vogler, S. and Kempermann, G. (2015) 'A co-culture model of the hippocampal neurogenic niche reveals differential effects of astrocytes, endothelial cells and pericytes on proliferation and differentiation of adult murine precursor cells', *Stem Cell Research*, 15(3), pp. 514–521. doi: 10.1016/j.scr.2015.09.010.

Eidet, J. R. *et al.* (2014) 'Objective assessment of changes in nuclear morphology and cell distribution following induction of apoptosis', *Diagnostic Pathology*, 9(1). doi: 10.1186/1746-1596-9-92.

Elahi, K. C. *et al.* (2016) 'Human mesenchymal stromal cells from different sources diverge in their expression of cell surface proteins and display distinct differentiation patterns', *Stem Cells International*. Hindawi Limited, 2016, p. 5646384. doi: 10.1155/2016/5646384.

Elvidge, J., Bullement, A. and Hatswell, A. J. (2016) 'Cost Effectiveness of Characterised Chondrocyte Implantation for Treatment of Cartilage Defects of the Knee in the UK', *PharmacoEconomics*. Springer International Publishing, 34(11), pp. 1145–1159. doi: 10.1007/s40273-016-0423-y.

Erggelet, C. and Vavken, P. (2016) 'Microfracture for the treatment of cartilage defects in the knee joint – A golden standard?', *Journal of Clinical Orthopaedics and Trauma*, 7(3), pp. 145–152. doi: 10.1016/j.jcot.2016.06.015.

Evans, C. H., Ghivizzani, S. C. and Robbins, P. D. (2013) 'Arthritis gene therapy and its tortuous path into the clinic', *Translational Research*, 161(4), pp. 205–216. doi: 10.1016/j.trsl.2013.01.002.

Faulkner-Jones, A. *et al.* (2013) 'Development of a valve-based cell printer for the formation of human embryonic stem cell spheroid aggregates', *Biofabrication*, 5(1). doi: 10.1088/1758-5082/5/1/015013.

Faulkner-Jones, A. *et al.* (2015) 'Bioprinting of human pluripotent stem cells and their directed differentiation into hepatocyte-like cells for the generation of mini-livers in 3D', *Biofabrication*. IOP Publishing, 7(4), p. 044102. doi: 10.1088/1758-5090/7/4/044102.

Faulkner-Jones, A. (2015) *Development of Multivalve - Based Bioprinting Technology*. Heriot-Watt University.

Fennema, E. *et al.* (2013) 'Spheroid culture as a tool for creating 3D complex tissues', *Trends in Biotechnology*. Elsevier Ltd, 31(2), pp. 108–115. doi: 10.1016/j.tibtech.2012.12.003.

Finger, F. *et al.* (2003) 'Molecular Phenotyping of Human Chondrocyte Cell Lines T/C-28a2, T/C-28a4, and C-28/I2', *Arthritis and Rheumatism*, 48(12), pp. 3395–3403. doi: 10.1002/art.11341.

Fitzgerald, J. B. *et al.* (2008) 'Shear- and compression-induced chondrocyte transcription requires MAPK activation in cartilage explants.', *The Journal of biological chemistry*. American Society for Biochemistry and Molecular Biology, 283(11), pp. 6735–43. doi: 10.1074/jbc.M708670200.

Foldager, C. B. *et al.* (2012) 'Cell Seeding Densities in Autologous Chondrocyte Implantation Techniques for Cartilage Repair', *Cartilage*, 3(2), pp. 108–117. doi:

10.1177/1947603511435522.

Foty, R. (2011) 'A Simple Hanging Drop Cell Culture Protocol for Generation of 3D Spheroids', *Journal of Visualized Experiments*. MyJoVE Corporation, (51). doi: 10.3791/2720.

Friedenstein, A. J., Chailakhjan, R. K. and Lalykin, K. S. (1970) 'The development of fibroblast colonies in marrow and spleen cells', *Cell Tissue Kinet.*, 3, pp. 393–403. doi: 10.1111/j.1365-2184.1970.tb00347.x.

Friedenstein, A. J., Gorskaja, J. F. and Kulagina, N. N. (1976) 'Fibroblast precursors in normal and irradiated mouse hematopoietic organs.', *Experimental Hematology*, 4(5), pp. 267–74. Available at: http://www.ncbi.nlm.nih.gov/pubmed/976387.

Frith, J. and Genever, P. (2008) 'Transcriptional control of mesenchymal stem cell differentiation', *Transfusion Medicine and Hemotherapy*. Karger Publishers, 35(3), pp. 216–227. doi: 10.1159/000127448.

Fromm, J. E. (1984) 'Numerical Calculation of the Fluid Dynamics of Drop-on-Demand Jets', *IBM Journal of Research and Development*, 28(3), pp. 322–333. doi: 10.1147/rd.283.0322.

Futrega, K. *et al.* (2015) 'The microwell-mesh: A novel device and protocol for the high throughput manufacturing of cartilage microtissues', *Biomaterials*, 62, pp. 1–12. doi: 10.1016/j.biomaterials.2015.05.013.

Gaber, T. *et al.* (2012) 'Osteoarthritis synovial fluid activates pro-inflammatory cytokines in primary human chondrocytes', *International Orthopaedics*, 37(1), pp. 145–151. doi: 10.1007/s00264-012-1724-1.

Gabriel, N. *et al.* (2010) 'Development of an in vitro model of feline cartilage degradation', *Journal of Feline Medicine and Surgery*. SAGE PublicationsSage UK: London, England, 12(8), pp. 614–620. doi: 10.1016/j.jfms.2010.03.007.

Ganesan, S. *et al.* (2019) 'Inkjet printing of zinc oxide and P3HT:ICBA in ambient conditions for inverted bulk heterojunction solar cells', *Optical Materials*. North-Holland, 94, pp. 430–435. doi: 10.1016/J.OPTMAT.2019.05.031.

Gebauer, M. *et al.* (2005) 'Comparison of the chondrosarcoma cell line SW1353 with primary human adult articular chondrocytes with regard to their gene expression profile and reactivity to IL-1β', *Osteoarthritis and Cartilage*. W.B. Saunders, 13(8), pp. 697–708. doi:

10.1016/J.JOCA.2005.04.004.

Gendron, C. *et al.* (2007) 'Proteolytic activities of human ADAMTS-5: comparative studies with ADAMTS-4.', *The Journal of biological chemistry*. American Society for Biochemistry and Molecular Biology, 282(25), pp. 18294–306. doi: 10.1074/jbc.M701523200.

Geurts, J. *et al.* (2018) 'Novel ex vivo human osteochondral explant model of knee and spine osteoarthritis enables assessment of inflammatory and drug treatment responses', *International Journal of Molecular Sciences*. Multidisciplinary Digital Publishing Institute (MDPI), 19(5). doi: 10.3390/ijms19051314.

Glasson, S. S. *et al.* (2005) 'Deletion of active ADAMTS5 prevents cartilage degradation in a murine model of osteoarthritis', *Nature*. Nature Publishing Group, 434(7033), pp. 644–648. doi: 10.1038/nature03369.

Glyn-Jones, S. *et al.* (2015) 'Osteoarthritis', *The Lancet*. Elsevier, 386(9991), pp. 376–387. doi: 10.1016/S0140-6736(14)60802-3.

Goldring, M. B. *et al.* (1994) 'Interleukin-1 beta-modulated gene expression in immortalized human chondrocytes.', *The Journal of Clinical investigation*, 94(6), pp. 2307–16. doi: 10.1172/JCI117595.

Graceffa, V. *et al.* (2019) 'Chasing Chimeras – The elusive stable chondrogenic phenotype', *Biomaterials*. Elsevier, 192, pp. 199–225. doi: 10.1016/j.biomaterials.2018.11.014.

Greenberg, D. D. *et al.* (2006) 'Biochemical effects of two different hyaluronic acid products in a co-culture model of osteoarthritis', *Osteoarthritis and Cartilage*, 14(8), pp. 814–822. doi: 10.1016/j.joca.2006.02.006.

van Griensven, M. *et al.* (2019) 'Mesenchymal Stem Cell Therapy for Osteoarthritis: The Critical Role of the Cell Secretome', *Front. Bioeng. Biotechnol*, 7(9), p. 9. doi: 10.3389/fbioe.2019.00009.

Groll, J. *et al.* (2016) 'Biofabrication: reappraising the definition of an evolving field.', *Biofabrication*, 8(1), p. 013001. doi: 10.1088/1758-5090/8/1/013001.

Gudapati, H., Dey, M. and Ozbolat, I. (2016) 'A comprehensive review on droplet-based bioprinting: Past, present and future', *Biomaterials*, 102, pp. 20–42. doi: 10.1016/j.biomaterials.2016.06.012.

Guillemot, F. *et al.* (2010) 'High-throughput laser printing of cells and biomaterials for tissue engineering', in *Acta Biomaterialia*. Elsevier BV, pp. 2494–2500. doi: 10.1016/j.actbio.2009.09.029.

Guillotin, B. *et al.* (2010) 'Laser assisted bioprinting of engineered tissue with high cell density and microscale organization', *Biomaterials*, 31(28), pp. 7250–7256. doi: 10.1016/j.biomaterials.2010.05.055.

Guillotin, B. and Guillemot, F. (2011) 'Cell patterning technologies for organotypic tissue fabrication', *Trends in Biotechnology*, pp. 183–190. doi: 10.1016/j.tibtech.2010.12.008.

Gutbier, S. *et al.* (2018) 'Major changes of cell function and toxicant sensitivity in cultured cells undergoing mild, quasi-natural genetic drift', *Archives of Toxicology*. Springer Berlin Heidelberg, 92(12), pp. 3487–3503. doi: 10.1007/s00204-018-2326-5.

Hadimioglu, B., Stearns, R. and Ellson, R. (2016) 'Moving Liquids with Sound: The Physics of Acoustic Droplet Ejection for Robust Laboratory Automation in Life Sciences', *Journal of Laboratory Automation*. SAGE Publications Inc., 21(1), pp. 4–18. doi: 10.1177/2211068215615096.

Hass, R. *et al.* (2011) 'Different populations and sources of human mesenchymal stem cells (MSC): A comparison of adult and neonatal tissue-derived MSC.', *Cell communication and signaling : CCS*. BioMed Central, 9, p. 12. doi: 10.1186/1478-811X-9-12.

Hassell, B. A. *et al.* (2017) 'Human Organ Chip Models Recapitulate Orthotopic Lung Cancer Growth, Therapeutic Responses, and Tumor Dormancy In Vitro', *Cell Reports*, 21(2), pp. 508–516. doi: 10.1016/j.celrep.2017.09.043.

Hendriks, J., Riesle, J. and van Blitterswijk, C. A. (2007) 'Co-culture in cartilage tissue engineering', *Journal of Tissue Engineering and Regenerative Medicine*, 1(3), pp. 170–178. doi: 10.1002/term.19.

Heo, J. S. *et al.* (2016) 'Comparison of molecular profiles of human mesenchymal stem cells derived from bone marrow, umbilical cord blood, placenta and adipose tissue', *International Journal of Molecular Medicine*. Spandidos Publications, 37(1), pp. 115–125. doi: 10.3892/ijmm.2015.2413.

Hermann, A. *et al.* (2006) 'Comparative analysis of neuroectodermal differentiation capacity

of human bone marrow stromal cells using various conversion protocols', *Journal of Neuroscience Research*. John Wiley & Sons, Ltd, 83(8), pp. 1502–1514. doi: 10.1002/jnr.20840.

Hino, K. *et al.* (2014) 'Master regulator for chondrogenesis, Sox9, regulates transcriptional activation of the endoplasmic reticulum stress transducer BBF2H7/CREB3L2 in chondrocytes', *Journal of Biological Chemistry*, 289(20), pp. 13810–13820. doi: 10.1074/jbc.M113.543322.

Hopp, B. *et al.* (2005) 'Survival and proliferative ability of various living cell types after laser-induced forward transfer', *Tissue Engineering*, 11(11–12), pp. 1817–1823. doi: 10.1089/ten.2005.11.1817.

Horvath, L. *et al.* (2015) 'Engineering an in vitro air-blood barrier by 3D bioprinting', *Scientific Reports*, 5. doi: 10.1038/srep07974.

Hu, K. *et al.* (2006) 'Pathogenesis of osteoarthritis-like changes in the joints of mice deficient in type IX collagen', *Arthritis & Rheumatism*. Wiley Subscription Services, Inc., A Wiley Company, 54(9), pp. 2891–2900. doi: 10.1002/art.22040.

Huang, S. Bin *et al.* (2015) 'Development of a pneumatically driven active cover lid for multi-well microplates for use in perfusion three-dimensional cell culture', *Scientific Reports*, 5. doi: 10.1038/srep18352.

Huang, Y. *et al.* (2017) 'Optical coherence tomography detects necrotic regions and volumetrically quantifies multicellular tumor spheroids', *Cancer Research*, 77(21), pp. 6011–6020. doi: 10.1158/0008-5472.CAN-17-0821.

Hurley, E. T. *et al.* (2018) 'Limited evidence for adipose-derived stem cell therapy on the treatment of osteoarthritis', *Sports Traumatology, Arthroscopy*, 26, pp. 3499–3507. doi: 10.1007/s00167-018-4955-x.

Hutchinson, G. H. (1978) 'Progress in water based printing inks', *Pigment & Resin Technology*, 7(11), pp. 4–13. doi: 10.1108/eb041437.

Hwang, N. S. *et al.* (2011) 'Chondrogenic priming adipose-mesenchymal stem cells for cartilage tissue regeneration', *Pharmaceutical Research*, 28(6), pp. 1395–1405. doi: 10.1007/s11095-011-0445-2.

Ikenoue, T. *et al.* (2003) 'Mechanoregulation of human articular chondrocyte aggrecan and type II collagen expression by intermittent hydrostatic pressure in vitro', *Journal of Orthopaedic Research*. Wiley Subscription Services, Inc., A Wiley Company, 21(1), pp. 110–116. doi: 10.1016/S0736-0266(02)00091-8.

Imaduwage, K. P. *et al.* (2017) 'Rapid LC-MS Based High-Throughput Screening Method, Affording No False Positives or False Negatives, Identifies a New Inhibitor for Carbonic Anhydrase', *Scientific Reports*, 7(1). doi: 10.1038/s41598-017-08602-w.

James, S. *et al.* (2015) 'Multiparameter Analysis of Human Bone Marrow Stromal Cells Identifies Distinct Immunomodulatory and Differentiation-Competent Subtypes', *Stem Cell Reports*. The Authors, 4(6), pp. 1004–1015. doi: 10.1016/j.stemcr.2015.05.005.

Jang, D., Kim, D. and Moon, J. (2009) 'Influence of fluid physical properties on ink-jet printability', *Langmuir*, 25(5), pp. 2629–2635. doi: 10.1021/la900059m.

Jean-Philippe, C. *et al.* (2012) 'A novel specific edge effect correction method for RNA interference screenings', *Bioinformatics*, 28(2), pp. 261–268. doi: 10.1093/bioinformatics/btr648.

Jeon, S.-J. *et al.* (2007) 'Bone marrow mesenchymal stem cells are progenitors in vitro for inner ear hair cells', *Molecular and Cellular Neuroscience*, 34(1), pp. 59–68. doi: 10.1016/j.mcn.2006.10.003.

Joh, D. Y. *et al.* (2017) 'Inkjet-printed point-of-care immunoassay on a nanoscale polymer brush enables subpicomolar detection of analytes in blood', *Proceedings of the National Academy of Sciences of the United States of America*, 114(34), pp. E7054–E7062. doi: 10.1073/pnas.1703200114.

Johnson, C. I., Argyle, D. J. and Clements, D. N. (2016) 'In vitro models for the study of osteoarthritis', *The Veterinary Journal*, 209, pp. 40–49. doi: 10.1016/j.tvjl.2015.07.011.

Joshi, P. and Lee, M.-Y. (2015) 'High Content Imaging (HCI) on Miniaturized Three-Dimensional (3D) Cell Cultures', *Biosensors*, 5, pp. 768–790. doi: 10.3390/bios5040768.

Jotanovic, Z. *et al.* (2012) 'Role of Interleukin-1 Inhibitors in Osteoarthritis', *Drugs & Aging*. Springer International Publishing, 29(5), pp. 343–358. doi: 10.2165/11599350-000000000-00000.

Jung, S. (2011) *Fluid characterisation and drop impact in inkjet printing for organic semiconductor devices*. University of Cambridge. Available at: https://core.ac.uk/download/pdf/1336887.pdf.

Junker, S. *et al.* (2016) 'Expression of adipokines in osteoarthritis osteophytes and their effect on osteoblasts', *Matrix Biology*, 62, pp. 75–91. doi: 10.1016/j.matbio.2016.11.005.

Kaartinen, L. *et al.* (1993) 'Rat Tracheal Epithelial Cell Diffeentiation In Vitro', *In Vitro Cell Development Biology*, (29A), pp. 481–492.

Kačarević, Ž. P. *et al.* (2018) 'An introduction to 3D bioprinting: Possibilities, challenges and future aspects', *Materials*. MDPI AG. doi: 10.3390/ma11112199.

Kahl, M. *et al.* (2019) 'Ultra-low-cost 3D bioprinting: Modification and application of an off-the-shelf desktop 3D-printer for biofabrication', *Frontiers in Bioengineering and Biotechnology*, 7(JUL), pp. 1–12. doi: 10.3389/fbioe.2019.00184.

Kämpfer, A. A. M. *et al.* (2017) 'Development of an in vitro co-culture model to mimic the human intestine in healthy and diseased state', *Toxicology in Vitro*. Pergamon, 45, pp. 31–43. doi: 10.1016/j.tiv.2017.08.011.

Kang, Y. B. *et al.* (2013) 'Layered long-term co-culture of hepatocytes and endothelial cells on a transwell membrane: Toward engineering the liver sinusoid', *Biofabrication*, 5(4), pp. 45008–45020. doi: 10.1088/1758-5082/5/4/045008.

Karlsen, T. A., Shahdadfar, A. and Brinchmann, J. E. (2011) 'Human primary articular chondrocytes, chondroblasts-like cells, and dedifferentiated chondrocytes: Differences in gene, MicroRNA, and protein expression and phenotype', *Tissue Engineering - Part C: Methods*, 17(2), pp. 219–227. doi: 10.1089/ten.tec.2010.0200.

Karnieli, O. *et al.* (2007) 'Generation of Insulin-Producing Cells from Human Bone Marrow Mesenchymal Stem Cells by Genetic Manipulation', *Stem Cells*. John Wiley & Sons, Ltd, 25(11), pp. 2837–2844. doi: 10.1634/stemcells.2007-0164.

Kartmann, S. *et al.* (2015) 'A disposable dispensing valve for non-contact microliter applications in a 96-well plate format', *Micromachines*, 6(4), pp. 423–436. doi: 10.3390/mi6040423.

Keenan, T. M. and Folch, A. (2007) 'Biomolecular gradients in cell culture systems', *Lab on a*

Chip, pp. 34–57. doi: 10.1039/b711887b.

Kellgren, J. H. and Lawrence, J. S. (1957) 'Radiological Assessment of Osteo-Arthrosis', *Annals of the Rheumatic Diseases*, 16(4), pp. 494–502. doi: 10.1136/ard.16.4.494.

Ketterl, N. *et al.* (2015) 'A robust potency assay highlights significant donor variation of human mesenchymal stem/progenitor cell immune modulatory capacity and extended radio-resistance', *Stem Cell Research & Therapy*. BioMed Central, 6(1), p. 236. doi: 10.1186/s13287-015-0233-8.

Kevorkian, L. *et al.* (2004) 'Expression profiling of metalloproteinases and their inhibitors in cartilage', *Arthritis & Rheumatism*. Wiley Subscription Services, Inc., A Wiley Company, 50(1), pp. 131–141. doi: 10.1002/art.11433.

Khalate, A. A. *et al.* (2012) 'A waveform design method for a piezo inkjet printhead based on robust feedforward control', *Journal of Microelectromechanical Systems*, 21(6), pp. 1365–1374. doi: 10.1109/JMEMS.2012.2205899.

Khan, A. *et al.* (2012) 'Direct printing of copper conductive micro-tracks by multi-nozzle electrohydrodynamic inkjet printing process', *Journal of Materials Processing Technology*. Elsevier, 212(3), pp. 700–706. doi: 10.1016/J.JMATPROTEC.2011.10.024.

Kim, H. A. and Cheon, E. J. (2012) 'Animal Model of Osteoarthritis', *Journal of Rheumatic Diseases*, 19(5), p. 239. doi: 10.4078/jrd.2012.19.5.239.

Kim, J. D. *et al.* (2010) 'Piezoelectric inkjet printing of polymers: Stem cell patterning on polymer substrates', *Polymer*. Elsevier Ltd, 51(10), pp. 2147–2154. doi: 10.1016/j.polymer.2010.03.038.

Kim, M. *et al.* (2019) 'Extracellular vesicles mediate improved functional outcomes in engineered cartilage produced from MSC/chondrocyte cocultures', *Proceedings of the National Academy of Sciences of the United States of America*, 116(5), pp. 1569–1578. doi: 10.1073/pnas.1815447116.

Kim, Y.-M. *et al.* (2008) 'Design and Fabrication of Electrostatic Inkjet Head using Silicon Micromachining Technology', *JSTS:Journal of Semiconductor Technology and Science*, 8(2), pp. 121–127. doi: 10.5573/jsts.2008.8.2.121.

King, S. M. *et al.* (2017) '3D proximal tubule tissues recapitulate key aspects of renal

physiology to enable nephrotoxicity testing', *Frontiers in Physiology*, 8(MAR), p. 123. doi: 10.3389/fphys.2017.00123.

Knight, E. (2013) *Influence of the micro-environment on the maintenance and differentiation of pluripotent stem cells*. University of Durham. Available at: http://etheses.dur.ac.uk.

Koch, L. *et al.* (2010) 'Laser printing of skin cells and human stem cells', *Tissue Engineering - Part C: Methods*. Mary Ann Liebert Inc., 16(5), pp. 847–854. doi: 10.1089/ten.tec.2009.0397.

Koch, L. *et al.* (2018) 'Laser bioprinting of human induced pluripotent stem cells - The effect of printing and biomaterials on cell survival, pluripotency, and differentiation', *Biofabrication*. Institute of Physics Publishing, 10(3). doi: 10.1088/1758-5090/aab981.

Kojima, N., Takeuchi, S. and Sakai, Y. (2012) 'Rapid aggregation of heterogeneous cells and multiple-sized microspheres in methylcellulose medium', *Biomaterials*. Elsevier, 33(18), pp. 4508–4514. doi: 10.1016/J.BIOMATERIALS.2012.02.065.

Kubosch, E. J. *et al.* (2016) 'The trans-well coculture of human synovial mesenchymal stem cells with chondrocytes leads to self-organization, chondrogenic differentiation, and secretion of TGFβ', *Stem Cell Research and Therapy*. BioMed Central, 7(1), p. 64. doi: 10.1186/s13287-016-0322-3.

Kuyinu, E. L. *et al.* (2016) 'Animal models of osteoarthritis: classification, update, and measurement of outcomes.', *Journal of orthopaedic surgery and research*. BioMed Central, 11, p. 19. doi: 10.1186/s13018-016-0346-5.

Kwon, K.-S. (2010) 'Experimental analysis of waveform effects on satellite and ligament behavior via in situ measurement of the drop-on-demand drop formation curve and the instantaneous jetting speed curve', *Journal of Micromechanics and Microengineering*, 20(11), p. 115005. doi: 10.1088/0960-1317/20/11/115005.

Kwon, K. S. (2009) 'Waveform design methods for piezo inkjet dispensers based on measured meniscus motion', *Journal of Microelectromechanical Systems*, 18(5), pp. 1118–1125. doi: 10.1109/JMEMS.2009.2026465.

Kyostio-Moore, S. *et al.* (2011) 'STR/ort mice, a model for spontaneous osteoarthritis, exhibit elevated levels of both local and systemic inflammatory markers', *Comparative Medicine*, 61(4), pp. 346–355.

Larson, B. *et al.* (2012) 'Automation of cell-based drug absorption assays in 96-well format using permeable support systems', *Journal of Laboratory Automation*, 17(3), pp. 222–232. doi: 10.1177/2211068211428190.

Lazzari, G. *et al.* (2019) 'Light sheet fluorescence microscopy versus confocal microscopy: in quest of a suitable tool to assess drug and nanomedicine penetration into multicellular tumor spheroids', *European Journal of Pharmaceutics and Biopharmaceutics*. Elsevier, 142, pp. 195–203. doi: 10.1016/J.EJPB.2019.06.019.

Lee, Geon Hui *et al.* (2018) 'Networked concave microwell arrays for constructing 3D cell spheroids', *Biofabrication*. IOP Publishing, 10(1), p. 015001. doi: 10.1088/1758-5090/aa9876.

Lee, V. *et al.* (2014) 'Design and fabrication of human skin by three-dimensional bioprinting.', *Tissue engineering. Part C, Methods*, 20(6), pp. 473–84. doi: 10.1089/ten.TEC.2013.0335.

Lemmo, A. V, Rose, D. J. and Tisone, T. C. (1998) 'Inkjet dispensing technology: Applications in drug discovery', *Current Opinion in Biotechnology*, 9(6), pp. 615–617. doi: 10.1016/S0958-1669(98)80139-0.

Van Lent, P. L. E. M. *et al.* (2012) 'Active involvement of alarmins S100A8 and S100A9 in the regulation of synovial activation and joint destruction during mouse and human osteoarthritis', *Arthritis and Rheumatism*. Wiley Subscription Services, Inc., A Wiley Company, 64(5), pp. 1466–1476. doi: 10.1002/art.34315.

Leung, B. M. *et al.* (2015) 'Media additives to promote spheroid circularity and compactness in hanging drop platform', *Biomaterials Science*, 3(2), pp. 336–344. doi: 10.1039/c4bm00319e.

Li, C. *et al.* (2015) 'Comparative analysis of human mesenchymal stem cells from bone marrow and adipose tissue under xeno-free conditions for cell therapy', *Stem Cell Research & Therapy*. BioMed Central, 6(1), p. 55. doi: 10.1186/s13287-015-0066-5.

Li, G. *et al.* (2013) 'Subchondral bone in osteoarthritis: insight into risk factors and microstructural changes', *Arthritis Research & Therapy*. BioMed Central, 15(6), p. 223. doi: 10.1186/ar4405.

Li, S. *et al.* (2015) 'Chondrogenic potential of human articular chondrocytes and skeletal stem cells: A comparative study', *Journal of Biomaterials Applications*, 29(6), pp. 824–836.

doi: 10.1177/0885328214548604.

Li, X. *et al.* (2016) 'Human Umbilical Cord Blood-Derived Mesenchymal Stem Cells Contribute to Chondrogenesis in Coculture with Chondrocytes', *BioMed Research International*, 2016. doi: 10.1155/2016/3827057.

Liberio, M. S. *et al.* (2014) 'Differential effects of tissue culture coating substrates on prostate cancer cell adherence, morphology and behavior', *PLoS ONE*. Edited by L. R. Languino. Public Library of Science, 9(11), p. e112122. doi: 10.1371/journal.pone.0112122.

Liberski, A. R., Delaney, J. T. and Schubert, U. S. (2011) '"One cell-one well": A new approach to inkjet printing single cell microarrays', *ACS Combinatorial Science*. American Chemical Society, 13(2), pp. 190–195. doi: 10.1021/co100061c.

Lin, C.-C. *et al.* (2009) 'IL-1β promotes A549 cell migration via MAPKs/AP-1- and NF-κB-dependent matrix metalloproteinase-9 expression', *Cellular Signalling*, 21(11), pp. 1652–1662. doi: 10.1016/j.cellsig.2009.07.002.

Ling, K. *et al.* (2015) 'Bioprinting-Based High-Throughput Fabrication of Three-Dimensional MCF-7 Human Breast Cancer Cellular Spheroids', *Engineering*. Elsevier, 1(2), pp. 269–274. doi: 10.15302/J-ENG-2015062.

Liu, Y. and Derby, B. (2019) 'Experimental study of the parameters for stable drop-on-demand inkjet performance', *Physics of Fluids*, 31(3), p. 32004. doi: 10.1063/1.5085868.

Loeser, R. F., Collins, J. A. and Diekman, B. O. (2016) 'Ageing and the pathogenesis of osteoarthritis', *Nature Reviews Rheumatology*, pp. 412–420. doi: 10.1038/nrrheum.2016.65.

Löffek, S., Schilling, O. and Franzke, C.-W. (2011) 'Biological role of matrix metalloproteinases: a critical balance', *European Respiratory Journal*, 38(1).

Lorber, B. *et al.* (2014) 'Adult rat retinal ganglion cells and glia can be printed by piezoelectric inkjet printing.', *Biofabrication*, 6(1), p. 015001. doi: 10.1088/1758-5082/6/1/015001.

Lu, T. J. *et al.* (2017) 'Chondrogenic differentiation of mesenchymal stem cells in three-dimensional chitosan film culture', *Cell Transplantation*, 26(3), pp. 417–427. doi: 10.3727/096368916X693464.

Lund, M. D. and Ward, J. P. (1998) 'On-page inkjet printhead spitting system system'. European Patent Office.

Lundholt, B. K., Scudder, K. M. and Pagliaro, L. (2003) 'A simple technique for reducing edge effect in cell-based assays', *Journal of Biomolecular Screening*, 8(5), pp. 566–570. doi: 10.1177/1087057103256465.

Luukkainen, A. *et al.* (2018) 'A Co-culture Model of PBMC and Stem Cell Derived Human Nasal Epithelium Reveals Rapid Activation of NK and Innate T Cells Upon Influenza A Virus Infection of the Nasal Epithelium', *Frontiers in Immunology*. Frontiers, 9, p. 2514. doi: 10.3389/fimmu.2018.02514.

Ma, B. *et al.* (2013) 'Gene expression profiling of dedifferentiated human articular chondrocytes in monolayer culture', *Osteoarthritis and Cartilage*, 21(4), pp. 599–603. doi: 10.1016/j.joca.2013.01.014.

Ma, L. D. *et al.* (2018) 'Design and fabrication of a liver-on-a-chip platform for convenient, highly efficient, and safe: In situ perfusion culture of 3D hepatic spheroids', *Lab on a Chip*. The Royal Society of Chemistry, 18(17), pp. 2547–2562. doi: 10.1039/c8lc00333e.

Macrory, L. *et al.* (2009) 'An exploration of the ability of tepoxalin to ameliorate the degradation of articular cartilage in a canine in vitro model', *BMC Veterinary Research*. BioMed Central, 5(1), p. 25. doi: 10.1186/1746-6148-5-25.

Madden, J. C. *et al.* (2012) 'Strategies for the optimisation of in vivo experiments in accordance with the 3Rs philosophy', *Regulatory Toxicology and Pharmacology*, 63(1), pp. 140–154. doi: 10.1016/j.yrtph.2012.03.010.

Madry, H. and Cucchiarini, M. (2016) 'Expert Opinion on Biological Therapy Gene therapy for human osteoarthritis: principles and clinical translation Gene therapy for human osteoarthritis: principles and clinical translation', *Expert Opinion on Biological Therapy*, 16(3), pp. 331–346. doi: 10.1517/14712598.2016.1124084.

Mahay, D., Terenghi, G. and Shawcross, S. G. (2008) 'Schwann cell mediated trophic effects by differentiated mesenchymal stem cells', *Experimental Cell Research*. Academic Press, 314(14), pp. 2692–2701. doi: 10.1016/J.YEXCR.2008.05.013.

Maksymowych, W. P. *et al.* (2012) 'Targeting tumour necrosis factor alleviates signs and symptoms of inflammatory osteoarthritis of the knee', *Arthritis Research and Therapy*. BioMed Central, 14(5), p. R206. doi: 10.1186/ar4044.

Malda, J. *et al.* (2004) 'Oxygen Gradients in Tissue-Engineered PEGT/PBT Cartilaginous Constructs: Measurement and Modeling', *Biotechnology and Bioengineering*, 86(1), pp. 9–18. doi: 10.1002/bit.20038.

Malfait, A. M., Little, C. B. and McDougall, J. J. (2013) 'A commentary on modelling osteoarthritis pain in small animals', *Osteoarthritis and Cartilage*. NIH Public Access, 21(9), pp. 1316–1326. doi: 10.1016/j.joca.2013.06.003.

Marga, F. *et al.* (2012) 'Toward engineering functional organ modules by additive manufacturing', *Biofabrication*. doi: 10.1088/1758-5082/4/2/022001.

Marshall, J., Barnes, A. and Genever, P. (2018) 'Analysis of the Intrinsic Self-Organising Properties of Mesenchymal Stromal Cells in Three-Dimensional Co-Culture Models with Endothelial Cells', *Bioengineering*, 5(4), p. 92. doi: 10.3390/bioengineering5040092.

Martel-Pelletier, J., Welsch, D. J. and Pelletier, J.-P. (2001) 'Metalloproteases and inhibitors in arthritic diseases', *Best Practice & Research Clinical Rheumatology*, 15(5), pp. 805–829. doi: 10.1053/berh.2001.0195.

Marx, U. *et al.* (2018) 'Bioengineering of a Full-Thickness Skin Equivalent in a 96-Well Insert Format for Substance Permeation Studies and Organ-On-A-Chip Applications', *Bioengineering*. Multidisciplinary Digital Publishing Institute (MDPI), 5(2), p. 43. doi: 10.3390/bioengineering5020043.

McCoy, A. M. (2015) 'Animal Models of Osteoarthritis: Comparisons and Key Considerations', *Veterinary Pathology*, 52(5), pp. 803–818. doi: 10.1177/0300985815588611.

McIlroy, C., Harlen, O. G. G. and Morrison, N. F. F. (2013) 'Modelling the jetting of dilute polymer solutions in drop-on-demand inkjet printing', *Journal of Non-Newtonian Fluid Mechanics*. Elsevier B.V., 201, pp. 17–28. doi: 10.1016/j.jnnfm.2013.05.007.

McKee, C. and Chaudhry, G. R. (2017) 'Advances and challenges in stem cell culture', *Colloids and Surfaces B: Biointerfaces*. Elsevier, 159, pp. 62–77. doi: 10.1016/J.COLSURFB.2017.07.051.

McKinley, G. H. and Renardy, M. (2011) 'Wolfgang von Ohnesorge', *Physics of Fluids*, 23(12). doi: 10.1063/1.3663616.

McMurtrey, R. J. (2016) 'Analytic models of oxygen and nutrient diffusion, metabolism

dynamics, and architecture optimization in three-dimensional tissue constructs with applications and insights in cerebral organoids', *Tissue Engineering - Part C: Methods*, 22(3), pp. 221–249. doi: 10.1089/ten.tec.2015.0375.

Melissaridou, S. *et al.* (2019) 'The effect of 2D and 3D cell cultures on treatment response, EMT profile and stem cell features in head and neck cancer 11 Medical and Health Sciences 1112 Oncology and Carcinogenesis', *Cancer Cell International*. BioMed Central, 19(1), p. 16. doi: 10.1186/s12935-019-0733-1.

Mennan, C. *et al.* (2018) 'Human Articular Chondrocytes Retain Their Phenotype in Sustained Hypoxia While Normoxia Promotes Their Immunomodulatory Potential', *Cartilage*. SAGE Publications Inc. doi: 10.1177/1947603518769714.

Meretoja, V. V *et al.* (2012) 'Enhanced chondrogenesis in co-cultures with articular chondrocytes and mesenchymal stem cells', *Biomaterials*. NIH Public Access, 33(27), pp. 6362–6369. doi: 10.1016/j.biomaterials.2012.05.042.

Meretoja, V. V *et al.* (2014) 'Articular chondrocyte redifferentiation in 3D co-cultures with mesenchymal stem cells', *Tissue Engineering - Part C: Methods*, 20(6), pp. 514–523. doi: 10.1089/ten.tec.2013.0532.

Michael, S. *et al.* (2008) 'A robotic platform for quantitative high-throughput screening', *Assay and Drug Development Technologies*, 6(5), pp. 637–657. doi: 10.1089/adt.2008.150.

Michael, S. *et al.* (2013) 'Tissue Engineered Skin Substitutes Created by Laser-Assisted Bioprinting Form Skin-Like Structures in the Dorsal Skin Fold Chamber in Mice', *PLoS ONE*, 8(3). doi: 10.1371/journal.pone.0057741.

Miers, J. C. and Zhou, W. (2017) 'Droplet formation at megahertz frequency', *AIChE Journal*, 63(6), pp. 2367–2377. doi: 10.1002/aic.15578.

Mikhailova, A. *et al.* (2014) 'Small-molecule induction promotes corneal epithelial cell differentiation from human induced pluripotent stem cells', *Stem Cell Reports*, 2(2), pp. 219–231. doi: 10.1016/j.stemcr.2013.12.014.

Miki, Y. *et al.* (2012) 'The advantages of co-culture over mono cell culture in simulating in vivo environment', *The Journal of Steroid Biochemistry and Molecular Biology*, 131(3), pp. 68–75. doi: 10.1016/j.jsbmb.2011.12.004.

Min, D. *et al.* (2018) 'Bioprinting of biomimetic skin containing melanocytes', *Experimental Dermatology*, p. 27. doi: 10.1111/exd.13376.

Minegishi, Y., Hosokawa, K. and Tsumaki, N. (2013) 'Time-lapse observation of the dedifferentiation process in mouse chondrocytes using chondrocyte-specific reporters', *Osteoarthritis and Cartilage*, 21(12), pp. 1968–1975. doi: 10.1016/j.joca.2013.09.004.

Mironov, V., Kasyanov, V. and Markwald, R. R. (2011) 'Organ printing: From bioprinter to organ biofabrication line', *Current Opinion in Biotechnology*, pp. 667–673. doi: 10.1016/j.copbio.2011.02.006.

Mistry, H. *et al.* (2015) *Autologous chondrocyte implantation in the knee*, *Health Technology Assessment*. doi: 10.1002/14651858.cd003323.pub3.

Mobasheri, A. and Batt, M. (2016) 'An update on the pathophysiology of osteoarthritis', *Annals of Physical and Rehabilitation Medicine*. Elsevier Masson, 59(5–6), pp. 333–339. doi: 10.1016/j.rehab.2016.07.004.

Mohanraj, B. *et al.* (2014) 'A high-throughput model of post-traumatic osteoarthritis using engineered cartilage tissue analogs', *Osteoarthritis and Cartilage*. NIH Public Access, 22(9), pp. 1282–1290. doi: 10.1016/j.joca.2014.06.032.

Moon, S. *et al.* (2011) 'Drop-on-demand single cell isolation and total RNA analysis', *PLoS ONE*, 6(3). doi: 10.1371/journal.pone.0017455.

Mosaad, E. *et al.* (2018) 'Using high throughput microtissue culture to study the difference in prostate cancer cell behavior and drug response in 2D and 3D co-cultures', *BMC Cancer*. BioMed Central, 18(1), p. 592. doi: 10.1186/s12885-018-4473-8.

Moseler, O. and Straky, H. (2000) 'Fault Detection of a Solenoid Valve for Hydraulic Systems in Vehicles', *IFAC Proceedings Volumes*, 33(11), pp. 119–124. doi: 10.1016/s1474-6670(17)37347-0.

Moskowitz, R. W. *et al.* (1973) 'Experimentally Induced Degenerative Joint Lesions Following Partial Meniscectomy in the Rabbit', *Arthritis & Rheumatism*. John Wiley & Sons, Inc., 16(3), pp. 397–405. doi: 10.1002/art.1780160317.

Mosmann, T. (1983) 'Rapid colorimetric assay for cellular growth and survival: Application to proliferation and cytotoxicity assays', *Journal of Immunological Methods*. Elsevier, 65(1–2),

pp. 55–63. doi: 10.1016/0022-1759(83)90303-4.

Mountain, D. J. H. *et al.* (2007) 'Interleukin-1β increases expression and activity of matrix metalloproteinase-2 in cardiac microvascular endothelial cells: Role of PKCα/β1 and MAPKs', *American Journal of Physiology - Cell Physiology*, 292(2), pp. C867-75. doi: 10.1152/ajpcell.00161.2006.

Murab, S. *et al.* (2013) 'Matrix-embedded cytokines to simulate osteoarthritis-like cartilage microenvironments.', *Tissue engineering. Part A*. Mary Ann Liebert, Inc., 19(15–16), pp. 1733–53. doi: 10.1089/ten.TEA.2012.0385.

Murphy, K. C. *et al.* (2016) 'Mesenchymal Stem Cell Spheroids Retain Osteogenic Phenotype Through α 2 β 1 Signaling', *STEM CELLS Translational Medicine*. Wiley-Blackwell, 5(9), pp. 1229–1237. doi: 10.5966/sctm.2015-0412.

Murphy, S. V., Skardal, A. and Atala, A. (2013) 'Evaluation of hydrogels for bio-printing applications', *Journal of Biomedical Materials Research - Part A*, 101 A(1), pp. 272–284. doi: 10.1002/jbm.a.34326.

Murphy, S. V and Atala, A. (2014) '3D bioprinting of tissues and organs.', *Nature Biotechnology*. Nature Publishing Group, 32(8), pp. 773–785. doi: 10.1038/nbt.2958.

Mwale, F. *et al.* (2006) 'Limitations of Using Aggrecan and Type X Collagen as Markers of Chondrogenesis in Mesenchymal Stem Cell Differentiation', *Journal of Orthopaedic Research*, pp. 1791–1798. doi: 10.1002/jor.

Nath, S. and Devi, G. R. (2016) 'Three-dimensional culture systems in cancer research: Focus on tumor spheroid model', *Pharmacology & Therapeutics*. Pergamon, 163, pp. 94–108. doi: 10.1016/J.PHARMTHERA.2016.03.013.

National Institute for Health and Care Excellence (2005) *The use of autologous chondrocyte implantation for the treatment of cartilage defects in the knee joints - Technical appraisal guidance TA89*. Available at: https://www.nice.org.uk/guidance/ta89.

National Institute for Health and Care Excellence (2014) *Osteoarthritis: care and management - Clinical guideline CG177*. doi: nice.org.uk/guidance/cg177.

National Institute for Health and Care Excellence (2017) *Autologous chondrocyte implantation for treating symptomatic articular cartilage defects of the knee - Technical*

appraisal guidance TA477. Available at: https://www.nice.org.uk/guidance/ta477/resources/autologous-chondrocyte-implantation-for-treating-symptomatic-articular-cartilage-defects-of-the-knee-pdf-82604971061701.

National Institute for Health and Care Excellence (2018) *Autologous chondrocyte implantation using chondrosphere for treating symptomatic articular cartilage defects of the knee - Technical appraisal guidance TA508*. Available at: www.nice.org.uk/guidance/ta508.

Niemeyer, P. *et al.* (2016) 'Autologous chondrocyte implantation (ACI) for cartilage defects of the knee: A guideline by the working group "Clinical Tissue Regeneration" of the German Society of Orthopaedics and Trauma (DGOU)', *Knee*, 23(3), pp. 426–435. doi: 10.1016/j.knee.2016.02.001.

Niles, W. D. and Coassin, P. J. (2005) 'Piezo- and Solenoid Valve-Based Liquid Dispensing for Miniaturized Assays', *Assay and Drug Development Technologies*, 3(2), pp. 189–202. doi: 10.1089/adt.2005.3.189.

Ong, C. S. *et al.* (2018) 'In vivo therapeutic applications of cell spheroids', *Biotechnology Advances*. Elsevier, 36(2), pp. 494–505. doi: 10.1016/J.BIOTECHADV.2018.02.003.

Osterman, C. *et al.* (2015) 'Platelet-Rich Plasma Increases Anti-inflammatory Markers in a Human Coculture Model for Osteoarthritis.', *The American Journal of Sports Medicine*, 43(6), pp. 1474–84. doi: 10.1177/0363546515570463.

Pampaloni, F., Ansari, N. and Stelzer, E. H. K. (2013) 'High-resolution deep imaging of live cellular spheroids with light-sheet-based fluorescence microscopy', *Cell and Tissue Research*, pp. 161–177. doi: 10.1007/s00441-013-1589-7.

Park, D. (2013) 'Method and Apparatus for Purging and Supplying Ink to an Inkjet Printing Apparatus'. United States of America: United States Patent and Trademark Office.

Park, J. *et al.* (2017) 'Hypergravity-induced multicellular spheroid generation with different morphological patterns precisely controlled on a centrifugal microfluidic platform', *Biofabrication*. IOP Publishing, 9(4), p. 045006. doi: 10.1088/1758-5090/aa9472.

Park, J. A. *et al.* (2017) 'Freeform micropatterning of living cells into cell culture medium using direct inkjet printing', *Scientific Reports*, 7(1), p. 14610. doi: 10.1038/s41598-017-14726-w.

Parrish, J. *et al.* (2018) 'A 96-well microplate bioreactor platform supporting individual dual perfusion and high-throughput assessment of simple or biofabricated 3D tissue models', *Lab on a Chip*, 18(18), pp. 2757–2775. doi: 10.1039/c8lc00485d.

Parsa, S. *et al.* (2010) 'Effects of surfactant and gentle agitation on inkjet dispensing of living cells', *Biofabrication*, 2(2), p. 025003. doi: 10.1088/1758-5082/2/2/025003.

Pas, H. I. *et al.* (2017) 'Stem cell injections in knee osteoarthritis: a systematic review of the literature', *British Journal of Sports Medicine*, 51(15), pp. 1125–1133. doi: 10.1136/bjsports-2016-096793.

Paul, S. M. *et al.* (2010) 'How to improve RD productivity: The pharmaceutical industry's grand challenge', *Nature Reviews Drug Discovery*, 9(3), pp. 203–214. doi: 10.1038/nrd3078.

Pawlowski, N. E. and Childers, W. D. (2001) 'Air purge apparatus for inkjet print cartridges'. European Patent Office.

Pennock, R. *et al.* (2015) 'Human cell dedifferentiation in mesenchymal condensates through controlled autophagy', *Scientific Reports*, 5(1). doi: 10.1038/srep13113.

Perelaer, J. *et al.* (2009) 'The Spreading of Inkjet-Printed Droplets with Varying Polymer Molar Mass on a Dry Solid Substrate', *Macromolecular Chemistry and Physics*, 210(6), pp. 495–502. doi: 10.1002/macp.200800569.

Pérez-García, S. *et al.* (2016) 'Healthy and Osteoarthritic Synovial Fibroblasts Produce a Disintegrin and Metalloproteinase with Thrombospondin Motifs 4, 5, 7, and 12: Induction by IL-1β and Fibronectin and Contribution to Cartilage Damage', *The American Journal of Pathology*, 186(9), pp. 2449–2461. doi: 10.1016/j.ajpath.2016.05.017.

Pfeifer, C. R. *et al.* (2018) 'Constricted migration increases DNA damage and independently represses cell cycle', *Molecular Biology of the Cell*, 29(16), pp. 1948–1962. doi: 10.1091/mbc.E18-02-0079.

Phillippi, J. A. *et al.* (2008) 'Microenvironments Engineered by Inkjet Bioprinting Spatially Direct Adult Stem Cells Toward Muscle- and Bone-Like Subpopulations', *Stem Cells*, 26(1), pp. 127–134. doi: 10.1634/stemcells.2007-0520.

Pierik, A. *et al.* (2008) 'Quality control of inkjet technology for DNA microarray fabrication', *Biotechnology Journal*, 3(12), pp. 1581–1590. doi: 10.1002/biot.200800121.

Pingguan-Murphy, B. and Nawi, I. (2012) 'Upregulation of matrix synthesis in chondrocyte-seeded agarose following sustained bi-axial cyclic loading', *Clinics*, 67(8), pp. 939–944. doi: 10.6061/clinics/2012(08)14.

Pond, M. J. and Nuki, G. (1973) 'Experimentally-induced osteoarthritis in the dog.', *Annals of the Rheumatic Diseases*. BMJ Group, 32(4), pp. 387–8. Available at: http://www.ncbi.nlm.nih.gov/pubmed/4726075.

Quent, V. M. C. *et al.* (2010) 'Discrepancies between metabolic activity and DNA content as tool to assess cell proliferation in cancer research', *Journal of Cellular and Molecular Medicine*, 14(4), pp. 1003–1013. doi: 10.1111/j.1582-4934.2010.01013.x.

Rahmati, M., Mobasheri, A. and Mozafari, M. (2016) 'Inflammatory mediators in osteoarthritis: A critical review of the state of the art, prospects, and future challenges.', *Bone*, 85, pp. 81–90. doi: 10.1016/j.bone.2016.01.019.

Ramirez, J. C. C. and Tumolva, T. P. (2018) 'Analysis and optimization of water-based printing ink formulations for polyethylene films', *Applied Adhesion Science*. Springer International Publishing, 6(1), pp. 1–21. doi: 10.1186/s40563-017-0102-z.

Razban, A. and Davies, B. L. (1991) 'An automated system for dispensing adhesives', *International Journal of Adhesion and Adhesives*, 11(3), pp. 187–191. doi: 10.1016/0143-7496(91)90022-A.

Reis, N. and Derby, B. (2000) 'Ink jet deposition of ceramic suspensions: Modelling and experiments of droplet formation', *Materials Research Society Symposium - Proceedings*, 624(January 2000), pp. 65–70. doi: 10.1557/PROC-625-117.

Rengel, Y., Ospelt, C. and Gay, S. (2007) 'Proteinases in the joint: Clinical relevance of proteinases in joint destruction', *Arthritis Research and Therapy*, 9(5), pp. 1–10. doi: 10.1186/ar2304.

Restouin, A. *et al.* (2009) 'A simplified, 96-well-adapted, ATP luminescence-based motility assay', *BioTechniques*, 47(4), pp. 871–875. doi: 10.2144/000113250.

Ribeiro, R. D. C. *et al.* (2017) 'Temporary Single-Cell Coating for Bioprocessing with a Cationic Polymer', *ACS Applied Materials and Interfaces*, 9(15), pp. 12967–12974. doi: 10.1021/acsami.6b16434.

Richardson, J. B. *et al.* (2017) 'Efficacy and safety of autologous cell therapies for knee cartilage defects (autologous stem cells, chondrocytes or the two): Randomized controlled trial design', *Regenerative Medicine*, 12(5), pp. 493–501. doi: 10.2217/rme-2017-0032.

Riffle, S. *et al.* (2017) 'Linking hypoxia, DNA damage and proliferation in multicellular tumor spheroids', *BMC Cancer*, 17(1). doi: 10.1186/s12885-017-3319-0.

Rigoglou, S. and Papavassiliou, A. G. (2013) 'The NF-κB signalling pathway in osteoarthritis', *The International Journal of Biochemistry & Cell Biology*, 45(11), pp. 2580–2584. doi: 10.1016/j.biocel.2013.08.018.

Rodríguez-Puente, S., Linacero-Blanco, J. and Guasch, A. (2013) 'A simple and effective calibration method to determine the accuracy of liquid-handling nano-dispenser devices', *Acta Crystallographica Section F: Structural Biology and Crystallization Communications*, 69(3), pp. 336–341. doi: 10.1107/S1744309113000791.

Roger, M. *et al.* (2019) 'Bioengineering the microanatomy of human skin', *Journal of Anatomy*. doi: 10.1111/joa.12942.

Roshanghias, A., Krivec, M. and Baumgart, M. (2017) 'Sintering strategies for inkjet printed metallic traces in 3D printed electronics', *Flexible and Printed Electronics*, 2(4). doi: 10.1088/2058-8585/aa8ed8.

Roth, E. A. *et al.* (2004) 'Inkjet printing for high-throughput cell patterning', *Biomaterials*, 25(17), pp. 3707–3715. doi: 10.1016/j.biomaterials.2003.10.052.

Russell, W. and Burch, R. (1959) *The Principles of Humane Experimental Technique*. London: Methuen.

Sakamoto, J. *et al.* (2009) 'Immobilization-Induced Cartilage Degeneration Mediated Through Expression of Hypoxia-Inducible Factor-1α, Vascular Endothelial Growth Factor, and Chondromodulin-I', *Connective Tissue Research*. Taylor & Francis, 50(1), pp. 37–45. doi: 10.1080/03008200802412454.

San Antonio, J. D. and Tuan, R. S. (1986) 'Chondrogenesis of limb bud mesenchyme in vitro: Stimulation by cations', *Developmental Biology*, 115(2), pp. 313–324. doi: 10.1016/0012-1606(86)90252-6.

Saunders, R. E., Gough, J. E. and Derby, B. (2008) 'Delivery of human fibroblast cells by

piezoelectric drop-on-demand inkjet printing', *Biomaterials*, 29(2), pp. 193–203. doi: 10.1016/j.biomaterials.2007.09.032.

Sawada, S. *et al.* (2016) 'Establishment of mesenchymal stem cell lines derived from the bone marrow of green fluorescent protein-transgenic mice exhibiting a diversity in intracellular transforming growth factor-β and bone morphogenetic protein signaling', *Molecular Medicine Reports*, 13(3), pp. 2023–2031. doi: 10.3892/mmr.2016.4794.

Schnabel, M. *et al.* (2002) 'Dedifferentiation-associated changes in morphology and gene expression in primary human articular chondrocytes in cell culture', *Osteoarthritis and Cartilage*, 10, pp. 62–70. doi: 10.1053/joca.2001.0482.

Secunda, R. *et al.* (2015) 'Isolation, expansion and characterisation of mesenchymal stem cells from human bone marrow, adipose tissue, umbilical cord blood and matrix: a comparative study', *Cytotechnology*. Springer, 67(5), pp. 793–807. doi: 10.1007/s10616-014-9718-z.

Shimizu, H., Yokoyama, S. and Asahara, H. (2007) 'Growth and differentiation of the developing limb bud from the perspective of chondrogenesis', *Development Growth and Differentiation*, 49(6), pp. 449–454. doi: 10.1111/j.1440-169X.2007.00945.x.

Shin, K. *et al.* (2013) 'The Efficacy of Diacerein in Hand Osteoarthritis: A Double-Blind, Randomized, Placebo-Controlled Study', *Clinical Therapeutics*, 35(4), pp. 431–439. doi: 10.1016/j.clinthera.2013.02.009.

Shterev, I. D. *et al.* (2018) 'Bayesian Multi-Plate High-Throughput Screening of Compounds', *Scientific Reports*. Nature Publishing Group, 8(1), p. 9551. doi: 10.1038/s41598-018-27531-w.

Shun, T. Y. *et al.* (2011) 'Identifying actives from HTS data sets: Practical approaches for the selection of an appropriate HTS data-processing method and quality control review', *Journal of Biomolecular Screening*, 16(1), pp. 1–14. doi: 10.1177/1087057110389039.

Sip, C. G., Bhattacharjee, N. and Folch, A. (2014) 'Microfluidic transwell inserts for generation of tissue culture-friendly gradients in well plates', *Lab on a Chip*, 14, pp. 302–314. doi: 10.1039/c3lc51052b.

Smith, C. M. *et al.* (2004) 'Three-dimensional bioassembly tool for generating viable tissue-

engineered constructs', *Tissue Engineering*, 10(9–10), pp. 1566–1576. doi: 10.1089/ten.2004.10.1566.

Smith, C. M. *et al.* (2007) 'Characterizing environmental factors that impact the viability of tissue-engineered constructs fabricated by a direct-write bioassembly tool', *Tissue Engineering*, 13(2), pp. 373–383. doi: 10.1089/ten.2006.0101.

Smyrek, I. and Stelzer, E. H. K. (2017) 'Quantitative three-dimensional evaluation of immunofluorescence staining for large whole mount spheroids with light sheet microscopy', *Biomedical Optics Express*, 8(2), p. 484. doi: 10.1364/boe.8.000484.

Solorio, L. D. *et al.* (2010) 'Chondrogenic differentiation of human mesenchymal stem cell aggregates via controlled release of TGF-β1 from incorporated polymer microspheres', *Journal of Biomedical Materials Research - Part A*. NIH Public Access, 92(3), pp. 1139–1144. doi: 10.1002/jbm.a.32440.

Song, R. *et al.* (2007) 'Aggrecan Degradation in Human Articular Cartilage Explants Is Mediated by Both ADAMTS-4 and ADAMTS-5', *Arthritis & Rheumatism*, 56(2), pp. 575–585. doi: 10.1002/art.22334.

Sophia Fox, A. J., Bedi, A. and Rodeo, S. A. (2009) 'The basic science of articular cartilage: Structure, composition, and function', *Sports Health*. SAGE Publications, 1(6), pp. 461–468. doi: 10.1177/1941738109350438.

Staat, E.-J. (2016) *Droplet dynamics during flight, impact and evaporation*. University of Twente. doi: 10.3990/1.9789036540810.

Stangegaard, M. *et al.* (2011) 'A Simple method for validation and verification of pipettes mounted on automated liquid handlers', *Journal of Laboratory Automation*, 16(5), pp. 381–386. doi: 10.1016/j.jala.2009.06.004.

Starkuviene, V. and Pepperkok, R. (2007) 'The potential of high-content high-throughput microscopy in drug discovery', *British Journal of Pharmacology*. Wiley-Blackwell, 152(1), pp. 62–71. doi: 10.1038/sj.bjp.0707346.

Stone, N. L., England, T. J. and O'Sullivan, S. E. (2019) 'A Novel Transwell Blood Brain Barrier Model Using Primary Human Cells', *Frontiers in Cellular Neuroscience*. Frontiers, 13, p. 230. doi: 10.3389/fncel.2019.00230.

Stow, C. D. and Hadfield, M. G. (1981) 'An Experimental Investigation of Fluid Flow Resulting from the Impact of a Water Drop with an Unyielding Dry Surface', *Proceedings of the Royal Society A: Mathematical, Physical and Engineering Sciences*, 373(1755), pp. 419–441. doi: 10.1098/rspa.1981.0002.

Sturgess, C. *et al.* (2017) '3D reactive inkjet printing of polydimethylsiloxane', *Journal of Materials Chemistry C*. The Royal Society of Chemistry, 5(37), pp. 9733–9743. doi: 10.1039/C7TC02412F.

Szymański, P., Markowicz, M. and Mikiciuk-Olasik, E. (2012) 'Adaptation of high-throughput screening in drug discovery-toxicological screening tests.', *International journal of molecular sciences*. Multidisciplinary Digital Publishing Institute (MDPI), 13(1), pp. 427–52. doi: 10.3390/ijms13010427.

Tat, S. K. *et al.* (2011) 'Strontium ranelate inhibits key factors affecting bone remodeling in human osteoarthritic subchondral bone osteoblasts', *Bone*, 49(3), pp. 559–567. doi: 10.1016/j.bone.2011.06.005.

Taylor, P. B. *et al.* (2002) 'A Standard Operating Procedure for Assessing Liquid Handler Performance in High-Throughput Screening', *Journal of Biomolecular Screening*. SAGE Publications, 7(6), pp. 554–569. doi: 10.1177/1087057102238630.

Teeple, E. *et al.* (2013) 'Animal models of osteoarthritis: challenges of model selection and analysis.', *The AAPS journal*. Springer, 15(2), pp. 438–46. doi: 10.1208/s12248-013-9454-x.

Thakur, M. *et al.* (2012) 'Characterisation of a Peripheral Neuropathic Component of the Rat Monoiodoacetate Model of Osteoarthritis', *PLoS ONE*. Edited by M. L. Baccei. Public Library of Science, 7(3), p. e33730. doi: 10.1371/journal.pone.0033730.

Thysen, S., Luyten, F. P. and Lories, R. J. U. (2015) 'Targets, models and challenges in osteoarthritis research', *Disease Models and Mechanisms*, 8(1), pp. 17–30. doi: 10.1242/dmm.016881.

Torsvik, A. *et al.* (2014) 'U-251 revisited: genetic drift and phenotypic consequences of long-term cultures of glioblastoma cells', *Cancer Medicine*. John Wiley & Sons, Ltd, 3(4), pp. 812–824. doi: 10.1002/cam4.219.

Trivedi, A. *et al.* (2019) 'Bone marrow donor selection and characterization of MSCs is critical

for pre-clinical and clinical cell dose production', *Journal of Translational Medicine*, 17(1), p. 128. doi: 10.1186/s12967-019-1877-4.

Trudel, G., Uhthoff, H. K. and Laneuville, O. (2005) 'Prothrombin gene expression in articular cartilage with a putative role in cartilage degeneration secondary to joint immobility.', *The Journal of Rheumatology*, 32(8).

Tse, C. (2015) *Utilising inkjet printing for tissue engineering*. University of Sheffield. Available at: http://etheses.whiterose.ac.uk/13950/1/THESIS_THESIS10alpha.pdf.

Tse, C. *et al.* (2016) 'Inkjet printing Schwann cells and neuronal analogue NG108-15 cells', *Biofabrication*. IOP Publishing, 8(1), p. 015017. doi: 10.1088/1758-5090/8/1/015017.

Tung, Y. C. *et al.* (2011) 'High-throughput 3D spheroid culture and drug testing using a 384 hanging drop array', *Analyst*, 136(3), pp. 473–478. doi: 10.1039/c0an00609b.

Uzarski, J. S. *et al.* (2017) 'Essential design considerations for the resazurin reduction assay to noninvasively quantify cell expansion within perfused extracellular matrix scaffolds', *Biomaterials*, 129, pp. 163–175. doi: 10.1016/j.biomaterials.2017.02.015.

Verma, P. and Dalal, K. (2011) 'ADAMTS-4 and ADAMTS-5: Key enzymes in osteoarthritis', *Journal of Cellular Biochemistry*. Wiley Subscription Services, Inc., A Wiley Company, 112(12), pp. 3507–3514. doi: 10.1002/jcb.23298.

Vinaiphat, A., Charngkaew, K. and Thongboonkerd, V. (2018) 'More complete polarization of renal tubular epithelial cells by artificial urine', *Cell Death Discovery*. Nature Publishing Group, 4(1), p. 47. doi: 10.1038/s41420-018-0112-z.

Vincent, T. L. *et al.* (2012) 'Mapping pathogenesis of arthritis through small animal models', *Rheumatology (United Kingdom)*, 51(11), pp. 1931–1941. doi: 10.1093/rheumatology/kes035.

Vos, T. *et al.* (2012) 'Years lived with disability (YLDs) for 1160 sequelae of 289 diseases and injuries 1990-2010: a systematic analysis for the Global Burden of Disease Study 2010.', *Lancet (London, England)*. Elsevier, 380(9859), pp. 2163–96. doi: 10.1016/S0140-6736(12)61729-2.

Walzl, A. *et al.* (2014) 'The resazurin reduction assay can distinguish cytotoxic from cytostatic compounds in spheroid screening assays', *Journal of Biomolecular Screening*. SAGE

Publications Inc., 19(7), pp. 1047–1059. doi: 10.1177/1087057114532352.

Wang, J. *et al.* (2019) 'Combined Autologous Chondrocyte and Bone Marrow Mesenchymal Stromal Cell Implantation in the Knee: An 8-year Follow Up of Two First-In-Man Cases', *Cell Transplantation*, 28(7), pp. 924–931. doi: 10.1177/0963689719845328.

Wasan, D. T. and Papoutsakis, E. T. (1995) 'Interfacial Properties of Cell Culture Media with Cell-Protecting Additives', *Biotechnology and Bioengineering*, 47(4), pp. 420–430.

Wheeler, J. S. R. *et al.* (2014) 'Polymer degradation during continuous ink-jet printing', *Polymer Degradation and Stability*, 105, pp. 116–121. doi: 10.1016/j.polymdegradstab.2014.04.007.

Wijshoff, H. (2018) 'Drop dynamics in the inkjet printing process', *Current Opinion in Colloid & Interface Science*. Elsevier, 36, pp. 20–27. doi: 10.1016/J.COCIS.2017.11.004.

Wilson, J. L. *et al.* (2014) 'Alginate encapsulation parameters influence the differentiation of microencapsulated embryonic stem cell aggregates', *Biotechnology and Bioengineering*, 111(3), pp. 618–631. doi: 10.1002/bit.25121.

Wilson, W. C. and Boland, T. (2003) 'Cell and organ printing 1: Protein and cell printers', *Anatomical Record - Part A Discoveries in Molecular, Cellular, and Evolutionary Biology*, 272(2), pp. 491–496. doi: 10.1002/ar.a.10057.

Woo, K. *et al.* (2013) 'Relationship between printability and rheological behavior of ink-jet conductive inks', *Ceramics International*, 39(6), pp. 7015–7021. doi: 10.1016/j.ceramint.2013.02.039.

Woodward, W. a and Tuan, R. S. (1999) 'N-Cadherin expression and signaling in limb mesenchymal chondrogenesis: stimulation by poly-L-lysine', *Developmental Genetics*, 24(1–2), pp. 178–187. doi: 10.1002/(SICI)1520-6408(1999)24:1/2<178::AID-DVG16>3.0.CO;2-M.

Wu, C. H. and Hwang, W. S. (2015) 'The effect of the echo-time of a bipolar pulse waveform on molten metallic droplet formation by squeeze mode piezoelectric inkjet printing', *Microelectronics Reliability*. Elsevier Ltd, 55(3–4), pp. 630–636. doi: 10.1016/j.microrel.2014.11.014.

Wu, L. *et al.* (2011) 'Trophic effects of mesenchymal stem cells increase chondrocyte proliferation and matrix formation', *Tissue Engineering - Part A*, 17(9–10), pp. 1425–1436.

doi: 10.1089/ten.tea.2010.0517.

Xia, Y. *et al.* (2019) 'Rescue of DNA damage after constricted migration reveals a mechano-regulated threshold for cell cycle', *The Journal of Cell Biology*, 218(8), pp. 2545–2563. doi: 10.1083/jcb.201811100.

Xing, D. *et al.* (2018) 'Mesenchymal stem cells injections for knee osteoarthritis: a systematic overview', *Rheumatology International*, pp. 1399–1411. doi: 10.1007/s00296-017-3906-z.

Xiong, W. *et al.* (2017) 'Experimental investigation on the height deviation of bumps printed by solder jet technology', *Journal of Materials Processing Technology*. Elsevier, 243, pp. 291–298. doi: 10.1016/J.JMATPROTEC.2016.12.031.

Xu, T. *et al.* (2005) 'Inkjet printing of viable mammalian cells.', *Biomaterials*, 26(1), pp. 93–9. doi: 10.1016/j.biomaterials.2004.04.011.

Xu, T. *et al.* (2006) 'Viability and electrophysiology of neural cell structures generated by the inkjet printing method', *Biomaterials*, 27(19), pp. 3580–3588. doi: 10.1016/j.biomaterials.2006.01.048.

Yamaguchi, S. *et al.* (2012) 'Cell patterning through inkjet printing of one cell per droplet', *Biofabrication*. IOP Publishing, 4(4), p. 045005. doi: 10.1088/1758-5082/4/4/045005.

Yang, Y.-H., Lee, A. J. and Barabino, G. A. (2012) 'Coculture-Driven Mesenchymal Stem Cell-Differentiated Articular Chondrocyte-Like Cells Support Neocartilage Development', *Stem Cells Translational Medicine*. Wiley-Blackwell, 1(11), pp. 843–854. doi: 10.5966/sctm.2012-0083.

Yasuda, T. (2006) 'Cartilage destruction by matrix degradation products', *Modern Rheumatology*. Springer, 16(4), pp. 197–205. doi: 10.1007/s10165-006-0490-6.

Yeung, P. *et al.* (2018) 'A human osteoarthritis osteochondral organ culture model for cartilage tissue engineering', *Biomaterials*. Elsevier, 162, pp. 1–21. doi: 10.1016/j.biomaterials.2018.02.002.

Yokoi, K. (2011) 'Numerical studies of droplet splashing on a dry surface: Triggering a splash with the dynamic contact angle', *Soft Matter*, 7(11), pp. 5120–5123. doi: 10.1039/c1sm05336a.

Yonker, L. M. *et al.* (2017) 'Development of a Primary Human Co-Culture Model of Inflamed

Airway Mucosa', *Scientific Reports*. Nature Publishing Group, 7(1), p. 8182. doi: 10.1038/s41598-017-08567-w.

Yus, J. *et al.* (2019) 'Semiconductor water-based inks: Miniaturized NiO pseudocapacitor electrodes by inkjet printing', *Journal of the European Ceramic Society*. Elsevier, 39(9), pp. 2908–2914. doi: 10.1016/J.JEURCERAMSOC.2019.03.020.

Yusof, A. *et al.* (2011) 'Inkjet-like printing of single-cells', *Lab on a Chip*. The Royal Society of Chemistry, 11(14), pp. 2447–2454. doi: 10.1039/c1lc20176j.

Zhang, S., Handa-Corrigan, A. and Spier, R. E. (1992) 'Foaming and media surfactant effects on the cultivation of animal cells in stirred and sparged bioreactors', *Journal of Biotechnology*, 25(3), pp. 289–306. doi: 10.1016/0168-1656(92)90162-3.

Zhang, X. *et al.* (2017) 'Coculture of mesenchymal stem cells and endothelial cells enhances host tissue integration and epidermis maturation through AKT activation in gelatin methacryloyl hydrogel-based skin model', *Acta Biomaterialia*. Elsevier, 59, pp. 317–326. doi: 10.1016/J.ACTBIO.2017.07.001.

Zhang, Z. *et al.* (2012) 'Quality control of cell-based high-throughput drug screening', *Acta Pharmaceutica Sinica B*. Elsevier, 2(5), pp. 429–438. doi: 10.1016/J.APSB.2012.03.006.

Zhou, S., Cui, Z. and Urban, J. P. G. (2008) 'Nutrient gradients in engineered cartilage: Metabolic kinetics measurement and mass transfer modelings', *Biotechnology and Bioengineering*, 101(2), pp. 408–421. doi: 10.1002/bit.21887.

Zimmermann, R. *et al.* (2019) 'High resolution bioprinting of multi-component hydrogels', *Biofabrication*, 11(4), p. 045008. doi: 10.1088/1758-5090/ab2aa1.

Appendix

MTT Calibration Curves

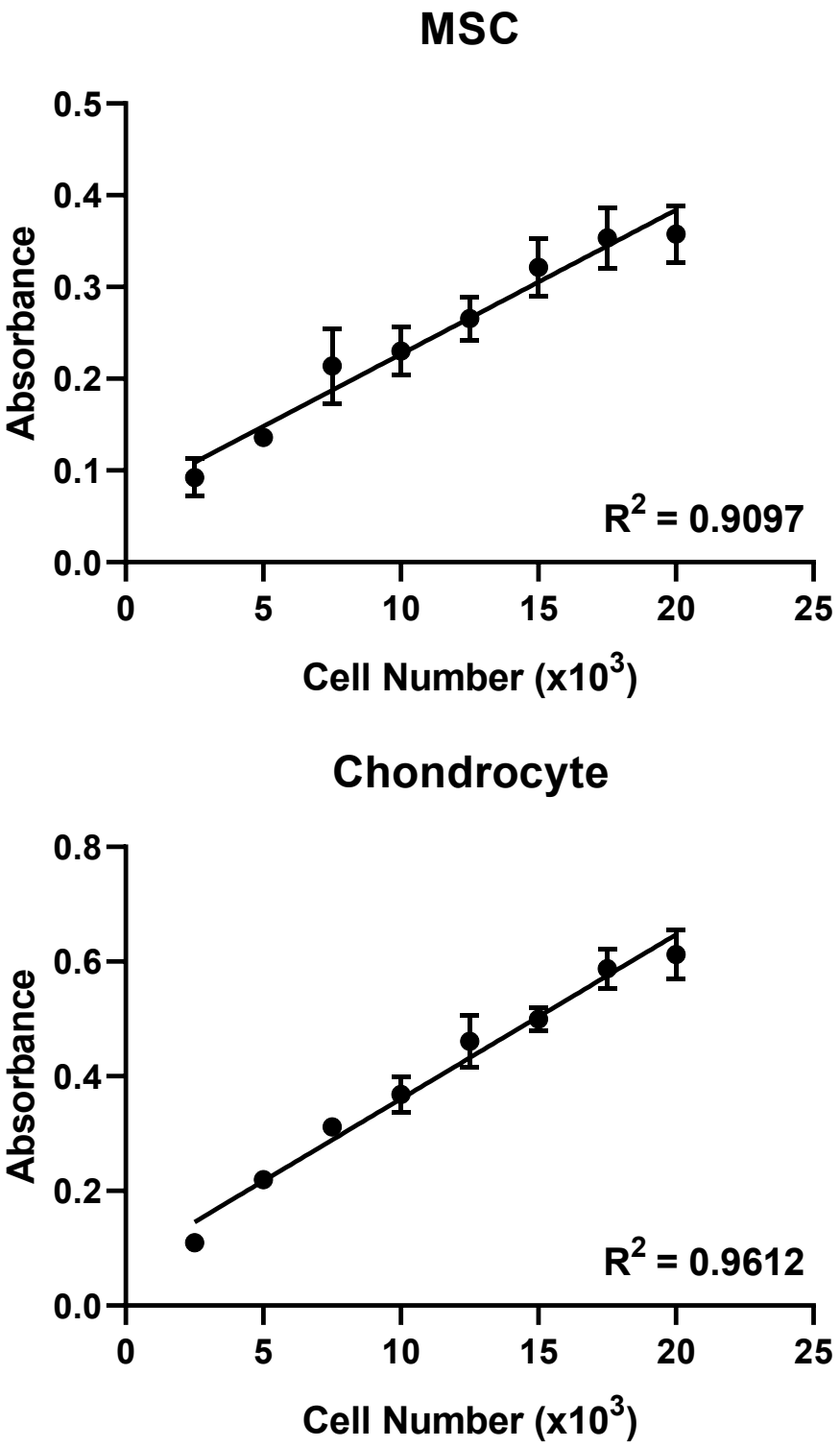

Appendix Figure 1 – MTT assay calibration curve data for the MSC and chondrocyte cell lines demonstrating the signal linearity across a concentration range of 2,500 - 20,000 cells per well. Data represents mean values ± SD. N=3.

PrestoBlue® Calibration Curves

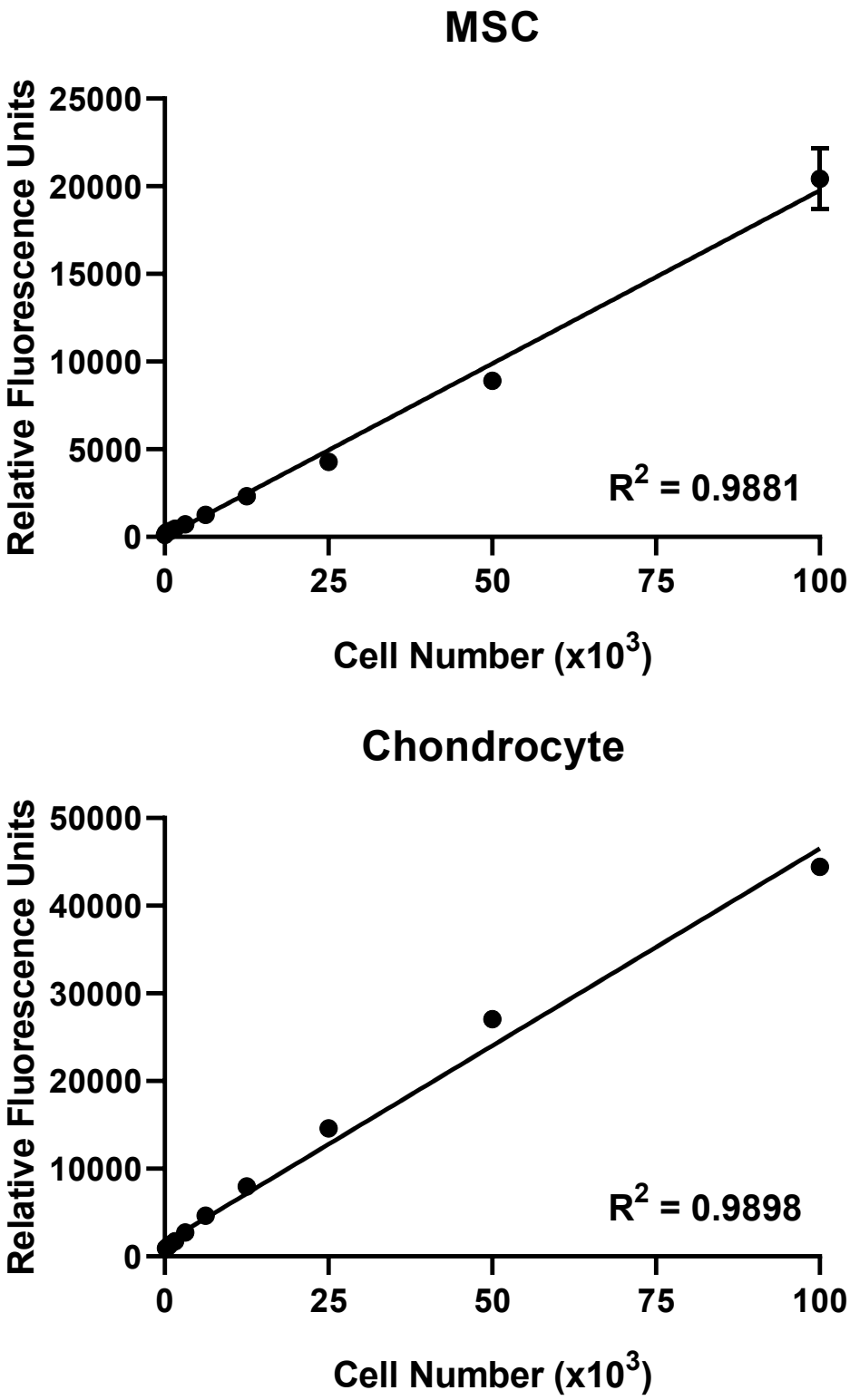

Appendix Figure 2 – PrestoBlue® assay calibration curve data for the MSC and chondrocyte cell lines demonstrating the signal linearity across a concentration range from 50 to 100,000 cells per well. Data represents mean values ± SD. N=6.

Indirect Immunofluorescence Staining Controls

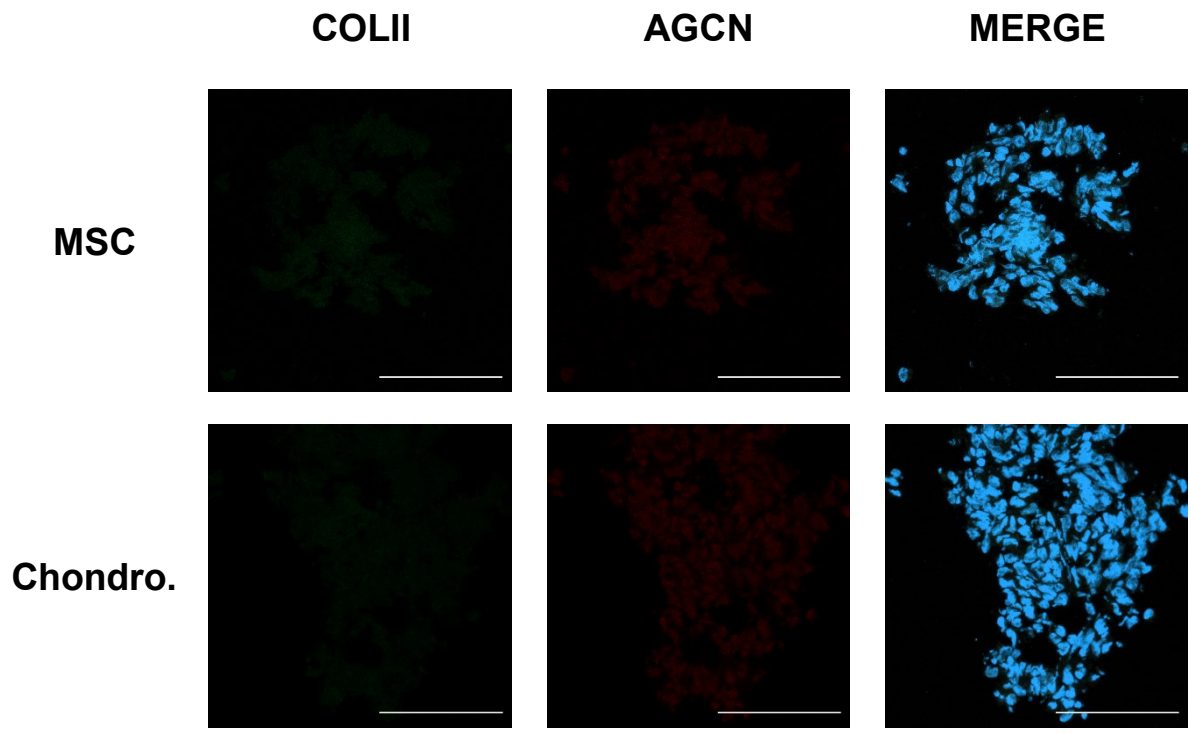

Appendix Figure 3 – Negative MSC and chondrocyte controls of collagen II (COLII, green) and aggrecan (AGCN, red) indirect immunofluorescence staining within sectioned tissue. Samples were stained using the primary antibody diluent alone followed by secondary antibody incubation. Scale bar = 100 µm.